# Structural Polymorphism of Amyloidogenic Peptides

**KAREN ELIZABETH MARSHALL**

A thesis submitted for the degree of Doctor of Philosophy

The University of Sussex
June 2010

# Declaration

I hereby declare that this thesis has not been and will not be, submitted in whole or in part to another University for the award of any other degree.

Signature:……

Karen Elizabeth Marshall

(June 2010)

# Acknowledgements

My sincere and unending gratitude goes to my supervisor, Louise, for giving me more support and guidance than I could ever have hoped for or expected, whilst allowing me to work and learn independently. The things I have to thank you for are too numerous to list here, but I will always be grateful for the continuing encouragement I have received. I hope for a long and lasting friendship both inside of science and out.

Thank you also to my second supervisor, Darren Thompson, for all the help, chats, advice both work related and otherwise, and of course the perpetual office entertainment.

I would like to thank Julian Thorpe for all his help with electron microscopy.

I am very grateful to those who have helped me with all matters spectroscopic, Alison Rodger, Tim Dafforn, Søren Vrønning Hoffmann and especially Matt Hicks, your thoughts and input have been invaluable.

To Tom, Kyle, Valia, Sharon and Lisa, thank you for making coming into work such a pleasure and for stimulating discussions in the office, lab and, not forgetting, the pub. I will miss you all very very much (I'm sure the feeling is mutual Kyle!) and look forward to many nights out with you all in the future (sausage competition, port and baileys anyone!?).

Thank you to the undergraduate project students who worked in the lab - Sam, Alex, Alastair and Debbie.

To my wonderful friends who have always listened with interest, genuine or not it is greatly appreciated.

By no means least, I would like to extend enormous thanks to my family - mum, dad, Anna, Nick and Donna. I am so grateful for your patience, support (financial and otherwise) and for always making me laugh, I am so lucky. My love to you all.

*“The best way to become acquainted with a subject is to write a book about it”*
Benjamin Disraeli

# CONTENTS

**List of figures**

**List of tables**

## Abbreviations

| | |
|---|---|
| **AD** | Alzheimer's Disease |
| **ADDL** | Amyloid β derived diffusible ligand |
| **AFM** | Atomic force microscopy |
| **APOE** | Apolipoprotein E |
| **APP** | Amyloid precursor protein |
| **CCD** | Charge-coupled device |
| **CD** | Circular dichroism |
| **cm** | Centimetres |
| **cryo EM** | Cryo-electron microscopy |
| **DMEM** | Dulbecco's modified Eagle's minimum |
| **DMSO** | Dimethyl sulfoxide |
| **DNA** | Deoxyribonucleic acid |
| ***E. coli*** | *Escherichia coli* |
| **EPR** | Electron paramagnetic resonance |
| **ER** | Endoplasmic reticulum |
| **FCS** | Foetal calf serum |
| **FTIR** | Fourier transform infra-red |
| **GuHCl** | Guanidinium hydrochloride |
| **h(IAPP)** | human Islet Amyloid Polypeptide |
| **H/D exchange** | Hydrogen deuterium exchange |
| **H/P** | Hydrophobic/Polar |
| **HFIP** | 1,1,1,3,3,3-Hexafluoro-2-propanol |
| **HT** | High tension |
| **kDa** | kilodalton |
| **kHz** | kilohertz |
| **LD** | Linear dichroism |
| **LDr** | reduced linear lichroism |
| **M** | Molar |
| **mg** | milligrams |
| **min** | minute |
| **ml** | millilitres |
| **mm** | millimetre |
| **mM** | millimolar |
| **MRE** | Mean residue ellipticity |
| **MTT** | (3-(4,5-Dimethylthiazol-2-yl)-2,5-diphenyltetrazolium bromide |
| **mV** | millivolts |
| **N/m** | Newtons per metre |
| **$Na_2HPO_4$** | disodium hydrogen phosphate |
| **NAC** | Non-amyloid component |
| **NaCl** | Sodium chloride |

| | |
|---|---|
| **NaF** | Sodium fluoride |
| **$NaH_2PO_4$** | sodium dihydrogen phosphate |
| **nm** | nanometre |
| **NM** | N terminal and middle region |
| **PBS** | Phosphate buffered saline |
| **pdb** | Protein data bank |
| **PEM** | Photoelastic modulator |
| **PMT** | Photomultiplier tube |
| **polyQ** | polyglutamine |
| **$PrP^C$** | Prion protein - cellular form |
| **$PrP^{Sc}$** | Prion protein - scrapie form |
| **PS1** | presenilin 1 |
| **PS2** | presenilin 2 |
| **RNA** | Ribonucleic acid |
| **rpm** | rotation per minute |
| **s** | second |
| **SAF** | Self assembled fibre |
| **SALSA** | Simple Algorithm for Sliding Averages |
| **SANS** | Small angle neutron scattering |
| **SH3** | Src homolgy 3 |
| **ss(NMR)** | solid state nuclear magnetic resonance |
| **TEM** | Transmission electron microscopy |
| **ThT** | Thioflavin T |
| **TSE** | Transmissible spongiform encephalopathies |
| **TTR** | Transthyretin |
| **UV** | Ultra-violet |
| **v** | volt |
| **v(CJD)** | variant Creutzfeldt-Jakob disease |
| **WT** | Wild type |
| **XRFD** | X-ray fibre diffraction |

# ABSTRACT

The folding of a protein from a linear chain of amino acids into its functional native state is one of the most widely investigated yet enigmatic events to take place in the natural world. An ever-increasing number of proteins and peptides are known to fold, or "misfold", into protease-resistant amyloid fibrils that share a common cross-β structure, despite having no apparent sequence homology. Self-assembly of particular proteins or peptides into amyloid is believed to be the molecular basis of many diseases, including Alzheimer's Disease, Type II diabetes and the transmissible spongiform encephalopathies. More recent evidence suggests a functional, non-pathogenic role for amyloid in certain organisms, which has inspired its use as a biomaterial. In order to understand these diseases and exploit amyloid for industrial use using a bottom-up design approach, detailed knowledge of the assembly process and structure of amyloid is required.

Many short peptides are known to assemble into amyloid-like fibres *in vitro* that have very similar properties to those formed *in vivo.* These "model systems" can give deeper insight into what triggers, drives and influences self-assembly. Furthermore, they can provide more detailed structural information than is often obtained from larger amyloid-forming proteins. Using two short peptides (the yeast prion fragment GNNQQNY and the designed peptide KFFEAAAKKFFE), which form amyloid-like microcrystals that have been structurally characterised previously, the roles of particular residues in assembly and structure were investigated. Results reveal that aromatic residues are fundamental determinants of assembly and may contribute to polymorphic propensity. Furthermore, non-aromatic sequence changes can have dramatic effects on fibril morphology both at a macromolecular level and in the underlying peptide packing arrangement. Structural variations were found between amyloid-like fibres and microcrystals formed from the same peptide, which has implications for how to examine amyloid structure in the future.

The balance of conditions required for proteins or peptides to adopt specific conformations is very fine. Polymorphism may be an inherent property of amyloidogenic proteins and peptides and detailing the structural intricacies of each form will be essential from both a biomedical and industrial perspective.

# 1. INTRODUCTION PART I: Amyloid – an overview

## 1.1. Nomenclature and classification

In 1854 the German physician Rudolf Virchow, while carrying out experiments on brain tissue that contained waxy, lardaceous deposits, observed a positive staining reaction after addition of iodine and sulphuric acid (Cohen, 1986). This led him to believe that these inclusions were composed of carbohydrate and he coined the term "amyloid", from the Latin *amylum*, meaning starch, to describe the deposits (Cohen, 1986). Five years later, while examining the same material, Friedreich and Kekule noted that amyloid had a high nitrogen content and concluded that the underlying component was not in fact carbohydrate but protein and that the positive iodine staining reaction observed by Virchow was due to co-deposited proteoglycans (Sipe and Cohen, 2000). Despite these new findings compromising its suitability, use of the term "amyloid" has been retained and 150 years later is still a subject of immense inquiry.

As technology has improved and methods have developed, our understanding of amyloid has moved on from these initial observations. Amyloid now more specifically refers to fibres formed from proteins that are said to have "misfolded" into a structure known as cross-$\beta$. It is these fibres that partially constitute the deposits observed by Virchow and others. Amyloid fibres are found in the body in a number of diseases and it was this apparent pathological association that originally stimulated interest in them. Defining exactly what amyloid is has been a subject of much debate and as attention to it has expanded outside of the medical profession its classification has become more controversial. The first criterion for determining the presence of amyloid in tissue was its observed apple green birefringence when viewed under cross-polarised light after staining with the dye Congo Red (figure 1.1a) (Glenner, 1980; Sipe and Cohen, 2000). This technique is still used on post-mortem specimens today, although the sensitivity of the test varies greatly (Pepys, 2006). In addition, amyloid fibrils can be extracted from affected tissues and observed using electron microscopy (EM) and in some cases have shown a common underlying structure to fibrils prepared

*in vitro* (figure 1.1b) (Serpell et al., 2000b). The first EM studies carried out on *ex-vivo* amyloid fibres revealed they are on average 75-100 Å in width and of indeterminate length (Cohen, 1982).

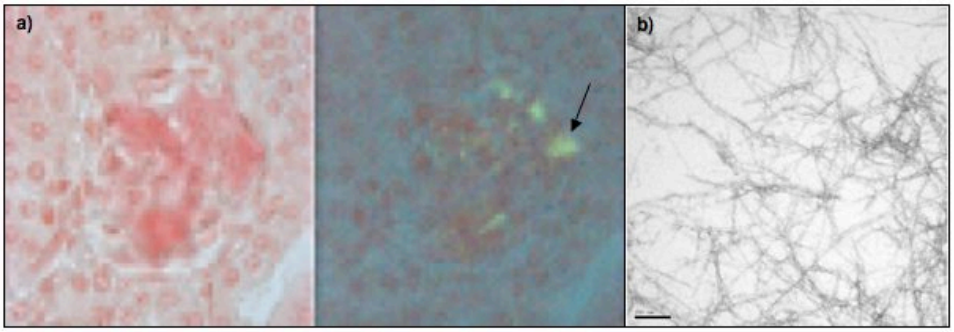


**Figure 1.1. a) Congo red staining of amyloid-containing mouse glomeruli and b) negative stain electron micrograph of synthetic IAPP at 2 mg/ml in PBS (courtesy of Dr. Louise Serpell).** The left image in a) shows the tissue after initial treatment with the dye, the image on the right is the same section viewed under cross-polarised light and shows the classic apple green birefringence characteristic of amyloid (indicated by the arrow). The scale bar in b) is 200 nm

The ability to bind Congo Red and the appearance of fibrillar material under the electron microscope were the first two criteria used to confirm the presence of amyloid in diseased tissues. However, as experiments have progressed and we see that amyloid can be formed not only from proteins that can cause disease but also many others, including those that are naturally occurring but non-pathogenic, or designed, or which are small fragments of larger proteins, the distinction is less clear. A recent definition of amyloid states: “to be included in the list, the protein has to be a major fibril protein in extracellular deposits, which have the characteristics of amyloid, including affinity for Congo Red with resulting green birefringence. Synthetic fibrils with amyloid properties are best named ‘amyloid-like’ ”, although the authors do acknowledge that the distinction is not always clear (Westermark et al., 2005). A later report suggested that because of the rate at which amyloid disorders were uncovered nomenclature should be based solely on the major protein constituent of the amyloid fibril (Westermark et al., 2007). This classification has moved on considerably from a definition in 1983 that considered amyloid simply to be any “naturally occurring mammalian protein polymers that exhibit a rod or fibril appearance by EM and show green birefringence after Congo Red staining” (Prusiner et al., 1983). As time has

proceeded, other definitions have been put forward such as the ability to bind another dye, Thioflavin T, or the co-deposition of other molecules e.g. amyloid P component (Pepys, 2006) although these are not necessarily essential. However, one criterion that has been widely accepted is that to be termed amyloid or amyloid-like, fibrils must exhibit a cross-β structure i.e. with β-strands formed from the precursor protein arranged perpendicularly to the length of the fibres (Fandrich, 2007; Sunde et al., 1997). To summarise, although no firm consensus has been reached on how to define amyloid (often due to divided opinions based on whether it is disease related or formed *in vitro*), here, it will be used to describe fibrils visible using EM and that show a cross-β structure.

It is well established that proteins can misfold into amyloid fibrils that are associated with disease. But interest in amyloid goes further than to fulfil the purpose of answering medical questions and finding treatments. The potential for proteins to "misfold" and self-assemble has led to a new view of protein folding. The precise way in which proteins achieve their functional three-dimensional shape is still unknown and proteins that can fold to form amyloid as well as their native state may help to unravel the mystery of folding. In addition, amyloid fibres are shown to have enormous strength and stability and may therefore provide the basis for an excellent material for industrial use (Smith et al., 2006). Furthermore, it has been observed that many organisms have exploited the properties of amyloid and used it for their benefit with no observable toxic effects (Fowler et al., 2007). Lessons in toxicity and how the cell operates to promote and prevent amyloid formation could be learned from these organisms. These aspects, along with how amyloid is implicated in disease, are discussed below.

## 1.2. Protein folding and misfolding

In 1958 Francis Crick and colleagues devised the "central dogma" of molecular biology and described the flow of genetic information from DNA to RNA and finally to the proteins that genes encode (Crick, 1970; Crick, 1958). It was known that proteins were produced from the ribosome as long polymers of covalently linked amino acids. In order to perform their function these chains fold up into a three dimensional shape, termed the native state, via metastable $\alpha$-helical or $\beta$-sheet secondary structures (Pauling and Corey, 1951). Investigations into how this process occurs remain a cornerstone of biological science and continue today.

In 1968 Cyrus Levinthal noted that if a polypeptide chain was to reach its correctly folded conformation (which it fundamentally requires to perform its function) by a systematic sampling of every possible stable bond angle available it would take a time far longer than what is actually observed for a protein to fold, thus formulating Levinthal's paradox (Levinthal, 1968). It is impossible that proteins could randomly search these possible conformations and there must be a way in which protein folding is guided. Levinthal postulated that proteins fold initially by the formation of local interactions between amino acids, which determine the final fold (Levinthal, 1968). He was careful to suggest that although logically the final folded state would be the one of lowest free energy and the most stable, this is not necessarily so, although the protein must be stable enough to remain folded and perform its function (Levinthal, 1968). These ideas built upon but also conflicted with those of Christian Anfinsen whose previous work on bovine pancreatic ribonuclease revealed that all of the information required for a protein to fold into its native structure is contained within the amino acid sequence of a polypeptide chain, and that this fold is the most thermodynamically stable i.e. of the lowest free energy (the thermodynamic hypothesis) (Anfinsen, 1973; Anfinsen et al., 1954). The controversy over whether protein folding is a thermodynamic process and the final conformation reached is that of the lowest free energy, or if the native state is determined by kinetic control and reaches a local, but not necessarily the lowest, free energy minima prevails (Govindarajan and Goldstein,

1998). It is believed that protein folding is driven initially by hydrophobic collapse followed by the formation of secondary structure elements within a polypeptide and finally stabilisation of the native state with stronger, covalent bonds (Gething and Sambrook, 1992). As the protein folds various intermediates form that are in equilibrium with the denatured state and which slowly convert to the native state (Gething and Sambrook, 1992; Ptitsyn, 1991; Brockwell and Radford, 2007). Protein folding in the cell is, of course, much more complicated and controlled than experiments carried out *in vitro* and much is known about the involvement of folding assistants, for example the enzyme protein disulphide isomerase and the heat shock protein family of chaperones (Gething and Sambrook, 1992).

Attempts to solve Levinthal's paradox have generated the idea of protein folding funnels and landscapes where there are multiple routes to the final folded state and no unique pathway exists (Dill and Chan, 1997; Dobson, 2003; Hartl and Hayer-Hartl, 2009). It is clear that all of the information required for a protein to fold correctly is contained within the polypeptide backbone; if a protein is denatured it will generally adopt the same original conformation after refolding (Honig, 1999; Levinthal, 1968). However, on occasion, proteins do not fold into their native structure, or functional conformations are perturbed in some way, despite the best efforts made by the cell to prevent this, and these events can give rise to protein misfolding diseases (figure 1.2) (Dobson, 2003). Many of these diseases show pathologies in which insoluble amyloid fibrils formed from normally soluble, and often functional, proteins are deposited. The formation of amyloid not only provides a molecular basis for these diseases but also demonstrates how amino acid sequences do not necessarily determine a unique structure and can deviate from their classical folding pathway to adopt alternative conformations. Indeed, it has been proposed that any protein is able to misfold into amyloid, given the appropriate conditions (Dobson, 2003).

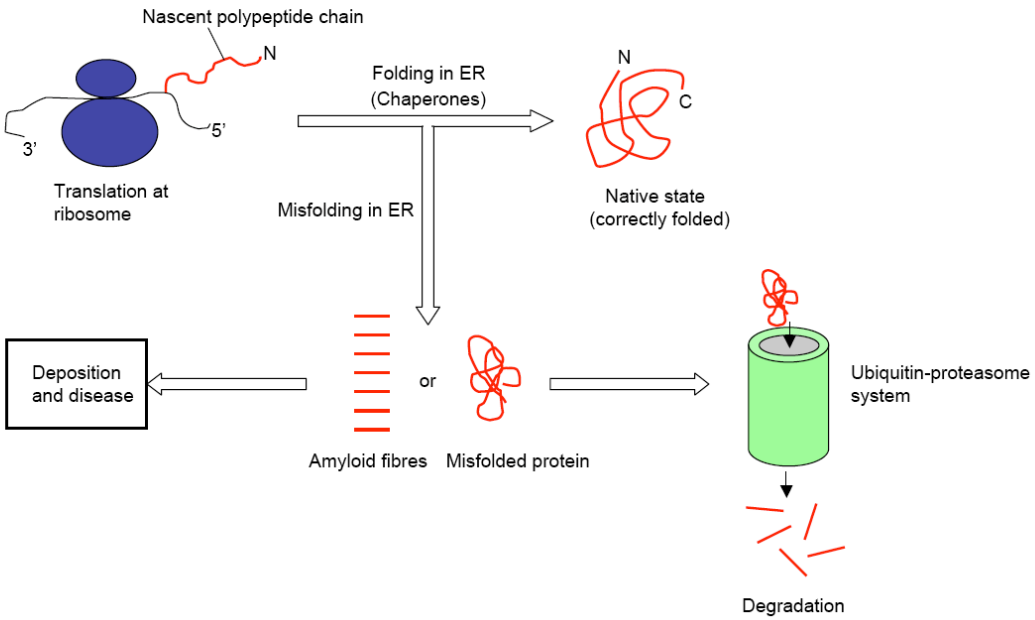


**Figure 1.2. Protein folding and misfolding *in vivo*.** Polypeptide chains enter the endoplasmic reticulum (ER) where they ideally fold into their native state. Incorrectly folded proteins are identified, targeted and may be degraded by the ubiquitin-proteasome system, although other systems exist and this is a simplified response. However, sometimes proteins misfold into structures such as amyloid that are not degraded and which can cause disease. Adapted from Dobson, 2003.

The forces that govern folding into the native state are the same as those that drive amyloid formation, such as hydrophobic interactions, hydrogen bonding, electrostatic interactions and π-π stacking, although the resulting structures indicate that the pathways are distinct and those side chains that drive folding into the native state are probably different to those contributing to amyloid formation. For example, in a similar manner to native folding, protein misfolding and aggregation is partly driven by hydrophobic interactions (Hartl and Hayer-Hartl, 2009). However, unlike the native state in which hydrophobic regions are buried, in misfolded proteins they are often exposed and this leads to aggregation of molecules, which may be amorphous or, as in the case of amyloid, ordered (Hartl and Hayer-Hartl, 2009). It is believed that amorphous aggregation and fibril formation in some cases compete (Zurdo et al., 2001). Proteins that have misfolded into amyloid are thought to be kinetically trapped intermediates (Lansbury, 1992). Figure 1.3 shows a protein-folding funnel, or energy

landscape, showing the pathways by which an unfolded protein might achieve one of many folded or misfolded states (Hartl and Hayer-Hartl, 2009).

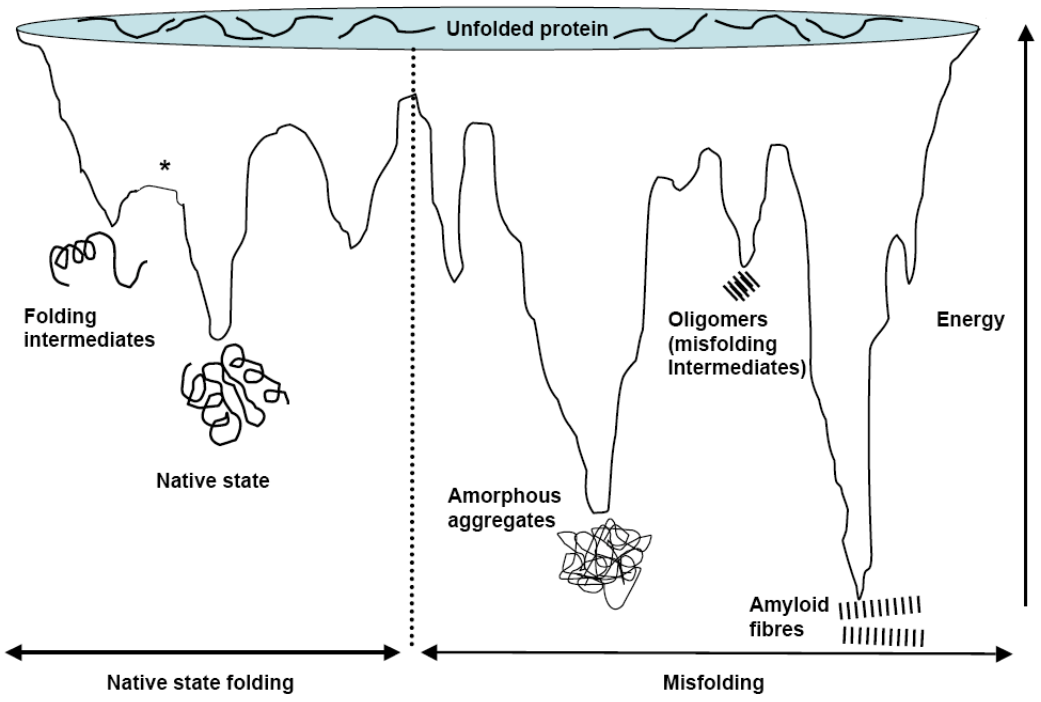


**Figure 1.3. Energy landscape of protein folding and misfolding.** On the left hand side are natively folded states and intermediates on pathway to the native state that can overcome small energy barriers (*). On the right hand side are off pathway misfolded states, however, these pathways can overlap and native state intermediates can eventually form misfolded states. The distinction between the right and left hand sides is that native states form intermolecular contacts only, whereas misfolded proteins and amorphous aggregates are intramolecularly bonded. Adapted from Hartl, 2009.

Denaturation of amyloid is generally more difficult compared to native state globular proteins, for example the dissolution of Aβ was shown only to occur with strong chaotropic agents or organic solvents e.g. phenol (Masters et al., 1985). Furthermore, a common characteristic of amyloid fibres is that they are resistant to proteases (Andersen et al., 2010; Dickson, 2002; Hartley et al., 2008; Hill et al., 1999; Soderberg et al., 2005). These observations have led to the suggestion that amyloid fibres represent the lowest possible energy conformation that a protein can adopt (Chiti and Dobson, 2006; Yang et al., 1999) which is alluded to in the diagram, where amyloid fibres are located at the lowest energy minima (Hartl and Hayer-Hartl, 2009). Also highlighted on figure 1.3 are oligomeric species that can be considered misfolding

intermediates, similar to those present in on-pathway native state folding (Jahn and Radford, 2005).

The number of proteins and peptides known to form amyloid *in vitro* is ever growing and brings increasing attention to the postulation that there is not just one structure dictated by amino acid sequence. The development of protein folding landscapes to include misfolded proteins, like the one shown in figure 1.3 have aided understanding in how proteins may misfold on a thermodynamic and kinetic basis. Other *in vitro* experiments have explored factors that may contribute to misfolding, such as mechanisms whereby local unfolded or partially unfolded protein concentration is increased which favours aggregation (Jahn and Radford, 2005; Stefani, 2008). However, the situation in the cell is far more complex and mechanisms have evolved to keep aggregation-prone partially folded states to a minimum (Jahn and Radford, 2005). Understanding how proteins misfold not only provides insight into protein folding from a theoretical point of view, for example how variations in sequence can influence folding pathways, but is also essential if the basis behind misfolding diseases is to be uncovered (Jahn and Radford, 2005)

## 1.3. Protein misfolding diseases and the Amyloid hypothesis

*In vitro*, many proteins and peptides are able to form amyloid. However, *in vivo* only around 23 proteins and peptides are known to misfold and cause disease (Pepys, 2006). This is perhaps not surprising since the cell has evolved to protect itself from toxicity. However, there are instances where the machinery of the cell falters and protein misfolding disease states manifest. The mechanisms for how this occurs are likely to be hugely complex given the intricate nature of the workings of the cell and the many components that play a role in its functioning. Furthermore, although these pathologies can be grouped into "protein misfolding diseases", their causes and effects are wide and varied. Not all of the protein misfolding diseases involves the deposition of amyloid fibrils and even the categorisation of those that do is not necessarily clear. One of the defining criteria for an amyloid-disease to be so-called is that the fibrils not only conform to the staining and visual criteria specified previously but that they are deposited extracellularly (Westermark et al., 2005). Intracellularly deposited fibrils, even if they can fit the other defining criteria, are termed "intracellular inclusions" from a medical standpoint (Westermark et al., 2005). For example, the polyglutamine expansion diseases show fibrillar aggregates deposited intracellularly and are therefore not classified as an amyloid disease (at least from a clinical perspective – the aggregates can be called amyloid as they conform to the necessary criteria – see section 1.1) (Pepys, 2006). Amyloidosis is a specific term used to describe any disorder that is *caused* by the extracellular deposition of insoluble amyloid fibrils formed from misfolded, self-assembled proteins (Pepys, 2006). This distinguishes the amyloidoses from other diseases where amyloid may be present but its causal effects are not absolutely confirmed. For example many neurodegenerative diseases such as Alzheimer's disease are associated with extracellular amyloid deposition, although intracellular inclusions composed of paired helical filaments of hyperphosphorylated tau protein also present in AD pathology (Sigurdsson, 2009). Some amyloid related protein misfolding diseases and their classification along with the peptide responsible or associated with the disease, are summarised in the table below:

| Disease | Protein or peptide (no. of residues) | Native structure |
|---|---|---|
| ***Systemic amyloidoses*** | | |
| AL amyloidosis | Immunoglobulin light chain or fragments (~90) | All β |
| AA amyloidosis | Fragments of serum amyloid A (76-104) | All α |
| Senile systemic amyloidosis | Wild type transthyretin (127) | Mostly β |
| Familial amyloidotic polyneuropathy | Transthyretin mutants (127) | Mostly β |
| Haemodialysis related amyloidosis | $\beta_2$-microglobulin (99) | All β |
| ApoAI amyloidosis | Apolipoprotein AI N-terminal fragments (80-93) | Natively unfolded |
| Finnish hereditary amyloidosis | Mutant gelsolin fragment (71) | Natively unfolded |
| Icelandic hereditary cerebral amyloid angiopathy | Mutant of cystatin C (120) | α and β |
| Lysozyme amyloidosis | Mutants of lysozyme (130) | α and β |
| Fibrinogen amyloidosis | Fibrinogen A α fragment (27-81) | Unknown |
| ***Non-neuropathic localised diseases*** | | |
| Type II diabetes | Islet amyloid polypeptide fragment (37) | Natively unfolded |
| Atrial amyloidosis | Atrial natriuretic factor (28) | Natively unfolded |
| Medullary carcinoma of the thyroid | Calcitonin (32) | Natively unfolded |
| Pituitary prolactinoma | Prolactin (199) | All α |
| Injection-localised amyloidosis | Insulin chains A (21) and B (30) | All α |
| *$\alpha_1$–antitrypsin deficiency | $\alpha_1$–antitrypsin (374) | α and β |
| Hereditary cerebral haemorrhage with amyloidosis | Mutants of Aβ (40 or 42) | Natively unfolded |
| Aortic medial amyloidosis | Medin (50) | Unknown |
| Cataract | γ-Crystallins (variable) | All β |
| Corneal amyloidosis associated with trichiasis | Lactoferrin (692) | α and β |
| ***Neurodegenerative diseases*** | | |
| Alzheimer's Disease | Aβ (40 or 42) | Natively unfolded |
| Spongiform encephalopathies | Prion protein or fragment (253) | Natively unfolded (1-120) and α (121-230) |
| *Parkinson's disease | α-Synuclein (140) | Natively unfolded |
| *Dementia with Lewy bodies | α-Synuclein (140) | Natively unfolded |
| *Frontotemporal dementia with Parkinsonism | Tau (352-441) | Natively unfolded |
| *Huntington's disease | Huntingtin with polyQ expansion in exon 1 (3144) | Mostly natively unfolded HEAT repeat |
| *Spinocerebellar ataxias | Ataxins with polyQ expansion (816) | All β (562-694), rest unknown |
| *Spinocerebellar ataxia 17 | TATA box binding protein with polyQ expansion (339) | α and β (159-339), rest unknown |
| *Spinal and bulbar muscular atrophy | Androgen receptor with polyQ expansion (919) | All α (669-919), rest unknown |
| *Familial encephalopathy with neuroserpin inclusion bodies (FENIB) | Neuroserpin (397) | α and β |

| | | |
|---|---|---|
| *Hereditary dentatorubral-pallidoluysian atrophy | Atrophin-1 with polyQ expansion (1185) | Unknown |
| Familial British dementia | ABri (23) | Natively unfolded |
| Familial Danish dementia | ADan (23) | Natively unfolded |

**Table 1.1. Some diseases associated with either the extra- or intracellular deposition of misfolded protein (Belorgey et al., 2007; Chiti and Dobson, 2006; Pepys, 2006; Sipe and Cohen, 2000).** The number in brackets refers to the number of residues in the protein that forms and deposits as aggregates; these are often cleaved from larger precursor proteins. Diseases may be predominantly sporadic e.g. Alzheimer's disease, senile systemic amyloidosis, or hereditary e.g. Huntington's disease and lysozyme amyloidosis. In most cases there are examples of both (Chiti and Dobson, 2006).
* Intracellular misfolding diseases

The previous section discussed the pathways by which proteins may misfold into amyloid from an unfolded protein (figure 1.3). Table 1.1 lists the native state structures of the disease associated proteins and peptides, and, while some are natively unfolded (and many of which have no known function e.g. Aβ, the Alzheimer's associated peptide) there are others that do adopt a functional native state (Chiti and Dobson, 2006). The structures of these native, globular proteins are varied in their topology (all α, all β or a mix) (table 1.1), indicating that not only is there no obvious link between sequences that are able to misfold and cause disease but also that the native structure bears no influence either. The way in which the tertiary or quaternary structures of native proteins may be perturbed to expose regions that can assemble into amyloid is discussed later.

Table 1.1 separates misfolding diseases into three categories: systemic amyloidoses and localised amyloid diseases which are both non-neuropathic and do not affect the nervous system, and neurodegenerative diseases. In the systemic diseases, amyloid deposition can occur throughout the body (except the brain) and in some cases huge deposits (up to kilogram quantities) of amyloid can be seen in organs, which would clearly place a strain on the tissue involved (Dobson, 2003; Pepys, 2006; Tan and Pepys, 1994). Diseases may also be localised to a particular region, for example type II diabetes is associated with amyloid deposition in the pancreas. In these examples tissue disruption is caused by deposition of amyloid fibrils (Pepys, 2006). In the

neurodegenerative diseases however, misfolded proteins are believed to cause damage through a "toxic gain of function" rather than from disruption of tissue structure and function from deposition (Pepys et al., 2002). A detailed picture of how aggregation is toxic to cells in neurodegenerative diseases is still to be established but over recent years it has become generally accepted that it is not fibrils that are responsible for this category of diseases but smaller intermediates, termed "toxic oligomers", which have become the primary therapeutic target (Caughey and Lansbury, 2003; Hardy and Selkoe, 2002; Irvine et al., 2008; Walsh et al., 2002) (although other work has suggested that fibrils themselves can exhibit toxicity (Deshpande et al., 2006; Loo et al., 1993)). There are various permutations on the term "toxic oligomer" including spherical oligomers, micelles, amyloid derived diffusible ligands (ADDLs) and prefibrillar aggregates (Glabe and Kayed, 2006). They all refer to intermediates on the amyloid-folding pathway that can be observed by TEM or AFM to be soluble spherical species approximately 3-10 nm in width (Anguiano et al., 2002; Harper et al., 1997a; Lashuel et al., 2002). At later stages of aggregation more linear species are observed, called protofibrils, thought to be composed of associated oligomers (Harper et al., 1997b). These various intermediates have been observed for a range of proteins that eventually go on to form amyloid and, like their fibrillar counterparts that all have a cross-$\beta$ arrangement, share common structural characteristics, suggesting a possible common mechanism of toxicity (Glabe and Kayed, 2006; Kayed et al., 2003; Kayed et al., 2004). Evidence for toxicity of the early-stage species has come from various studies. For example, protofibrillar species of $\alpha$-synuclein have been implicated in membrane permeabilisation and toxicity (Volles et al., 2001). In another study, ADDLs and protofibrils formed by synthetic A$\beta$ disrupted neuronal cell cultures (Hartley et al., 1999; Lambert et al., 1998). Furthermore, these small species can cause neurological impairment in mice before the formation of amyloid fibres (Hsia et al., 1999). It has been proposed that amyloid oligomers may exert their toxic effects primarily by membrane permeabilisation, possibly by forming a pore in the membrane (the "channel hypothesis" (Kagan et al., 2004; Lashuel et al., 2002)), and toxicity has shown to be linked with an increase in intracellular calcium concentration (Mattson, 1994). Although it is not entirely agreed on how oligomers

perturb membranes it is accepted that this disruption triggers a cascade of downstream events that are responsible for pathogenesis such as calcium dyshomeostasis and production of reactive oxygen species, alteration to signalling pathways and mitochondrial dysfunction via direct mitochondrial membrane permeabilisation (Glabe, 2006). It has been postulated that the large deposits of amyloid seen in these neurodegenerative diseases act as reservoirs that are in equilibrium with smaller, toxic material but are themselves inactive (Hardy and Selkoe, 2002).

Although there may be a common mechanism of toxicity between some of the amyloid diseases and oligomeric species may be responsible for pathology, each disease has its own individual characteristics. To illustrate this, the most widely known amyloid associated disease, Alzheimer's disease, is discussed in more detail below.

### 1.3.1. Alzheimer's disease and Amyloid-β

Alzheimer's disease (AD) is increasingly prevalent among the world's population accounting for over 50% of the estimated 30 million cases of dementia worldwide (www.alzheimers.org.uk). Alois Alzheimer first identified AD in 1906 after post-mortem examination of brain tissue from a patient that had suffered from an unknown mental illness (Alzheimer, 1904). He noticed that the brain had an abnormal appearance (figure 1.4) and contained clumps of material which we now know to be amyloid plaques, along with bundles of tangled fibres (neurofibrillary tangles), composed of the protein tau (Alzheimer, 1904; Goedert et al., 2006).

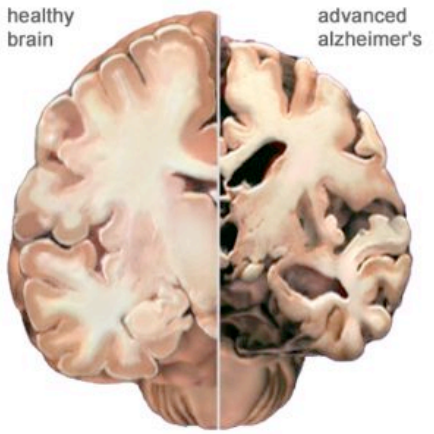


**Figure 1.4. Section through healthy (left) and Alzheimer (right) brains.** Reproduced from http://www.bio.davidson.edu/.

AD is a neurodegenerative disorder that results from neuronal dysfunction and death in parts of the brain that ultimately lead to dementia (Selkoe, 2000). It is generally accepted that the cause of AD is due to the accumulation of the peptide Aβ in the brain that arises from an imbalance between its production and clearance which triggers a cascade of events that ultimately lead, over many years, to the presentation of the disease (Selkoe, 2000). This is known as the "amyloid hypothesis of Alzheimer's disease" (or the Aβ hypothesis, to clarify that it could be any of the species formed by the peptide that cause the disease, and not just amyloid fibrils) and was proposed as a result of the mounting evidence showing a strong correlation between Aβ production and AD (Selkoe, 2000). Amyloid fibrils formed from Aβ are the primary component of brain plaques that are characteristic of AD (figure 1.4). As mentioned, fibrillary tangles composed of the protein tau are also seen in AD, however, it is believed that these form after and possibly as a consequence of Aβ processing from APP (for example, Aβ toxicity in mouse hippocampal neurons has been shown to be tau dependent) (Hardy et al., 1998; Lewis et al., 2001; Rapoport et al., 2002). In addition, the strongest genetic risk factor for developing both early and late onset AD is the ε4 allele of apolipoprotein E (APOE), thought to influence Aβ metabolism (Fagan et al., 2002; Kim et al., 2009). These examples along with a wealth of other evidence strongly suggest that Aβ is the causative agent of AD.

Aβ is universally encoded for by the β amyloid precursor protein (*APP*) gene (Hardy and Selkoe, 2002). This gene is located on chromosome 21; the observation that Downs syndrome, caused by a third copy of chromosome 21, leads to AD provided more evidence that Aβ is responsible for AD (Olson and Shaw, 1969; Selkoe, 2000). Further evidence comes from the identification of mutations in *APP* that serve to increase either the production of Aβ from APP or its inherent propensity to aggregate (Cai et al., 1993; Citron et al., 1992; Suzuki et al., 1994; Wisniewski et al., 1991). Certain mutations in the presenilin proteins PS1 and PS2, part of the γ-secretase complex that is responsible for the intramembrane cleavage of Aβ from APP, can also cause AD (Kimberly et al., 2003; Scheuner et al., 1996; Takasugi et al., 2003; Wolfe et al., 1999). The proteolytic processing of Aβ is shown in figure 1.5.

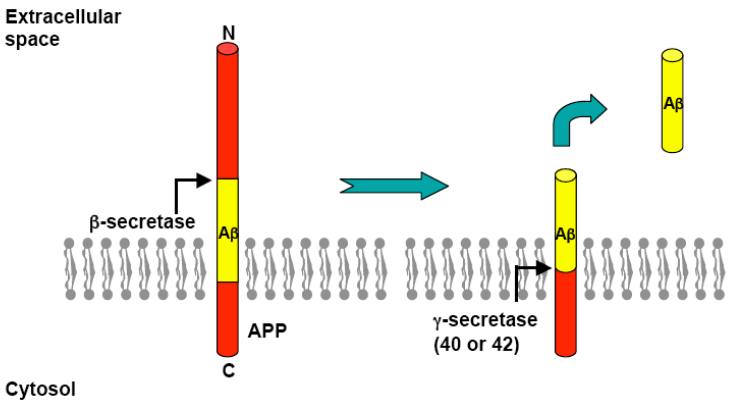


**Figure 1.5. Production of Aβ from APP.** α-, β- and γ-secretases cleave APP at certain sites; cleavage by β- and γ-secretases result in the production of Aβ. Many mutations that favour the production of Aβ are located around these cleavage sites or within the Aβ region of APP (Hardy and Selkoe, 2002).

Aβ is produced normally in all individuals when the transmembrane protein APP is cleaved at different sites by secretases to produce a 38, 40 or 42 residue proteolytic fragment, of which the 40 and 42 residue forms are associated with AD ($A\beta_{1\text{-}40}$ or $A\beta_{1\text{-}42}$ respectively) (Klein et al., 2001; Roher et al., 2000; Selkoe, 1994; Selkoe, 2001). In most individuals the production of $A\beta_{1\text{-}40}$ is much higher than $A\beta_{1\text{-}42}$; the latter has shown to be much more fibrillogenic (Jarrett et al., 1993b). Early-onset hereditary forms of the disease present due to specific mutations but most cases are sporadic with onset of symptoms correlating with increasing age (Chiti and Dobson, 2006). In

early-onset cases, the mutations appear to affect Aβ processing that leads to increased production of both $A\beta_{1-40}$ and $A\beta_{1-42}$, or a higher ratio of $A\beta_{1-42}$ to the shorter form (Walsh and Selkoe, 2007).

Although there are strong indications that Aβ is responsible for AD, concerns are still voiced over the hypothesis and not all clinical symptoms can be explained by it (Hardy and Selkoe, 2002). For example, the appearance and size of amyloid plaques deposited in the brain do not correlate well with severity of symptoms and in some cases amyloid plaques can be found in the post mortem brains of individuals with no AD symptoms at all (Hardy and Selkoe, 2002). However, the increasing evidence that points towards small soluble oligomeric species as the toxic conformer, and the better correlation between Aβ levels that are determined biochemically with dementia, make this lack of association less significant (Hardy and Selkoe, 2002).

A comprehensive understanding of the causes of AD is yet to be obtained and is essential for more accurate and early stage diagnoses and therapeutic intervention. Most treatments at present are palliative and only work to alleviate symptoms induced by destroyed neurons, although some newer treatments work on a different basis, such as regulating cholesterol metabolism or preserving the function of neuronal mitochondria (Tillement et al., 2010). However, despite gaps in the knowledge, the amyloid hypothesis has been used to develop drugs that specifically target Aβ pathways, primarily the removal or inhibition of oligomerisation. The relationship between over-production of Aβ and onset of AD suggests that higher concentrations promote assembly, so some strategies have been directed towards reducing monomer concentration by inhibiting γ-secretases (Siemers et al., 2006). Others focus on: up-regulation of enzymes that are able to degrade Aβ e.g. Cathepsin B (Mueller-Steiner et al., 2006), using small molecules to bind to and stabilise Aβ monomers (Gervais et al., 2007), inhibition of Aβ aggregation (McLaurin et al., 2006; Walsh et al., 2002) and the development of antibodies to bind to and prevent the toxic effects of Aβ oligomers (Dodart et al., 2002; Schenk et al., 2005). So far, several of these drugs have come to clinical trials but most have been discontinued due to various side effects.

## 1.4. Prions

Prions (proteinaceous infectious agents) are the cause of the fatal transmissible spongiform encephalopathies (TSE's), referred to in table 1.1, and their unusual ability to cause infection despite containing no genetic material, along with their link to amyloid, deserves them further explanation (Griffith, 1967; Prusiner, 1998). Prions have been identified in mammals, yeast and in the fungus *Podospora anserina* and are able to confer particular traits onto species, although unlike for mammals the alternative conformations in yeast and fungal prions are in general not harmful and are discussed in further detail in section 1.5 (Derkatch et al., 2001; Krammer et al., 2009; Uptain et al., 2001). These traits arise from the ability of certain proteins to undergo a change in conformation that leads to the formation of amyloid fibrils (figure 1.3) (Lipfert et al., 2005). Crucially however, unlike amyloid that forms in the diseases mentioned in the previous section, prions are able to cross species barriers and transmit their aberrant fold to other protein monomers (Lipfert et al., 2005). For example, variant Creutzfeldt-Jakob disease (vCJD) has developed in humans that have consumed BSE infected beef, and kuru, a disease which has now been wiped out due to intervention, was caused by inhabitants of Papua New Guinea eating the CJD infected brains of deceased relatives during ritual ceremonies (Derkatch et al., 2001; Gajdusek et al., 1966; Wadsworth et al., 2008). Most cases of CJD occur spontaneously and are not due to infection; however, there are genetic factors that can influence susceptibility to disease, whether it is acquired or sporadic (individuals with CJD are homozygous for either methionine or valine at position 129) (Collinge et al., 1991; Palmer et al., 1991; Wadsworth et al., 2008). Kuru was the first human prion disease discovered and in some cases the time since infection has shown to exceed 50 years, although the mean incubation period is 10-15 years (Collinge, 2001; Collinge et al., 2006). In both cases, the transmission of prions was responsible for pathogenesis although kuru prions have shown to be more similar to sporadic CJD prions than vCJD prions, suggesting that the disease originated from a person that had developed CJD spontaneously and also highlighting that differences do exist between the diseases (Wadsworth et al., 2008).

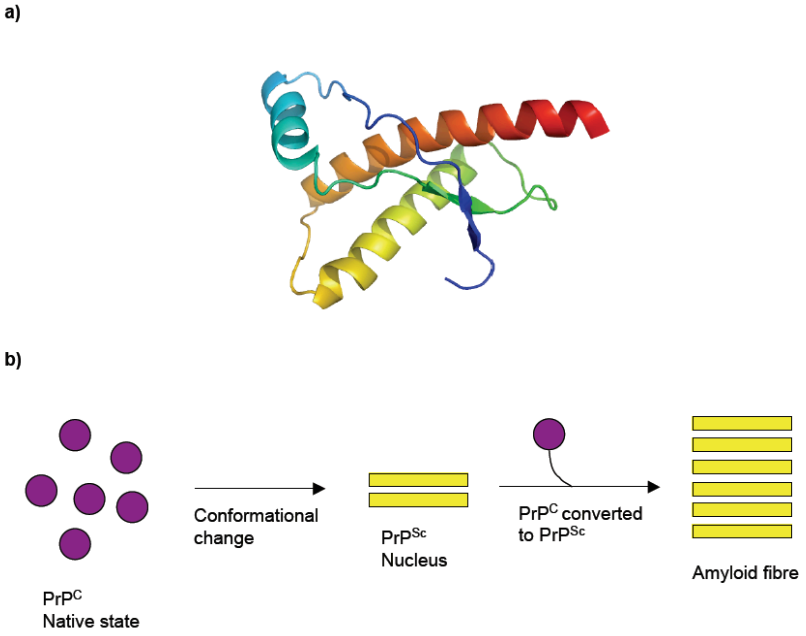


**Figure 1.6. a) Crystal structure of $PrP^C$. b) Schematic of the conversion of normally soluble, non-infectious $PrP^C$ to insoluble, infectious and aggregated $PrP^{Sc}$.** $PrP^C$ is converted to $PrP^{Sc}$ via a templated mechanism, this new conformation is able to aggregate into the amyloid fibrils that are associated with prion diseases. $PrP^{Sc}$ can act as an infectious agent and is able to cross species barriers.

$PrP^C$, the non-pathogenic form of human prion (the superscript C denotes "cellular") is present in all individuals, although its function has not been fully determined, and its crystal structure is shown in figure 1.6a. $PrP^{Sc}$ is the nomenclature given to the infectious form of $PrP^C$, the Sc superscript referring to "scrapie", the CJD equivalent in sheep (McGowan, 1922). The X-ray structure of $PrP^{Sc}$ is not known but it has a much higher β-sheet content than the cellular form as determined by FTIR (43% compared to 3%); these findings support the idea that a conformational transition is vital in prion propagation (Pan et al., 1993). Prion diseases have been identified in a wide range of animals and the prion protein shows great sequence homology across mammalian species (Collinge, 2001).

Why prions are able to cross species barriers but other forms of amyloid cannot is still not understood. Proposed mechanisms for methods of transmission are the heterodimer model (Cohen et al., 1994), the co-operative model (Eigen, 1996) and the model of seeded polymerisation (Harper and Lansbury, 1997). The mechanism by

which prions form is also unknown but it is thought to be a result of increased concentration of prion proteins that promotes either its spontaneous folding or raises the probability of collision of two molecules that induces conformational change (Derkatch et al., 2001; Wickner, 1994).

## 1.5. Non-pathogenic amyloid

In recent years a new role for amyloid has been uncovered. It has become clear that many organisms, including mammals, are able to use amyloid for beneficial purposes (Badtke et al., 2009). Some of the properties of amyloid that in some cases may contribute to pathogenicity, for example their strength and ability to avoid degradation by the normal cellular pathways, have been exploited for a variety of functions (Chiti and Dobson, 2006).

Curli protein fibres expressed by *E. coli* are involved in surface adhesion and, as they are essential for biofilm formation, aid the bacteria's ability for host colonisation (Hammar et al., 1996; Kikuchi et al., 2005). They have been classified as amyloid based on conclusions from electron microscopy (straight and unbranching fibres), resistance to protease digestion, birefringence under cross polarised light when stained with Congo Red dye, a shift in fluorescence of the dye Thioflavin T upon binding, and computer modelling studies which indicate a cross-β formation due to the sequence being rich in glutamine and asparagines (Barnhart and Chapman, 2006; Chapman et al., 2002). Curli is formed by the protein CsgA, the assembly of which depends on the membrane-bound protein CsgB that is thought to act as a nucleator for the polymerisation of CsgA (Hammer et al., 2007). The hydrophobins, proteins that are present on the surface of some filamentous fungi and bacteria also have amyloid characteristics (Gebbink et al., 2005). These proteins share very little sequence similarity but all form β-barrel structures held together by eight conserved cysteine residues (de Vocht et al., 2000). Their function is to aid in the formation of and attachment of hyphae to surfaces (Wosten, 2001). Hydrophobins are secreted and self-assemble at hydrophilic-hydrophobic interfaces to form an amphipathic monolayer that shares structural similarities to amyloid fibrils (Kwan et al., 2006; Sunde et al., 2008).

Yeast prions, unlike their mammalian counterparts, are able to confer non-pathogenic traits across cells (Chien et al., 2004; True et al., 2004; True and Lindquist, 2000).

Sup35 (eukaryotic peptide chain release factor GTP-binding subunit) is a protein in the yeast *Saccharomyces cerevisiae.* In its native state the role of Sup35 is to terminate translation in wild-type [psi] cells (Stansfield and Tuite, 1994). However, it has also been shown to behave in a prion-like manner conferring a specific phenotype to yeast, namely that [PSI+] cells have a higher rate of read-through of stop codons due to the aggregated state of Sup35 (Liebman and Sherman, 1979; Patino et al., 1996). The translation termination domain is fused to a so-called NM (referring to the N terminus and middle regions) domain (residues 1-253) (figure 1.7).

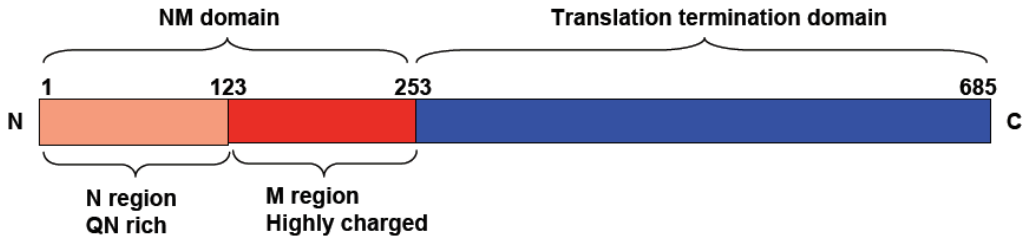


**Figure 1.7. Regions of the Sup35 protein.** The NM domain is split into the N (N-terminal, residues 1-123) and M (middle, residues 124-253) regions that are rich in Q, N, G and Y and charged residues respectively. The N region is responsible for fibre formation. The C terminal domain contains GTP-binding subunits and provides Sup 35 with its functional role (Xu et al., 2001).

The N region, or prion determining domain, (residues 1-123) is rich in asparagine and glutamine (and contains the sequence GNNQQNY which is able to form amyloid-like fibrils and crystals and has been used as a model system for many structural studies (Marshall et al., 2010; Nelson et al., 2005; Sawaya et al.; van der Wel et al., 2007) while the M region (residues 124-253) is highly charged (Chernoff, 2004; Glover et al., 1997; Krammer et al., 2008; Patino et al., 1996; Uptain et al., 2001). Interactions between these polar residues are believed to be responsible for the aggregation properties of Sup35 (Bousset et al., 2008). Two other yeast prions, Ure2 and Rnq1, are also Q and N rich; it is believed that these residues propagate the assembly of amyloid via polar zipper interactions (Bousset et al., 2008; Michelitsch and Weissman, 2000; Perutz, 1994; Tuite, 2000). Ure2 in its native form is a regulator of nitrogen metabolism; in its [URE3] prion form it loses this function and promotes uptake of nitrogen in poor

resources (Lian et al., 2006). Rnq1 forms the [PIN+] prion and is able to induce formation of [PSI+] and [URE3] prions (Sondheimer and Lindquist, 2000; Wickner et al., 2008) Structural studies using solid state NMR have shown that the aggregated amyloid forms of all three of these yeast prions have a parallel, in-register cross-β arrangement (Baxa et al., 2007; Shewmaker et al., 2006; Wickner et al., 2008). Another fungal prion, [Het-s], of *Podospora anserina*, forms HET-s amyloid fibrils that are infectious but does not have a Q/N rich region, instead a protease-resistant core has been identified as the possible prion domain (Maddelein et al., 2002).

Silk shares many characteristics with amyloid. The production of silk by spiders is a tightly controlled process where various soluble proteins only become aggregated after passing through the spinning duct (Rammensee et al., 2008). The mechanism by which this occurs is not fully understood which is not surprising given the different types of threads that are produced, each with different properties and designed for different functions (Vollrath, 2000). Some structural detail is known about synthetic dragline silk, which shows similar X-ray fibre diffraction patterns to that of amyloid suggesting a similar arrangement in at least part of the silk (Slotta et al., 2007).

Most examples of non-pathogenic amyloid, such as those described above, have been found in prokaryotes, however, more recently, functional amyloid has been found in mammals. Pmel17 is a transmembrane glycoprotein involved in the maturation of melanosomes, organelles that synthesise and store melanin pigments (Berson et al., 2003). An 80kDa cleaved fragment of Pmel17 is able to self-assemble into amyloid fibres that act as a template for the polymerisation of melanin (Berson et al., 2003; Fowler et al., 2006). There is a repeat region in this fragment that is essential for fibril formation and which can form fibres *in vitro* alone, although only when exposed to slightly acidic conditions like those in the melanosome lumen; at neutral pH the fibres become soluble (McGlinchey et al., 2009; Watt et al., 2009).

These cases not only demonstrate how the mechanical properties of amyloid can be taken advantage of to perform useful functions but also how nature has evolved to

carefully control the manufacture of these structures. Their production is often compartmentalised, as in the case of Pmel17 and spider silk which presumably hinders the possibility that they might reach other tissues and begin uncontrolled aggregation, like that seen in disease. Uncovering the differences between these amyloids and pathogenic forms may not only aid in understanding how diseases present but also in how they can be exploited for use in technical applications.

## 1.6. Amyloid in nanotechnology

The exploitation of amyloid by the natural world has prompted vision for its use in technology. To use amyloid as a biomaterial in industry, it is necessary to understand how peptides self assemble so that bottom-up design approaches can be used to manufacture "useful" amyloid. Furthermore it must be possible to exert control over these systems; the propensity many proteins and peptides have to self-assemble significantly impedes the ability to do this. However, the knowledge gained so far on the assembly, structure and function of disease-related and non-pathogenic amyloid has gone some way in enabling its use as a material. Self-assembling peptide systems such as amyloid are desirable for use in industry as they easily form defined structures, are of nanoscale dimensions, and are comparatively low in cost (Cherny and Gazit, 2008).

Some of the properties of amyloid (which have been taken advantage of by the species described above) that have inspired the possibility for using it as a biomaterial include its mechanical strength and stiffness. Using force spectroscopy techniques, the strength of insulin amyloid fibrils has shown to be comparable with that of spider silk which has mechanical properties similar to steel (Gosline et al., 1999; Smith et al., 2006). Other physical measurements including the shear modulus, thermal stability and Young's modulus also show amyloid to be strong materials that could make them suitable for use as nanomaterials (Ali et al., 2006; Knowles et al., 2007; Knowles et al., 2010).

A range of protein biomaterials has been created using a bottom up approach to their design based on first principles that include tissue scaffolds, hydrogels, nanotubes, biosensors and molecular motors (Banta et al., 2007; Woolfson and Ryadnov, 2006). Many examples focus on the ability of proteins to act as a support as they do in nature, such as in collagen and the microtubule network in cells. The efficacious assembly of structures like those found in life is a challenge for researchers but the establishment of some rules means progress can be made. Compared to the designed assembly of

fibrous constructs based on α-helical motifs, for example the self-assembling fibre (SAF) system that is based on two leucine zipper peptides (Woolfson and Ryadnov, 2006), the manufacture of β-sheet based materials is complicated by the lack of such defined principles. The observation that even short peptides form cross-β structures that are heterogeneous in their morphology compared to the uniformity displayed in the SAF system illustrates the lack of control in these β-based systems. It is thought that seeding mechanisms, which are very difficult to control or exclude completely from any system, are crucial in propagation of amyloid and these could be responsible at least in part for the disparity.

Despite this, the number of examples of β-structures used in biotechnology is ever increasing. One of the best examples is the production of peptide hydrogels, which have potential for use in drug delivery and tissue engineering (Lee and Mooney, 2001). In tissue engineering a new organ or tissue can be formed from a combination of the patients own cells and a polymer scaffold that is injected into the patients body. Synthetic polymers require an incision to be made in the body, whereas hydrogel polymers are injectable (Lee and Mooney, 2001). Hydrogels have historically been based on high molecular weight polymers but more recently the self-assembly of peptides has been used. In one example, a peptide was designed to form flat, non twisting fibrils by inserting a diproline peptide in between two β-sheet forming strands consisting of alternating valine and lysine residues (Schneider et al., 2002). Under basic conditions, when lysine residues have no charge, β-hairpins form that can self-assemble into β-sheet fibres: the hydrophobic valine face encourages lateral association and H-bonding occurs between β-hairpins in the axis direction (Schneider et al., 2002). However, when the pH is lowered below the $pK_a$ of lysine, the resulting charge causes the lysine residues to repulse, the hairpins unfold and a hydrogel forms (Schneider et al., 2002). pH has been used in other studies as a way of controlling hydrogelation (Aggeli et al., 2003; Rajagopal et al., 2009; Zhao et al., 2008) and similar investigations have used light (Haines et al., 2005) and temperature (Pochan et al., 2003) as mechanisms to control stimulation of hydrogelation. Interestingly, depending on whether a combination of D and L or L and L proline residues is used affects the

resulting structure; only the construct with the D isomer forms β-hairpins and hydrogels (Schneider et al., 2002). The sequence containing two L isomers of proline adopts an extended β-strand conformation and forms amyloid like fibres (Lamm et al., 2005). Work by another group used a similar system of two alternating charged/neutral amino acid sequences, determined as random coil by CD, to form a hydrogel when mixed together (Ramachandran et al., 2005). The hydrogel was able to recover from damage induced by shearing. As in the previous example, valine was used as the neutral amino acid due to its high propensity to form β-sheets and lysine and glutamate were used as the positive and negatively charged residues respectively (Ramachandran et al., 2005).

A hydrogel has also been formed from amyloidogenic sequences. The central hydrophobic segment comprising residues 16-20 (KLVFF) of Aβ has been shown to be critical in fibrillisation of the full-length peptide (although it is not firmly established to form fibrils as a fragment alone) (Chebaro et al., 2009; Gordon et al., 2001; Hilbich et al., 1992; Kallberg et al., 2001; Krysmann et al., 2008; Lu et al., 2009; Tjernberg et al., 1996). Krysmann *et. al*. reported that when the peptide is put into concentrated phosphate buffered saline (PBS) a hydrogel is formed; it is suggested this is due to screening of the electrostatic charges from the K residues by the buffer salts thus enabling β-sheets to aggregate into a gel (Krysmann et al., 2008) (although other studies have shown that screening of side chain charges requires very high (>1 M) salt concentrations (Dzubiella, 2009; Jelesarov et al., 1998; Lopez De La Paz et al., 2002)). It was possible to rebuild the gel after disruption by vortexing, indicating that any damage incurred during injection could be rectified once inside the body (Krysmann et al., 2008).

There is potential that amyloid fibres could be fuctionalised with, for example, enzymes by adding the units to the end of protein monomers and then allowing the monomers to assemble into fibrils (Baldwin et al., 2006). Several constructs of the yeast prion Ure2p were made that contained enzymes on the end of the native sequence. These constructs were then allowed to form amyloid filaments and the

activity of the enzymes was retained (Baxa et al., 2002). A similar approach was taken to produce amyloid fibrils with cytochrome b attached along the length of the fibrils that was able to bind haem and potentially act as a molecular wire through electron transfer (Baldwin et al., 2006). Amyloid based structures have also been used to construct nanowires for use in electronics. One of the first examples was peptide-based nanotubes that used D and L amino acids to form cyclic structures that associate on top of each other in a β-sheet fashion to form cylindrical structures (Ghadiri et al., 1993). In other work, gold nanoparticles were covalently attached to cysteine residues on the NM region of Sup35 and were bridged to form nanowires with a thickness of 80-200 nm (Scheibel et al., 2003). Furthermore, diphenylalanine formed nanotubes around 100 nm wide and several micrometres long that were shown by FTIR to have a β-sheet like conformation. They also stain with the dye Congo red, indicative of an amyloid like structure. Ionic silver was added to the nanotubes that was then reduced using sodium citrate. The peptide was then degraded with proteinase K to produce silver nanowires with a diameter of around 20 nm (Reches and Gazit, 2003). DNA can also be used as a scaffold for building nanowires (Aldaye et al., 2008). It is much easier to program the self- assembly of DNA than proteins but proteins have the advantage of increased stability (Scheibel et al., 2003). Furthermore, peptide based materials provide a range of binding sites so different substrates can bind at controlled positions illustrating the need for development in the use of protein fibres as biomaterials (Scheibel et al., 2003).

These examples illustrate how the self-assembly of β-structures, although harder to control than some other peptide based or molecular self-assembling systems, can be tuned to show responsiveness to particular conditions. Furthermore, by using short peptides to investigate self-assembly, design principles emerge that give clues as to how amyloid forms and how its characteristic properties are imparted onto it.

## 1.7. Model systems and sequence propensity for amyloid formation

Many proteins and peptides are able to form amyloid fibres, despite high sequence diversity, an ability that has been proposed as an inherent property of the polypeptide backbone (Dobson, 2001; Fandrich and Dobson, 2002). This proposition implies that, under the correct conditions, sequence has little influence but the widely varying rates of fibrillogenesis observed with different peptides, and the mutations in disease related proteins that increase propensity for fibril formation suggest that amino acid sequence, or at least features thereof, do play an important role. For example, human IAPP is extremely fibrillogenic, but rat IAPP, which differs in sequence at only six of the 37 residues, five of which are in the 20-29 region is not known to form amyloid (Cao et al., 2010). In addition, residues 20-29 region of human IAPP forms amyloid-like fibrils *in vitro*, whereas the same region of rat IAPP does not (Westermark et al., 1990). Attempting to identify motifs or regions of full-length disease related peptides or proteins that are responsible for or contribute to fibril formation is challenging, particularly for larger proteins, so often the proteins are analysed as a series of smaller fragments. These short sequences, or model systems, can provide information on which regions or motifs of larger proteins are necessary for self-assembly into amyloid. Furthermore, experiments have shown that short, model proteins can have cytotoxic effects making their study all the more relevant (Bucciantini et al., 2002; Ventura et al., 2004). A table of short peptides able to form amyloid is given in the appendix (i).

Some simple rules have been established that have aided the design of particular secondary structural elements. The formation of $\alpha$-helices is promoted by an HPPHPPP pattern of amino acid residues whereas $\beta$-sheets generally form from an HPHPHP sequence (MacPhee and Woolfson, 2004; Woolfson and Ryadnov, 2006). This alternating pattern generates a hydrophilic and hydrophobic face that encourages self-assembly whereby the hydrophobic sides interact. This is the basis of assembly of amyloid fibres. In addition, particular residues have greater propensity for forming $\beta$-sheets than do others and a number of studies have been carried out to try to assign numerical values to amino acids to describe how likely they are to be involved in a $\beta$-

strand (Chou and Fasman, 1974; Kim and Berg, 1993; Minor and Kim, 1994a; Minor and Kim, 1994b; Smith et al., 1994). The propensity to form β-sheet can be measured by substituting in each of the 20 amino acids at a particular position in a small protein of known structure and examining the effect. For example, this has been carried out on a small domain of bacterial IgG binding protein G (Smith et al., 1994) and a zinc finger peptide (Kim and Berg, 1993). The data from these studies do not perfectly correlate but overall trends are apparent, for example all three tables place tyrosine, threonine, isoleucine, phenylalanine, tryptophan and valine as being the residues most likely to be part of a β-sheet (Smith et al., 1994). Similarly, sequences that form amyloid often lack proline and glycine, which both have low scores, as these residues are β-sheet breakers (Rauscher et al., 2006). Incidentally, with the exception of threonine, these residues are hydrophobic and hydrophobicity is known to affect fibril formation. α-synuclein contains an central hydrophobic region known as the NAC domain that is required for fibrillisation of the peptide (Waxman et al., 2009). Certain deletions made to this region significantly impaired its ability to form fibrils, although others only reduced formation rate and did not abrogate assembly completely (Giasson et al., 2001; Waxman et al., 2009).

Aβ also contains hydrophobic regions believed to be important for its amyloid forming ability (Serpell, 2000). As mentioned in the previous section, the motif KLVFF in Aβ has shown to be important in assembly of the full-length peptide (Chebaro et al., 2009; Gordon et al., 2001; Kallberg et al., 2001; Lu et al., 2009; Tjernberg et al., 1996). However, there are discrepancies in whether the fragment is able to form fibrils alone *in vitro* with some groups reporting that it does (Gordon et al., 2002) and others that it cannot (Tjernberg et al., 2002). Tjernberg *et. al.* found that the shortest fibril forming fragment of Aβ was HQKLVFFAED (residues 14-23) (Tjernberg et al., 1999) and that another peptide KLVFFAE could form fibrils alone (Balbach et al., 2000). Kim *et. al.* performed a nonpolar scan across the hydrophobic region of $A\beta_{1\text{-}42}$ and showed that removal of only one hydrophobic residue does not diminish fibril forming propensity indicating that a hydrophobic region is required, not specific residues (Kim and Hecht, 2006). Regions identified as important in fibrillisation of Aβ have been suggested as

possible inhibitor binding sites and may be blocked by small peptides with identical sequences to that of the binding site – so-called "self recognition elements" (Ghanta et al., 1996; Hughes et al., 2000; Tjernberg et al., 2002). The observation that the speed of fibril growth can only be enhanced by seeding with fibrils formed from the same peptide and not by fibrils formed from similar sequences also suggests particular regions are important in aggregation (Jarrett and Lansbury, 1992). The amyloidogenic, hydrophobic C-terminal region of Aβ, residues 25-42, is homologous with the highly conserved residues 96-111 of PrP which has also been shown to form amyloid fibrils in isolation (Come et al., 1993; Stahl and Prusiner, 1991). Hydrophobicity and β-sheet forming propensity of amino acids are therefore closely linked to amyloid formation (Chiti et al., 2003).

As well as the stretches of proteins that have been shown to be crucial in fibrillisation, particular residues have been highlighted as playing a role. Phenylalanine features in many amyloidogenic sequences and in the cross-β core of amyloid fibrils, particularly as pairs, and is thought to drive amyloid assembly by aromatic π-π stacking (Gazit, 2002; Makin et al., 2005). For example, the FF motif is present in residues 16-20 of Aβ and is thought to play a significant role in amyloid formation (Tjernberg et al., 1996). Furthermore, phenylalanine is believed to play an essential role in IAPP fibrillogenesis (Azriel and Gazit, 2001). It is believed that the high frequency at which aromatic residues feature in amyloidogenic sequences points towards the importance of π-π stacking (Gazit, 2002). It has been shown that replacing phenylalanine residues in $A\beta_{1-42}$ slowed down assembly (Fraser et al., 1994). Aggregation of human muscle acylphosphatase was also decreased following aromatic to non-aromatic substitution (Bemporad et al., 2006). Single point mutations in a 14 residue fragment from acetylcholinesterase supported the importance of aromatic residues in amyloid formation and also highlighted the stabilising role of salt-bridges (Jean et al., 2008).

Charge-charge interactions between ionisable residues have also shown to be important in stabilisation of amyloid fibres (Caplan et al., 2002; Fraser et al., 1994; Lopez De La Paz et al., 2002; Makin et al., 2005; Ulijn and Smith, 2008; Zhang et al.,

1993; Zhang and Rich, 1997). However, the presence of charged side chains in a sequence of hydrophobic residues has been proposed as a hindrance to aggregation, acting as "structural gatekeepers" that maintain the integrity of the non-aggregated structure (Otzen et al., 2000; Otzen and Oliveberg, 1999; Rousseau et al., 2006). Furthermore, many diseases are accelerated by point mutations within proteins linked to diseases (table 1.2) which suggests that it is not only hydrophobic collapse that promotes fibrillogenesis (Lopez De La Paz et al., 2002). Examples of some of the mutations that can give rise to inherited disease states are given below.

| Protein/peptide | Mutation | Name of mutation |
|---|---|---|
| Aβ | E22Q | Dutch |
| Aβ | E22K | Italian |
| Aβ | E22G | Arctic |
| Aβ | D23N | Iowa |
| α-synuclein | A30P | n/a |
| α-synuclein | E46K | n/a |
| α-synuclein | A53T | n/a |

**Table 1.2. Some mutations affecting aggregation propensities of disease related natively unfolded proteins (Waxman et al., 2009).**

Methods for predicting sequences that are prone to form β-structures have been developed using data from *in vitro* experiments and computer simulations investigating the aggregation and structure of these short peptides. The development of algorithms is an ongoing process; some sequences that have been predicted to form β-strands actually occur in helical regions, termed "discordant helices", although it has been shown experimentally that these sequences can convert to β conformations more easily than those predicted to be α-helical (Broome and Hecht, 2000; Kallberg et al., 2001). Several algorithms are now available that aim to predict regions of proteins that are likely to form amyloid. The SALSA algorithm works by calculating average β-propensity scores of a peptide "window" and by moving this window along one residue at a time plots the score for each amino acid in the peptide (Zibaee et al., 2007). These measures of β-strand propensity are termed β-strand contiguity and have been plotted for α-synuclein, $A\beta_{1\text{-}40}$ and tau; the results were found to correlate well with experimentally determined amyloidogenic regions (Zibaee et al., 2007). The

algorithm PERLA (Lopez de la Paz et al., 2001) was used to search for and predict six residue amyloidogenic sequences which were verified experimentally (Lopez De La Paz et al., 2002). Assembly showed to be heavily influenced by the overall net charge on the peptide and only formed fibrils with an overall charge of +1 (Lopez De La Paz et al., 2002). This work and others (Aggeli et al., 2001; Jimenez et al., 1999; Kim and Hecht, 2006; Kim and Hecht, 2008; Zerovnik et al., 2007; Zhang et al., 1993; Zhang and Rich, 1997; Zurdo et al., 2001) highlights the crucial importance of solution conditions in *in vitro* experiments, such as pH and salt concentration. For example, lysozyme is able to form fibrils after various treatments, such as low pH or denaturation with GuHCl although the structural differences between the fibrils, if any, are unknown (Jahn et al., 2008). The peptide STVIIE was shown to be very amyloidogenic and a further examination of it, involving a full positional scanning of each residue, led to the development of a sequence pattern that could be used to detect other fibril-forming regions in proteins (Lopez de la Paz et al., 2001). The TANGO and Zyggregator algorithms also locate aggregation-prone sequences in peptides and denatured proteins (Fernandez-Escamilla et al., 2004; Pawar et al., 2005). Pawar *et. al.* used similar approaches to ascribe specific amyloid forming propensity to each amino acid and developed a method to predict sequences in $A\beta_{1-42}$, $\alpha$-synuclein and tau that are crucial for fibril formation (Pawar et al., 2005). These regions were verified experimentally and found to correlate well, for example $A\beta_{17-21}$ and $A\beta_{30-42}$ were predicted as being highly amyloidogenic, which correlates well with previous experimental data (Balbach et al., 2000; Pawar et al., 2005; Petkova et al., 2002; Tjernberg et al., 1999; Torok et al., 2002; Williams et al., 2004).

Much of this work focuses on the potential to design therapeutics or inhibitors for fibrillisation (Lopez De La Paz et al., 2002; Lynch et al., 2008; Pawar et al., 2005). If regions of disease forming peptides can be uncovered that are essential for fibril formation, then designing agents to bind to these regions would block assembly and thus prevent disease (Schenk, 2002).

## 1.8. Structural features of the cross-β amyloid core

Despite the lack of any obvious sequence similarity between precursor proteins and peptides, amyloid fibrils all share common structural characteristics and properties. Knowledge of the structure of amyloid fibrils observed by EM has progressed greatly since they were first generically described as "cross-β" (Eanes and Glenner, 1968). Cross-β refers to the perpendicular orientation of β-strands with respect to the fibre axis, which results in the characteristic fibre diffraction pattern seen for most amyloid fibrils with a meridional reflection at around 4.7 Å and an equatorial spacing at 10-11 Å (Fandrich and Dobson, 2002; Kirschner et al., 1987; Makin and Serpell, 2005a; Serpell et al., 2000a; Serpell and Smith, 2000; Sikorski et al., 2003). The advancement of technology and ability to form amyloid fibrils *in vitro* for analysis has revealed the intricate differences between fibrils and highlighted the structural features they share. A combination of high and low-resolution techniques has provided essential information on both the long and short-range order in amyloid.

### 1.8.1. Low-resolution macromolecular substructure of amyloid fibrils

Most of the low-resolution knowledge of amyloid structure has come from visual methods such as EM, cryo-EM and AFM. In addition, X-ray fibre diffraction can report on protofilament substructure (Serpell et al., 2007; Serpell et al., 2000b). Mature amyloid fibrils of the type seen in electron microscopy are generally around 60-120 Å in diameter, are straight, long and unbranching (Serpell et al., 2000b) and there is often a twist present (Goldsbury et al., 2000; Jimenez et al., 1999; Jimenez et al., 2002; Kajava et al., 2005; Petkova et al., 2006; Sachse et al., 2006; Sumner Makin and Serpell, 2004). Visible striations parallel to the length of the fibre and cross-sections of fibres reveal that smaller, laterally associated protofilaments comprise the underlying level of organisation (Cohen, 1982; Kirschner et al., 1987; Serpell et al., 2000b; Shirahama and Cohen, 1965). Protofilaments are distinct from proto*fibrils* mentioned in section 1.3, which describe the small species formed at the early stages of assembly (Harper et al., 1997b; Walsh et al., 1997). The number and width of protofilaments that make up the mature fibril varies depending on the precursor protein or peptide (table 1.3). A

schematic of the hierarchy of amyloid formation from monomeric peptide to mature fibril is shown in figure 1.8.

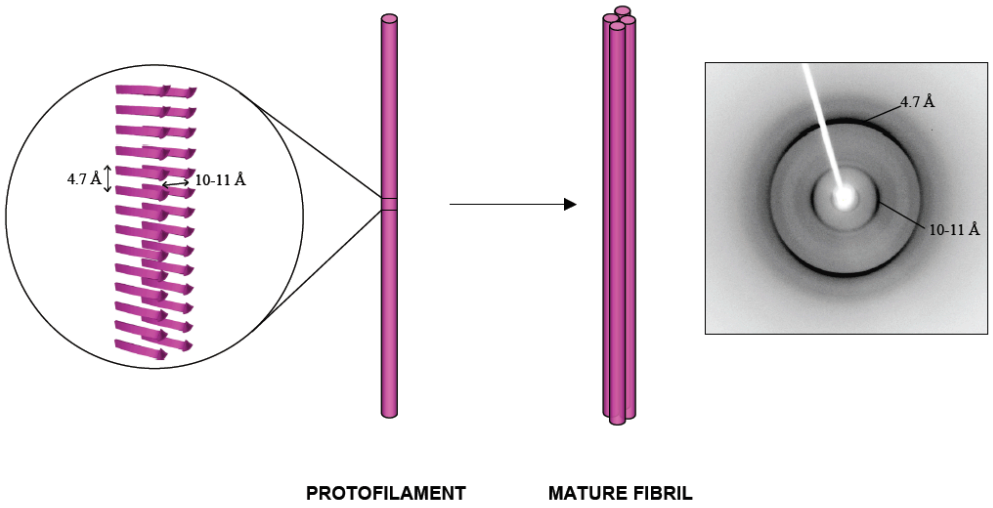


**Figure 1.8. Schematic of the assembly of amyloid-forming peptide monomers into mature fibrils.** Peptide monomers are arranged in a cross-β manner perpendicular to the fibre axis into a β-sheet. A pair of β-sheets constitute the protofilament. Protofilaments assemble laterally to become mature fibres. The width of each species varies but protofilaments are typically around 30-50 Å and ~4-6 assemble to form mature fibres around 60-120 Å in diameter (Serpell et al., 2000b).

| Protein | Technique | No. of protofilaments in mature fibril | Diameter of mature fibril (Å) | Diameter of each subunit (Å) | Reference |
|---|---|---|---|---|---|
| **Monoclonal Ig γ light chain** | EM | 4-6 | 90 | 30 | (Serpell et al., 2000b) |
| **L60R apolipoprotein A1** | EM | 5-6 | 100 | 32 | (Serpell et al., 2000b) |
| **Amyloid A protein** | EM | 5 | 100 | 30 | (Serpell et al., 2000b) |
| **D67H lysozyme** | EM | 5 | 95 | 30 | (Serpell et al., 2000b) |
| **TTR 10-19** | EM | 6 | 90 | 28 | (Serpell et al., 2000b) |
| **AL (immunoglobulin light chain)** | EM | 5 | 75-80 | 25-35 (formed from 10 Å sub-protofilaments) | (Shirahama et al., 1973) |
| **Aβ 6-25** | EM | 5-6 | 50-80 | 20-30 | (Fraser et al., 1991) |
| **Aβ 22-35** | EM | - | Helical, 120 at widest, 50-60 at narrowest | - | (Fraser et al., 1991) |
| **$A\beta_{1-38}$ $A\beta_{1-40}$** | EM | - | 70-90 | - | (Fraser et al., 1991) |
| **V30M TTR** | EM | 4 | 120 | 50-60 | (Serpell et al., 1995) |
| **SH3 domain** | Cryo-EM | 4 | 80 | 20 | (Jimenez et al.,1999) |
| **$A\beta_{1-42}$** | Cryo-EM | 1 | 130 | n/a | (Schmidt et al., 2009) |
| **$A\beta_{1-40}$** | Cryo-EM | 2 | 200 | 100 | (Meinhardt et al., 2009) |
| **$\beta_2$-microglobulin** | Cryo-EM | 6 | 180 | n/a | (White et al., 2009) |
| **PrP 91-231** | EM | 2 | 60 | 30-35 | (Tattum et al., 2006) |
| **Insulin** | Cryo-EM | 2,4 or 6 | 60-180 | 30 | (Jimenez et al., 2002) |

**Table 1.3. Reported numbers of protofilament subunits in mature fibrils formed from different proteins and peptides.** Adapted from Serpell, 2000.

Cryo-EM combined with single particle analysis has given particular insight into the macromolecular structure of amyloid. Analysis of fibrils formed by insulin and the SH3 domain of phosphatidylinositol-3'-kinase showed a variety of morphologies in the same sample, composed of different numbers of flat protofilaments (Jimenez et al.,

1999; Jimenez et al., 2002). Recent experiments on $\beta_2$-microglobulin have elucidated the structure of the fibril that shows a complex tetrameric arrangement of full-length proteins within the fibre (White et al., 2009). A combination of cryo-EM, magic angle spinning NMR and fibre diffraction on fibrils formed from residues 105-115 of transthyretin showed that the protofilaments were composed of four extended $\beta$-sheets and that the mature fibril is made up of four protofilaments (Jaroniec et al., 2004). Similar methods were used to determine that both straight and twisted mature $\alpha$-synuclein fibrils, formed from WT or residues 30-110 respectively, were both made up of two protofilaments (Vilar et al., 2008).

While many studies have shown that particular numbers of protofilaments make up mature fibrils, the emerging view of amyloid structure is that fibrils are polymorphic, where even within the same sample mature fibrils of different morphologies can be observed (Fandrich et al., 2009; Malinchik et al., 1998; Petkova et al., 2005). Polymorphism within amyloid may occur at any of three levels of organisation; the number of protofilaments that compose the mature fibril, the arrangement of the protofilaments, or the peptide packing within the protofilaments or other larger assemblies such as crystals (see section 1.8.2) and has been observed in fibrils formed from a number of different proteins and peptides (Fandrich et al., 2009). It is becoming increasingly evident that polymorphism in amyloid is common and has also been observed in *ex vivo* samples (Jimenez et al., 2001). It is believed that these different conformations are responsible for the different strains seen in prion diseases, where different fibril morphologies exhibit different physiological effects (Toyama et al., 2007; Wiltzius et al., 2008). A similar conformation dependent disease mechanism has been proposed for non-infectious amyloid (Telling et al., 1996). Two strains of amyloid formed from Sup35 have been characterised using a combination of H/D exchange, solution NMR and mutagenesis and revealed that one conformation contained a larger proportion of the sequence in the amyloid core than the other (Toyama et al., 2007). A variety of fibril morphologies have been observed including smooth, straight filaments, twisted fibres or ribbons, sheet-like structures, tubes and microcrystals (Jimenez et al., 2001; Reches and Gazit, 2003; Sachse et al., 2008; Wiltzius et al., 2008). The generation

of particular morphologies often depends on experimental conditions, for example fibrils of $A\beta_{1-40}$ that were grown with and without agitation showed to have different structures (Petkova et al., 2005). Flat ribbons with two fold symmetry have previously been observed for fibrils of agitated $A\beta_{1-40}$ (Petkova et al., 2006) and twisted fibrils with three-fold symmetry were produced by the same peptide that had been left quiescent (Paravastu et al., 2008). In both of these models it is the quaternary arrangement of the peptides within the fibrils that varies; the internal peptide contacts and arrangement of the $\beta$- sheets (parallel and in-register) is the same (Paravastu et al., 2008). Propagation of single morphologies has been achieved by adding parent seeds to solutions with particular macromolecular morphologies predominating in the daughter fibrils (Petkova et al., 2005). Importantly, these different morphologies observed using low-resolution methods were shown to have underlying polymorphism at an atomic level and, critically, exhibited varying cytotoxicity (Petkova et al., 2005).

### 1.8.2. High-resolution structural detail of amyloid protofilaments

Until recently, the high-resolution structural determination of amyloid fibres has been prohibited due to their insolubility and heterogeneity. For most globular proteins, X-ray crystallography is the preferred method for looking at structure in atomic detail. However, because of its fibrillar nature, most attempts at crystallising amyloid have been unsuccessful. Furthermore, recent evidence suggests that single crystal diffraction may not be the most appropriate method for the structural determination of amyloid as fibres and crystals formed from the same peptide were shown to vary in their structures (Marshall et al., 2010; van der Wel et al., 2007). For these reasons, the high-resolution structural characterisation of amyloid and assignment of side chain conformations has come mostly from other methods, in particular solid state NMR and EPR, although the Eisenberg group have reported over thirty crystal structures of nineteen short amyloid forming peptides, some in two crystal forms (see table 1.4 and appendix (ii)) (Nelson et al., 2005; Sawaya et al., 2007). The crystals were mostly grown by the hanging drop method and others grew in batch from lyophilised peptide dissolved in water or buffer (Nelson et al., 2005; Sawaya et al., 2007). However, no peptide longer than seven residues has been crystallised, suggesting that peptide

length is a limitation to growing crystals of amyloid-forming peptides. Nevertheless, the crystal structures corroborate the cross-β arrangement. The first peptide to be crystallised and its structure determined was the Sup35 fragment GNNQQNY, further details on which are given in section 4.1 (Nelson et al., 2005). The structure showed the peptides arranged parallel to one another in a β-sheet with the sheets anti-parallel (Nelson et al., 2005). The peptide side chains were modelled as being closely interlocked in an anhydrous "steric zipper", thought to account for the strength of amyloid, with a wet interface between pairs of sheets (Nelson et al., 2005). This arrangement of residues featured in all of the crystal structures in a later publication, which were defined according to one of eight classes that depend upon the organisation of peptides within the crystals, although no examples have yet been discovered for three of the classes (Sawaya et al., 2007). Crystal structures have been used to model structures of full-length peptides (Ivanova et al., 2009; Wiltzius et al., 2008). NNFGAIL and SSTNVG from IAPP were both crystallised, with only one peptide (SSTNVG) showing a steric zipper arrangement leading to the conclusion that this sequence features in the core of amyloid fibrils formed from full-length IAPP (Wiltzius et al., 2008). An alternative model of IAPP was similar overall but featured differences in side chain packing (Luca et al., 2007) and yet another structure differed from both of these, featuring NFGAILS as part of a β-strand instead of part of the turn motif (Nielsen et al., 2009). IAPP has also been modelled as a superpleated β structure with three β-strands forming a S shape 'serpentine' fold and stacked parallel and in-register, similar to Ure2p fibrils (Kajava et al., 2005; Kajava et al., 2004). Most data suggests that the most common arrangement for amyloid is parallel and in-register β-strands (table 1.4) (Margittai and Langen, 2008).

| Peptide | Arrangement | Method | Reference |
|---|---|---|---|
| $A\beta_{10-35}$ | Parallel, in-register | ssNMR | (Benzinger et al., 1998) |
| $A\beta_{10-35}$ | Antiparallel | FTIR | (Fraser et al., 1994) |
| $A\beta_{10-35}$ | Parallel, in-register | ssNMR | (Antzutkin et al., 2002) |
| $A\beta_{1-40}$ | Parallel, in-register | ssNMR | (Antzutkin et al., 2000) |
| $A\beta_{34-42}$ | Antiparallel | ssNMR | (Lansbury et al., 1995) |
| $A\beta_{16-22}$ | Antiparallel | ssNMR | (Balbach et al., 2000) |
| $A\beta_{1-42}$ | Parallel, in-register | ssNMR | (Antzutkin et al., 2002) |
| Various short peptides | Various | X-ray crystallography | (Nelson et al., 2005; Sawaya et al., 2007) |
| IAPP | Parallel, in-register | EPR | (Jayasinghe and Langen, 2004) |
| $\alpha$-synuclein | Parallel, in-register | EPR | (Der-Sarkissian et al., 2003) |
| PrP | Parallel, in-register | EPR | (Cobb et al., 2007) |
| $A\beta_{34-42}$ | Antiparallel | ssNMR | (Lansbury et al., 1995) |
| HETs prion domain (218-289) | $\beta$-solenoid | ssNMR and H/D exchange | (Ritter et al., 2005) |
| $A\beta_{10-35}$ | Parallel, in-register | ssNMR, EM, SANS | (Benzinger et al., 2000) |
| Rnq1 [PIN+] | Parallel, in-register | ssNMR | (Wickner et al., 2008) |
| Sup35NM | Parallel, in-register | ssNMR | (Shewmaker et al., 2006) |
| Ure2 prion domain (1-89) | Parallel, in-register | ssNMR | (Baxa et al., 2002) |
| IAPP | Parallel, in-register | ssNMR | (Luca et al., 2007) |
| KFFEAAAKKFFE | Antiparallel | XRFD | (Makin et al., 2005) |
| $TTR_{105-115}$ | Extended $\beta$-sheet | ssNMR | (Jaroniec et al., 2004) |

**Table 1.4. Structures of amyloid determined by different methods.**

Solid state NMR has provided a wealth of information on the structure of amyloid fibrils and brought attention to the molecular level polymorphisms that exist within fibres formed from the same peptide (Antzutkin et al., 2000; Antzutkin et al., 2002; Balbach et al., 2000; Balbach et al., 2002; Benzinger et al., 1998; Gregory et al., 1998; Griffiths et al., 1995; Ishii et al., 2001; Lansbury et al., 1995; Luhrs et al., 2005; Madine et al., 2009; Paravastu et al., 2009; Petkova et al., 2005). Most results also support a cross-$\beta$ model. Two models have been reported for microcrystals formed from residues 42-49 of medin that both feature parallel, in-register strands (Madine et al., 2009). An anti-parallel arrangement was observed for residues 20-29 of IAPP, although another group found that the same fragment formed both anti-parallel and parallel structures, again highlighting molecular level polymorphisms (Madine et al., 2008; Nielsen et al., 2009). ssNMR studies on the Iowa mutant of A$\beta$ (D23N) also revealed

fibrils with both parallel and anti-parallel β-strands, although the antiparallel form was more abundant (Tycko et al., 2009). Examination of the K3 fragment of $\beta_2$-microglobulin showed that the peptide as it exists within fibrils was similar to the native crystal structure i.e. β-strand-loop-β-strand, except that phenylalanine 22 and serine 28 are flipped from the outside to a location on the interior of the fibril which was presumed to optimise inter- rather than intra-molecular packing (Iwata et al., 2006). Work by the Tycko group and others has focused on the molecular structure of Aβ fibrils using ssNMR. A model of amyloid fibrils from residues 10-35 of Aβ consistent with data from ssNMR, EM and small angle neutron scattering features parallel β-strands that are off-set slightly to produce a twist observable by EM (Benzinger et al., 2000). Full-length $A\beta_{1-40}$ forms a β-bend with the two β-strands stacking up to form parallel β-sheets (figure 1.9) and a similar model has been proposed for the WW domain of CA150, a protein associated with Huntington's Disease (Ferguson et al., 2006). However, later work suggested that in fact $A\beta_{1-40}$ forms a variety of morphologies with differing molecular structures (Petkova et al., 2002; Petkova et al., 2005). There are significant structural differences between this and the model for $A\beta_{1-42}$ (figure 1.9) (Luhrs et al., 2005). While both form parallel β-hairpins, in $A\beta_{1-42}$ the interaction between the β-strand on one β-hairpin is with the β-strand on the next molecule, whereas in $A\beta_{1-40}$ the β-strands interact within the same molecule (Luhrs et al., 2005; Petkova et al., 2002). Electroparamagnetic resonance (EPR) and site directed spin labelling has also provided atomic level structural detail on fibrils formed by $A\beta_{1-40}$ and $A\beta_{1-42}$ (both in-register and parallel) (Torok et al., 2002) and α-synuclein (which showed the core as consisting of residues 36-98) (Chen et al., 2007; Der-Sarkissian et al., 2003). X-ray fibre diffraction and electron diffraction produced a high-resolution model for the amyloid-forming designed peptide KFFEAAAKKFFE (see section 6.1) (Makin et al., 2005). Some of the structures mentioned here are shown in figure 1.9 with details of specific interactions in table 1.5.

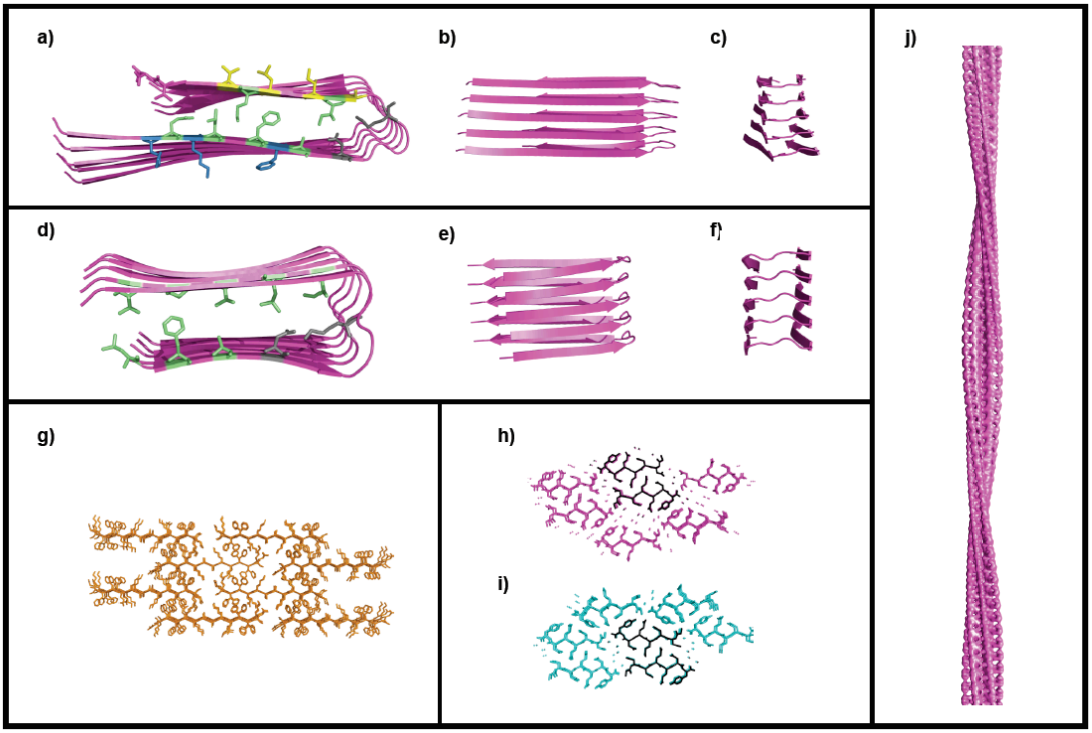


**Figure 1.9. Structural models for amyloid fibrils.** a) view down the fibre axis, b) side on to the fibre axis and c) at the end of the axis of $A\beta_{1\text{-}40}$ (Petkova et al., 2002). Residues that interact in the hydrophobic core are coloured green, yellow residues form the hydrophobic face, side chains on the opposite face are in blue and D23 and K28 which are thought to form a salt bridge are coloured in grey. d) down, e) side and f) end views of $A\beta_{1\text{-}42}$ (Luhrs et al., 2005). The structure differs to $A\beta_{1\text{-}40}$ in that the interactions are inter- rather than intramolecular. g) model of the structure of the designed peptide KFFEAAAKKFFE (Makin et al., 2005). h) and i) two crystal forms of the peptide GNNQQNY (Nelson et al., 2005; Sawaya et al., 2007). j) the macromolecular structure of $\beta_2$-microglobulin fibrils from cryo-EM (Jimenez et al., 2002; White et al., 2009).

| Peptide | Technique | Key features | Side chain contacts | Reference |
|---|---|---|---|---|
| $A\beta_{1-40}$ (a-c) (Structure provided by Dr. R. Tycko, personal communication) | Solid State NMR | Parallel, in register<br>Residues 1-10 disordered<br>Residues 12-24 β strand 1<br>Residues 25-29 β turn<br>Residues 30-40 β strand 2 | Residues Q15, L17, F19, A21, I31, M35, V39 in the same molecule interdigitate. A30, I32, L34, V36 and V40 form a hydrophobic face. Residues H14, K16, F20 are on the opposite face. D23 and K28 form a salt bridge. | (Petkova et al., 2002) |
| $A\beta_{1-42}$ (d-f) (pdb code: 2BEG) | HD exchange NMR Mutagenesis | Parallel, in register<br>Residues 1-17 disordered<br>Residues 18-26 β strand 1<br>Residues 27-20 β turn<br>Residues 31-42 β strand 2 | Residues L17, F19 and A21 of β strand 1 on the nth molecule interdigitate with I32, L34, V36, G38 and V40 in β strand 2 in the (n-1)th molecule. D23 and K28 form a salt bridge. | (Luhrs et al., 2005) |
| KFFEAAAKKFFE (g) (designed peptide) (pdb code 2BFI | X-ray fibre diffraction Electron diffraction | Antiparallel sheets | π-π stacking (Phe)<br>Salt bridges (E and K) | (Makin et al., 2005) |
| GNNQQNY from the yeast prion Sup35 (h and i) (pdb code: form 1 1YJP, form 2 2OMM) | X-ray crystallography | Parallel, in register<br>Class 1 steric zipper; pair of β-sheets with a dry interface | N2, Q4, N6 interdigitate in the dry interface<br>Amide stacks (Asn)<br>Tyrosine stacks | (Nelson et al., 2005; Sawaya et al., 2007) |
| Insulin (j) | Cryo-EM | Long-range interactions between protofilaments, helical twisting | N/A | (Jimenez et al., 2002) |

**Table 1.5. Methods used to determine the structures shown in figure 1.9 with detail of key structural features.**

### 1.8.3. Alternative models for amyloid structure

The most widely accepted generic model for amyloid structure is the cross-β arrangement discussed in the previous sections. However, several other models have been suggested for amyloid. β-helix type structures, which includes β-solenoids and nanotubes, have been proposed as an alternative model. The "water-filled nanotube" was originally suggested by Perutz from data collected from fibrils formed by the polyglutamine peptide $D_2Q_{15}K_2$ (Perutz et al., 2002). Fibre diffraction data from these fibrils did not give the classical 10-11 Å equatorial reflection and therefore was assessed as being inconsistent with a cross-β structure (Perutz et al., 2002; Jahn et al., 2010). Subsequent analysis of the data revealed a strong 8.3 Å equatorial reflection

which although lower than the usual position could be fitted to a model in which the glutamine side chains packed very close together (Sikorski and Atkins, 2005). Furthermore, the texture of the sample used to collect diffraction data had a remarkable effect on the patterns observed (Jahn et al., 2010). Calculation of fibre diffraction patterns from the nanotubes model do not compare well with experimental diffraction patterns, suggesting that this structure may not be correct (Jahn et al., 2010). The structure of Het-s fibrils has been described as a β-solenoid, indicating that it shares a similar helical structure to the nanotubes, however inspection of the structure reveals that it is more likely consistent with a cross-β arrangement (Ritter et al., 2005; Wasmer et al., 2008; Jahn et al., 2010). Insulin fibrils have been suggested as having a similar β-roll structure (Choi et al., 2009).

Stacking of native structures, particularly in the case of larger precursor proteins that would require significant unfolding, has also been suggested as a possible underlying fibril conformation (Colon and Kelly, 1992). $\beta_2$-microglobulin is believed to retain some native-like structure in amyloid fibrils (Eakin et al., 2004). However, the recent structure of amyloid fibres formed from $\beta_2$-microglobulin determined by cryo-EM was inconsistent with this report of stacked native structures, or of fibrils that featured a cross-β arrangement of peptides (Ivanova et al., 2004; Ivanova et al., 2006; Iwata et al., 2006) or domain swapped dimers (Benyamini et al., 2003; Calabrese et al., 2008) and suggested that a non-native but globular dimer-of-dimers formed the protofilament subunit (White et al., 2009).

Most structural knowledge obtained so far on amyloid has come from mature fibrils. The heterogeneity of prefibrillar species and their transient nature makes them much less amenable to structural characterisation. Although characterising the structure of mature fibrils can give insights into possible arrangements of these smaller species there is potential that they may take on some other conformation, so more recently work has focused on the structural determination of early intermediates. The structure of the $A\beta_{1\text{-}40}$ oligomer was presented as a spherical intermediate that contained parallel β-sheet structure and was shown to be more toxic than fibrils that formed at

later time points (Chimon et al., 2007). Dimerisation of Aβ monomers followed by monomer addition has also been shown to be a key step in the formation of oligomers (Ono et al., 2009). The exact structural nature of the toxic species is still to be determined however, and it may be that oligomers, like other assemblies in the amyloid hierarchy, are polymorphic.

## 1.9. Mechanisms of amyloid assembly

The ability of some proteins with very different sequences to misfold into fibres with similar structures makes the mechanism of assembly of amyloid all the more intriguing. Precisely how normally soluble proteins form insoluble amyloid fibrils is not fully understood at present and the process by which this occurs will inevitably be far more complicated in a cellular environment. However, *in vitro* experiments can provide insight. It is believed that unfolded monomers first form partially folded intermediates that assemble into small prefibrillar species (protofilaments) around 5-10 nm in width and then lengthen into protofibrils and finally mature amyloid fibres (figure 1.8), as has been shown for $\alpha$-synuclein (Conway et al., 2000; Uversky et al., 2001). Kinetics of assembly are in turn governed by the properties of the partially unfolded state which forms at the start of the process, for example charge (Krebs et al., 2008). Proteins that are folded in their native state are likely to require a degree of unfolding first, unless native structures are stacked (Guijarro et al., 1998; Litvinovich et al., 1998). The extent to which unfolding is required will vary, for example experiments on TTR showed that it was not necessary to fully denature the protein in order for fibrils to form and that many of the proteins' secondary (and some tertiary) structural features were retained in the fibril (Colon and Kelly, 1992). $\beta_2$-microglobulin forms different fibrils depending on preparation conditions; at pH 2 the native protein is partially denatured and at neutral pH native-structure is retained (McParland et al., 2000; Platt et al., 2009). A detailed representation of amyloid assembly is shown in figure 1.10.

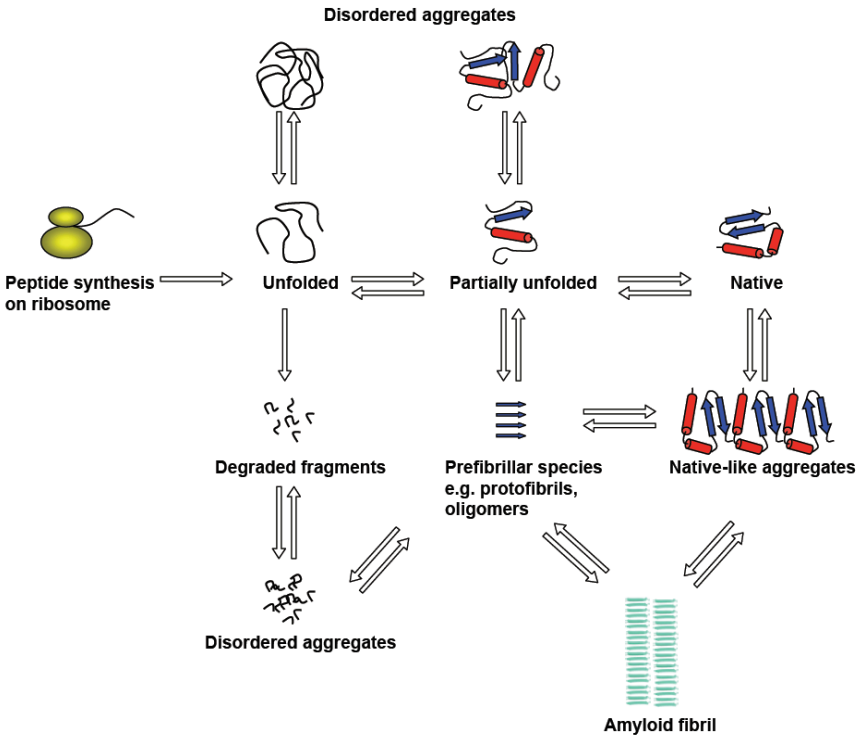


**Figure 1.10. Possible pathways of assembly of amyloid. Adapted from Chiti, 2006 and Hartl, 2009.**

The assembly of amyloid fibres can be followed using the dye Thioflavin T, or by monitoring turbidity, and often shows a sigmoidal growth curve that consists of a lag phase, followed by a period of rapid growth and ending with a plateau indicating that fibril formation has fully proceeded (for further information see 2.4.3) (Naiki and Nakakuki, 1996). The lag phase can be shortened or even eliminated by adding preformed seeds, which are able to convert soluble protein into amyloid in a similar mechanism to the templating observed for prion proteins (Tanaka et al., 2006). Fragmentation of amyloid fibres can create seeds that leads to the faster proliferation of fibres and has also been shown to increase cytotoxic potential, adding to evidence that fibres may act as a reservoir for toxic species (Ban et al., 2006; Xue et al., 2009a). Visual methods such as EM and AFM can also be used to follow assembly, while spectroscopic methods like CD, LD, Raman and FTIR and various fluorescence methods can be used to probe changes in secondary structure, in particular the transition from natively unfolded or $\alpha$-helical monomer to $\beta$-sheet rich fibres and the structural environments of particular residues respectively (Adachi et al., 2007; Andersen et al.,

2010; Ban et al., 2006; Bulheller and Hirst, 2009; Jean et al., 2008; Lee et al., 2007; Marshall et al., 2010; Martel et al., 2008; Padrick and Miranker, 2001). Solution NMR and H/D exchange can be used to gain information on the early stage dynamic interactions between and within monomers and the structure of the resulting soluble species (Hoshino et al., 2002; Jahn et al., 2006; Olofsson et al., 2006).

The first phase in amyloid formation is thought to be the assembly of oligomeric structures. This may be through non-specific association of monomers or a more specific mechanism, such as domain swapping (Nagarkar et al., 2008; Nelson and Eisenberg, 2006). Domain swapping occurs when a molecule undergoes a conformational rearrangement so that one of its domains is "swapped" with the same domain of an identical but separate molecule to restore the original structure and has been observed in amyloid forming proteins such as cystatins (Staniforth et al., 2001), T7 endonuclease I (Guo and Eisenberg, 2006) and prion protein (Knaus et al., 2001). The pathways by which fibres and oligomers form is unclear and it has not been ascertained if oligomers are intermediates in fibril formation, or whether they form in a separate pathway (Collins et al., 2004). Oligomers formed during Sup35 amyloid formation have been observed localised to fibre ends, indicating that oligomer formation is a step on the pathway to fibril elongation (Serio et al., 2000). Similarly, oligomer rather than monomer addition was suggested as the primary mechanism for insulin fibril elongation (Vestergaard et al., 2007). A three stage assembly process has been proposed by Nelson *et. al.* which involves firstly monomer assembly into β-sheets, followed by formation of a nucleus and finally the interaction of pairs-of-sheets to form elongated fibrils (see section 4.1 for further detail) (Nelson et al., 2005). An alternative model of amyloid growth that features fragmentation as a step has been suggested for the yeast prion protein Sup35. It was shown using single molecule fluorescence experiments that monomers, and not oligomeric intermediates, add to fibre ends suggesting that oligomers form separately to fibres (Collins et al., 2004). The growth of fibrils formed by a mutant of $A\beta_{1\text{-}40}$ (F19P) has been followed using surface plasmon resonance and shown to elongate by monomer addition in a reaction that is initially reversible but over time becomes more stable (Cannon et al., 2004).

Fibrillogenesis has been characterised using a model termed phase mediated fibrillogenesis, where the fibril lengthening is split into a concentration independent lag phase and a concentration dependent growth phase (Padrick and Miranker, 2002). These examples make it clear that no single mechanism for amyloid (or oligomer) formation has been agreed upon and most likely infer that there are many different pathways by which amyloid can form.

Amyloid fibres are stabilised by a number of interactions. It is believed that mature fibrils may associate via hydrophobic interactions between exposed residues on the opposite side to the amyloid core, and that this non-specific interaction may be partly responsible for the polymorphisms seen (Iwata et al., 2006; Petkova et al., 2006). Stabilisation within the protofilament at a molecular level is also achieved by side-chain interactions which may be intra- or inter-molecular, for example aromatic interactions and $\pi$-$\pi$ stacking (Fandrich and Dobson, 2002; Gazit, 2002; Iwata et al., 2006; Makin et al., 2005) or salt bridges between oppositely charged residues (Makin et al., 2005; Petkova et al., 2005). Asparagine ladders, where aligned polar N residues are hydrogen-bonded in the fibre axis direction have also been highlighted as a stabilising interaction that overcome the energetic disadvantage of the residue being in a hydrophobic environment i.e. within the fibril core (Iwata et al., 2006; Kajava et al., 2005; Nelson et al., 2005). A similar arrangement has been observed for glutamine side chains (Sikorski and Atkins, 2005).

## 1.10. Summary

The reasons, therefore, for carrying out investigations on amyloid are multiplicitous; to understand the molecular basis of the diseases with which amyloid is linked and develop therapeutics to treat them, to gain knowledge about how proteins go from a disordered polypeptide chain to ordered, stable and not necessarily unique structures, to fathom why some organisms, even mammalian, use amyloid in a beneficial way and to be able to learn from nature and exploit it as a material for industrial use. Underlying all of these problems is a simple question: How do very different protein sequences form very similar structures? The propensity so many proteins and peptides have to form amyloid suggests there may be a common mechanism for amyloid formation and possible rules to uncover that can be used as predictive tools. If the properties of amyloid, whether good or bad, are to be understood it is fundamental that these structures are known in detail. By using short peptides as model systems some of the elusive “rules” that govern amyloid formation may be uncovered which are essential for both bottom-up design strategies and therapeutic intervention.

# 2. INTRODUCTION PART II: Methods to characterise amyloid

## 2.1. Introduction

Knowledge of the structure of amyloid is essential if progress is to be made in understanding how misfolding events are initiated and how assembly proceeds. Accumulating evidence suggests that in some pathologies, particularly the neurodegenerative amyloid-associated diseases, oligomeric species are responsible for toxicity (Hardy and Selkoe, 2002) but their transient nature makes their structural elucidation problematic. For this reason most structural work has been carried out on amyloid fibrils that are presumed to share similar structural features with early-stage species. Proteins and peptides that are involved in amyloid-associated diseases range in amino acid length and there may be large segments that do not contribute to the amyloid core and which appear to play no role in the formation of amyloid fibrils. Techniques such as H/D (hydrogen-deuterium) exchange and limited proteolysis, as well as bioinformatics tools such as prediction algorithms have identified sequences that are involved in the cross-β core of fibrils (Hoshino et al., 2002; Trovato et al., 2007; Williams et al., 2004; Zhang et al., 2009; Zibaee et al., 2007). These shorter sequences often have the ability to form amyloid fibrils alone, with similar properties and characteristics to their full-length counterparts. They are often preferable for use in biophysical studies as they form more ordered structures, thought to be representative of the cross-β core of the full-length proteins to which they relate. Another benefit of using short peptide sequences is the ability to relate sequence to structure and function by mutating one residue at a time and due to the simplicity of the systems, to understand how each amino acid contributes to amyloid formation and structure.

A wide range of biophysical techniques have been used to attempt to elucidate the structure and assembly mechanisms of amyloid. In the majority of cases the use of X-ray crystallography and solution NMR has been precluded due to the insoluble and

heterogeneous nature of amyloid fibres, although there have been several short amyloid-forming sequences that have been crystallised by the Eisenberg group for which crystal structures have been published (Nelson et al., 2005; Sawaya et al., 2007). It is mainly for this reason that structural information has had to come from other techniques. Also, whether the crystal structure represents the fibril structure remains controversial (see chapter 4) (Marshall et al., 2010; van der Wel et al., 2007). Furthermore, other techniques can give information on fibrillisation and the structural changes that may occur on the pathway from monomer to fibre, which are not obtainable by X-ray crystallography. It is this collective information that will provide a more global view of amyloid structure and formation and aid in understanding of the molecular basis of amyloid diseases. The biophysical techniques used to study the peptides presented here are detailed below.

## 2.2. Circular Dichroism

### 2.2.1. Theory and Instrumentation

Circular Dichroism (CD) is the differential absorption of left and right circularly polarised light by an optically active molecule (Fasman, 1996). Due to the chiral nature of amino acids CD spectroscopy is particularly useful for studying proteins. The use of CD for measuring elements of protein secondary structure is well established and it is often used to monitor conformational changes that occur as proteins fold. Proteins absorb left and right circularly polarised light to different extents; this difference is the CD signal and is wavelength dependent:

$$CD = A_\ell - A_r \qquad \text{(Equation 1)}$$

Circularly polarised light is generated by superposing two out of phase waves of plane polarised light oriented perpendicular to each other. A phase difference of + or -90° causes the electric field vector to rotate in a circle, i.e. the light is now circularly polarised in either a right (+) or left (-) handed direction. Figure 2.1 shows the basic experimental setup in a CD spectrometer.

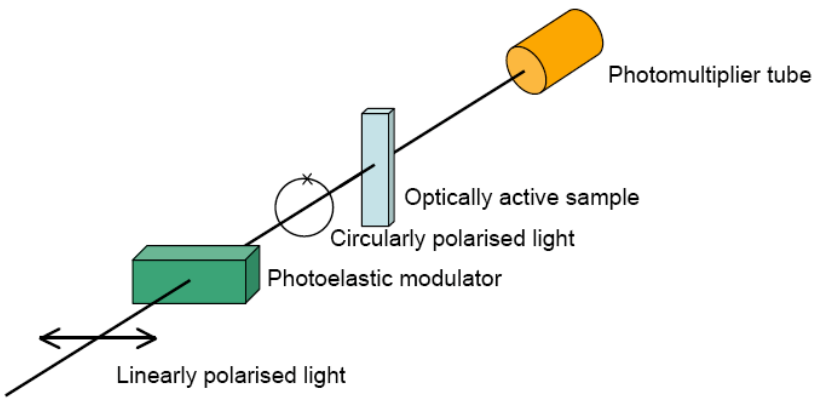


**Figure 2.1. Experimental setup inside a CD spectrometer.**

Monochromatic linearly polarised light from a xenon arc lamp is turned into alternatively right and left circularly polarised light by a photoelastic modulator (PEM) (Kelly and Price, 2000). The PEM consists of a piezoelectric element attached to a block of silica. When the piezoelectric element is driven at 50 kHz it causes the silica to become birefringent and act as a dynamic quarter wave plate that slows one of the linearly polarised beams by a quarter-wave so that they are out of phase by + or - 90°. Thus, left and right circularly polarised light is produced that alternates at 50,000 times per second (Kelly and Price, 1997). If this light hits an optically active sample the two polarisations of light will be absorbed to different extents and this preferential absorption is detected with a photomultiplier tube and recorded. As the circular polarisations of light will be absorbed differently the resulting beam will no longer trace a circle but an ellipse (Fasman, 1996). Hence, CD is normally measured in units of ellipticity.

Proteins contain chromophores that absorb in the ultraviolet (UV) region of the electromagnetic spectrum. Typically secondary structure (backbone) measurements are made in the far-UV region (180-250 nm) where the peptide bond absorbs. Signals obtained in the near-UV region come from transitions associated with aromatic residues. The differences between far- and near-UV are shown in table 2.1.

| | **Far UV** | **Near UV** |
|---|---|---|
| **Wavelength range (nm)** | < 250 | 250-300 |
| **Contributions from** | Peptide backbone<br>Some side chains (although generally very difficult to detect) | Aromatic residues (Phe, Tyr, Trp)<br>Disulphide bonds |
| **Transition energies (nm)** | 210-230 ($n \rightarrow \pi^*$)<br>190 ($\pi \rightarrow \pi^*$) | See table 2.3 |

**Table 2.1. Near- and far-UV spectroscopic characteristics.** Information taken from Rodger and Norden, 1997.

### 2.2.2. Far-UV CD: Electronic transitions in the peptide chromophore

The transitions that are seen in the far-UV arise primarily from the peptide chromophore (figure 2.2).

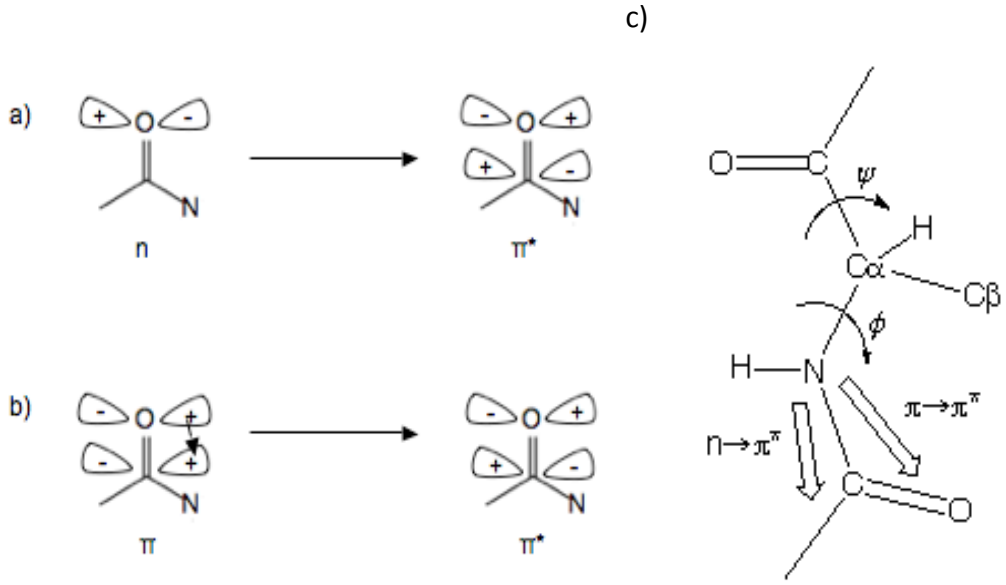


**Figure 2.2. The peptide chromophore and its associated amide orbital transitions.** a) n → π* and b) π → π*. The n → π* transition is of lower energy (210-230 nm) and lower intensity (ε = ~ 100 $mol^{-1}$ $dm^3$ $cm^{-1}$) and is polarised along the carbonyl bond. The π → π* transition is at 190 nm, has a much higher intensity (ε = ~ 7000 $mol^{-1}$ $dm^3$ $cm^{-1}$) and is polarised between the oxygen and the nitrogen. Adapted from Rodger and Nordén, 1997. c) shows an alternative view of the transitions in relation to the peptide bond (reproduced from www.proteinchemist.com)

The broader n → π* transition (figure 2.2a) is polarised along the carbonyl bond and is centred at around 220 nm. The more intense π → π* amide transition (figure 2.2b) occurs at around 190 nm (Rodger and Norden, 1997). The energy and intensity of these transitions depend on the ϕ and ψ angles in the peptide bond (figure 2.2c), hence they are affected by their conformational environment and therefore give rise to different CD spectra depending on the protein secondary structure. α-helices, β-sheets and random coil conformations will each give different spectra due to the long range order in the peptide chromophores (Fasman, 1996). Typical protein secondary structures for pure α-helix, β-sheet and random coil are shown in figure 2.3 and their characteristic spectral features are given in the table below:

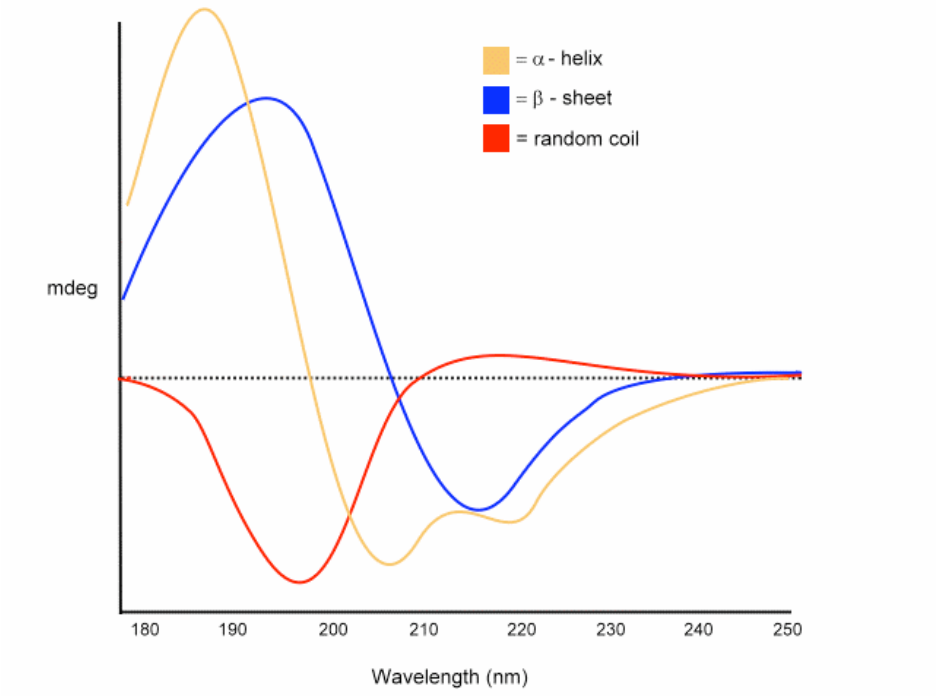


| | **Positive (nm)** | **Negative (nm)** |
|---|---|---|
| **α-helix** | 190 | 208, 222 |
| **β-sheet** | 195 | 216-218 |
| **Random coil** | 215 (weak) | 195 |

**Figure 2.3 and table 2.2. Typical CD spectra for α-helical (black line), β-sheet (blue line) and random coil (green line) structures.** Reproduced from http://www.proteinchemist.com**.**

In an α-helix the minimum at 222 nm arises from the n → π* transition. The minimum at 208 nm and the maximum at 190 nm arise from splitting of the π → π* transition where one component is polarised parallel to the helix axis (208 nm) and the other perpendicular to the helix axis (190 nm) (Bulheller and Hirst, 2009; Rodger and Norden, 1997). The positive band at 195 nm in a β-sheet is from the π → π* transition (the exciton splitting in this motif is less significant than for α-helices (Fasman, 1996) and the negative band near 215 nm is attributed to the n → π* transition. These transitions are depicted pictorially in figure 2.2. It should be noted that despite the reported characteristic spectrum for a β-sheet as given in the table above (which comes from poly-L-lysine as it exists in this conformation) there is no real standard and β-sheets are much less well characterised than α-helices and their spectra more open to interpretation (Nesloney and Kelly, 1996).

There are some side chains that can contribute to far-UV spectra, for example, arginine, glutamine, the acidic side chains and the aromatic side chains (table 2.3) (Rodger and Norden, 1997). Despite their transitions being stronger than that of the peptide backbone they are often not detected as they are generally in much lower abundance than the peptide transitions. However, their occurrence can complicate CD spectra (Rodger and Norden, 1997). For example, positive CD bands in the 225-235 nm region have been observed for avidin (Green and Melamed, 1966) while calculations on tryptophan-containing proteins suggest that this residue may contribute significantly to spectra in the same region (Andersson et al., 2001; Vuilleumier et al., 1993; Woody, 1994). It has been calculated that tyrosine can contribute significantly to the CD spectra of helical proteins at 220 nm which could cause an underestimation of the % helical content (Bhattacharjee et. al.,, 2003; Chakrabartty et al., 1993). Furthermore, there are examples where tyrosine and tryptophan have contributed to CD spectra in the 225-250 nm region as positive bands (e.g. for the gene 5 protein of bacteriophage fd) (Woody, 1978). Several algorithms have been developed that aim to calculate CD spectra for proteins of known structure, for example Dichrocalc (Bulheller and Hirst; Rogers and Hirst, 2004; Sreerama et al., 1999). Calculated CD spectra can be compared with experimental data to establish relative proportions of secondary structure, verify models and facilitate the analysis of observed CD spectra (Whitmore and Wallace, 2008).

### 2.2.3. Near-UV CD: Aromatic transitions and tertiary structure

The transitions that contribute to near-UV CD are from aromatic residues (the amide group has no transitions in the near-UV) and have the potential to give information on the conformational changes that these residues may experience e.g. more mobile residues will show a lower intensity (Bulheller et al., 2007; Kelly and Price, 2000). Furthermore, while near-UV CD spectra cannot report directly on tertiary structure (although folding can be inferred) they can be used to compare differences that may arise, for example after changing pH or concentration. All of the transition energies of the aromatic side chains (including those in the far-UV which are in italics) along with the total maximum extinction coefficient and the corresponding intensity are given in

the table below and are shown in figure 2.4c and d. Phenylalanine and tyrosine have one transition in the near-UV while tryptophan has two.

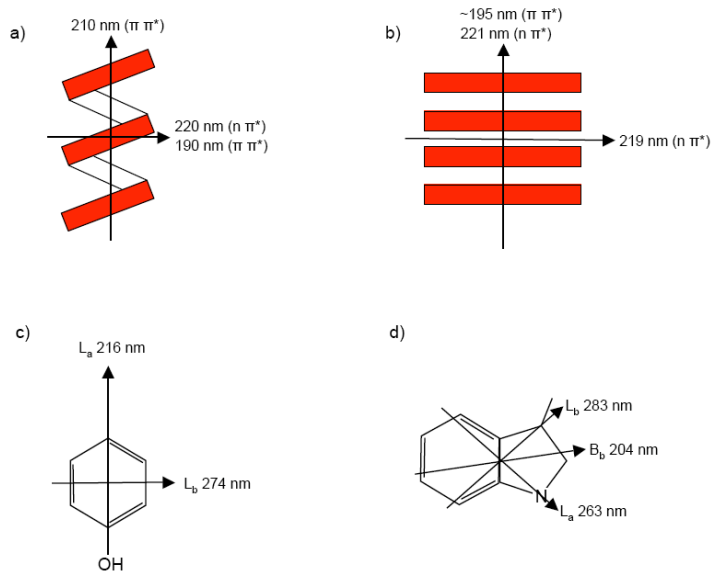


**Figure 2.4. Orientations of transition moment polarisations in a) α-helix, b) β-sheet, c) Tyrosine and d) Tryptophan.** a and b are determined by calculations (Rodger et al., 2006). Approximate wavelength maxima for each transition are given (adapted from (Bulheller and Hirst, 2009; Dafforn and Rodger, 2004; Fasman, 1996; Rodger et al., 2006).

| | $\varepsilon_{max}$ (nm) | $\varepsilon_{max}$ ($mol^{-1}$ $dm^3$ $cm^{-1}$) | Transition energy (nm) |
|---|---|---|---|
| **Phenylalanine** | 263 | ~190 | *190 ($^1B_b$)*<br>*191 ($^1B_a$)*<br>*209 ($^1L_a$)*<br>**263 ($^1L_b$)** |
| **Tyrosine** | 274 | ~1400 | *193 ($^1B_b$)*<br>*196 ($^1B_a$)*<br>*216 ($^1L_a$)*<br>**274 ($^1L_b$)** |
| **Tryptophan** | 279 | ~5000 | *196 ($^1B_a$)*<br>*204 ($^1B_b$)*<br>**263 ($^1L_a$)**<br>**283 ($^1L_b$)** |

**Table 2.3. Transitions in both the near and far-UV from the three aromatic residues (Bulheller and Hirst, 2009; Rodger and Norden, 1997).** The transition energies are calculated and have been verified experimentally (Bulheller and Hirst, 2009). L (near-UV) and B (far-UV, more intense) represent the low and high-energy transitions respectively (Bulheller et al., 2007). The superscript notation of the transition energies means that the state is a singlet state and the subscript refers to the orientation of the transition dipole moment along the axis of the ring, a being the long and b the short axis (Bulheller et al., 2007).

The phenol on tyrosine affects the absorption bands compared to the simpler phenylalanine and shifts them to a longer wavelength (Fasman, 1996). The intensity of the maximum absorption is also much higher making it easier to detect.

Experiments in the near-UV are less common than far-UV and information can be harder to extract but there are a significant number of examples and extensive research has been carried out into the theoretical basis and interpretation of near-UV data (Strickland, 1974). Near-UV CD analysis on bovine pancreatic ribonuclease showed the extent of burial of the six tyrosine residues it contains (Horwitz et al., 1970) and similar experiments have been carried out on RNase A (Woody and Woody, 2003). Insulin forms oligomers that are affected by the presence of zinc and this can be seen from changes in the near-UV CD spectra (Wood et al., 1975).

### 2.2.4. CD from amyloid-forming peptides and proteins

CD has been a useful tool for following the conformational changes that occur as amyloid forms. In general, it would be expected that an increase in a β-sheet signal would be observed in the far-UV region as fibrillisation proceeded and there are many examples where this is the case (Lopez De La Paz et al., 2002). Near-UV CD on amyloid has been carried out on fibrils formed from transthyretin (Colon and Kelly, 1992), the SH3 domain of phosphatidylinositol 3-kinase (Guijarro et al., 1998), IAPP (Kayed et al., 1999), α-synuclein (Ulrih et al., 2008) and $\beta_2$-microglobulin (Eakin et al., 2004) to look at conformational changes that occur as aggregation proceeds.

CD spectra of short peptides that contain aromatic residues often show significant differences to regular CD spectra. CD of a diphenylalanine peptide that formed nanotubes showed positive bands at 197 nm ($\pi \rightarrow \pi^*$ transition) and 220 nm ($n \rightarrow \pi^*$ transition) and a broad negative maximum at around 280 nm that was thought to come from the aromatic residues (Gupta et. al., 2007). It was proposed that the phenylalanine residues were stacked in the nanotube structure. A similar spectrum had been observed previously for a peptide that was believed to form a β-turn motif (Tinker et al., 1988). Similarly, work carried out on the peptide KLVFF which constitutes residues 16-20 of Aβ and forms amyloid by itself gave unusual spectral characteristics with a peak at 198 nm and broader peak at 210-220 nm (Krysmann et al., 2008). In a related study, AAKLVFF gave different CD spectra depending on its preparation. In a dried film it gave a characteristic β-sheet spectrum whereas in solution the negative maximum was red-shifted to 228 nm with a weaker positive signal at 209 nm, generally found in β-turn structures (Castelletto et al., 2009; Krysmann et al., 2008). However, the spectrum in this case was interpreted to arise from $n \rightarrow \pi^*$ aromatic stacking interactions between phenylalanine residues. CD carried out on a variant of KLVFF that contained methylated K and V residues showed a β-sheet spectrum although the minima was red-shifted from 217 nm to 226 nm. This red-shift has been seen for other β-sheet forming peptides and has been attributed to a twist (Cerpa et al., 1996; Manning et al., 1988; Orpiszewski and Benson, 1999).

CD from amyloid may be difficult to interpret for various reasons. CD experiments are generally carried out on isotropic samples i.e there is no directional dependence. However, some systems are inherently oriented and can complicate data interpretation by contributing a linear dichroism to the CD spectra, which is orders of magnitude greater than CD signals (Davidsson et al., 1980). Amyloid fibrils could be considered to be an inherently ordered system and therefore spectra may not be straightforward to interpret. Furthermore, amyloid formation means the size of the aggregates are increasing which will influence the amount of light that is scattered away from the detector and thus distort the signal, specifically the PMT will mistake the scattered light for absorbed light and falsely increase measured absorbance (Ji and Urry, 1969). In addition, particulate systems such as those that are prone to aggregation often exhibit flattened absorption bands (Duysens, 1956). Absorption flattening occurs where the concentration of particles able to absorb light are reduced as they are incorporated into the aggregate, thus falsely decreasing measured absorbance (Ji and Urry, 1969). Light scattering and absorption flattening have both been previously observed to affect CD spectra by imposing a red-shift on observed minima and reducing intensity (Calloni et al., 2008; Castiglioni et al., 2007; Ji and Urry, 1969; Starck and Sutherland-Smith, 2010; Wallace and Mao, 1984). An example of unusual CD spectra from an amyloid fibre was that from a fragment of the non-amyloid β component (NAC) that gave a band at 285 nm as well as showing typical β structure in the far-UV, despite the absence of any aromatic residues or cysteine (Abe and Nakanishi, 2003).

## 2.3. Linear Dichroism

Linear Dichroism (LD) is similar to CD in that it refers to the different extents to which a molecule absorbs polarised light at different wavelengths, except that the incident light is linearly instead of circularly polarised. An essential requirement of an LD experiment is that the sample is somehow oriented, either naturally or during the experiment, so that the light is linearly polarised both parallel and perpendicular with respect to an axis (Bulheller et al., 2007). It is this differential absorption that is calculated:

$$LD = A_{\parallel} - A_{\perp} \qquad \text{(Equation 2)}$$

where $A_{\parallel}$ is the absorbance of parallel polarised light and $A_{\perp}$ is the absorption of perpendicularly polarised light. According to this equation, transitions polarised parallel to the axis will give a positive band in an LD spectrum and those polarised perpendicular will result in negative bands (Rodger and Norden, 1997). When a chromophore in a molecule absorbs a photon of light, its energy is increased as the radiation displaces the electronic arrangement from a lower starting level to a higher one (Rodger and Norden, 1997). This redistribution of charge is defined by the transition moment in a molecule, which has a specific polarisation (the direction of the transition), length (proportional to the square root of the absorbance) and intensity (Rodger and Norden, 1997). Maximum absorbance occurs when the transition moment is parallel to the propagation direction of the electric field component of the light (Rodger and Norden, 1997). The electronic transitions associated with various peptide chromophores can be seen in figures 2.2 and 2.4 and are described in the CD section above.

For an $\alpha$-helix, an LD spectrum that is negative at 190 nm and positive at 210 nm arises due to absorptions that are polarised perpendicular and parallel to the axis respectively. A negative spectrum at 220 nm would come from an $n \rightarrow \pi^*$ transition that is perpendicularly polarised with respect to the helix axis. Because of the

requirement to align, only certain systems are amenable to study using LD, these include DNA, membrane proteins and fibrous proteins; amyloid fibrils fit into this last category.

A common method for aligning fibres is using shear flow in a Couette cell (figure 2.5).

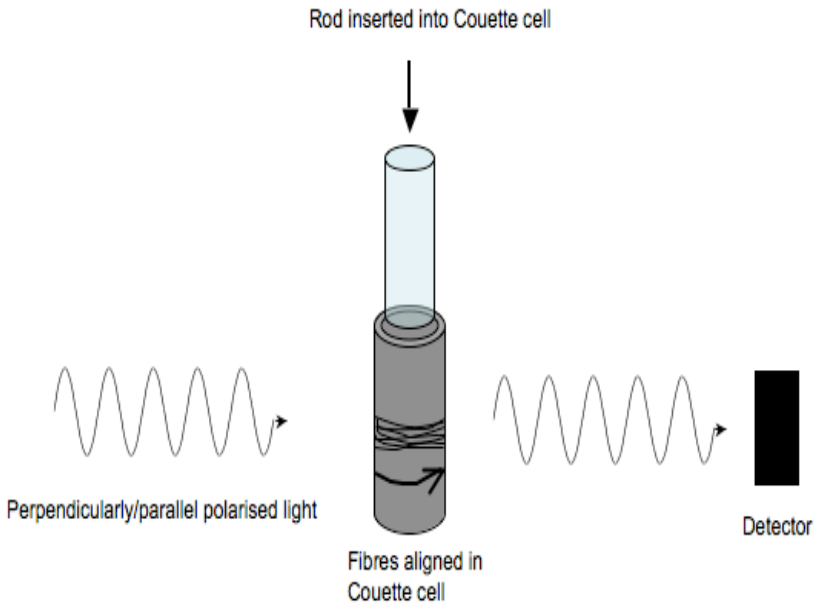


**Figure 2.5. Basic experimental setup for an LD experiment**. The sample is placed into a quartz Couette cell and a rod inserted. Rotation of either the rod or the cell will expose the long molecules to shear flow that will aid in their alignment. Plane polarised light is transmitted through the sample at parallel and perpendicular orientations to the fibre axis. The sample will absorb depending on the orientation of the electronic transitions within the chromophores in the molecules and the resulting transmitted light is detected.

With this system it is possible to use very low sample volumes (<30μl) (Marrington et al., 2005). The spectra produced are similar to CD spectra in that they are wavelength dependent and there are characteristic signals representative of particular structural elements. However, much more is known about the theory behind CD and how secondary and tertiary structural features in proteins contribute to the observed spectra (Kelly et al., 2005; Schellman, 1975). LD, by comparison, is an emerging technique with initial studies being mostly carried out on DNA (Norden and Kurucsev, 1994). Its use in studying proteins is relatively recent, although a number of fibrous

proteins have been investigated including actin, collagen and FtsZ, as well as membrane proteins which, by being membrane-bound, are provided with an orientation axis (Dafforn et al., 2004; Dafforn and Rodger, 2004; Marrington et al., 2004; Marrington et al., 2006). The formation of fibrils and crystals from amyloidogenic proteins has also been studied using LD (Adachi et al., 2007; Dafforn et al., 2004; Marshall et al., 2010). The LD spectrum of Aβ gave a positive maximum at 205 nm supporting the perpendicular orientation of the peptide chains with respect to the fibre axis. There was no signal in the near-UV region despite a large proportion of the residues (around 10%) being aromatic, suggesting that they are not rigid within the structure (Dafforn and Rodger, 2004). Another explanation for an LD signal of 0 is if the transitions are at the magic angle of 54.7° with respect to the axis (Dafforn and Rodger, 2004; Rodger et al., 2006; Rodger and Norden, 1997).

To quantitatively characterise the orientation of the chromophore in relation to the fibre axis and gain structural information the reduced LD ($LD^r$) is calculated:

$$LD^r = \frac{LD}{A} = \frac{A_{\parallel} - A_{\perp}}{A} = \frac{3}{2} S(3\cos^2\alpha - 1) \qquad \text{Equation 3.}$$

where A is the absorbance of the anisotropic sample i.e. not oriented, S is the orientation factor which lies between 1 and 0 (1 being perfectly oriented and 0 being completely random) and $\alpha$ is the angle between the transition moment and the orientation axis (Rodger et al., 2006). In practise it can be difficult defining S as subjecting fibres to shear flow does not orient them perfectly.

For systems such as amyloid where light scattering is significant there is the potential that the "real" LD spectrum can be distorted for more concentrated samples by as much as 30 nm (Bulheller et al., 2007). The correct spectra can be determined by reducing the concentration, which will either shift the peak to the correct position, or reduce the intensity if the peak is already in the right place. As the use of LD has developed, algorithms similar to those used in CD calculations have been established

to attempt to predict LD spectra from known structures (Bulheller and Hirst, 2009; Bulheller et al., 2007).

## 2.4. Fluorescence

### 2.4.1. Intrinsic protein fluorescence

Fluorescence occurs when a photon of light that has been absorbed by a molecule falls from a higher energy state to a lower one and consequently a photon is emitted. Proteins contain fluorophores that, when excited with light of the appropriate wavelength, emit a photon at another characteristic wavelength that can be measured using a fluorimeter. The emission is generally at a lower energy and therefore longer wavelength than the absorbed photon, the difference between maximum absorption and emission is called the Stokes shift. This process is shown in figures 2.6 and 2.7 below.

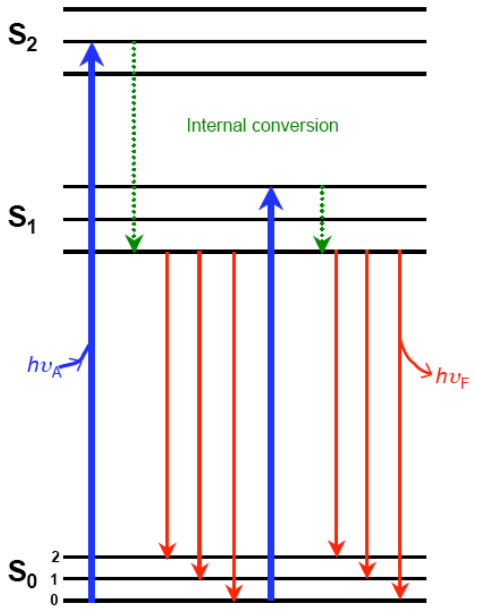


**Figure 2.6. A simplified form of a Jablonski diagram (Lakowicz, 1999).** Photons of light are absorbed ($h\upsilon_A$) and emitted ($h\upsilon_F$ ). $\upsilon$ is the frequency of the photon and $h\upsilon$ is the energy it has. $S_0$ $S_1$ and $S_2$ are the singlet ground, first and second electronic energy levels respectively. Within these electronic levels are different vibrational energy levels (0,1 and 2). When the fluorophore has been displaced to a higher energy level it undergoes internal conversion to the lowest vibrational state of $S_1$ before returning to the ground state ($S_0$) and emission of another photon (Lakowicz, 1999).

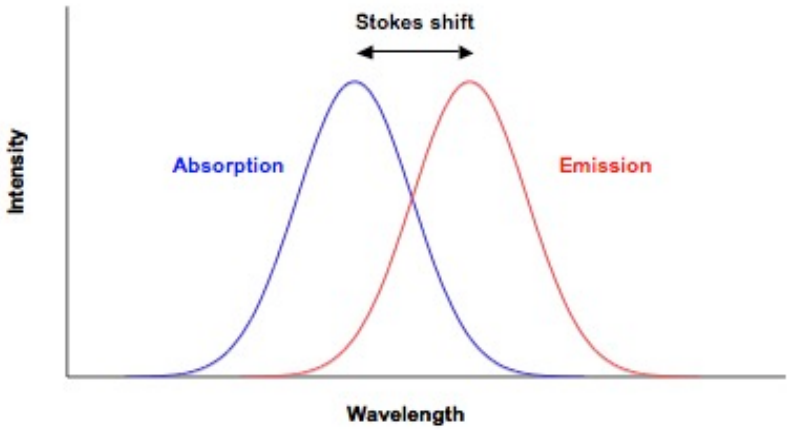


**Figure 2.7. Typical absorption and emission spectra of a fluorophore.** In most cases, the photon absorbed is of higher energy and shorter wavelength than the photon emitted during fluorescence. The difference between these maxima is the Stokes shift.

After a photon of light has been absorbed the fluorophore is excited to $S_1$ or $S_2$ (figure 2.6). If it is excited to $S_2$ the fluorophore will quickly drop to the $S_1$ level in a process called internal conversion. Emission then results from the fluorophore relaxing from the lowest vibrational energy level of $S_1$ to, in most instances, the highest vibrational state in $S_0$. Fluorophores may occupy different vibrational energy levels, illustrated by the emission profile of some molecules that show several peaks at different wavelengths, for example phenylalanine (figure 2.8).

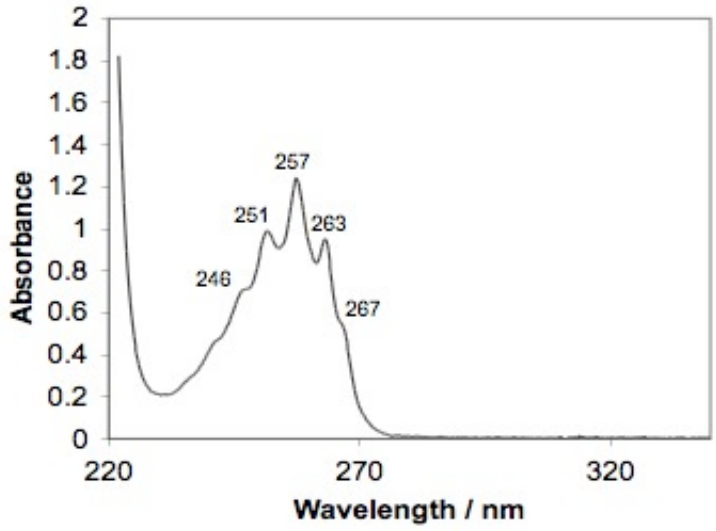


**Figure 2.8. Absorbance spectrum of phenylalanine. (Hu et al., 1998)**

Fluorescence normally arises from aromatic molecules. In proteins phenylalanine, tyrosine and tryptophan are able to absorb light and fluoresce at a particular wavelength (table 2.4).

| **Residue** | **Absorption** | | **Fluorescence (λ/nm)** |
|---|---|---|---|
| | **λ/nm** | **ε** | |
| Phenylalanine | 257 | 200 | 282 |
| Tyrosine | 274 | 1400 | 303 |
| Tryptophan | 280 | 5600 | 348 |

**Table 2.4. The three aromatic amino acids with their absorption and emission maxima and molar absorptivity (ε).** Tryptophan fluoresces the most strongly whereas phenylalanine fluorescence is very weak.

The fluorescence characteristics of these side chains can give structural information on proteins and the environment of the residue. Tryptophan fluorescence is very dependent on solvent and demonstrates a blue shift to shorter wavelength and an increase in intensity as the solvent polarity decreases (Seidel et al., 1993). This may be achieved by burial in the hydrophobic core (Cowgill, 1975). Unlike tryptophan, tyrosine does not undergo any environment dependent spectral shifting. However, its intensity varies depending on environment and following changes in tyrosine fluorescence can inform of the extent of burial of the residue (Lakowicz, 1999). Tryptophan, tyrosine, and phenylalanine fluorescence have all been used to investigate the assembly of amyloid. Dusa *et. al.* mutated tyrosine 39 in $\alpha$-synuclein to tryptophan, which has a much higher fluorescence yield, and monitored its change in fluorescence as the peptide aggregated identifying oligomeric intermediates that existed at different stages of assembly (Dusa et al., 2006). Similar experiments have been carried out on $\beta_2$-microglobulin (Kihara et al., 2006) and A$\beta$ (Touchette et al., 2010). Although tryptophan lends itself best to fluorescence studies, tyrosine fluorescence in amyloid has also been monitored to follow aggregation (Maji et al., 2005; Padrick and Miranker, 2001). The fluorescence of phenylalanine in amyloidogenic peptides has also been investigated (Krysmann et al., 2008).

### 2.4.2. Fluorescence Quenching

In addition to the information on residue solvent accessibility that can be provided by intrinsic fluorescence studies on proteins, similarly their ability to be quenched can be revealing. Collisional, or dynamic, quenching describes the collision of a molecule with another, which is able to quench a fluorophore by returning it from an excited state to the ground state (Lakowicz, 1999). This phenomenon is separate from static quenching where a non-fluorescent complex is formed between the quencher and the fluorophore, as in the case of self-quenching (Lakowicz, 1999). Self-quenching can occur between groups in the same molecule, for example tryptophan can be quenched by nearby protonated acidic groups i.e. aspartate or glutamate or it can quench tyrosine by energy transfer effects. Tyrosine can undergo excited state ionisation at high pHs and lose a proton on its OH group, which also quenches fluorescence (Chen and Edelhoch, 1975).

The Stern-Volmer equation is used to describe collisional quenching (Chen and Edelhoch, 1975):

$$F_0/F = 1+K_{SV}[Q] \qquad \text{Equation 4.}$$

where $F_0$ is the fluorescence intensity in the absence of any quenching agent, F is the fluorescence intensity in the presence of quencher, [Q] is the concentration of quenching agent and $K_{SV}$ is the Stern-Volmer quenching constant. Data are presented as plots of $F_0/F$ vs. [Q], the slope of the resulting line is equal to $K_{SV}$ with higher values indicating increased ability to quench a fluorophore (Lakowicz, 1999).

Due to their higher fluorescence yield, tryptophan and tyrosine are generally the protein fluorophores that are examined using quenching methods. A number of effective quenchers are known, including iodide, $O_2$ and acrylamide (Eftink and Ghiron, 1981). Fluorescence quenching experiments have been carried out previously on amyloidogenic peptides to determine the solvent accessibility of particular regions of

proteins as they form amyloid protofibrils and fibres (Dusa et al., 2006; Padrick and Miranker, 2001; Relini et al., 2010; Sakata et al., 2008).

### 2.4.3. Thioflavin T fluorescence

Thioflavin T (ThT) is a dye that binds to amyloid and, upon binding, undergoes a red-shift in its emission absorbance maximum from 445 nm to 485 nm (LeVine, 1993; LeVine, 1999; Naiki et al., 1989; Vassar and Culling, 1959). Its structure is shown below:

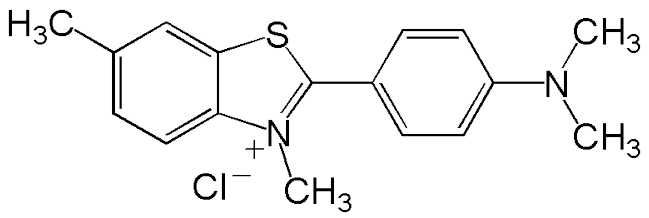


**Figure 2.9. Structure of Thioflavin T**

Little is known about the mechanism by which ThT binds to amyloid but it is believed that the cross-β arrangement forms channels that are able to accommodate linear dyes like ThT, thus giving it its specificity (Biancalana and Koide, 2010). Observations from polarised fluorescence spectroscopy have indicated that the long axis of the ThT molecule is aligned parallel to the fibre axis (Krebs et al., 2005). ThT has shown to form micelles and it is these that bind to amyloid, although the critical micellar concentration is not agreed upon and varies from 4 μM (Khurana et al., 2005) to 30 μM (Sabate et al., 2008). Another suggestion is that ThT does not form micelles but excited dimers, termed excimers, that are able to bind to hydrophobic channels in amyloid fibrils (Groenning et al., 2007a; Groenning et al., 2007b). Electrostatic interactions are also known to be important in ThT binding and its affinity is significantly reduced at low pH as positive net charges are likely to cause repulsion and therefore reduce fluorescence emission (Kelenyi, 1967; LeVine, 1993). These ionic interactions would help to explain the occasional cross-reactivity of ThT with non-fibrillar material (Biancalana and Koide, 2010). A crystal structure of ThT bound to

globular acetylcholinesterase shows the dye binding in an α-helical hydrophobic pocket mediated by π-π stacking with tyrosine and tryptophan residues (Harel et al., 2008). However most models are consistent with ThT binding specifically to amyloid, and provided sufficient precautions are taken, it can be used for this purpose (Biancalana and Koide, 2010).

Because ThT selectively binds to amyloid and not the protein precursor or amorphous aggregates it has been extensively used to follow amyloid formation, to the extent that it is now considered by some to be essential in defining a substance as amyloid (Nilsson, 2004). Thioflavin T is most often used to follow kinetics of amyloid formation. An excitation wavelength of approximately 450 nm is used and emission at ~485 nm measured over time. The resulting sigmoidal curve correlates with species observed using other methods, for example electron microscopy (figure 2.10).

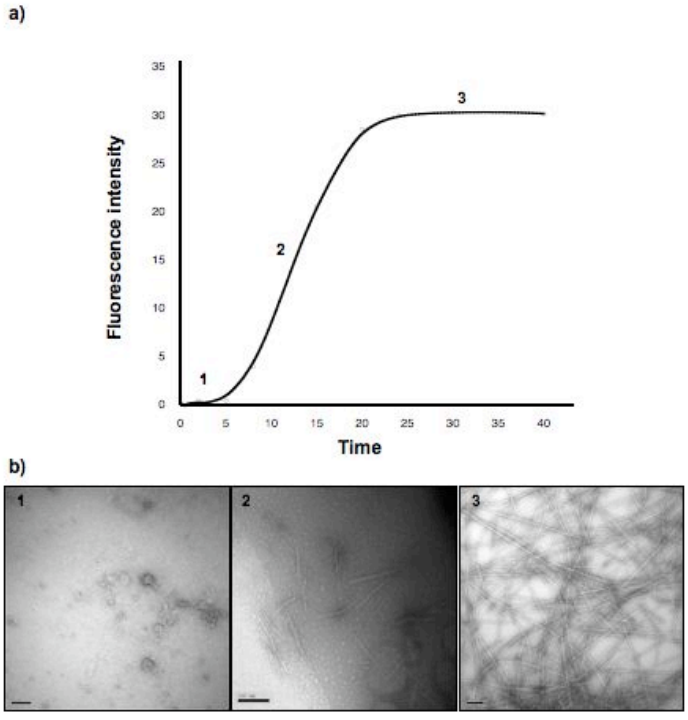


**Figure 2.10. a) Typical plot of Thioflavin T fluorescence against time as fibres assemble b) Typical corresponding EM images at each stage of assemble.** In the initial rate-limiting lag phase (stage 1) small oligomeric species assemble, followed by protofibrils (stage 2) and finally mature, full-length fibrils (stage 3). At this point there in no further increase in Thioflavin T fluorescence. Scale bars are 200 nm.

The lag phase (stage 1) corresponds with the slow formation of a critical nucleus that defines the rate-determining step in fibrillogenesis and which can be overcome by the addition of preformed seeds (Asakura et al., 1964; Come et al., 1993). After this phase monomers can add to the stable unit more rapidly and fibrils lengthen (2 in figure 2.10). The final stage (3) occurs when fibres are fully formed and no more dye is able to bind to the growing fibres.

Although Thioflavin T is specific for amyloid, as mentioned its binding affinity varies depending on peptide and solution conditions. Experiments are normally carried out at around pH 8 as this has been shown to increase the affinity of the dye (LeVine, 1999). However, this basic pH may not always be appropriate for the fibrils being grown so experiments must be carried out rapidly to avoid fibril dissociation (LeVine, 1999). Furthermore, ThT has shown to be much more weakly fluorescent with short peptides, for example $A\beta_{25-35}$ which is known from EM to form amyloid-like fibrils (LeVine, 1999). It also shows great sequence specificity and the presence of aromatic residues, in particular tyrosine and phenylalanine appear to promote binding, probably through hydrophobic interactions and $\pi$-$\pi$ stacking (Biancalana et al., 2009; Wu et al., 2009). Conversely, sequences that feature a high number of positively charged residues show a lower affinity for binding (Wu et al., 2009).

## 2.5. X-ray fibre diffraction

### 2.5.1. Diffraction theory

X-ray fibre diffraction was one of the first techniques to be used to examine amyloid and is still essential in structure determination (Eanes and Glenner, 1968; Jahn et al., 2010; Serpell et al., 2007). As amyloid fibres are heterogeneous and insoluble they are not amenable to X-ray single crystal crystallography or solution NMR studies. Fibre diffraction enables structural elucidation whilst preserving the sample integrity, as no alternative conditions are required to produce fibrils for this method, unlike single crystal diffraction.

In order to gain a high-quality diffraction pattern, fibres must be aligned in some way. There are several methods for doing this including using a stretch-frame, by drying out in a glass capillary, aligning fibres as a thin film deposited on a suitable material such as Teflon or glass, or by magnetic alignment (Makin and Serpell, 2005b). These methods will each give a different texture to the sample, referring to the way in which the fibres are aligned and their orientation with respect to the incident X-ray beam (Makin and Serpell, 2005b).

Much of the diffraction theory relevant to X-ray crystallography also applies to fibre diffraction. Crystals are composed of identical molecule-containing subunits, termed unit cells, that are ordered in a three dimensional manner. The repeating nature of the unit cells within a crystal allows the signal to be amplified into a diffraction pattern. A unit cell will have its own characteristic dimensions defined by vectors *a*,*b* and *c* and angles $\alpha$, $\beta$ and $\gamma$ (figure 2.12a). Because each unit cell is identical, the positions of the molecules, and therefore the atoms of the molecules in each unit cell are identical. Unit cells generally contain more than one copy of a molecule, related to one another within the cell by crystallographic symmetry that will be present throughout the whole crystal. The asymmetric unit describes the part of the unit cell that can be copied using symmetry operations to generate the unit cell and the rest of the crystal. The symmetrical relationships between molecules within a crystal are described by a

specific space-group. The most common method used to describe a space group is using a specific notation which first defines the centring with a letter and then a number denoting the point group. The point group may be further annotated to describe the presence of screw axes. There are 14 Bravais lattices that are each included in one of 7 crystal systems, each of which is defined by particular vector (a, b and c) and angle arrangements. The screw axis is the rotation about an axis i.e. how many turns would be required to make one full turn, subscript numbers refer to the degree of translation along that axis. For example, the space group $P2_12_12_1$ describes a primitive Bravais lattice (i.e. where lattice points are on the corners of the cell only), with a twofold rotation along each of the *a*,*b* and *c* axes and the subscript 1 denotes a translation of ½ of the lattice vector. Each space group can only belong to one crystal system, in this case this would be orthorhombic, the properties of which are $a \neq b \neq c$, and $\alpha=\beta=\gamma= 90^\circ$ (Blow, 2002).

When X-rays interact with a crystal some will scatter due to interaction with the electrons on each atom; because protein molecules in a crystal are arranged in an ordered way, the scattered waves are able to add up through constructive interference and produce a diffraction signal. The result is a series of spots on a detector that gives information not on the atoms specifically, but on the electron density in the molecule although the two are closely linked and hence can provide a structure. The electron density, and therefore structural, information in a diffraction pattern is generated by performing a Fourier transform on the data. Only waves that are in phase will add up and produce a signal. Most waves are out of phase and will cancel out which is why only spots are seen on the detector, rather than a continuous distribution of intensity, which is what would be observed if only one molecule was able to successfully diffract (Blow, 2002).

The relationship between the X-rays that hit a crystal with the spots that are observed on the detector is described by Bragg's law and is shown in figure 2.11. The figure shows two incident, in-phase X-ray beams of a particular wavelength ($\lambda$) that diffract at a specific angle ($\theta$) off atomic planes within the crystal that are separated by

distance d. Bragg's law is described mathematically as $2d\sin\theta = n\lambda$ and is satisfied only when waves are in-phase, which will produce a spot on the detector. Waves will constructively interfere when they are in phase by an integer number of wavelengths; half-integer multiples will cancel out and no spot will be observed. In any one orientation only some of the atomic planes will be in the right position for diffraction to occur in phase and a spot to appear. In order to sample every possible plane, the crystal must be rotated 360°, each data set producing new spots. The unit cell defines the position of the spots on the diffraction pattern, whilst the arrangement of atoms within the unit cell determines the amplitude and phase (the position of a peak in a wave) of the diffracted X-ray wave. However, the detector is able to record only the amplitude of the resultant wave, which is proportional to the square root of the intensity of the spot observed, and not the phase, which is known in crystallography as the "phase problem" (Blow, 2002).

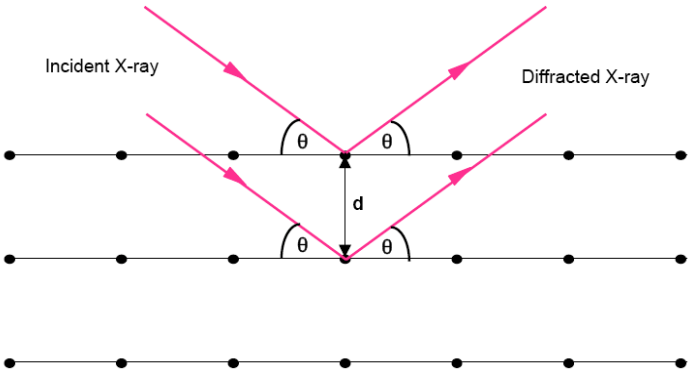


**Figure 2.11. Interaction of X-rays with a crystal lattice illustrating Bragg's law.**

There is an inverse relationship between d and θ: the lower the spacing, the higher the angle required to achieve constructive interference. The structure in the crystal is said to be in real space, whereas the diffraction pattern that is observed on the detector is in reciprocal space i.e. the relationship of the spots to the crystal is $1/a$, $1/b$ and $1/c$, or $a^*$, $b^*$ and $c^*$. Therefore, the smaller the unit cell (and the smaller the protein), the larger the distance between the spots. The reciprocal lattice vectors $a^*$, $b^*$ and $c^*$ are related to the Miller indices, h, k and l, which specify the atomic plane in the crystal lattice that produces a particular reflection. The atomic planes pass through the unit

cells at various positions and those that go through the same points in each unit cell will diffract in-phase (Blow, 2002). An example is shown in figure 2.12.

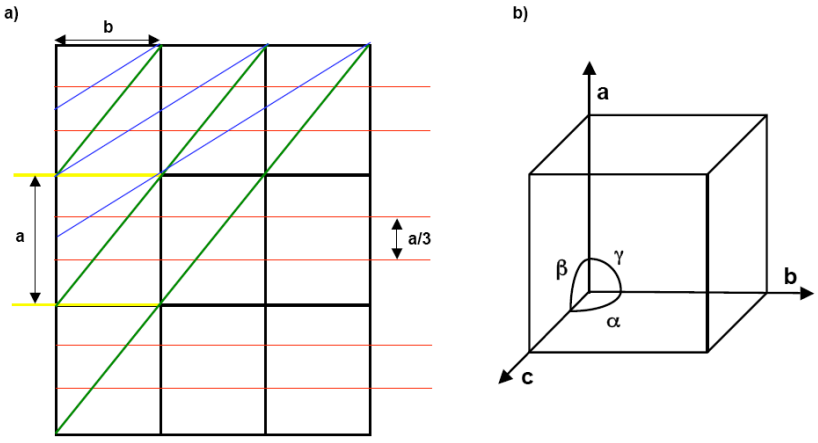


**Figure 2.12. a) Bragg planes intersecting unit cells in a crystal. b) a three-dimensional representation of a unit cell showing the a,b and c vectors and related angles.**

In figure 2.12 unit cells are shown in black, and the atomic planes that will pass through the same part, and therefore the same atoms (hence "atomic plane"), of each unit cell are in yellow, red, green and blue. The yellow planes are separated by distance *a* i.e one unit cell edge and, as this distance is related to the h indexing, are described as [1 0 0]. The red planes are separated by 1/3 of distance *a* and are therefore indexed to [3 0 0]. Planes in the *b* direction are [0 k 0] and in the *c* direction are [0 0 l]. The diagonal blue and green lines are planes that will cut the unit cell in two dimensions (the *a* and *b* directions). The distance between the green lines is a full unit cell edge along the *a* direction and also the *b* direction, therefore this is the [1 1 0] plane. The blue lines are related by ½ the unit cell *a* edge and a full *b* distance, therefore this plane would be indexed to [2 1 0]. As the planes cut through identical atoms in each unit cell, this indexing system can be used to assign each reflection in a diffraction pattern to a particular location in the unit cell. Screw axes in certain space groups can give rise to systematic absences, meaning that only certain reflections will be present. For example in the space group $P2_12_12_1$ odd reflections at [h 0 0][0 k 0] and [0 0 l] will not be present (Blow, 2002).

### 2.5.2. Fibre diffraction

The same theory as that described above applies to diffraction from fibres, however, the resulting diffraction patterns from fibres differ quite significantly compared to crystals.

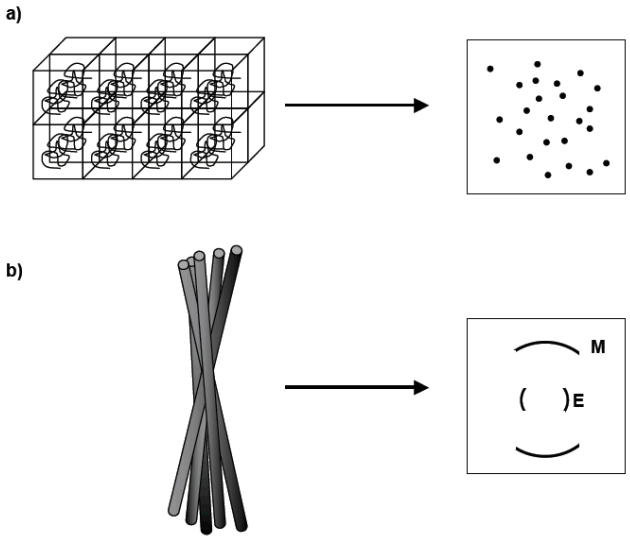


**Figure. 2.13. Schematic showing X-ray diffraction of a) crystals and b) a bundle of aligned fibres.** M refers to meridional, E refers to equatorial.

The obvious difference between the data that is obtained is that arcs are present on the detector instead of spots. This is because in a fibre the order is not three-dimensional, as it is in a crystal (figure 2.13). Within each fibre there are repeating units that are bonded in a regular arrangement along the length of the fibre axis. However, because fibres are not perfectly aligned along an axis, the spots are spread out over a wider area, forming arcs due to overlapping reflections (Makin and Serpell, 2005b). The reason fibres are aligned is to try and introduce more order into the sample that is being analysed, which will result in better diffraction. In a fibre diffraction pattern there are two notable reflections that show symmetry. The meridional reflection (M in figure 2.13b) contains information on the more crystalline (i.e. ordered) arrangement of the fibre in the axis direction. The equatorial direction (E) contains information on the other two directions (Makin and Serpell, 2005b). The general convention and that which is used here is for direction *a* to correspond to the hydrogen bonding distance between peptides in the fibre axis direction (see chapter 1,

figure 1.8), with directions *b* and *c* referring to the sheet spacing distance and the chain length respectively. Therefore, the *a* dimension for a fibre can be determined by measuring the position of the reflection in the meridional direction. Indexing the reflections in the equatorial direction may be more difficult as they are a combination of both *b* and *c* directions (Makin and Serpell, 2005b). Depending on the unit cell, certain reflections in diffraction patterns from fibres may be systematically absent. For example, an anti-parallel arrangement of peptides within a β-sheet may be expected to produce an additional reflection on the meridian to the one seen at 4.7 Å at double this distance, i.e at around 9.4 Å. However, a $2_1$ screw axis would forbid the generation of this reflection and lead to incorrect interpretation (Makin and Serpell, 2005b). If fibres are aligned well and sufficiently ordered, fibre diffraction data can reveal much about the underlying molecular structure.

# 3. METHODS

## 3.1. Methods pertaining to chapters 4 and 5 (GNNQQNY)

### 3.1.1. Peptide synthesis and sample preparation of NH3+-GNNQQNY-COO-

NH3+-GNNQQNY-COO- was purchased in lyophilised form from Pepceuticals (Biocity, Nottingham) at > 97% purity. Stock solutions were made up in MilliQ 0.2 μm filtered water at concentrations of between 0.57-15 mg/ml. After addition of water, samples were vortexed briefly and centrifuged for 5 minutes at 13000 rpm to remove any preformed aggregates using an Eppendorf MiniSpin® microcentrifuge (Eppendorf AG, Hamburg, Germany). Any pellet that formed was discarded. The concentration of the supernatant was determined using a Molar Extinction Coefficient (ε) of 1490 $M^{-1}cm^{-1}$. ε was calculated using ε of tyrosine at 280 nm, as only one tyrosine residue was present (Gill and von Hippel, 1989). Absorbance at a wavelength of 280 nm was measured using an Eppendorf Biophotometer (Eppendorf AG, Hamburg, Germany).

### 3.1.2. Transmission electron microscopy (TEM)

4 μl of peptide solution was placed onto a carbon-coated copper grid (Agar Scientific, Essex, UK) left for 2 minutes. The grid was washed once using water and negatively stained twice with 4 μl filtered 2% (w/v) uranyl acetate solution. Negative staining enhances contrast by coating the specimen with a thin layer of the staining solution, which scatters electrons more than the sample itself does (Lashuel and Wall, 2005). At each stage excess liquid was blotted with filter paper. The grid was allowed to air dry before examining in a Hitachi 7100 microscope (Hitachi, Germany) operating at 100 kV fitted with a Gatan Ultrascan 1000 CCD camera (Gatan, Abingdon, UK). All measurements of EM images were made using ImageJ (Abramoff et al., 2004).

### 3.1.3. Tyrosine Fluorescence

Samples were prepared at a concentration of 3 mg/ml, centrifuged and any pellet that formed discarded then placed in a microvolume cuvette with a 1 cm pathlength and fluorescence emission from tyrosine measured at various time points using a Varian Cary Eclipse fluorimeter (Varian, Oxford, UK) using an excitation wavelength of 278 nm. Fluorescence intensities at 305 nm were plotted against time. Excitation and emission slits were set to 5 and 10 nm respectively. The scan rate was 600 nm/min with 1 nm data intervals and an averaging time of 0.1 s. The voltage on the photomultiplier tube was set to medium (600 v) and experiments were carried out in triplicate to confirm trends. The temperature was maintained at 20 °C using a peltier device. Cuvettes were cleaned both before and after experiments by washing with water, 2% Hellmanex (Hellma, Southend-on-Sea, UK) and ethanol, and then air-drying.

### 3.1.4. Atomic force microscopy

For early stage species, GNNQQNY was dissolved in water to a concentration of 2 mg/ml. The peptide solution was applied to cleaved mica and then allowed to dry. For crystals, peptide was dissolved to a concentration of 2 mg/ml, incubated for 8 days to ensure formation of crystals then diluted 1 in 5. Peptide solutions were applied to cleaved mica and allowed to dry then imaged using 10 nm silicon nitride cantilever tips with a force constant of 0.06-0.58 N/m and a resonance frequency of 18-57 kHz (Veeco, Cambridge, UK and μMasch, San Jose, CA, USA). Early stage species were imaged using an Asylum MFP-3D atomic force microscope (Asylum Research, Santa Barbara, CA, USA) and crystals were imaged using a Veeco Dimension 3100 scanning probe microscope (Veeco, Cambridge, UK). All experiments were performed in tapping mode at room temperature.

### 3.1.5. Acrylamide quenching

Samples were prepared as for tyrosine fluorescence and fluorimeter settings were identical. The effect of quenching tyrosine fluorescence with acrylamide was observed on fibrils (after an incubation time of 0 hours) and crystals (after an incubation time of

168 hours). Acrylamide was titrated into the samples at increasing final concentrations between 0.1 M and 0.4 M at various time points and a fluorescence reading taken. In addition, a reading was taken with no acrylamide present. Data were fitted to the Stern-Volmer equation, used to describe collisional quenching (Lakowicz, 1999):

$$F_0 / F = 1 + K_{SV}[Q]$$

where $F_0$ is the fluorescence intensity in the absence of acrylamide, $F$ is the fluorescence intensity in the presence of acrylamide, $Q$ is the concentration of acrylamide and $K_{SV}$ is the Stern-Volmer quenching constant (Lakowicz, 1999). Linear plots of $F_0/F$ against $[Q]$ give $K_{SV}$ values for fibrils and crystals (higher values indicate more quenching i.e tyrosine is more solvent-accessible).

### 3.1.6. Circular dichroism

Lyophilised peptide was dissolved, centrifuged and the concentration of the supernatant measured to be 5 mg/ml. This was incubated in for several weeks to ensure crystal formation (verified by EM) then diluted to 2.5 mg/ml and placed in a 0.1 cm quartz cuvette (Starna, Essex, UK) and CD measurements taken using a JASCO J-715 spectropolarimeter. The time constant (response) was set to 1 s and the scan rate to 200 nm/min. The bandwidth was 1 nm and the sensitivity set to standard. Scans were performed from 300-190 nm with a 0.2 nm data pitch and continuous scan mode. A peltier device was used to maintain a temperature of 20 °C. Scans were taken in triplicate and the data averaged. A water baseline was subtracted and cuvettes cleaned by washing before and after experiments with water, 2% Hellmanex (Hellma, Southend-on-Sea, UK) and ethanol then air-drying. Only data recorded with a high tension (HT) voltage of less than 600 were plotted.

All measurements were originally measured in millidegrees and converted to units of mean residue ellipticity (MRE) to standardise for concentration and pathlength (Kelly et al., 2005). Raw data were converted using the following equation:

$$MRE = \frac{(mdeg \times Mr)}{(10 \times c \times l \times Na)}$$

Equation 5.

Where Mr is the molecular weight of the monomeric peptide, c is the concentration in mg/ml, l is the pathlength and Na is the number of amino acids in the monomer.

### 3.1.7. Linear Dichroism

Linear dichroism measurements were carried out on both end-stage species of GNNQQNY i.e. crystals, and a kinetic analysis on the assembly process. For backbone LD measurements on crystals, peptide was incubated at a concentration of 2 mg/ml for several weeks to ensure crystal formation (verified by EM) then diluted to 0.2 mg/ml to gain far-UV data. Measurements were carried out on a MOS-450 spectrometer (Biologic, France) from 350-180 nm with a bandwidth of 2 nm, scanning speed of 100 nm/min, response time of 1 s, standard sensitivity and a data pitch of 0.2 nm. Samples were aligned using a microvolume Couette cell rotating at 3000 rpm built in-house at the University of Warwick, Coventry, UK. Eight scans were averaged and a water spectrum subtracted from this to correct for the inherent LD signal that arises from the optics and detector. Data are reported in $\Delta$ absorbance units.

LD tilt measurements were performed on a JASCO-715 spectropolarimeter with identical settings to those used for CD. Water baselines were subtracted and data are reported in $\Delta$ absorbance units.

Kinetic LD measurements were carried out on peptide that was freshly solubilised, vortexed, centrifuged and measured to have a concentration of 2 mg/ml. Alignment was induced using a microvolume Couette cell (Kromatek, Great Dunmow, UK) with a pathlength of 0.5 mm (Rodger et al., 2006). Samples were rotated at 3000 rpm, as in previous experiments. Kinetic experiments were carried out on the UV1 beamline at the Synchrotron Radiation Facility ASTRID at the Institute for Storage Ring Facilities, University of Aarhus (Aarhus, Denmark). Synchrotron radiation increases the signal/noise ratio and thus allowed rapid scanning required for samples such as

amyloid fibres and crystals that inherently scatter at low wavelengths. Spectra were measured from 350-180 nm with 1 nm data steps (Dicko et al., 2008). A water baseline was subtracted. Synchrotron radiation LD spectra are reported in units of millivolts (mV) that are related to $\Delta$ absorbance units (1 mV = ~6 x $10^{-4}$ Å).

### 3.1.8. X-ray fibre diffraction, data processing and unit cell optimisation

Peptide was prepared at 10 mg/ml and incubated at room temperature. At particular time points this sample was analysed for presence of fibres, crystals or a mixture of both using EM. Samples that contained fibres or a mixture of fibres and crystals were set up for fibre diffraction by placing 20 μl of solution between two wax filled capillaries and allowed to air-dry at room temperature. The crystalline sample did not align using this method so an alternative method was used. The sample was placed into a siliconised 0.7 mm capillary tube, sealed with wax at one end and allowed to air-dry at room temperature to produce a disk across the capillary. The capillary was then sealed at the other end, the sample placed on a goniometer head and data collected using a Rigaku rotating anode (CuK$\alpha$) and Raxis IV++ detector (Rigaku, Sevenoaks, UK) with specimen to film distances of either 160 mm or 250 mm. Experiments were carried out on at least two separately prepared samples to confirm results.

The program CLEARER was used for processing experimental diffraction data and unit cell determination(Sumner Makin et al., 2007). Diffraction patterns were loaded into the program and centred to ensure that reflections were in opposite symmetrical positions. Diffraction settings were as follows: the sample to detector distance was 160 mm or 250 mm, the wavelength was 1.5419 Å and the pixel size was 400 μm. The program then measured the signal positions and these were compared to those measured by hand using a function of the program. Using these signal positions, possible unit cells were generated. Initially guessed lattice vectors were defined as: a = 4.69 Å, b = 15 Å, c = 25 Å based on expected unit cell dimensions and $\alpha=\beta=\gamma= 90°$. *a** was defined as the fibre axis and *b** and *c** were optimised. The most intense d-spacings (reflections) measured were entered and a unit cell calculated. See section 5.2.4 for further information.

### 3.1.9. X-ray diffraction simulation from co-ordinates

Model co-ordinates from 1YJP.pdb and 2OMM.pdb were used to calculate diffraction patterns using published unit cell dimensions. Inputting the published structural co-ordinates into the fibre diffraction analysis program CLEARER generated fibre diffraction patterns (SUMNER MAKIN ET AL., 2007). The fibre axis was assigned as parallel to the hydrogen bonding direction of the co-ordinates ([0 1 0]) and the beam direction perpendicular ([0 0 1]). In order to allow direct comparison with experimental data, settings used for experimental data collection were accounted for in the diffraction pattern calculations. The specimen to film distance was 160 mm or 250 mm, the pixel size was 400 μm and the crystallite size was 40 nm x 40 nm x 40 nm.

Reflections from the calculated diffraction patterns were indexed using the signal position prediction function in CLEARER (Sumner Makin et al., 2007). Diffraction settings were input as per section 3.1.8 and the unit cell co-ordinates for 1YJP.pdb (Nelson et al., 2005) and 2OMM.pdb (Sawaya et al., 2007) entered. The beam and fibre axis were oriented to [0 0 1] and [0 1 0] respectively.

## 3.2. Methods pertaining to chapters 6 and 7 (KFFEAAAKKFFE and variants)

### 3.2.1. Peptide synthesis and sample preparation of NH3+-KFFEAAAKKFFE –COO- and variants thereof

NH3+-KFFEAAAKKFFE-COO-, Ac-KFFEAAAKKFFE-NH2 and F/A variants of KFFEAAAKKFFE were purchased in lyophilised form from Bachem (St. Helens, UK) at > 97% purity. K/A and K/R variants of KFFEAAAKKFFE were a gift from Dr. Helen Walden, Cancer Research UK and were >95% purity. Peptide solutions were made up to concentrations of between 5 and 20 mg/ml in either milliQ 0.2 μm filtered water or phosphate buffered saline (PBS) diluted x10 (stock PBS; 19 mM sodium dihydrogen phosphate ($NaH_2PO_4$), 81 mM disodium hydrogen phosphate ($Na_2HPO_4$), 1.5 M NaCl or NaF, pH 7.4). Samples set up at pH 2 and pH 12 were dissolved in filtered 10 mM phosphoric acid and 10 mM disodium hydrogen phosphate ($Na_2HPO_4$) respectively. The pH was measured prior to dissolution. After addition of water, samples were vortexed briefly and centrifuged for 5 minutes at 13000 rpm to remove any preformed aggregates using an Eppendorf MiniSpin® microcentrifuge (Eppendorf AG, Hamburg, Germany). Any pellet that formed was noted as present then discarded. Due to the lack of any tryptophan, tyrosine or cysteine residues the concentration determination of these peptides is not possible by UV absorbance at 280 nm. The Bradford method of protein determination concentration, which is based on the shift in absorbance that occurs on the binding of the dye Coomassie blue to basic and aromatic residues in proteins (Compton and Jones, 1985) is also not appropriate as the aromatic residue phenylalanine constitutes a large proportion of the sequence. Furthermore, the BCA assay, which works on the basis that amide groups in peptide bonds reduce $Cu^{2+}$ to $Cu^{+}$ ions that then chelate with bicinchoninic acid, cannot be used with these peptides due to the requirement of either elevated temperatures or a long incubation period, both of which would result in formation of fibrils and thus inaccurate protein concentration (Smith et al., 1985; Wiechelman et al., 1988). Therefore, concentration was determined by careful weighing out of the peptide using a microbalance (Sartorius, MA, USA) and calculating the appropriate volume of solvent to be added to achieve

the required concentration. Samples were either left quiescent at room temperature or agitated at a speed of 100 rpm at 20 °C.

### 3.2.2. Transmission electron microscopy (TEM)

Samples were prepared and imaged as in section 3.1.2.

### 3.2.3. Circular dichroism

Lyophilised peptide was dissolved in either PBS or water to a concentration of 5 mg/ml. Due to the interference of $Cl^-$ ions in circular dichroism measurements PBS was made using NaF instead of NaCl. The supernatant was diluted to 0.5 mg/ml with the same buffer that the peptide had originally been dissolved in and CD measurements taken immediately after placing in a 0.02 cm quartz cuvette (Starna, Essex, UK) using a JASCO J-715 spectropolarimeter. The time constant (response) was set to 4 s and the scan rate to 50 nm/min. The bandwidth was 1 nm and the sensitivity set to standard. Scans were performed from 320-180 nm with a 0.1 nm data pitch and continuous scan mode. A peltier device was used to maintain a temperature of 20 °C. Scans were taken in triplicate and the data averaged. Buffer or water baselines were subtracted and cuvettes cleaned in between readings by washing with water, 2% Hellmanex (Hellma, Southend-on-Sea, UK) and ethanol then air-drying. Only data recorded with an HT voltage of less than 600 were plotted. Samples were agitated at 100 rpm for 7 days and then another reading taken. CD rotation measurements were taken with the same settings.

All measurements were originally measured in millidegrees and converted to units of mean residue ellipticity (MRE) as described in section 3.1.6.

### 3.2.4. Intrinsic phenylalanine fluorescence

Lyophilised peptides were made up to a concentration of 5 mg/ml in either PBS or water and diluted to 0.5 mg/ml with the same buffer that the peptide had originally

been dissolved in. Samples were placed in a microvolume cuvette with a 1 cm pathlength and fluorescence emission from phenylalanine measured at various time points using a Varian Cary Eclipse fluorimeter (Varian, Oxford, UK) using an excitation wavelength of 265 nm. Water and PBS baselines were subtracted from the data. Triplicate measurements were taken and averaged. Fluorescence intensities at 305 nm were plotted against time. Excitation and emission slits were both set to 5 nm. The scan rate was 600 nm/min with 1 nm data intervals and an averaging time of 0.1 s. The voltage on the photomultiplier tube was set to high (800 v) and experiments were carried out in triplicate to confirm trends. The temperature was maintained at 20 °C using a peltier device. Samples were agitated at 100 rpm for 7 days and then another reading taken. Cuvettes were cleaned before and after experiments with water, 2% Hellmanex (Hellma, Southend-on-Sea, UK) and ethanol then air-drying.

### 3.2.5. Thioflavin T fluorescence

Lyophilised peptides were made up to a concentration of 5 mg/ml in either PBS (NaF) or water and diluted to 0.5 mg/ml with the same buffer that the peptide had originally been dissolved in. A 1 mg/ml (3.14 mM) stock ThT solution was made by dissolving ThT (Sigma, UK) in water and filtering with a 0.2 μm filter. Stock ThT was added to the diluted peptide sample to a final concentration of 50 μM, gently vortexed, and allowed to bind for 5 minutes before reading were taken.

Samples were placed in a microvolume cuvette with a 1 cm pathlength and fluorescence emission from Thioflavin T measured at various time points using a Varian Cary Eclipse fluorimeter (Varian, Oxford, UK) using an excitation wavelength of 450 nm. Water and PBS baselines were subtracted from the data. Fluorescence intensities at 485 nm were plotted against time. Excitation and emission slits were set to 5 nm and 10 nm respectively. The scan rate was 600 nm/min with 1 nm data intervals and an averaging time of 0.1 s. The voltage on the photomultiplier tube was set to high (800 v) and experiments were carried out in triplicate to confirm trends. The temperature was maintained at 20 °C using a peltier device. Cuvettes were

cleaned before and after experiments with water, 2% Hellmanex (Hellma, Southend-on-Sea, UK) and ethanol then air-drying.

### 3.2.6. In-house fibre diffraction

Peptide was prepared at 5 mg/ml and incubated at room temperature. Samples were set up for fibre diffraction by placing 20 μl of solution between two wax filled capillaries and allowed to air-dry at room temperature. The samples were placed on a goniometer head and data collected using a Rigaku rotating anode (CuKα) and Raxis IV++ detector (Rigaku, Sevenoaks, UK) with specimen to film distances of either 160 mm or 250 mm. Experiments were carried out on at least two separately prepared samples to confirm results.

### 3.2.7. Synchrotron fibre diffraction

Peptide was prepared and aligned as for in-house fibre diffraction. The samples were placed on a goniometer head and data collected on the I24 Microfocus MX beamline at Diamond Light Source, Oxford, UK.

### 3.2.8. Data processing and unit cell optimisation

The program CLEARER was used for processing experimental diffraction data and unit cell determination. Diffraction patterns were loaded into the program and centred to ensure that reflections were in opposite symmetrical positions. Diffraction settings depended upon the data collection method. For in-house data the sample to detector distance was 160 mm, the wavelength was 1.5419 Å and the pixel size was 400 μm. For synchrotron data the settings were 312 mm, 0.9778 Å and 440 μm. The program then measured the signal positions and these were compared to those measured by hand using a function of the program. Using these signal positions, possible unit cells were generated. Initially guessed lattice vectors were defined as: a = 4.69 Å, b = 15 Å, c = 25 Å based on expected unit cell dimensions and $\alpha=\beta=\gamma= 90°$. a was defined as the fibre axis and b* and c* were optimised. The most intense d-spacings (reflections)

measured were entered and a unit cell calculated. See section 7.2 for further information.

### 3.2.9. MTT cell toxicity assay

DMEM/F12 medium without phenol red was supplemented with 1/100 v/v penicillin/streptomycin, 1/100 v/v L-glutamine and 15% fetal calf serum (FCS) (Gibco) (Complete medium). SH-SY5Y human neuroblastoma cells were placed in a 37 °C water bath until just thawed (for storing method see 'freezing cells' below). 1 ml of the cell suspension was added to 4 ml of complete medium in a universal tube and centrifuged for 5 minutes at 1500 rpm on a bench top centrifuge. The medium was aspirated and the pellet resuspended in 20 ml complete medium. This solution was transferred to a T175 flask and 15 ml complete medium added to a total volume of 35 ml. The cells were grown overnight at 37 °C in a humidified incubator in the presence of 5% $CO_2$ and atmospheric pressure $O_2$. The following day medium was exchanged with 35 ml fresh complete medium and warmed up to 37 °C in a water bath.

Splitting and counting cells

At approximately 80-90% confluency, the cells were split to prevent over-proliferation. The medium was aspirated and the cell layer was rinsed with 10 ml of PBS before adding 10 ml of 0.25% trypsin and placing the flask in the incubator for 5 minutes in order to detach the cells. The flask was then agitated by hand to further dislodge cells from the flask wall and 10 ml of medium added to prevent any further trypsinisation.

A few μl of this 20 ml cell suspension was applied to a haemocytometer in order to count the number of cells present in 1 ml of cell suspension. More specifically, cells included in the 1 mm x 1 mm squares A and C in the top chamber and B and D in the bottom chamber were counted and averaged.

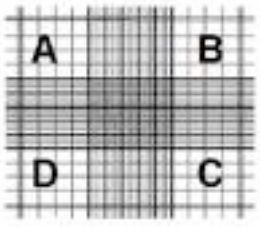

The total number of cells per millilitre was calculated by multiplying this averaged number by $10^4$. For a T175 flask, 1 x $10^6$ cells were used.

The rest of the 20 ml cell suspension was transferred to a universal tube and centrifuged at 1500 rpm for 5 minutes before aspirating the trypsin and medium supernatant from the tube. The cell pellet was resuspended in 20 ml fresh medium and mixed thoroughly. This solution was split between new T175 flasks and the cell passage number increased by 1. 25 ml of complete medium was added to each flask and the cells were allowed to proliferate in the incubator.

Freezing cells

In order to create a stock bank of cell aliquots for future use, when the cells reached 80-90 % confluency (approximately 4 days) they were split and counted as described above. To preserve the cells during storage in liquid nitrogen, the cell pellet resulting after trypsinisation and centrifugation was resuspended in medium containing 10 % DMSO. Cells were frozen in cryotubes in aliquots of 1 ml (containing approximately 2x $10^6$ cells per tube). The cryo tubes were placed in a freezing vessel and filled with isopropanol, stored overnight at -80 °C and transferred to liquid nitrogen the following day.

Adding peptides to SH-SY5Y cells

Frozen cells were thawed and grown to 80-90% confluence and split as described above. A number of 1 x $10^5$ cells/well was used for seeding into a 96-well plate. To calculate the volume of solution to add to each well the number of cells per well required i.e 1 x $10^5$ was divided by the number of cells/ml counted. The appropriate volume of cell suspension was added to each well (approximately 100 μl), using one plate per time point and accounting for each concentration in triplicate. Plates were incubated overnight so that cells adhered to the walls of the wells.

Peptides used for cytotoxicity assays were:

i) capped peptide in PBS at 5 mg/ml at time 0

ii) capped peptide in PBS at 5 mg/ml after 2 hours incubation

iii) K1A K8A in PBS at 5 mg/ml left quiescent

iv) K1A K9A in PBS at 5 mg/ml left quiescent

The peptide solutions were made up in a sterile environment. 0.2 μm sterile filtered PBS was added to non-sterile lyophilised peptide aliquots to a concentration of 5 mg/ml. As the purchased peptide was not sterile it was necessary to also filter the peptide solution. This was carried out by firstly washing a syringe and Whatman Anotop 0.1 μm filter (Sigma, UK) through with sterile PBS. The low volumes of peptide solution used (< 300 μl) meant that the solution had to be pipetted into the syringe and then pushed through the filter. The solution was agitated at 100 rpm for 7 days to ensure the formation of fibres. Half of the incubated capped sample was then sonicated for 20 minutes. The low concentration peptide was made up and added to cells immediately after preparation. In each case, after filtering, samples were prepared for electron microscopy to examine the nature of the species added. The peptide concentrations used for these experiments were kept in line with previous reports in the literature of amyloid cytotoxicity and were chosen as 10 μM and 50 μM.

The following day the plates were visualised to ensure presence of live cells. Peptide solutions containing fibres had been prepared in advance and those containing early stage species prepared immediately before the experiment. Peptides were diluted with complete medium to the desired concentrations (10 μM and 50 μM). The medium was aspirated from all wells except the untreated cells and the calculated volume of medium-diluted peptide solution added to each well. Plates were returned to the incubator and MTT assays carried out at 1 hour, 5 hours and 24 hours according to the manufacturers protocol after adding peptide solutions. More specifically, due to the high cell density (>1 x $10^5$ cells per well) the incubation time was 2 hours at 37 °C. After this time all but 25 μl of medium was removed from the wells and 50 μl DMSO added to dissolve the insoluble formazan and thoroughly mixed. The plates were incubated for 10 minutes at 37 °C and the absorbance at 540 nm with a reference at 620 nm.

All experiments were carried out under aseptic conditions.

Data analysis

Statistical data analysis was carried out using the GraphPad Prism software package. The D'Agostino-Pearson omnibus test was used to determine the normality of the data and the probability value at 5 % significance ($p<0.05$) was calculated using the Mann-Whitney two-tailed test for non-normally distributed, non-parametric data.

## 3.3. Difficulties of working with amyloid

The work here describes systems that are by their nature prone to aggregation. Working with amyloid brings about a number of issues to overcome that may not be apparent in the first instance. Some of these are detailed below.

### 3.3.1. Concentration

Electron micrographs of all the amyloid forming peptides used in these experiments taken immediately after dissolution of the peptide indicate that they start fibrillising straight away. This has implications for concentration determination; protein that is in a fibrillar form is not the same as monomeric peptide i.e peptide incorporated into a fibre will have different absorbance profile to monomeric peptide. Attempts have been made to obtain monomeric solutions of peptide by dissolving in organic solvents such as HFIP and are often used to prepare stock solutions of Aβ (Bitan et al., 2005). Whilst this method has proven successful for other peptides, including hIAPP (Higham et al., 2000) electron micrographs of the peptide GNNQQNY prepared in this way show evidence of fibrillar structures forming (figure 3.1).

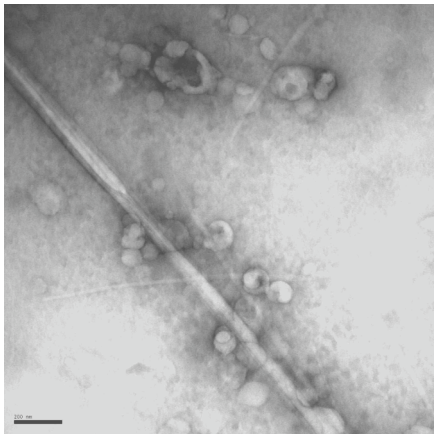

**Figure 3.1. GNNQQNY in HFIP at a concentration of 3.3 mg/ml after 48 hours.** Scale bar is 200 nm.

Furthermore, dissolving peptide in these solvents may affect the structure of the fibrils formed so that they are not comparable to those produced under physiological or other experimental conditions. Therefore, obtaining solutions of monomeric peptide to measure concentration provides a significant challenge in concentration determination of amyloid forming peptides.

The absorbance at 280 nm of proteins or peptides that contain either tryptophan, tyrosine or cysteine residues can be measured and the concentration calculated according to the Beer-Lambert law. However, when using short peptide sequences there may not be any of these residues present, as is the case for the peptide KFFEAAAKKFFE and variants thereof. In these cases the peptide concentration can only be determined by weight (see Methods for further detail), which imposes an inherent limitation on accuracy.

### 3.3.2. Crystallisation

In most cases in structural biology, the preferable method to obtain atomic level structural detail of proteins at high resolution is X-ray crystallography. One of the prerequisites to form single crystals is a homogenous solution of protein molecules. Amyloid fibrils are heterogeneous in length and are therefore theoretically precluded from crystallisation. However, microcrystals formed from over 30 amyloid forming peptides have shown to be amenable to single crystal diffraction, although none are longer than 7 residues (Nelson et al., 2005; Sawaya et al., 2007). Attempts at crystallising the 12 residue peptide KFFEAAAKKFFE and variants thereof, as reported here, were generally unsuccessful, possibly due to the length of the peptide. Furthermore, as mentioned previously, obtaining a monomeric solution of amyloid forming peptide is difficult even at low concentrations as the formation of fibres is favoured, hence the starting solution will be heterogeneous and therefore unable to crystallise.

It is commonly conceived that the inherent inability of amyloid to form, large, well ordered three-dimensional crystals has been a limiting factor in the progress of structural determination and presents a problem across the field. However, it is not clear how relevant a crystal structure of amyloid would be to the fibril structure. For example, transthyretin has been crystallised (Sunde et al., 1996) but the crystal structure of the monomer does not explain how it assembles into fibrils, or what their structure is. The precipitation of crystals from a supersaturated solution is normally a forced event with a careful balancing of different conditions required to form a crystal.

Making crystals from amyloidogenic peptides may not therefore be as essential a prerequisite as initially thought.

# 4. RESULTS AND DISCUSSION: Assembly of GNNQQNY fibres and crystals

## 4.1. Introduction

### 4.1.1. Structure

GNNQQNY is a peptide fragment corresponding to residues 7-13 from the 685 amino acid prion-like protein Sup35 found in the yeast *Saccharomyces cerevisiae.* Both full-length Sup35 and the glutamine and asparagine rich NM (N-terminal and middle) domain (residues 1-253) form amyloid fibrils *in vitro* (Glover et al., 1997). To aid in the structural characterisation of fibrils formed from Sup35, short fragments, including the sequence GNNQQNY, were prepared that formed fibrils and/or microcrystals with similar properties to that of the full-length peptide, for example the ability to bind Congo Red and ThT (Balbirnie et al., 2001; Nelson et al., 2005).

Initial studies on GNNQQNY produced fibrils (formed at a concentration of 1 mg/ml) and microcrystals (formed at 10 mg/ml) (Balbirnie et al., 2001). The latter were subject to powder diffraction and data were interpreted to produce a structure in which there were 4 GNNQQNY molecules per unit cell, each in a separate β-sheet. The strands within each sheet are parallel and the sheets are packed in an anhydrous manner. The polar N and Q side chains hydrogen-bond together in what is termed an amide stack in the fibre axis direction forming a polar zipper, similar to that suggested for polyglutamine proteins that form amyloid (Perutz, 1994; Tsai et al., 2005). Together with the additional hydrogen bonds between the backbones of each peptide, this network of intermolecular bonding was said to account for the high stability of the fibres (Balbirnie et al., 2001). It was proposed that partial unfolding of the NM region of Sup35 would be sufficient to expose the glutamine and asparagines side chains and lead to the formation of amyloid.

Later work by Diaz-Avalos *et. al*. built upon these results using electron diffraction (Diaz-Avalos et al., 2003). This group reported that at a concentration of less than 5 mg/ml the peptide did not aggregate even after an extended period, at 10 mg/ml "clumps" formed that gave powder diffraction patterns and at 20 mg/ml and above a viscous gel formed consisting of fibres (table 4.1). These results highlight the difficulty in reproducing solutions of fibres or crystals from GNNQQNY; the previous experiments produced fibres at a concentration of 1 mg/ml whereas in this case there was no observable aggregation at the same concentration (table 4.1). The microcrystals were examined by electron diffraction and this confirmed that the β-sheets i) were tightly packed with hydrogen-bonded neighbouring side chains ii) excluded water and iii) were parallel (Diaz-Avalos et al., 2003).

| **Reference** | **Fibres** | **Crystals** | **Other notes** |
|---|---|---|---|
| Balbirnie, 2001 | 1 mg/ml | 10 mg/ml | |
| Diaz-Avalos, 2003 | >= 20 mg/ml (form in 30 minutes) | 10 mg/ml (form in 1 week) | No assembly at < 5 mg/ml after 1 year |
| Nelson, 2005 | ~400μM (0.3 mg/ml) (form after a few hours) | ~10-100 mM (8-80 mg/ml) | |
| van der Wel, 2007 | 20-25 mg/ml | 10 mg/ml (both types although more monoclinic unless seeded)<br>2 mg/ml (less crystals, orthorhombic) | A mixture of fibres and monoclinic crystals is obtained at 12 mg/ml). |
| Sawaya, 2007 | n/a | 10 mg/ml (hanging drop – monoclinic)<br>10 mg/ml (orthorhombic) | |

**Table 4.1. Conditions required to form fibres and crystals from GNNQQNY from previously published results.**

Whilst powder and electron diffraction provide information on the packing of the peptide in the unit cell these methods are unable to give precise details on the interactions that occur between the side chains and backbones of the molecules. The elucidation of crystal structures of the peptides GNNQQNY and NNQQNY were the first examples of their kind for amyloid forming peptides (figure 4.1) (Nelson et al., 2005). Since then, other short (7 residues or less), amyloid-forming peptides have been crystallised and their structure determined (Ivanova et al., 2009; Sawaya et al., 2007;

Wiltzius et al., 2008). It is proposed that these structures are similar to the structure of both the amyloid-like fibrils formed from these peptides and the amyloid core of the full-length proteins from which the segments were taken. The arguments behind this are that: a) both fibrils and crystals grow under the same conditions and are often found to co-exist in solution, and that the experimental fibril diffraction patterns and simulated patterns calculated from the crystal structures share similarities; b) crystalline seeds of a short peptide (LVEALYL) are able to reduce the lag time for fibril growth of the full-length peptide to which they are related (insulin), and vice versa (Sup35 is able to seed growth of GNNQQNY fibrils) and c) mutating residues within the segment affects fibril formation in the parent protein (Sawaya et al., 2007). A noteworthy feature of most of the crystal structures is the so-called “steric zipper”, a term used to describe the tight interdigitation of the peptide side chains due to their high self-complementarity (quantified by the $S_C$ parameter (Lawrence and Colman, 1993)) to form a dry interface (Sawaya et al., 2007).

Two crystal structures have now been reported for GNNQQNY with the pdb codes 1YJP (Nelson et al., 2005) and 2OMM (Sawaya et al., 2007) (figure 4.1 and table 4.2). Whilst there are similarities between the two structures there are also some striking differences. The two crystal forms are shown in figure 4.1 along with their measurements and the previously reported unit cells (table 4.2).

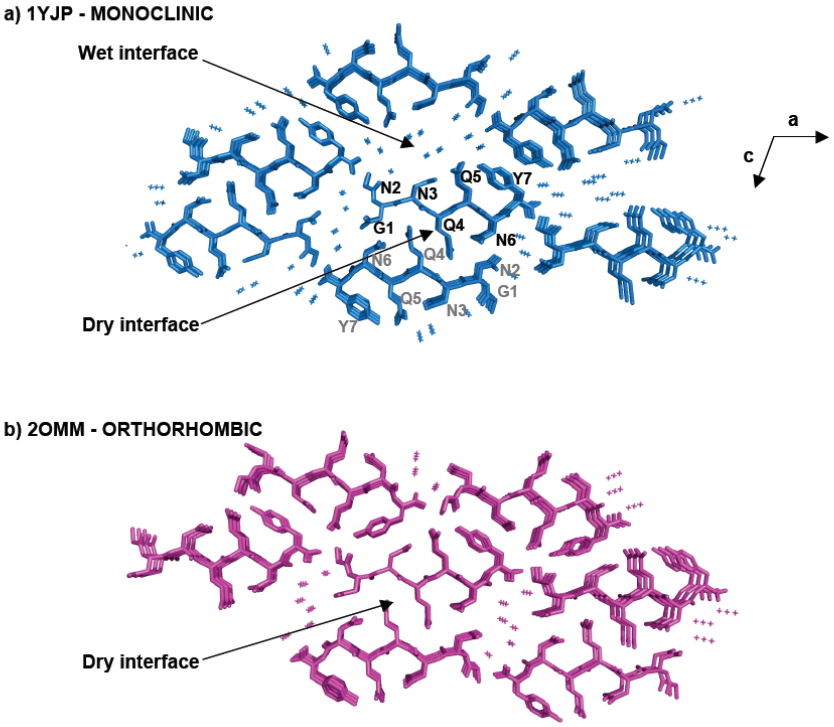


**Figure 4.1. Two crystal structures of the amyloid forming peptide GNNQQNY.** View is looking down the fibre axis. a) Crystal form 1 (pdb code 1YJP) (Nelson et al., 2005). The residues of 2 different peptides are labelled in black and grey. b) Crystal form 2 (pdb code 2OMM) (Sawaya et al., 2007). Water molecules are shown in the structures; there is considerably higher water content in the structure for 1YJP. Also of note is the interaction between tyrosine residues across sheets in 1YJP that is lacking in 2OMM.

| Reference | Method | Space group | a | b | c | α | β | γ |
|---|---|---|---|---|---|---|---|---|
| Balbirnie, 2001 | Powder diffraction | P 2 $2_1$ $2_1$ or P 2 $2_1$ 2 (orthorhombic) or P $2_1$ (β nearly 90°) (monoclinic) | 22.63 | 39.44 | 4.81 | 90 | 90 | 90 |
| Diaz-Avalos, 2003 | Electron diffraction | P $2_1$ $2_1$ $2_1$ (orthorhombic) | 22.7-21.2 | 39.9-39.3 | 4.89-4.86 | 90 | 90 | 90 |
| *Nelson, 2005* | *X-ray crystallography* | *P $2_1$ (monoclinic) 1YJP* | *21.94* | *4.87* | *23.48* | *90.00* | *107.08* | *90.00* |
| *Sawaya, 2007* | *X-ray crystallography* | *P $2_1$$2_1$$2_1$ (orthorhombic) 2OMM* | *23.32* | *4.93* | *37.55* | *90.00* | *90.00* | *90.00* |

**Table 4.2. Summary of reported unit cell dimensions for microcrystals of the peptide GNNQQNY.** a, b and c are given in Å and α, β and γ are given in degrees. The unit cells from the crystal structures for 1YJP and 2OMM are in italics.

In both crystal models the β-strands are arranged parallel and in-register. Figure 4.1a shows the monoclinic crystal form 1 (pdb code 1YJP). This structure has 2 monomers in the unit cell that are related by a $2_1$ screw axis i.e. the strands in the facing sheets are antiparallel to each other and are shifted in the fibre axis direction by half the hydrogen bonding distance of 4.87 Å. The steric interactions (non-hydrogen bonded) between N2, Q4 and N6 in the dry interface can be clearly seen. The wet interface is larger (about 15 Å compared to around 8.5 Å in the dry interface) and water molecules hydrate the polar residues on this side of the β-strand (Nelson et al., 2005). It was suggested from this model that the pair-of-sheets that formed the dry interface constituted the protofilament, although later a four-sheet twisted model was proposed which reconciled with EM measurements of protofibrils that also suggested 4 sheets (Diaz-Avalos et al., 2003; Esposito et al., 2006; Periole et al., 2009; Sawaya et al., 2007). The cross-β spine is stabilised in the fibre axis direction (*b*) by 11 hydrogen bonds between β-strands. 5 of these are backbone-backbone C=O…H-N bonds and 4 are amide stacks (mentioned previously) between adjacent N and Q residues that are responsible for the parallel and in-register arrangement (Nelson et al., 2005). There is also a bond between the nitrogen on the amide sidechain of Q5 and the hydroxyl on Y7, and between the N2 backbone nitrogen and the N2 sidechain oxygen (Sawaya et al., 2007). Finally, the tyrosine rings stack in an edge-to-face manner across the wet interface (Nelson et al., 2005).

Figure 4.1b shows the structure of GNNQQNY in the second, orthorhombic, form (pdb code 2OMM). This structure has 4 monomers in the unit cell and features a very similar dry interface (steric zipper) to that in the monoclinic structure (Sawaya et al., 2007). However, in this structure the wet interface is much less well defined and it appears that N3 and Y7 on one molecule interact with Y7 and N3 on different molecules. In this model the tyrosine side chains do not interact in the sheet-spacing direction (*c*).

Solid-state NMR measurements on GNNQQNY fibres and crystals showed that the peptide could adopt a number of conformations (van der Wel et al., 2007). The

preparation methods are given in table 4.1 and produced fibres and both types of crystals. These assemblies were compared to the previously published monoclinic crystal form 1YJP (the orthorhombic crystal structure 2OMM had not yet been published). In the crystals the mobility of the tyrosine ring was shown to vary and was much more rigid in the monoclinic form, as might be expected from the crystal structure. The attenuated resonances for the orthorhombic form indicated that the tyrosine ring is able to undergo two-fold flips in these crystals and is therefore more mobile. At least three different structural forms for the fibres were produced (not distinguishable by EM) depending on preparation method. In addition to concentration, variables included temperature (4-30 °C), pH and lyophilisation and rehydration of the sample. Fibril forms 1 and 2 were not similar to either crystal structure but also showed some deviations from each other; form 1 was β-sheet whereas form 2 was more consistent with α-helical structure. It was proposed that form 2 might represent oligomers; previous work suggested that Sup35 oligomers were helical (Narayanan et al., 2006). Fibril 3, which was the least abundant species, was also β-sheet but showed most similarity to the monoclinic crystals. The two crystal structures were very alike overall but showed chemical shift differences around the ends of the peptide. Comparison of all species showed the least differences were around Q4 indicating that in both fibres and crystals the dry interface is maintained. As for the crystal structures, the largest deviations between all samples were around the ends of the peptide (van der Wel et al., 2007). It is clear that there are polymorphisms within fibres and crystals formed from GNNQQNY and this has also been investigated using simulations (Berryman et al., 2009). However, it is not known whether the different NMR signals arise from different conformations within the same fibre or from three separate polymorphic structures in the same sample (van der Wel et al., 2007). Both fibres and crystals gave narrow line widths on their NMR spectra suggesting a very high degree of order at an atomic level for both species, although the fibres would be macroscopically disordered (van der Wel et al., 2007).

### 4.1.2. Assembly

Elucidation of the first crystal structure of GNNQQNY, the monoclinic form 1YJP, led Nelson *et. al.* to suggest three stages of assembly. In the first stage, β-strands rapidly align to form a parallel β-sheet (Nelson et al., 2005). The β-sheets then associate more slowly to form the pair-of-sheets structure that has the characteristic dry interface. Because this association is not well defined it is conceivable that this stage could be responsible for the polymorphisms seen for this peptide (Nelson et al., 2005; Sawaya et al., 2007; van der Wel et al., 2007). Molecular dynamics simulations verified the stability of this structure even when it is composed of very few β-strands, although the number required to form the nucleus varied, and some results suggested the formation of antiparallel oligomers (Berryman et al., 2009; Esposito et al., 2008; Esposito et al., 2006; Lipfert et al., 2005; Meli et al., 2008; Strodel et al., 2007; Vitagliano et al., 2008; Wang et al., 2008; Zhang et al., 2008; Zheng et al., 2006). The formation of this nucleus is the rate-limiting step to fibril formation and is proposed to account for the lag-phase observed for most amyloid assembly. After this unit has formed, peptides can add on more efficiently and the fibre grows rapidly. Van der Waals interactions between the side chains of the steric zipper and the formation of backbone hydrogen bonds and amide stacks stabilise the structure (Nelson et al., 2005). Once the rate-limiting step is overcome and a nucleus is formed, high concentrations of monomer can drive fibrillisation (Nelson et al., 2005). Lastly, fibrils form from the assembly and formation of a wet interface between the pair-of-sheets structures (Nelson et al., 2005). This process is depicted in figure 4.2.

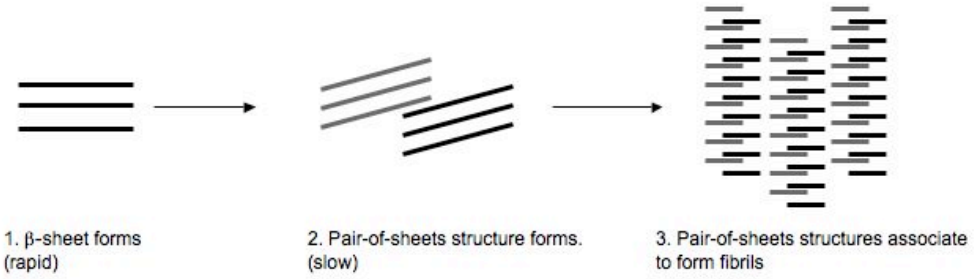


**Figure 4.2. Schematic showing the proposed assembly of GNNQQNY by Nelson *et.al.* (Nelson et al., 2005).** In the second stage residues interdigitate, variations in these bonding patterns may be responsible for polymorphisms (Nelson et al., 2005).

### 4.1.3. Experimental aims

GNNQQNY is one of the few amyloidogenic peptides that has been characterised by X-ray crystallography and therefore provides an excellent model system for further investigation. Although the previous work shows that both fibres and crystals share the cross-β arrangement (Nelson et al., 2005; van der Wel et al., 2007), it is not known if either crystal structure more accurately reflects that of the fibre, or whether they take on a different conformation. The polymorphism observed for GNNQQNY may be due to preparation conditions, in which case it is appropriate to question the relevance of the crystal structures of this peptide to fibrillar forms. Conditions required to form crystals of amyloid forming peptides may promote a molecular arrangement that may be dramatically different to that in fibrils. Furthermore, crystal structures represent a static view and would miss any structural changes that may accompany assembly. Understanding the conformational changes that occur as amyloid forms is as important as structural knowledge of the final polymorphs and may hold the key to elucidating what drives assembly and how to interfere with it. To investigate the assembly and structures of species observed on the pathway further, a combination of biophysical techniques were used to characterise the assembly and structural relationships between GNNQQNY fibres and crystals. Previous reports in the literature describe the assembly of GNNQQNY fibres and microcrystals to be concentration dependent phenomena and both are prepared by dissolving the peptide in water.

Table 4.1 summarises the different preparations other groups have used to obtain fibres and crystals. It is clear that there is no defined method for producing either form and the concentrations required vary greatly, for example Nelson *et. al.* report fibril formation at 0.3 mg/ml whereas Diaz-Avalos *et. al*. see no assembly at concentrations up to 5 mg/ml. A number of different concentrations were prepared and monitored over time to see if any of the above results could be duplicated and a single population of fibres and crystals obtained for further characterisation. In addition, there has been little investigation into the time-dependent assembly of fibres or crystals and only the end-point structures have been studied. In order to address this, at each of the concentrations tested, electron micrographs were taken at a series of time points in order to follow assembly. Tyrosine fluorescence measurements were taken concurrently with the EM images to investigate specifically the role of the tyrosine residue in the assembly of fibres and crystals. Circular dichroism (CD) and linear dichroism (LD) spectroscopy were also used to probe assembly and the environment of the tyrosine residue, and X-ray fibre diffraction carried out to compare the different forms structurally. This combination of techniques was used to give further insight and knowledge into the assembly and structure of GNNQQNY fibres and crystals and how they relate to one another.

## 4.2. Results and discussion

### 4.2.1. Following the assembly of fibres to crystals with microscopy, intrinsic tyrosine fluorescence and acrylamide quenching.

Several concentrations were prepared between 0.5 mg/ml and 15 mg/ml GNNQQNY peptide in water. Electron microscopy images showed that assembly began as soon as the peptide was dissolved in water (figure 4.3), therefore the concentration that was measured immediately after dissolution could not be altered. Attempts to keep the peptide in a monomeric state using other solvents proved unsuccessful (see section 3.3.1 and figure 3.1). As soon as the peptide was dissolved the concentration was measured and experiments started with no further treatment of the peptide solution.

For all concentrations tested between 0.5 mg/ml and 10 mg/ml fibres form initially, followed by crystals. Figure 4.3i and ii shows electron micrographs of fibres and crystals at three concentrations and are representative of all concentrations tested up to 10 mg/ml. For the lower concentration shown (1 mg/ml) very few fibres were visible at time 0, probably because assembly is limited by low peptide concentrations. However, even at <1 mg/ml some fibrillar material was seen at time 0 in almost all cases, despite centrifugation immediately after dissolution to attempt to remove preformed aggregates (data not shown). At 5 mg/ml assembly is apparently much faster and long fibres can be observed at time 0 (figure 4.3b.i). At the higher concentration of 10 mg/ml fibres can be seen to bundle at time 0 (figure 4.3c.i). In all cases crystals eventually form and the population of fibres is completely depleted. Previous reports(table 4.1) show that the production of fibres compared to crystals is concentration dependent, although the exact concentrations and times required for formation of either crystals or fibres vary between groups (Balbirnie et al., 2001; Diaz-Avalos et al.; Nelson et al., 2005; Sawaya et al., 2007; van der Wel et al., 2007). However, these studies have focused on the characterisation of the final stage species formed and not the assembly process. The results here show that crystals form *from* fibres and as concentration is increased, there is a higher abundance of fibres seen at time 0 which also correlates with a reduction in the lag phase in tyrosine fluorescence

(figure 4.3iii). van der Wel *et. al.* produced a sample that was a mixture of both orthorhombic and monoclinic crystals (van der Wel et al., 2007). Over time, the NMR signal that arose from the monoclinic crystals disappeared indicating a structural conversion from one crystal form to another (van der Wel et al., 2007). This is concurrent with these results that indicate the formation of crystals from fibres over time.

Corresponding tyrosine fluorescence plots for each concentration are shown in figure 4.3iii. There is a distinct lag phase at early time points that decreases in time as the concentration is raised.

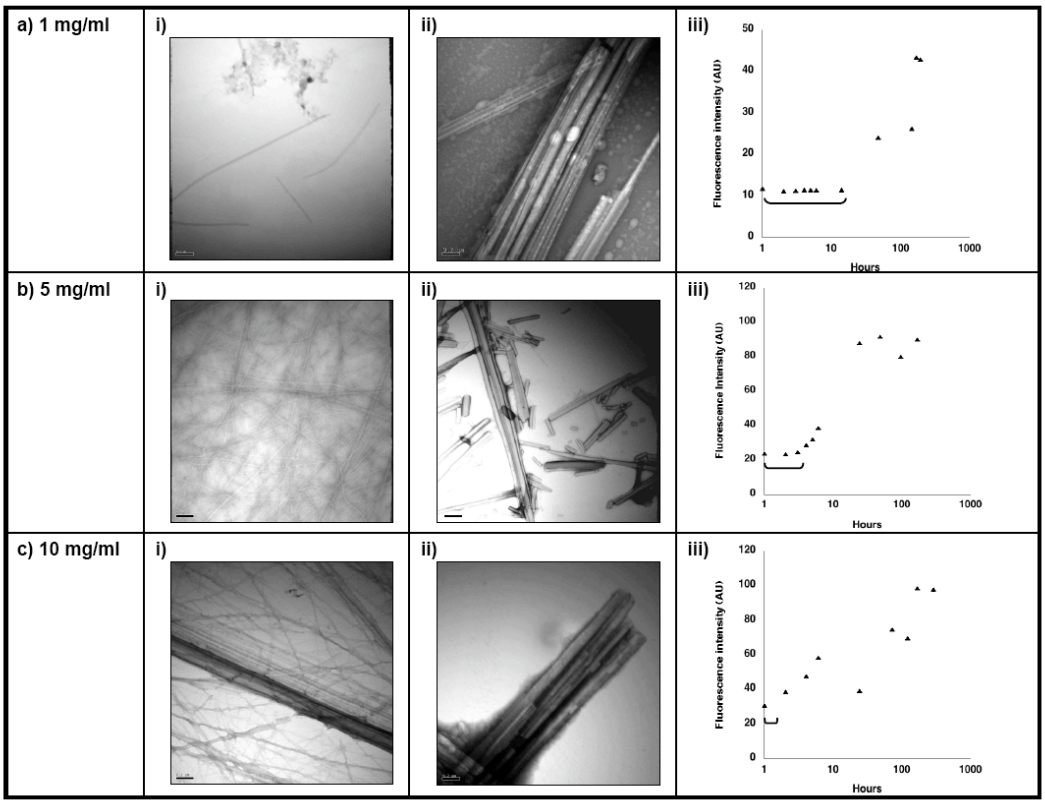


**Figure 4.3. Electron micrographs and tyrosine fluorescence of GNNQQNY at various concentrations.** a) 1.0 mg/ml at i) time 0 and ii) after 168 hours b) 5.0 mg/ml at 1) time 0 and ii) after 192 hours. c) 10 mg/ml at i) time 0 and ii) after 336 hours. Tyrosine fluorescence at 305 nm for each concentration is plotted on a log scale to show early time points more clearly and is shown in iii). The bars on the plots in iii illustrate the decreasing lag-phase with increasing concentration. The EM images shown in ii correspond to the last time point on the tyrosine fluorescence curves. Fibrillar species are observed during the exponential phase (see figure 4.5 for detailed EM analysis). Scale bars are 200 nm.

The width of fibres is generally around 5-10 nm although lateral association of fibres can be seen in some samples prior to crystal formation. These “ribbons” are around 20-60 nm, an example of this is given in figure 4.3c. The width of crystals varies but is generally between 200 nm and 400 nm. Atomic force microscopy measurements corroborated the results from electron microscopy (figure 4.4). AFM measurements on species with a width of around 80 nm (laterally associated fibres or ribbons) are around 4 nm (figure 4.4a), consistent with measurements on $\beta_2$-microglobulin fibrils (Gosal et al., 2005; Xue et al., 2009b). The height of the crystals is around 10 nm showing that the crystals are relatively flat (figure 4.4b.iii). This suggests that as crystals form there is growth in both width and height directions. AFM measurements also support the observation that crystals are much wider than the ribbons (300-400 nm and ~80 nm respectively). No AFM data from early stage fibres was obtained.

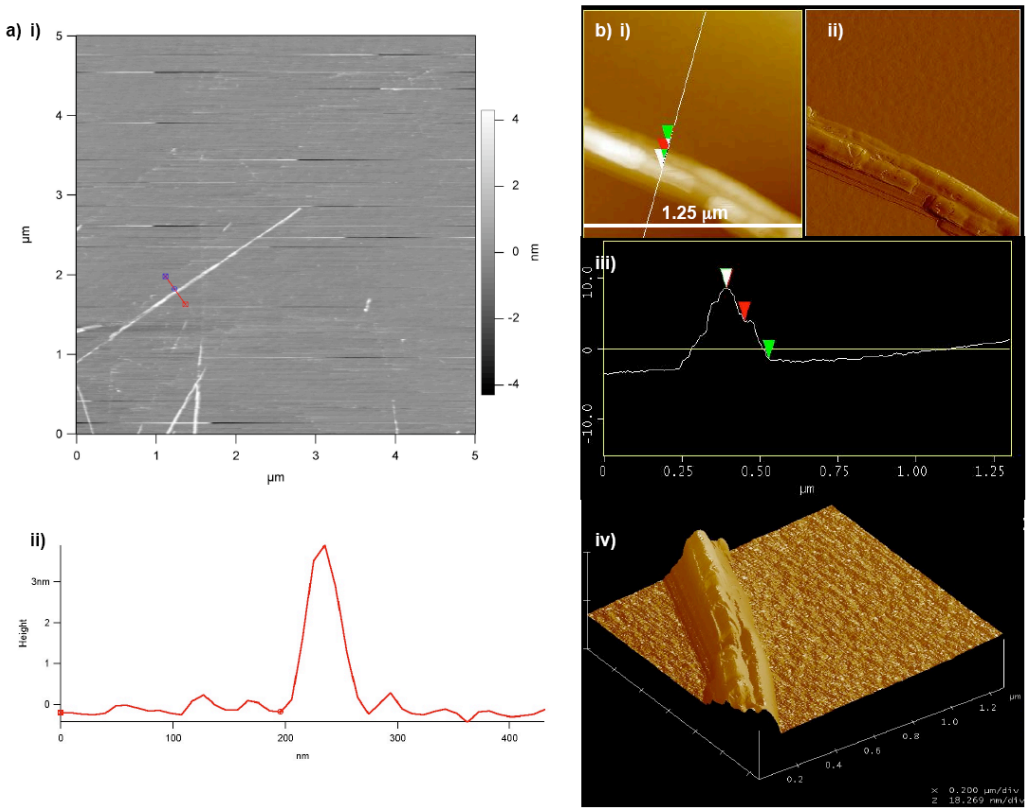


**Figure 4.4. Atomic force microscopy images and height measurements of GNNQQNY.** a) i) Height image of thinner species and ii) cross section showing height and width measurements. b) i) Height and ii) amplitude images of crystals. The width of the images is 1.25 µm. The amplitude image shows the height variations in the crystal. iii) Section of the crystal indicated by the line in i). The distance between the white and green points is 10.13 nm and between the white and red points is 4.69 nm. The width of the crystal is approximately 300 nm. iv) Surface image of the crystal.

The time it took for crystals only to form, and their resulting morphology, varied, even when it was possible to repeat the same concentration suggesting that assembly could be influenced by a wide number of external factors, for example agitation during transportation, exposure to surfaces (different types of container or cuvette may have an effect) and environmental temperature that is beyond control. This observation correlates with crystallisation experiments generally where formation of crystals can be promoted or hindered by many unintended influences (McPherson, 1999). The appearance of fibrils initially suggests that bonding is favoured in the hydrogen bonding direction i.e. the association of peptides into β-sheets. However, although the conversion to crystals is much slower, crystalline forms may represent the most stable arrangement that GNNQQNY can adopt.

The emergence of crystals and disappearance of fibres could potentially be explained by one of two pathways: either the fibres associate laterally to become crystalline, or crystals form via an entirely separate pathway. This pathway may involve monomer dissociation or fragmentation of existing fibres, which creates a pool of monomer (or other small species e.g. oligomers) that then go on to form crystals. It would seem that this dissociation is not reversible once crystals have formed, indicating their stability. In addition, it is possible that not all monomer is incorporated into the fibres, and this may add to the crystal rather than fibres. It is clear that there is a concentration dependence and that high peptide concentrations results in faster fibril formation. It may be that over time the fibrils formed at 15 mg/ml would convert to crystals, although this could not be ascertained during the course of these experiments. The crystals show characteristic features that distinguish them from other protein crystals grown and used for single crystal diffraction; they show directionality as one axis is significantly longer than the other in two dimensions, possibly indicating that even though the crystals are bigger in three dimensions compared to the fibres, they still retain a fibrous nature i.e. bonding is favoured in the fibre axis direction. Therefore, although these crystals are referred to as such, based on their appearance, ‘fibrous crystal’ is perhaps a more accurate term. Similar events have been observed previously in gelator systems where, fibres and crystals both formed from the same initial starting

material have shown to be structurally distinct (Moffat and Smith, 2008; Wang et al., 2008). It is not known which process is responsible for the formation of crystals from fibres but it is possible that that there is some kind of structural rearrangement occurring that leads to the formation of different species..

The previous work carried out on crystals and fibres of this peptide indicated that the tyrosine residue plays an important role in structure and assembly (Nelson et al., 2005; Sawaya et al., 2007; van der Wel et al., 2007). In particular, tyrosine showed to be mobile and MD simulations indicated that Y7A mutants of GNNQQNY had a decreased propensity to aggregate (Gsponer et al., 2003; van der Wel et al., 2007). The role of the tyrosine residue was investigated further by monitoring its fluorescence over time as crystals form and the population of fibres is depleted. Tyrosine fluorescence intensity was shown to increase as crystals formed, eventually reaching a plateau when crystals only were observed in EM (figure 4.3 iii). In order to attribute this increase specifically to changes in the environment of the tyrosine residue as the crystals form a sample was prepared that did not form crystals in the same time period and its tyrosine fluorescence also measured. Previous studies had shown that at higher concentrations it was less likely that crystals would be the predominant species (Diaz-Avalos et al., 2003; van der Wel et al., 2007) so a concentration of 15 mg/ml was monitored by EM and did remain as fibres in this time frame. This is shown in the figure below, along with a more detailed time course for a sample representative of those in figure 4.4 above, prepared at 3 mg/ml.

It is clear from these results that low tyrosine fluorescence arises from the presence of fibres and an increase correlates with the formation of crystals. The 15 mg/ml sample remained fibrillar throughout the course of the experiment and no increase in tyrosine fluorescence was observed. The tyrosine fluorescence curve for 3 mg/ml shows a lag phase up to 3 hours at which time the intensity starts to increase. At 72 hours EM images show the presence of crystals only and it is at this time point that the tyrosine fluorescence no longer increases and remains constant. Similar results are seen for concentrations up to 10 mg/ml with tyrosine fluorescence showing a lag phase, then a

steady increase and finally a plateau where only crystals are present and all fibrillar material has disappeared from the background completely (figure 4.3iii).

Tyrosine fluorescence increases when the residue goes from a more solvent-exposed environment, where its fluorescence is quenched, to a more buried environment and has been used previously to examine structural changes that occur during amyloid fibril formation (Maji et al., 2005; Padrick and Miranker, 2002). Previous work by Maji *et. al.* showed that tyrosine fluorescence from $A\beta_{1-40}$ (where the phenylalanine residue at position 20 had been substituted for tyrosine) was sigmoidal in shape, similar to the results observed here (Maji et al., 2005). However, the assembly of this peptide is much slower than GNNQQNY (the time course was over several days) and the lag phase was attributed to small oligomeric intermediates, with the increase in fluorescence coinciding with the formation of fibrillar material, as corroborated by CD experiments (Maji et al., 2005). This work supports the conclusion that an increase in tyrosine fluorescence coincides with a structural rearrangement, in this case the formation of crystals. Indeed, if it were possible to measure tyrosine fluorescence on a much-reduced time-scale for the concentration used in these experiments, a two-stage assembly might be apparent as smaller species are depleted and fibres form, and then crystals at later time points. These results therefore show that the tyrosine residue becomes more buried as crystals form. To corroborate this, acrylamide quenching was used to monitor the extent of solvent exposure in the crystals and fibrils. Acrylamide has been used previously to quench the fluorescence of tyrosine in amyloid and give information on changes in its environment during fibrillisation (Dusa et al., 2006; Padrick and Miranker, 2001). A Stern-Volmer plot was generated for both fibres (taken at time 0) and crystals (formed after 168 hours) and is shown below.

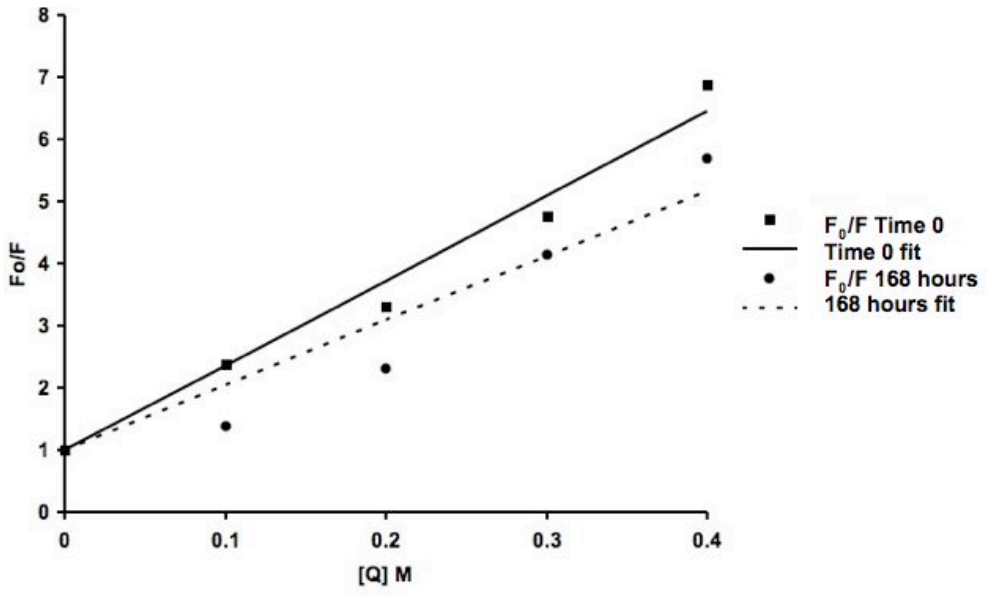


**Figure 4.6. Stern-Volmer plot for fibres and crystals formed from GNNQQNY.** Fibres are shown as squares and the straight line of best fit and crystals are shown as circles and the dashed line of best fit.

The slope of the line of best fit gives the $K_{SV}$ values for fibres and crystals. The $K_{SV}$ value is an indicator of how easily quenched a residue is; the higher it is the more readily the tyrosine is quenched. $K_{SV}$ values for fibres and crystals were 13.6 ± 0.6 $M^{-1}$ and 10.4 ± 0.1 $M^{-1}$ respectively suggesting that the tyrosine residue is more readily quenched, and therefore more accessible to solvent in fibres than in crystals. This is in agreement with the tyrosine fluorescence data where the fluorescence intensity was lower in the fibrils as it was more solvent-exposed, and therefore more quenched.

The reason for the tyrosine being more solvent exposed in the fibrils compared to the crystals may be because in the fibrils either the tyrosine residue is located on the surface, or it is exposed to solvent contained within the structure. Fluorescence from tyrosine that is solvent exposed is quenched by the carbonyl group in the peptide bond and only occurs when the peptide bond is in an aqueous environment (in non-aqueous solvents such as dioxane quenching is diminished), although the exact mechanism by which this occurs is unknown (Cowgill, 1975). Locating the tyrosine in a buried, hydrophobic environment will have the same effect of alleviating quenching (Cowgill, 1975). The tyrosine is located at the C-terminus of the peptide; as crystals form it is likely that this residue will become buried and therefore less solvent exposed. Changes

in the tyrosine fluorescence intensity are therefore due to changes in the environment of the tyrosine residue in fibres compared to crystals and it is possible that this change in environment coincides with a structural rearrangement.

### 4.2.2. Probing the structure of the fibres and crystals and the conformations accessed by the tyrosine residue using circular and linear dichroism

The results from tyrosine fluorescence and acrylamide quenching suggest that the tyrosine is undergoing a conformational change as crystals form. To further investigate any structural rearrangements that may be taking place as crystals form, circular dichroism (CD) and linear dichroism (LD) were carried out on fibres and crystals of GNNQQNY. For further experiments only concentrations below 10 mg/ml were used so that fibres and crystals that had grown from the same solution could be examined. The fibrils produced in the sample prepared at 15 mg/ml were not analysed further.

Initially, CD was used to further investigate the structures of the final stage species i.e. crystals formed from GNNQQNY. A typical spectrum that was obtained is shown in figure 4.7a and shows three positive maxima: a dominant peak at 204 nm, a smaller peak at approximately 235 nm and a small peak in the near-UV region at around 280 nm. This spectrum does not correspond to any of the classically observed CD signals and was thought to be due to LD effects. Linear dichroism is the differential absorption of light polarised parallel and perpendicular to an orientation axis and differs from CD in that signals will be obtained only from samples that are aligned and show directional dependence, e.g. amyloid fibres and crystals. Due to inefficiencies in the photoelastic modulator (required for light polarisation) in the CD instrument some linearly polarised light will be produced as well as circularly polarised light and, provided the sample is aligned, LD effects will be more pronounced than CD effects (Davidsson et al., 1980; Drake et al., 1988; Rodger et al., 2010). In order to test whether this unusual CD spectrum could be attributed to LD effects, LD was measured and is shown in figure 4.7b. In order to orient the fibres or crystals the sample is rotated in a Couette cell (figure 4.7b schematic). This aligns the sample so that the long axis of the fibre or crystal is oriented with the flow direction. Transition dipole moments within the

structure will also be aligned and by measuring the difference between the absorption of parallel and perpendicular linearly polarised light the orientations of these transition moments, and therefore particular chromophores, can be determined. This spectrum is very similar to the CD plot and confirms that LD effects are dominating CD signals, probably due to inherent alignment of the fibres or crystals.

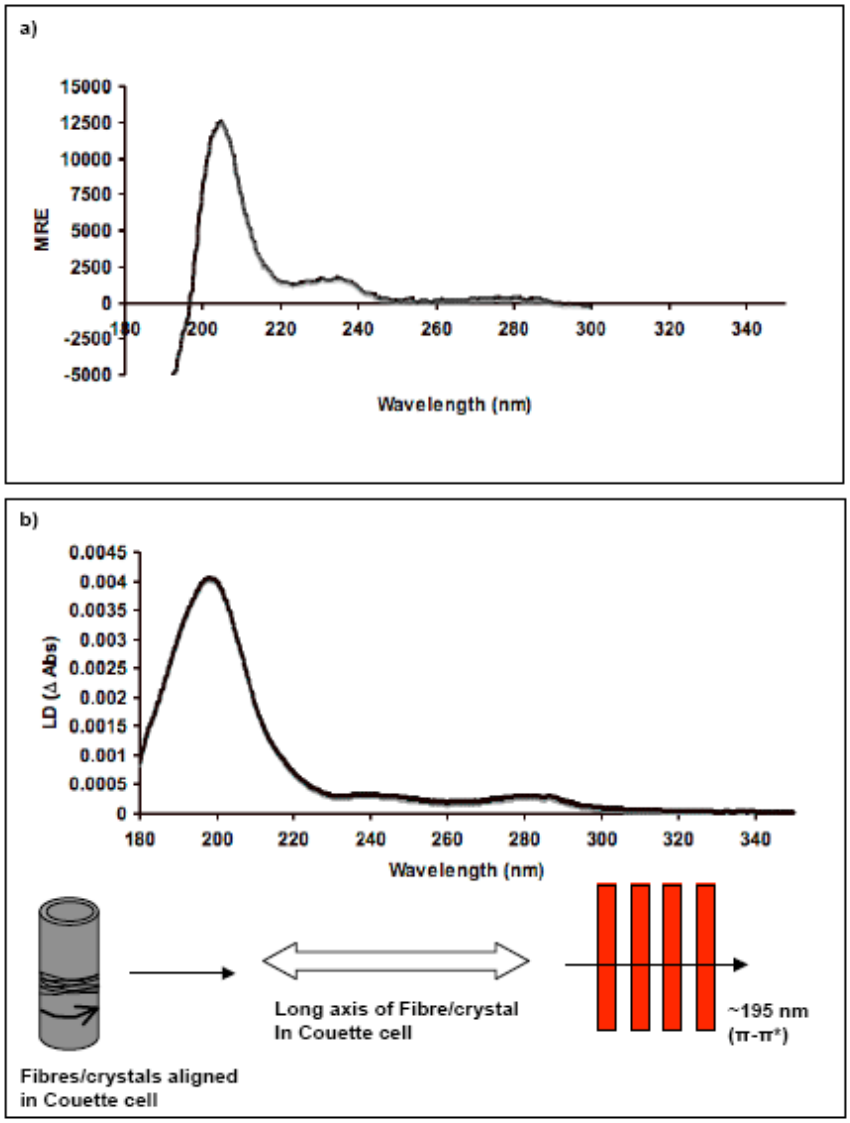


**Figure 4.7. a) CD and b) LD spectra of GNNQQNY crystals.** Samples were prepared at 5 mg/ml (CD) or 2 mg/ml (LD), incubated for several weeks to ensure the formation of crystals, then diluted to 2.5 mg/ml (CD) or 0.2 mg/ml (LD) (dilution was required to reduce absorbance and light scattering effects that would prevent sufficient light reaching the detector at lower wavelengths). The schematic shows the alignment of fibres or crystals in a Couette cell and the amide backbone transition moment at 195 nm perpendicular to the β-strands but parallel to the long axis of the fibre or crystal.

The dominant positive maximum at ~195 nm arises from the π-π* amide transition dipole moment being oriented perpendicular to the β-strands and is consistent with a cross-β structure (figure 4.7b) (Dafforn and Rodger, 2004). In addition to this signal, a smaller positive signal can be observed at ~230-240 nm along with a splitting of a peak in the aromatic region with maxima at 278 nm and 286 nm (shown in more detail in figure 4.8 below). When tyrosine residues are in close enough proximity they can undergo exciton coupling and contribute to LD spectra at these positions (Khan et al., 2007), suggesting that the tyrosine residues are also ordered within the crystal.

Inherent alignment of GNNQQNY crystals that were subject to CD was further investigated by measuring LD at a range of tilt angles from a sample in a CD cuvette. Crystalline samples were positioned in the holder and an LD scan taken. This gave a spectrum that showed similar maxima to the samples aligned in the Couette cell (figure. 4.7), except the signals were inverted i.e. were negative instead of positive. This inversion is due to the long axis of the crystals being oriented at 90° to those in the previous experiment. To demonstrate the directional nature of LD signals, this inherently aligned sample was rotated through 90° with readings taken at 10° tilt intervals. The resulting spectra are shown in figure 4.8.

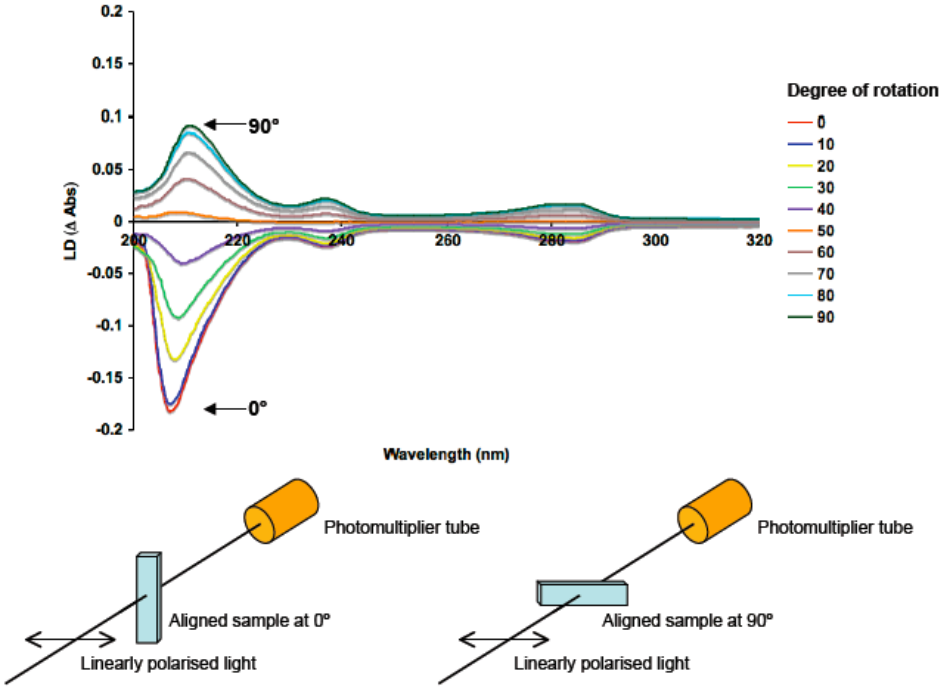


**Figure 4.8. LD spectra from an inherently aligned sample of GNNQQNY crystals at 10° interval tilts.** The schematic below shows the position of the cuvette at 0° and 90°. See chapter 6 figure 6.6 for further experimental details.

The magnitude of LD signals from a fibre depends on the following relationship:

$$LD^r = \frac{LD}{A} = \frac{3S}{2}\left(3\cos^2\alpha - 1\right)$$

where A is absorbance, S is the orientation parameter that defines how oriented the fibrils are (S=1 describes a perfect orientation and 0 is randomly oriented) and $\alpha$ is the angle between the orientation axis (i.e. the fibre axis) and the transition moment (Adachi et al., 2007; Dafforn and Rodger, 2004). If the angle of the transition moment is at 54.7° (the so-called "magic angle") relative to the parallel polarisation of light, the LD signal will be zero, as $(3\cos^2(54.7)-1)$ is zero (Bulheller and Hirst, 2009). Therefore, as the sample is tilted and the transition moment angles approach the magic angle, the LD signal reaches near zero. This illustrates how the orientation of the sample can affect LD (and in this case CD) signals and that an aligned sample is required in order to

gain an LD signal. Adachi *et. al.* carried out similar experiments to those shown here, whereby the CD of amyloidogenic fragments from $\beta_2$-microglobulin that were subject to flow were measured (Adachi et al., 2007). The resulting spectra were not typical of previously observed CD spectra and were similar to LD signals, except that the spectra were inverted, similar to the results here (Adachi et al., 2007). Measuring accurate CD spectra under these conditions is therefore not possible because of artefacts induced by inherent alignment. CD and LD measurements carried out at 2.5 mg/ml (figure 4.7a and figure 4.8) showed low wavelength peaks (204 nm and 210 nm respectively) that were shifted from the LD spectra obtained using Couette flow alignment (195 nm) measured at 0.2 mg/ml (figure 4.7b). Higher concentrations are generally required to achieve alignment in the absence of flow. At these raised concentrations the absorbance is too high at low wavelengths, so insufficient light reaches the detector. There may also be artefacts due to stray light and absorbance flattening (when signal intensity is reduced due to a decrease in concentration of particles able to absorb light, often observed in aggregating systems (Castiglioni et al., 2007; Ji and Urry, 1969)). This can result in a 'false' peak being created at an incorrect, higher wavelength (Hicks et al., 2010). The spectrum shown in figure 4.7b was more dilute to avoid these effects and can be considered 'correct'. These low wavelength data support a cross-$\beta$ structure for crystals of GNNQQNY.

Shear-flow LD, the most common method used for LD measurements as it provides effective alignment in dilute solution (figure 4.7b), was used for further experiments to obtain directional information on how the features observed in the previous spectra develop over time as crystals form and fibrils are depleted. LD has been used previously on fibres formed from the 22 residue K3 peptide fragment of $\beta_2$-microglobulin to reveal structural details regarding the orientation of the tyrosine residue with respect to the fibre axis (Adachi et al., 2007). The smaller peaks visible in the near-UV can report on the position of the tyrosine residue with respect to the fibre axis. Previous work on GNNQQNY fibres and crystals using solid state NMR highlighted the importance of the tyrosine residue in the structure of GNNQQNY and drew attention to its mobility (van der Wel et al., 2007). To investigate this further a time

course experiment was carried out on the peptide using linear dichroism to monitor any conformational changes, in particular in the tyrosine residue. The peptide was dissolved at a concentration of 2 mg/ml to ensure that the data could be compared with other experiments carried out previously. This concentration increased absorbance and light scattering and meant that data could be collected only at wavelengths greater than 215 nm i.e. only the aromatic contributions were measured. The peptide was dissolved in water placed into a Couette cell to induce alignment and spectra were taken at 8 minute intervals for approximately 8 hours.

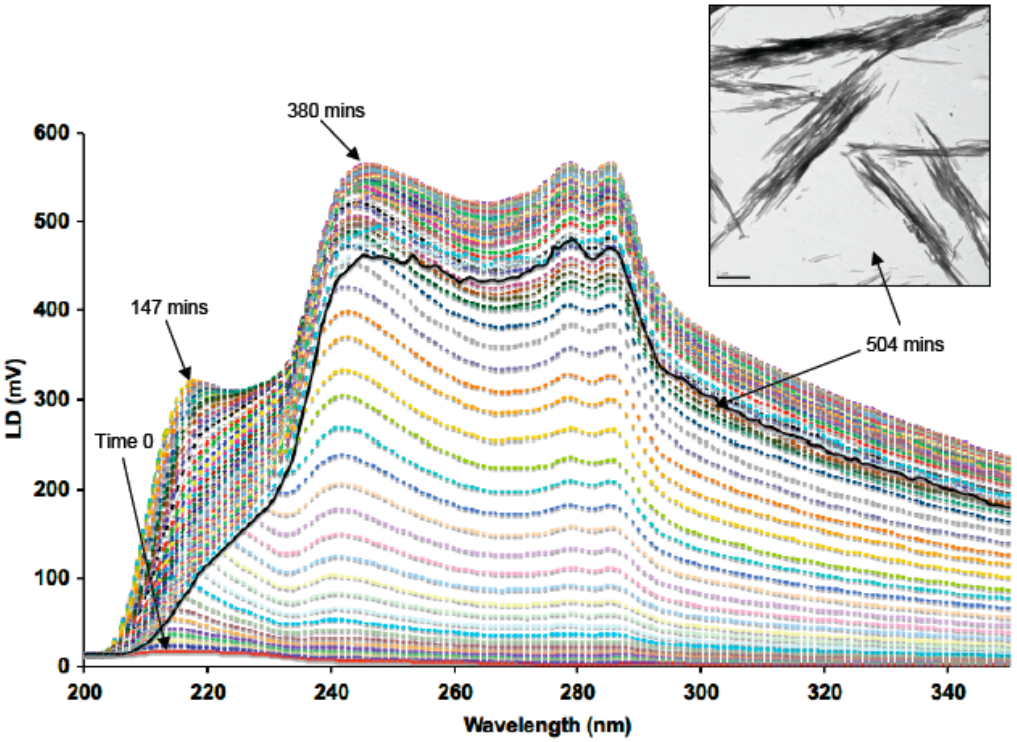


**Figure 4.9. Kinetic LD data of fibre and crystal formation from GNNQQNY under alignment.** Data shown from time 0 to 504 minutes (black line). The signal at 218 nm begins to decrease at 147 minutes and the signals at ~244 nm, 279 nm and 285 nm decrease much later, at approximately 380 minutes. The signals decrease due to the crystals being of sufficient size that they are precipitating out of the line of the beam (shown in the EM image in the inset (scale bar = 2 μm).

Figure 4.9 shows the LD signal over time up to the end point of 504 minutes (the black line). Generally, the signal increases as time proceeds, which correlates with the

lengthening and increased alignment of fibres and crystals induced by the Couette flow. This is consistent with the increase in light scattering that results in the increase in the baseline signal. At wavelengths where there is no absorbance (e.g. 300-320 nm) the baseline should be zero. The increase of the sloping baseline with time at these wavelengths means that the particles are increasing in size and therefore scattering more light away from the detector, which the instrument cannot distinguish from absorbance. It was not possible to accurately correct for light scattering in this instance, therefore positive and negative signals are regarded as such with respect to this baseline. The aromatic peaks at around 280 nm are clear in the spectra. From previous EM studies at this concentration (2 mg/ml) it is known that at time 0 fibres will be present. It should be noted that subjecting the sample to Couette flow from the initial time point is probably responsible for speeding up fibre and crystal formation (Hill et al., 2006) and at the final time point of 504 minutes only crystals are observed (figure 4.9 inset), much earlier than for the quiescent samples used in previous experiments.

The maxima at 218 nm arise from the n-$\pi^*$ backbone transition and the longer wavelength signals are from the tyrosine residues. As mentioned previously, the aromatic signals at ~280 nm suggest that the tyrosine residues are ordered within the fibres and crystals. Figure 10a shows the LD signal from the aromatic region for the first 10 scans (0 – 80 minutes).

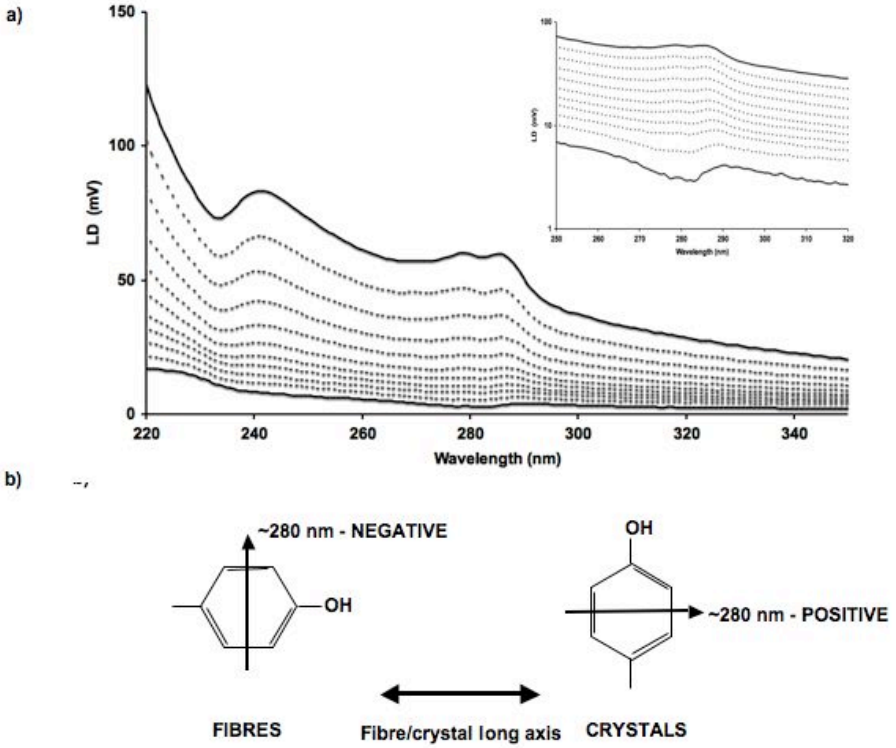


**Figure 4.10. LD spectra corresponding to the first 80 minutes of fibril/crystal formation by GNNQQNY.** The inset shows the inversion of the signal in the aromatic region 250-320 nm on a log scale.

The development of the signal from the tyrosine residues as crystals form can clearly be observed. Close inspection of the near-UV aromatic region shows splitting of the 280 nm peak that occurs when tyrosine residues are in close proximity, in this case either because they are located close to each other in the fibre axis direction and are stacked on top of one another, or potentially from proximity in the sheet spacing direction. In addition, an inversion of the aromatic signal (figure 4.10 inset) reveals a flip in the orientation of the tyrosine residue with respect to the fibre axis. As this signal depends on the directional nature of the tyrosine residues it can be deduced that inversion corresponds to a change in the orientation of the tyrosine side chain under conditions that lead to the development of crystals, consistent with other data that shows a change in environment. Therefore, the tyrosine residue occupies a different position in the two species; in the fibres the transition moment around 280 nm is oriented more perpendicular to the fibre axis whereas in the crystals it is more parallel to the fibre axis and gives a positive LD signal. The opposite can be seen for the

transition moment around 230 nm because this transition is perpendicular to the 280 nm transition in the aromatic ring of the tyrosine side chain.

These results clearly indicate that, at the concentrations tested, fibres form and then crystals and that the crystalline form of GNNQQNY is structurally different to the fibrillar form at the same concentration, especially in terms of the tyrosine residue. In order to further investigate the structures of fibres and crystals and how they compare to the crystal structures already published, fibre diffraction was carried out on these different species, continued in chapter 5.

## 4.3. Summary

In order to investigate the assembly of GNNQQNY into fibres and crystals, based on previous reports, concentrations of peptide in water were prepared ranging from 0.5 to 15 mg/ml and their assembly monitored by EM and tyrosine fluorescence. EM showed that at concentrations up to 10 mg/ml fibres form initially, followed by the appearance of crystals and eventually there is a complete depletion of fibrillar material. This suggests that crystals are the most stable form GNNQQNY can adopt, although the crystals do retain some fibril-like features. Tyrosine fluorescence experiments carried out alongside EM show a change in fluorescence intensity as crystals form from fibres. At 15 mg/ml, no crystals, only fibrils, formed in the time scale monitored, which provided a control sample. The lag phase seen at earlier time points corresponds with a population of fibres and is shortened with higher peptide concentrations. An increase in intensity is concurrent with a depletion of fibres and appearance of crystals. Eventually tyrosine fluorescence reaches a plateau where crystals only are observed in EM images. These results show that tyrosine is more solvent exposed in the fibrils than in the crystals, corroborated by acrylamide quenching experiments that gave higher $K_{SV}$ values for fibres. Further investigation into the change in environment of the tyrosine residue using LD revealed an inversion of the LD signal. This suggests that the tyrosine residue undergoes a flip in orientation, again coinciding with the change from fibres to crystals. CD experiments on crystals of

GNNQQNY gave unusual spectra that, after carrying out LD experiments, were interpreted as being due to overpowering LD contributions, as the LD signal from GNNQQNY crystals was remarkably similar. These results show that GNNQQNY is able to convert from one species to another, and that this conversion appears to be associated with a change in conformation of the tyrosine residue, resulting in different underlying structures between GNNQQNY polymorphs.

# 5. RESULTS AND DISCUSSION: Comparison of experimental and calculated fibre diffraction from GNNQQNY

## 5.1. Introduction

Previous studies have shown that GNNQQNY can form fibres, crystals and heterogenous mixtures of both (Balbirnie et al., 2001; Diaz-Avalos et al., 2003; Nelson et al., 2005; Sawaya et al., 2007; van der Wel et al., 2007). It has been established that the crystals can take on two forms, orthorhombic and monoclinic, and the structures of these have been elucidated and are shown in figure 4.1 (Balbirnie et al., 2001; Diaz-Avalos et al., 2003; Nelson et al., 2005; Sawaya et al., 2007; van der Wel et al., 2007). The existence of these two forms that differ significantly in the packing of the peptide, in particular around the tyrosine residue, along with evidence of multiple structural forms from solid-state NMR experiments (van der Wel et al., 2007) prompted further investigation into the structures of fibrils and crystals observed in the previous chapter using fibre diffraction. Firstly, experimental fibre diffraction was carried out on partially aligned fibres, crystals and a mixture of both species. Although crystals are referred to as such, compared to crystals generally used for single crystal diffraction those formed by GNNQQNY are significantly smaller and their size made in-house crystal data collection impossible. Furthermore, the crystals show obvious striations and their high ratio of length to width made them more amenable to fibre diffraction analysis.

## 5.2. Results and discussion

### 5.2.1. Experimental fibre diffraction

Data presented in chapter 4 shows that GNNQQNY forms fibres (at early time points), crystals (at late time points) or a mixture of both. Each of these preparations were placed in an X-ray beam and the resulting diffraction patterns are shown in figure 5.1. Reflection positions in the diffraction patterns were measured using the program CLEARER (Sumner Makin et al., 2007) (see section 3.1.8 for further details). As expected, all three patterns show reflections typical of a cross-β arrangement, with a strong meridional reflection at ~4.75 Å representing the hydrogen-bonding distance between the β-strands in the fibre axis direction. The characteristic cross-β equatorial reflections at around 10 Å thought to arise from the distance between the β-sheets are also present but interestingly these are at slightly different positions in the different preparations. The positions of the reflections are listed in the table below:

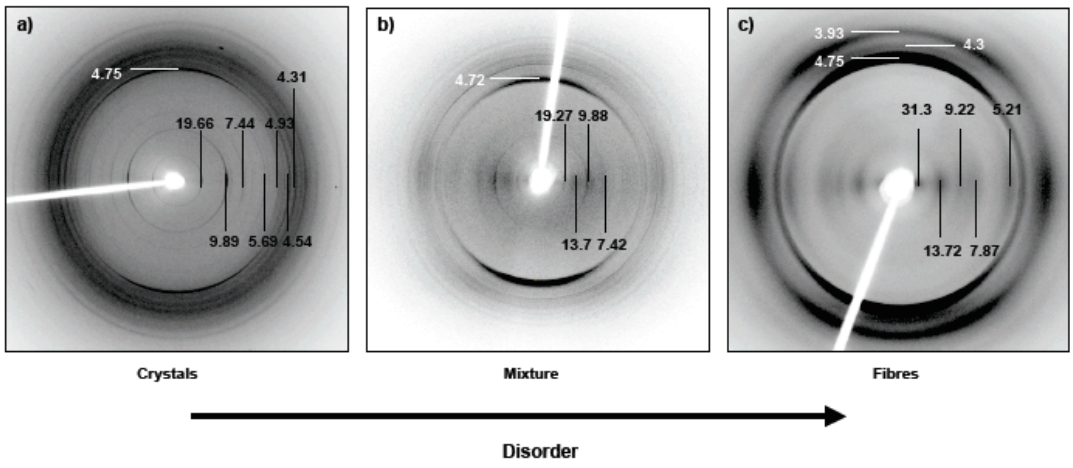


**Figure 5.1. Experimental fibre diffraction patterns from GNNNNQNY crystals, fibres and a mixture of both.** Numbers in black refer to equatorial reflections; numbers in white refer to meridional reflections. Units are given in Å.

| | Crystals | Mixture | Fibres |
|---|---|---|---|
| **Equatorial (Å)** | - | - | **31.30** |
| | **19.66** | - | - |
| | - | **19.27** | - |
| | 14.80 | **-** | **-** |
| | - | **13.70** | **13.72** |
| | 11.43 | - | - |
| | **9.89** | **9.88** | - |
| | - | - | **9.22** |
| | 9.06 | - | - |
| | - | - | **7.87** |
| | **7.44** | **7.42** | - |
| | **5.69** | - | - |
| | 5.47 | 5.49 | - |
| | - | - | **5.21** |
| | **4.93** | - | - |
| | 4.82 | - | - |
| | **4.54** | - | - |
| | **4.31** | - | - |
| | 4.02 | - | - |
| **Meridional (Å)** | **4.75** | **4.72** | **4.75** |
| | - | - | **4.30** |
| | - | - | **3.93** |
| | 3.50 | - | - |
| | - | - | 2.4 |

**Table 5.1. Reflection positions measured from experimental diffraction patterns of GNNQQNY fibres, crystals and a mixture of both**. Similarly positioned reflections (<=0.1 Å difference) are placed on the same row, a dash indicates no similar reflection was present. Numbers in bold are indicated in figure 5.1.

The sharpness of reflections decreases from crystals through to fibres, as would be expected for samples that have increasingly shorter coherence lengths, therefore making analysis somewhat less accurate for these samples. Coherence length refers to the length of a crystallite (ordered unit). When there is a long coherence length and crystallites are ordered over a long range, a reflection will be very intense and sharp. In a fibre, there will be most order along the length of the fibre axis where the β-strands stack on top of each other, and longer fibres will obviously have longer-range order. This means that for a fibrillar sample, there will generally be sharper reflections on the meridian compared to the equator, as the meridian corresponds to the fibre axis direction. Crystalline samples will have longer coherence lengths in not only the axis direction but also laterally, and therefore both meridional and equatorial reflections

will be strong and sharp. It should be noted that although for purposes of simplicity the term “crystal” is used, in fact the crystals of GNNQQNY are not as ordered as a protein crystal that undergoes single crystal diffraction might be. This observation is based on the appearance of a fibre diffraction pattern (arcs rather than spots), and inferences from EM images that show striated material, suggesting that they are more ordered in a particular direction. The fibre diffraction patterns arise because a bundle of crystals are placed into the X-ray beam, and not a single crystal, so they are not fully aligned to a vertical axis. Therefore, for fibrillar samples of GNNQQNY the reflections are more diffuse and less intense in the equatorial direction compared to crystals and compared to the meridional direction. However, approximate positions can still be determined. Table 5.1 lists the equatorial and meridional reflections measured in each sample. These measurements can give structural information on the species in each sample as they correspond to particular distances that are repeated throughout the fibre or crystal. For example, low-angle reflections i.e. those closer to the centre of the diffraction pattern, relate to long-range repeats in structures and arise from the chain length or width of protofilaments. On the meridian, low angle reflections may represent regularly spaced twists whereas on the equator they are likely to come from sheet spacing or chain length i.e width of protofilaments. Other reflections in the meridional direction will give detail on repeating units in the direction of the fibre axis i.e. the hydrogen bonding arrangement of the β-strands. Similarly, spacings in the equatorial direction will correspond to spacings in the other two dimensions (between β-sheets and along the length of the β-sheets, also known as the chain length). Comparison and analysis of reflection positions can reveal similarities and differences between species and inferences can be made with regards their structure.

Both crystals and fibres have unique reflections on the equator (19.66 Å in the crystals and 31.3 Å and 13.72 Å in the fibres) suggesting their internal architecture varies. The most intense equatorial reflections in the crystals, mixture and fibre samples are at 9.89 Å, 9.88 Å and 13.72 Å respectively. The fact that these reflections are the strongest is suggestive that they arise from the distance between β-sheets, which will be repeated throughout the whole of the fibre or crystal. The smaller distance in the crystals suggests that the steric zipper may be more tightly interdigitated in the crystal

than the fibre. Although the strongest reflection in the mixture is more consistent with the crystals, there is also an equatorial spacing similar to that in the fibres at 13.7 Å, showing that this sample contains both polymorphs. It is likely that the reason for the 9.88 Å reflection being more intense in the mixture sample is because the more ordered crystalline species give more intense reflections. Overall, all of the reflections in the mixed sample appear to be a combination of those from the crystals and fibres. To investigate the relationship between the experimental patterns to the published structures further, the experimental diffraction was compared to simulated patterns.

### 5.2.2. Simulation of fibre diffraction patterns from crystal structures

In order to compare the fibre diffraction patterns obtained experimentally with the published crystal structures, the pdb co-ordinates from the published structures 1YJP (Nelson et al., 2005) and 2OMM (Sawaya et al., 2007) were used to generate simulated fibre diffraction patterns using the program CLEARER (Sumner Makin et al., 2007) (figure 5.2 and table 5.2). In order to calculate a diffraction pattern, firstly the minimum unit (distinct from the unit cell) required to recreate the correct packing arrangement in the entire crystal must be generated from a model structure, in this case the crystal structures 1YJP and 2OMM (Nelson et al., 2005; Sawaya et al., 2007). The minimum units required for 1YJP and 2OMM were 2 and 4 molecules respectively. Once the minimum units had been generated using PyMol (DeLano scientific, CA, USA) they were input into CLEARER along with the corresponding unit cell dimensions. The program then built up repeating units into a crystal lattice using symmetry operations as defined in the pdb file. The lattice arrangement was verified as correct by comparison to the crystal structures visualised in PyMol (DeLano scientific, CA, USA). Diffraction settings were input to correspond to experimental data and the structure oriented so that the axes matched those used experimentally i.e. that the X-ray beam was oriented perpendicular to the fibre axis (see section 3.1.9). Structures were also generated with and without water molecules present, although this was found to make no difference to the resulting simulation.

Reflection positions in the calculated patterns were measured and indexed using the unit cell dimensions from the relevant pdb file (table 5.2). CLEARER generates a list of reflections that would be expected in a diffraction pattern from the unit cell entered (see appendix iii and iv for lists). Using this list, the observed reflections can be identified and indexed, which would give detail on where particular reflections come from in a known structure. This allows a more complete examination of the experimental data and will also help to determine the relationship between fibre diffraction patterns and crystal structures.

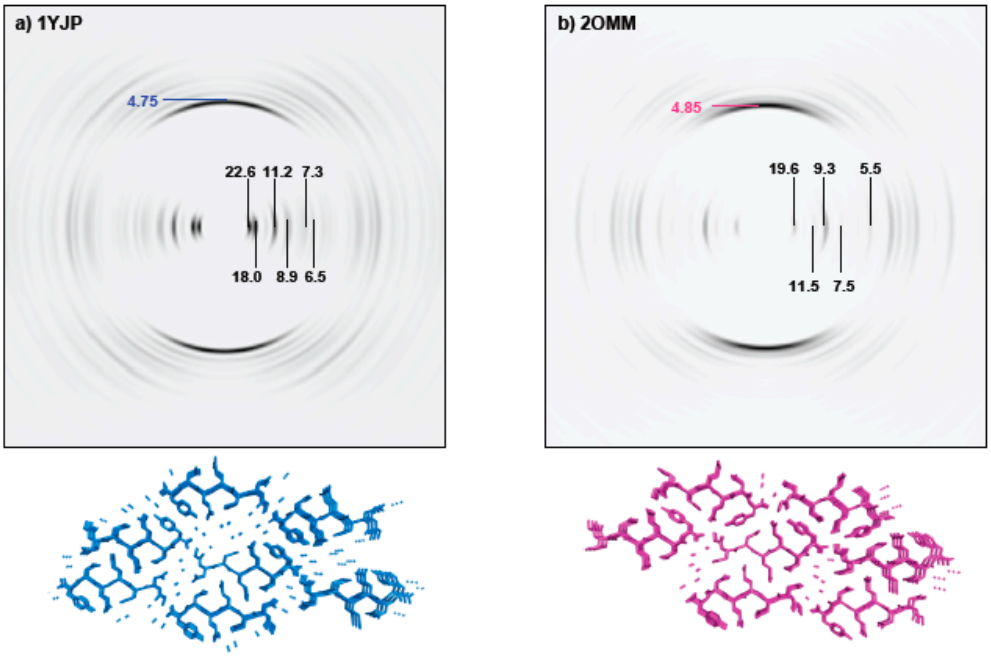


**Figure 5.2. Calculated fibre diffraction patterns and corresponding models of GNNQQNY crystal structures.** Simulations of diffraction patterns from 1YJP and 2OMM were produced using published unit cell co-ordinates (Nelson et al., 2005; Sawaya et al., 2007). Below each image are the corresponding models.

| | ***a*=21.94 Å *b*=4.87 Å *c*=23.48 Å** | | | ***a*=23.32 Å *b*=4.93 Å *c*=37.55 Å** | | |
|---|---|---|---|---|---|---|
| | **1 YJP ($P 2_1$)** | | | **2OMM ($P2_12_12_1$)** | | |
| | **Measured reflection** | **Miller indices [h k l]** | **Predicted reflection** | **Measured reflection** | **Miller indices [h k l]** | **Predicted reflection** |
| **Equatorial (Å)** | **22.6** | **[0 0 1]** | **22.44** | - | - | - |
| | - | - | - | **19.6** | **[0 0 2]** | **18.77** |
| | **18.0** | **[1 0 0]** | **20.97** | - | - | - |
| | - | - | - | 14.44 | [1 0 2] | 14.62 |
| | 13.8 | [1 0 1] | 13.48 | - | - | - |
| | **-** | **-** | **-** | **11.5** | **[2 0 0]** | **11.66** |
| | **11.2** | **[0 0 2]** | **11.22** | **-** | **-** | **-** |
| | **-** | **-** | **-** | **9.3** | **[0 0 4]** | **9.39** |
| | **8.9** | **[1 0 2]** | **8.87** | - | - | - |
| | **-** | **-** | **-** | **7.5** | **[3 0 1]** | **7.61** |
| | **7.3** | **[0 0 3]** | **7.48** | **-** | **-** | **-** |
| | **6.5** | **[1 0 3]** | **6.47** | - | - | - |
| | **-** | **-** | **-** | 6.2 | [0 0 6] | 6.25 |
| | 5.8 | [0 0 4] | 5.61 | - | - | - |
| | 5.4 | [2 0 3] | 5.39 | **5.5** | **[2 0 6]** | **5.51** |
| **Meridional (Å)** | - | - | - | **4.85** | **[0 1 1]** | **4.89** |
| | **4.75** | **[0 1 1]** | **4.76** | - | - | - |

**Table 5.2. Reflection positions measured and indexed from diffraction patterns calculated from co-ordinates published in 1yjp.pdb and 2omm.pdb**. Similarly positioned reflections (<=0.1 Å difference) are placed on the same row, a dash indicates no similar reflection was present. Those numbers in bold are indicated in the diagram above.

Analysis of the reflections reveals clear differences, as would be expected from the variations in the two structures, which crystallise in different unit cells and space groups and show different side chain packing, with particular differences around the tyrosine residue (Nelson et al., 2005; Sawaya et al., 2007). Using CLEARER, it was possible to index the reflections in the calculated patterns, as the unit cell dimensions are known. 1YJP crystallises in a monoclinic $P2_1$ space group. According to the unit cell for 1YJP, the *a* direction is defined as the sheet spacing (21.94 Å), *b* is the fibre axis direction and is 4.87 Å and *c* is the chain length (23.48 Å). However, because of the non-90° $\beta$ angle, these positions change slightly when indexed. Therefore, [1 0 0], instead of being 21.94 Å is actually at 20.97 Å. Similarly, [0 0 1], instead of being at 23.48 Å is at 22.44 Å. Both of these reflections are present in the simulation, although there is some error. This is because in addition to the information given by the unit cell

dimensions the structure will also have an impact on the resulting reflections. Furthermore, low angle reflections are more prone to error than those at high angles. For this space group, there will be systematic absences at odd [0 h 0], which corresponds to the fibre axis direction in the model. This means that the 4.87 Å reflection indexed as [0 1 0] (this spacing is not changed because the non-90° β angle lies between the *a* and *c* axes, therefore the *b* axis is not affected) in the list (see appendix iii) would not be expected to be present on the simulation, which it is not. The meridional reflection on the 1YJP calculation is measured as 4.75 Å, which is indexed as an off-meridional [0 1 1]. Therefore, the meridional reflection observed for the calculated diffraction pattern is not actually representative of the "real" spacing between the β-strands.

For the 2OMM calculation, the dimensions defined by the unit cell are identical to those predicted because in this case the unit cell is orthorhombic and therefore α, β and γ angles are all 90°. However, because of the space group ($P2_12_12_1$), systematic absences would be expected at odd [h 0 0], [0 k 0] and [0 0 l]. This explains why the reflections indexed as [1 0 0] (23.32 Å, the *a* dimension), [0 1 0] (4.93 Å, the *b* dimension) and [0 0 1] (37.55 Å, the *c* unit cell dimension) are not observed in the diffraction simulation. However, the [2 0 0] and [0 0 2] reflections (11.66 Å and 19.6 Å respectively) are present, although there is some error on the [0 0 2] reflection.

The "real" meridional spacings measured in the crystal structures using PyMOL are identical to the *b* dimensions for both structures, as would be expected from their [0 1 0] indexing. However, these distances (4.87 Å and 4.93 Å in 1YJP and 2OMM respectively) are somewhat larger than is typically expected for amyloid structures, which are commonly around 4.76 Å. This may reflect a slightly different packing arrangement in the crystals compared to how the peptides would be positioned in a fibril. The equatorial reflections come from sheet spacings and chain length and also differ between the two structures. Classically, in experimental patterns, the reflection with the highest intensity on the equator is at around 10-11 Å, depending on side chain composition and packing. In both unit cells the sheet spacing is in the *c* direction. In the two simulations the reflections are at 11.2 Å (indexed to 0 0 2]) and 9.3 Å

(indexed to [0 0 4]) in 1YJP and 2OMM respectively. The structures of 1YJP and 2OMM with their unit cells overlaid are shown below.

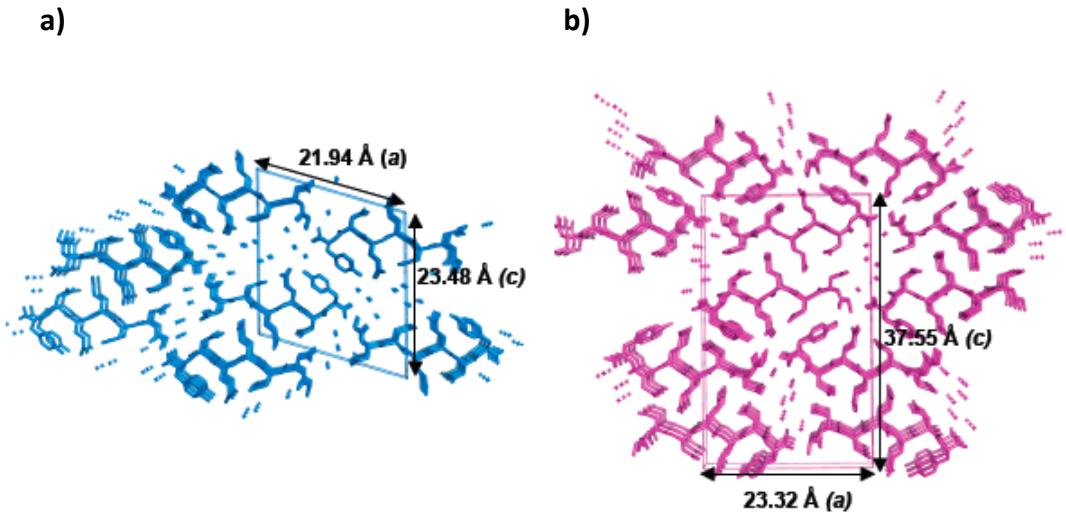


**Figure 5.3. Structures of a) 1YJP and b) 2OMM with unit cell overlaid (Nelson et al., 2005; Sawaya et al., 2007).**

It is clear from the crystal structures shown in figure 5.3 that 2OMM is more tightly packed than 1YJP, which would result in these variations on the equator.

### 5.2.3. Comparison of experimental and simulated fibre diffraction

Comparing the fibre diffraction patterns from experimental samples to simulations generated using the crystal structures can give information on how well the different species relate structurally to the published crystal structures. It also gives indications on how similar the fibres and crystals are to one another and therefore whether any structural rearrangement is taking place on the assembly pathway. A comparison of diffraction patterns from fibres, crystals and a mixture of both to the patterns calculated from the published unit cell co-ordinates from 1YJP and 2OMM along with a table of reflections are given below:

| | 1YJP | 2OMM | Crystals | Mixture | Fibres |
|---|---|---|---|---|---|
| **Equatorial (Å)** | - | - | - | - | 31.30 |
| | 22.6 | - | - | - | - |
| | - | 19.6 | 19.66 | 19.27 | - |
| | 18.0 | - | - | - | - |
| | - | 14.44 | 14.80 | - | - |
| | 13.8 | - | - | 13.70 | 13.72 |
| | - | 11.5 | 11.43 | - | - |
| | 11.2 | - | - | - | - |
| | - | - | 9.89 | 9.88 | - |
| | - | 9.3 | - | - | 9.22 |
| | 8.9 | - | 9.06 | - | - |
| | - | - | - | - | 7.87 |
| | - | 7.5 | 7.44 | 7.42 | - |
| | 7.3 | - | - | - | - |
| | 6.5 | - | - | - | - |
| | - | 6.2 | - | - | - |
| | 5.8 | - | - | - | - |
| | - | - | 5.69 | - | - |
| | 5.4 | 5.5 | 5.47 | 5.49 | - |
| | - | - | - | - | 5.21 |
| | - | - | 4.93 | - | - |
| | - | - | 4.82 | - | - |
| | - | - | 4.54 | - | - |
| | - | - | 4.31 | - | - |
| | - | - | 4.02 | - | - |
| **Meridional (Å)** | - | 4.85 | - | - | - |
| | 4.75 | - | 4.75 | 4.72 | 4.75 |

**Table 5.3. Comparison of reflection positions for fibre diffraction patterns calculated from 1yjp.pdb and 2omm.pdb with experimental patterns from fibres, crystals and a mixture of both.**

All three samples bear semblance to the simulations in some respect although less so for the fibres. Only the strongest meridional reflections are shown and match better to 1YJP. The difference between the hydrogen bonding dimensions in the two crystal structures is 0.06 Å; at the resolutions determined for these structures (1.8 Å for 1YJP and 2.0 Å for 2OMM) this is not significant and within experimental error compared to the experimentally determined reflections. Therefore, no further analysis was performed for the meridional spacings. However, the equatorial reflections from the crystals match more closely to 2OMM. In terms of equatorial reflections, there are five shared reflections between the experimental crystal pattern and the calculated 2OMM pattern, and two shared reflections between the experimental crystal and calculated 1YJP patterns. The water content of the two crystal structures varies, there is a wide

spacing at the wet interface of approximately 15 Å in 1YJP not present in 2OMM which is more tightly packed. This spacing would affect the structure and the resulting simulation and as the equatorial reflections do not match to 1YJP as well it could be conceived that for our samples 2OMM is the predominating crystal form. Importantly, the equatorial reflections in the diffraction patterns from fibres do not match either simulation well (only one shared reflection with both simulations). In particular the strong 13.7 Å reflection is missing in both 1YJP and 2OMM, perhaps corroborating the conclusion made earlier that fibres must rearrange structurally somehow to become crystals.

### 5.2.4. Unit cell measurements from experimental diffraction data

The information provided from the experimental fibre diffraction data made it possible to calculate unit cells that could be further compared to the previously published structural data (see table 4.2). For the unit cell optimisation, vector *b* was defined as the fibre axis and was set to 4.69 Å. The length of the peptides in both structures is around 20 Å, which corresponds well to a calculated length of 24.5 Å, using an approximation of 3.5 Å per amino acid in the peptide chain, since the peptides are not arranged end to end. It would be expected that this length would agree to one of the unit cell dimensions *b* or *c* (either is possible as all angles were set to 90°). The tables below show the unit cells calculated using the input experimental data.

**Table 5.4 CRYSTALS.** Unit cell prediction: a= 4.69 Å, b=19.68 Å, c= 22.82 Å

| Miller indices | | | d-spacings (Å) | | Error |
|---|---|---|---|---|---|
| **h** | **k** | **l** | **Calculated** | **Empirical** | % |
| 1 | 0 | 0 | 19.68 | 19.66 | -0.09 |
| 1 | 0 | 1 | 14.90 | 14.80 | -0.70 |
| 0 | 0 | 2 | 11.41 | 11.43 | 0.14 |
| 1 | 0 | 2 | 9.87 | 9.89 | 0.17 |
| 2 | 0 | 1 | 9.03 | 9.06 | 0.27 |
| 2 | 0 | 2 | 7.45 | 7.44 | -0.16 |

**Table 5.5 FIBRES.** Unit cell prediction: a= 4.69 Å, b=15.74 Å, c=27.61 Å

| Miller indices | | | d-spacings (Å) | | Error |
|---|---|---|---|---|---|
| **h** | **k** | **l** | **Calculated** | **Empirical** | % |
| 1 | 0 | 1 | 13.67 | 13.72 | 0.32 |
| 0 | 0 | 3 | 9.20 | 9.22 | 0.17 |
| 2 | 0 | 0 | 7.87 | 7.87 | -0.01 |
| 1 | 0 | 5 | 5.21 | 5.21 | -0.02 |

**Tables 5.4 and 5.5. Calculation of unit cells for crystals and fibres of GNNQQNY from experimental fibre diffraction data.**

The unit cells and indexings are compared to the previously published unit cell dimensions in the tables below.

| **Reference** | **Method** | **Space group** | **a** | **b** | **c** | **α** | **β** | **γ** |
|---|---|---|---|---|---|---|---|---|
| Balbirnie, 2001 | Powder diffraction | P 2 $2_1$ $2_1$ or P 2 $2_1$ 2 (orthorhombic) or P $2_1$ (β nearly 90°) (monoclinic) | 22.63 | 39.44 | 4.81 | 90 | 90 | 90 |
| Diaz-Avalos, 2003 | Electron diffraction | P $2_1$ $2_1$ $2_1$ (orthorhombic) | 22.7-21.2 | 39.9-39.3 | 4.89-4.86 | 90 | 90 | 90 |
| *Nelson, 2005* | *X-ray crystallography* | *P $2_1$ (monoclinic) 1YJP* | *21.94* | *4.87* | *23.48* | *90.00* | *107.08* | *90.00* |
| *Sawaya, 2007* | *X-ray crystallography* | *P $2_1$ $2_1$ $2_1$ (orthorhombic) 2OMM* | *23.32* | *4.93* | *37.55* | *90.00* | *90.00* | *90.00* |
| **CRYSTAL** | **FD** | | **19.68** | **4.69** | **22.83** | **90** | **90** | **90** |
| **FIBRE** | **FD** | | **15.74** | **4.69** | **27.61** | **90** | **90** | **90** |

**Table 5.6. Comparison of unit cells to previously published results.**

| *1YJP* | *2OMM* | [h k l] | Crystals | Fibres |
|---|---|---|---|---|
| *20.97* | *23.32* | **[1 0 0]** | 19.66 | - |
| *13.48* | *19.81* | **[1 0 1]** | 14.80 | 13.72 |
| *11.22* | *18.72* | **[0 0 2]** | 11.43 | - |
| *8.87* | *14.62* | **[1 0 2]** | 9.89 | - |
| *8.53* | *11.13* | **[2 0 1]** | 9.06 | - |
| *6.74* | *9.90* | **[2 0 2]** | 7.44 | - |
| *7.48* | *15.52* | **[0 0 3]** | - | 9.20 |
| *10.49* | *11.66* | **[2 0 0]** | - | 7.87 |
| *4.15* | *7.15* | **[1 0 5]** | - | 5.21 |

**Table 5.7. Comparison of indexed reflections from crystal data to experimental data.** See appendix iii and iv for crystal data.

Consistent with other data, the unit cell from the fibre diffraction pattern least matches any of the previously observed cell dimensions. Comparison of the indexed reflections from the calculated patterns with those observed experimentally (table 5.7) reveals that although on initial inspection the experimental pattern from GNNQQNY crystals match more closely to 2OMM, in fact the indexing is more like 1YJP. However, caution should be taken with this interpretation, as by default CLEARER will use an orthorhombic unit cell to index to, and 1YJP is monoclinic. Most importantly however, once again, the indexing of the reflections from the fibres does not match to either crystal structure.

## 5.3. Summary

Fibre diffraction was used on GNNQQNY fibres, crystals and a mixture of both to understand more about the underlying structures of the different species and compare them to the known crystal structures. Experimental fibre diffraction patterns from each sample show a typical cross-β diffraction pattern. Comparison of the measured reflections showed variations, suggesting differing internal architectures between fibres and crystals. The mixture contained reflections characteristic of both samples. There was a smaller sheet spacing in the crystals, suggesting this structure is more tightly interdigitated.

Using the two crystal structures of GNNQQNY (Nelson et al., 2005; Sawaya et al., 2007), diffraction patterns were calculated and their reflections measured and indexed. Comparing experimental diffraction patterns to those calculated from the crystal structures revealed that the fibres differ in structure not only to the crystals used in these experiments, but also to both crystal structures. The crystals used in experiments appear more like 2OMM, based on the positions of the reflections. Unit cells calculated from experimental data corroborates that fibres cannot be indexed to a unit cell consistent with either crystal type. Overall the FD results support a structural rearrangement as crystals form from fibres.

## 5.4. Conclusions (chapters 4 and 5)

This work aimed to explore the structural relationship between different polymorphs (fibres and crystals) formed by the same peptide GNNQQNY and highlight any similarities or differences that may exist between them. This investigation was partly based on the proposal that crystal structures of short amyloidogenic peptides are an accurate representation of amyloid structure (Sawaya et al., 2007).

Monitoring the assembly of GNNQQNY crystals showed that fibrils form initially and crystals at later time points and this is concurrent with a change in the environment of the tyrosine residue. CD proved to be an ineffective method for following secondary structure changes. LD was therefore used as the main spectroscopic technique for the analysis of fibres and crystals of GNNQQNY. LD analysis showed a change in the orientation of the tyrosine residue over time as crystals appear. Eventually, only crystals are observed indicating that these are the most stable form that GNNQQNY can adopt, as fibres do not appear at yet later time points (figure 5.5).

Experimental fibre diffraction patterns from fibres, crystals and a mixture of both also reveal that the peptide packing is different in the species and may arise from structural rearrangements that occur as crystals form. Other results that suggest the tyrosine residue is undergoing a conformational rearrangement indicate this may be associated with the gradual changes observed in diffraction patterns as crystals form from fibres. The lack of any disparity between the meridional reflections in experimental patterns suggests that it is the sheet spacing of the fibres that rearranges over time (figure 5.5). The larger sheet spacing in the fibres indicates that the interface is more solvent exposed, as the crystal forms (possibly driven by rearrangement of the tyrosine residue) a dry interface i.e. the steric zipper is formed, and the position of the reflection changes. This would fit well with the tyrosine fluorescence being more quenched in the fibrils, which may contain more solvent, compared to the crystals. As time proceeds the fibres appear to structurally rearrange themselves, suggesting that inherent differences must exist between fibres and crystals. Comparison of experimental diffraction patterns to those calculated from the two published

structures suggest that the crystals formed here are most consistent with the orthorhombic crystal form 2OMM and the fibrils do not closely relate to either crystal form published. This may be because the fibres take on some very different conformation to either crystal form. Unit cell comparisons corroborate that the fibrils are structurally different to the crystals and may indicate that both types of crystal structure are formed. These observations are illustrated in figure 5.5.

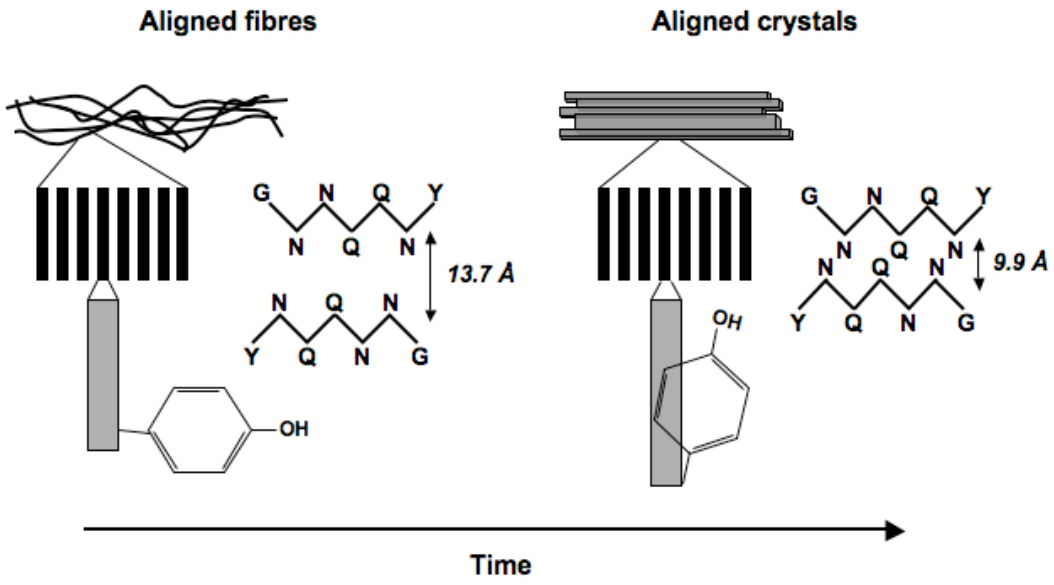


**Figure 5.5. Schematic showing differing structural features in fibrillar and crystalline GNNQQNY polymorphs.** As time proceeds, fibres form initially and crystals at later time points. Linear dichroism results from aligned fibres and crystals suggest a change in the orientation of the tyrosine residue as crystals form and fibre diffraction analysis supports a wider sheet spacing in fibres compared to crystals, possibly because they are more hydrated.

It has been proposed previously that crystals of GNNQQNY share many structural similarities with fibrils formed from the same peptide. The data presented here highlights both the similarities and differences between these species. In particular the role of the tyrosine residue is highlighted in line with other work that specifies aromatic residues as important drivers of fibrillisation and structure, for example FF pairs feature in Aβ and serum amyloid A protein (Gazit, 2002).

Using GNNQQNY as a model system provides information that has wider relevance to the field of amyloid formation from Q/N rich proteins such as Sup35. It was previously proposed that partial unfolding of the Q/N rich NM region of Sup35 would be sufficient for the instigation of self-assembly of the protein into amyloid fibrils and thus the $PrP^{Sc}$ conformation (Balbirnie et al., 2001). The results here support this finding, as the assembly of GNNQQNY is extremely fast with fibres visible immediately on dissolution of the peptide even at concentrations below 1 mg/ml. The main insight from these results however relates to the structures formed from GNNQQNY and its potential for polymorphism. The previous structural data suggested that the peptide could take on a variety of conformations and this is supported by this data. The fibres produced using the methods employed do not appear to share many similarities with either crystal structure previously published suggesting that perhaps this method, whilst supporting previous observations such as the cross-β arrangement, may not be the most appropriate way to determine amyloid structure. Rather, a combination of techniques, such as those employed here, can provide a more detailed analysis.

# 6. RESULTS AND DISCUSSION: Biophysical characterisation of variants of KFFEAAAKKFFE

## 6.1. Introduction

The peptide KFFEAAAKKFFE was designed based on the sequence KFFE, shown to be one of the shortest amyloid forming peptides known that meet electron microscopy (EM) and staining criteria (Tjernberg et al., 2002). KFFE was chosen for investigation based on evidence that short fragments from amyloidogenic proteins were capable of forming fibrils, suggesting that aggregation is initiated by particular regions (Taddei et al., 2001), and that these regions often contain hydrophobic residues, at least one of which is aromatic (Tjernberg et al., 2002). For example, FF pairs are present in Amyloid-β (Aβ) and serum amyloid A protein and the motif AAXK is found in α-synuclein (Makin et al., 2005). Original investigations were carried out on KFFE and the similar peptides KLLE and KAAE, which did not form fibrils and were observed only as random coil in circular dichroism (CD) spectra, whereas KFFE (and KVVE) showed partial β-strand conformation in solution (Tjernberg et al., 2002). Interestingly, the investigators also observed that the peptides KFFK and EFFE do not form fibrils on their own but do when mixed together. These results led to the conclusions that 1) β-strands are strong determinants of fibril formation, 2) the presence of aromatic residues is related to a high β-strand propensity, probably due to π-π stacking and 3) charge interactions are important in fibril formation; in this case the strands would be predicted to run anti-parallel to each other as K and E residues are known to pair (Tjernberg et al., 2002). The effect of the structural environment of KFFE on polymerisation was then investigated using either a turn motif (YNGK) or the less rigid hydrophobic sequence AAAK to fuse two KFFE peptides (Hosia et al., 2004). Only the AAAK construct formed fibrils, with the YNGK peptide forming a β-hairpin that could oligomerise into 12-mers but not fibrils (Hosia et al., 2004). It was suggested that AAAK forms more backbone hydrogen bonds (8 instead of 4 made by the β-hairpin) with neighbouring peptides due to its extended conformation as determined by CD, nuclear

magnetic resonance (NMR) and hydrogen-deuterium (H/D) exchange enabling it to form longer fibrils (Hosia et al., 2004).

Further work was subsequently undertaken to produce a high-resolution structural model using X-ray diffraction. Incubation of the peptide dissolved in phosphate buffered saline (PBS) at 5 mg/ml and agitated for 7 days produced fibrous crystals that were large and ordered enough to give X-ray fibre and electron diffraction data to resolutions of 2 Å and 0.9 Å respectively (Makin et al., 2005). The structure of the polypeptide as it exists in the crystal was solved; the consequent model revealing that β-strands run anti-parallel to one another, phenylalanine side chains closely interlock and electrostatic interactions help to stabilise the structure (Makin et al., 2005). The modelled structure is shown below, along with a schematic of the assembly of monomeric peptide into crystals. Peptide monomers are believed to assemble in an anti-parallel arrangement stabilised by salt bridges in the hydrogen bonding (fibre axis, *a*) direction between E4 on peptide 1 and K9 on peptide 2 and E12 on peptide 1 and K1 on peptide 2. Anti-parallel β-sheets make up the basic cross-β structure of the protofilament and these associate laterally into the crystalline species seen in the electron microscope.

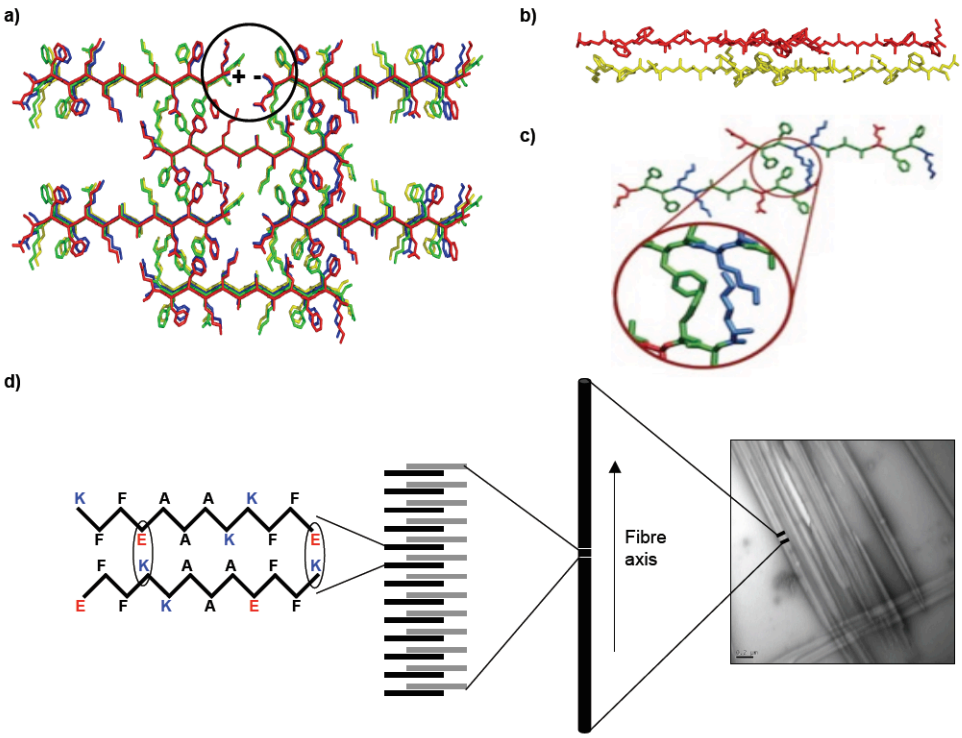


**Figure 6.1. Structure and assembly of amyloid-like fibrous crystals formed from the peptide KFFEAAAKKFFE (Makin et al., 2005).** a) View down the fibre axis (*a* axis). The peptides are stacked anti-parallel within each β-sheet and the β-sheets are in a cross-β arrangement. The resulting structure is held together by hydrogen bonds, π-π bonds between phenylalanine pairs and electrostatic interactions between E and K residues and is very rigid. b) Side view perpendicular to the fibre axis (*b* axis). c) Detail of the interaction between phenylalanine pairs within the structure. The peptide chains are coloured by residue type (blue: basic, red: acidic, green: non-polar) (Makin et al., 2005). d) Schematic of the structural hierarchy of KFFEAAAKKFFE fibrous crystals. Scale bar is 200 nm.

### 6.1.1. Experimental aims

The high-resolution structural detail available for amyloid fibres formed from KFFEAAAKKFFE made it an ideal model system on which to carry out further investigations into sequence-structure relationships i.e. how individual residues influence the structure and assembly of amyloid. The results could add to the understanding of how certain amino acids, or groups of residues, increase or decrease the propensity for amyloidogenicity and would aid in the establishment of rules for amyloid formation. Various mutants of KFFEAAAKKFFE (referred to hereafter as the

wild-type (WT) peptide) were constructed to explore the effects of making small changes to sequence on amyloid formation. Specifically, the roles of 1) hydrophobic interactions, in particular π-π stacking, 2) electrostatic interactions and 3) the charged N- and C-termini in amyloid formation and structure were examined. A range of biophysical techniques were used to examine differences in assembly and structure between the variants.

Phenylalanine/alanine (F/A) variants were constructed to examine the role of hydrophobic interactions and π-π stacking in fibrillisation and electrostatic interactions were investigated by mutating lysine residues to either alanine or arginine (lysine variants). In addition, a peptide with an acetyl cap on the N terminus and an amidated C terminus was made to examine the role of the charges at the end of the peptide in fibril and crystal formation. EM was used in the first instance to determine whether any fibrillar or crystalline species formed from both the WT peptide and the variants. Following this, CD, intrinsic phenylalanine fluorescence and thioflavin T fluorescence (ThT) were carried out alongside EM to give some information on how structure and assembly change over time by characterising the species at the start and end of fibrillisation. Far-UV CD was used to examine changes in secondary structure elements i.e. the peptide backbone that occur during assembly. The fluorescence of phenylalanine serves as a useful probe into its conformational environment (Krysmann et al., 2008; Sudhakar et al., 1993) and differences in the fluorescence intensity of the residue over time were measured. Amyloid specifically binds the dye Thioflavin T and this was also monitored using fluorescence to determine whether the species observed fit the classic amyloid defining criteria. Collating this information and correlating results from these techniques would gain insights into how the peptides assemble and how they compare structurally to the WT peptide. In addition, some of the peptide variants were added to cell cultures to determine any relationship between structure and toxicity.

The variants constructed were as follows:

$H_2N$-KFFEAAAKKFFE-COOH (WT peptide)
$CH_3CO$ – KFFEAAAKKFFE – $CONH_2$ (capped peptide)

Phenylalanine/Alanine (F/A) variants:
K**A**FEAAAKKFFE (F2A)
K**AA**EAAAKKFFE (F2AF3A)
KF**A**EAAAKKF**A**E (F3AF11A)
KFFEAAAKK**AA**E (F10F11A)
KFFEAAAKKF**A**E (F11A)

Lysine variants:
Lysine/Arginine (K/R) variants:
KFFEAAA**R**KFFE (K8R)
KFFEAAA**RR**FFE (K8RK9R)
KFFEAAAK**R**FFE (K9R)
**R**FFEAAAKKFFE (K1R)
**R**FFEAAA**R**KFFE (K1RK8R)
**R**FFEAAAK**R**FFE (K1RK9R)

Lysine/Alanine (K/A) variants:
KFFEAAA**A**KFFE (K8A)
KFFEAAA**AA**FFE (K8AK9A)
KFFEAAAK**A**FFE (K9A)
**A**FFEAAAKKFFE (K1A)
**A**FFEAAA**A**KFFE (K1AK8A)
**A**FFEAAAK**A**FFE (K1AK9A)

Lysine was mutated to either alanine or arginine to examine the effect of electrostatic interactions in amyloid assembly and structure, as lysine participates in the salt bridges that feature in the crystals formed by the WT sequence. Alanine was chosen because it diminished the positive charge of lysine that is thought to be important in fibrillisation and stabilisation. Also, its small size meant it should not impose any steric hindrance on the cross-$\beta$ structure. Arginine was chosen as an alternative mutation because of its close similarity to lysine and therefore may act as a control. Any differences in structural information between the K/R variants and the WT sequence would indicate that lysine is specifically required in the charge pairing interaction and that variations can occur from even small chemical differences between residues. The structures of

the residues are shown below and illustrate the similarities and differences between lysine, arginine and alanine. The core of amyloid fibrils are composed of β-sheets, therefore the propensity of each residue to form a β-sheet, based on the Chou-Fasman method, is indicated as P(b); higher numbers refer to increased propensities (Chou and Fasman, 1974). It should be noted that there are a number of different scales that describe the preference of an amino acid to be in a β-sheet that vary depending on the method of calculation (Chou and Fasman, 1974; Kim and Berg, 1993; Minor and Kim, 1994a; Minor and Kim; Smith et al., 1994). The structural context of the amino acid within the β-strand, for example whether it is near the N or C terminus, also influences its β-sheet forming propensity (Minor and Kim, 1994a; Street and Mayo, 1999). However, despite these discrepancies, the overall trends are the same and the values used here (the Chou-Fasman method) are a general representation.

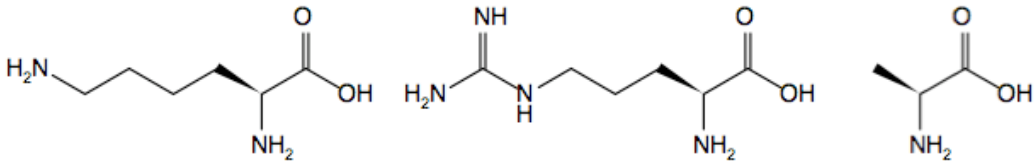


| | Lysine | Arginine | Alanine |
|---|---|---|---|
| **MW** | 146.19 | 174.20 | 89.09 |
| **p$K_a$ (R)** | 10.0 | 12.0 | n/a |
| **HI** | - 3.9 | -4.5 | 1.8 |
| **Volume (Å$^3$)** | 168.6 | 173.4 | 88.6 |
| **P(b)** | 74 | 93 | 83 |
| **pI** | 9.74 | 10.76 | 6.00 |

**Figure 6.2. Structures of lysine, arginine and alanine and their chemical properties.** HI refers to the hydropathy index and indicates how hydrophobic a residue is; the larger the number the more hydrophobic. The scale ranges from -4.5 (arginine) to 4.5 (isoleucine) (Kyte and Doolittle, 1982; Zamyatnin, 1972). pI refers to the isoelectric point of the individual amino acid and is the pH at which it has no net charge (Lide, 1991).

Both single and double K/A and K/R variants were made. In the WT structure the salt bridge is believed to form between antiparallel β-strands within the same β-sheet in the hydrogen bonding (fibre axis) direction. Specifically, E4 and E12 on one peptide form electrostatic interactions with K9 and K1 on another peptide, respectively (figure 6.1d). By systematically changing the K residues the influence of the salt bridge can be

investigated, with the K1AK9A variant expected to have the most dramatic effect as this variant should not be able to form salt bridges. Furthermore, because electrostatic interactions rely on charge, the effect of changing the overall net charge of the protein by dissolution in either PBS or water was investigated. Water was chosen to maintain simplicity in the system and to remove salt contributions to fibre diffraction patterns carried out later that can complicate interpretation (Makin and Serpell, 2005b). Preliminary experiments indicated that samples that were left quiescent underwent slower growth and at the end point fibres were either less abundant or shorter, although they did show similar morphologies in EM images. Therefore, to ensure the propagation of sufficient fibres on which to carry out biophysical analyses, all samples in the experiments carried out here were agitated.

The role of π-π stacking of aromatic residues in the WT sequence was examined in a similar way by performing an alanine scan of some of the phenylalanine residues. For these samples there are no appropriate controls as the residue closest in structure, tyrosine, contains an additional hydroxyl group on its benzene ring that dramatically alters its chemical properties. The aromatic interactions are shown in figure 6.1c. All four phenylalanine residues are thought to participate in the zipper and are believed to drive self-assembly via energetic contributions from π-π stacking (Makin et al., 2005). Therefore, selections of single and double variants were constructed to investigate if phenylalanine residues were essential for fibrillisation and whether pairs were required or a single phenylalanine residue within a pair would suffice. The mutations made were not exhaustive, the aim being to obtain preliminary insight into the role of these residues. As for the lysine variants, the F/A variants were dissolved in both PBS and water and agitated.

The association of KFFEAAAKKFFE into microcrystals may be partly influenced by the charged the N and C termini (positive and negative at pH 7.4 respectively). The role of the charged N and C termini in lateral association was explored using a peptide variant that had an amidated C terminus and an acetylated N terminus (referred to as the capped peptide). This abolished the charges at the N- and C-termini (at pH 7.4) and would give information on whether these charges are required for crystal formation. If

it was possible to form fibres from the peptide variants these could be analysed using the same biophysical methods and their structure and assembly compared to the crystals formed by the WT sequence. There is some controversy over the relationship between the structures of fibres and crystals formed from amyloidogenic peptides. This work would give insight into the possible mechanisms of crystal and fibril formation and any similarities or differences the two may share.

In summary, using the WT sequence, KFFEAAAKKFFE, and variants thereof, the roles of particular residues were examined to provide precise information on which interactions drive the assembly of amyloid and what structural features are imposed by changing the sequence. The results can be used to aid in the understanding of the general rules that accompany fibril formation, and the exploitation of self-assembly for designing materials using a bottom-up approach.

## 6.2. Results and discussion

### 6.2.1. Biophysical characterisation of the WT sequence, KFFEAAAKKFFE

The previous studies on KFFEAAAKKFFE provided some information on assembly and later work gave a full structural description of the peptide within the amyloid-like crystals (Hosia et al., 2004; Makin et al., 2005). In order to obtain data that would provide a basis for comparison of the variants, a more complete biophysical characterisation than had been performed in previous studies was initially carried out on the WT peptide. Firstly, electron microscopy was used to observe any macromolecular structures formed by the peptide both in water and PBS (pH 7.4) at time 0 (immediately after the peptide has been dissolved, vortexed, centrifuged and any pellet discarded) and 7 days. Previous results showed that KFFEAAAKKFFE did not assemble when agitated in water at 5 mg/ml and this was confirmed by electron microscopy (even after 1 year no fibrous or crystalline material formed). The concentration was increased up to 20 mg/ml to determine whether this was a concentration dependent phenomenon but still no material formed in water after 7 days with agitation, even at the highest concentration (figure 6.3).

a)

| *Time 0* | 5 mg/ml | 10 mg/ml | 20 mg/ml |
|---|---|---|---|
| Water | No fibrils observed | No fibrils observed | No fibrils observed |
| PBS | 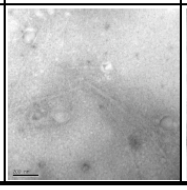 | 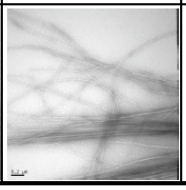 | 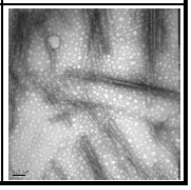 |

b)

| *7 days* | 5 mg/ml | 10 mg/ml | 20 mg/ml |
|---|---|---|---|
| Water | No fibrils observed | No fibrils observed | No fibrils observed |
| PBS | 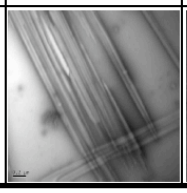 | 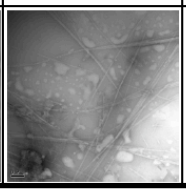 | 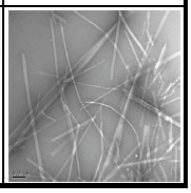 |

**Figure 6.3. Electron micrographs of KFFEAAAKKFFE at time 0 (a) and after 7 days agitation (b) at 5, 10 and 20 mg/ml.** Peptides were dissolved in either water or PBS (pH 7.4). Scale bars are 200 nm.

The inability of KFFEAAAKKFFE to form fibres or crystals in water may be due to the high positive net charge on the peptide in the solvent. In water, despite the lack of any buffer, the pH remained stable at pH 3.0 ± 0.5 (the low pH is likely to be due to residual trifluoroacetic acid in the lyophilised peptide preparation). At this pH the peptide will carry an overall charge of +4, whereas in PBS at pH 7.4 the charge will be +1. The net charge varies depending on pH and is calculated from the p$K_a$ of the ionisable groups in the peptide, in this case these are lysine (basic, p$K_a$ of 10.0) and glutamate (acidic, p$K_a$ of 4.4) and the N and C termini (p$K_a$'s of 8.0 and 3.1 respectively) (Stryer, 1999). When the p$K_a$ is higher than the pH of the solution, a proton will be transferred from the solution to the ionisable group because the solution will be the stronger acid. At pH 7.4 (when the peptide is dissolved in PBS) lysine and the N terminus will carry a charge of +1 and glutamate and the C terminus will have a charge of -1. Therefore the overall net charge of the WT sequence in PBS is +1, as there are three lysine residues and one N terminus carrying positive charges and two glutamate residues and one C terminus carrying a negative charge. In water, at low pH, the ionisable residues will be protonated, so lysine and the N terminus will be positively charged and glutamate and the C terminus will have no charge. Therefore, the WT peptide in water will carry an overall charge of +4. The higher charge on the peptide in water may cause repulsion of the molecules and prevent assembly.

KFFEAAAKKFFE assembled in PBS at all concentrations between 5 and 20 mg/ml although the species formed appeared to vary in morphology. At 5 mg/ml, thinner (10-50 nm) fibres appear initially (i.e. at time 0) with large, striated crystals (approximately 1 μm in width) of the type used in previous experiments forming at 7 days after agitation. At time 0, at 10 mg/ml and 20 mg/ml, fibres form in higher abundance and with a higher degree of lateral association (bundles are 200-300 nm in width) than at 5 mg/ml but after 7 days do not form crystals of the type seen at 5 mg/ml and remain as thinner, semi-crystalline looking species i.e. flat and straight but limited in width and lacking striations. It is clear from figure 6.3a (time 0) that increasing the concentration leads to faster growth, possibly because there are more nucleation points present. The formation of amyloid fibrils can be compared to the phases a protein goes through when forming a crystal, illustrated in the diagram below.

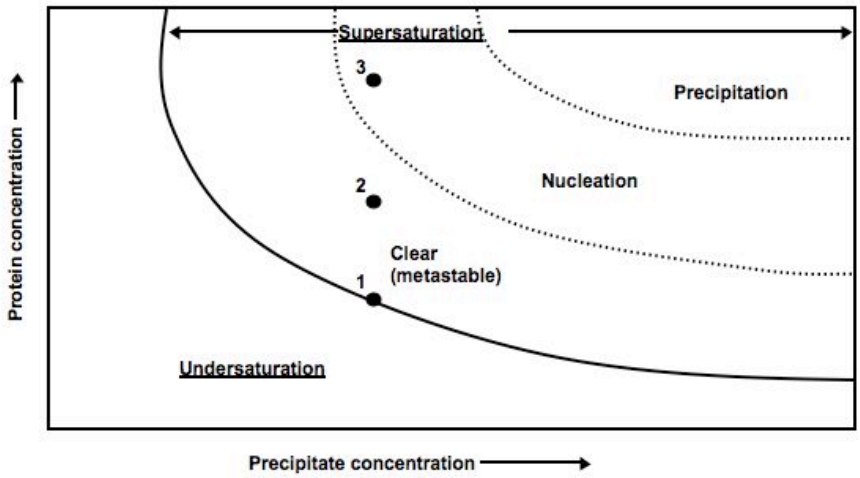


**Figure 6.4. A phase diagram of protein crystallisation relating protein and precipitate concentration.** Crystals will form only when the solution is supersaturated, when the concentration of protein or precipitate is too low the solution is undersaturated and no crystals will form. The events that may be occurring at 5, 10 and 20 mg/ml are indicated as circles 1,2 and 3 on the diagram respectively.

The diagram is divided into 2 regions: undersaturated and supersaturated (composed of clear, nucleation and precipitation regions). Saturation occurs when a system is in equilibrium and no more of the protein will dissolve in solvent. In an undersaturated solution, when protein or precipitant concentration is low, the protein will be fully dissolved and no precipitation will occur. If the protein or precipitant concentration is raised the solution starts to become supersaturated and the process of nucleation can begin. Nucleation points, or seeds, form in the metastable and nucleation zones of the diagram and this is where crystal growth takes place. After the primary nucleation event (seed formation) crystal growth is perpetuated by contact of the seed with other molecules to build up a three dimensional lattice. If the initial protein concentration is too high ordered nuclei will not form and the protein will precipitate out of solution as an amorphous aggregate.

The self-assembly of peptide molecules could be viewed as related to the ordered precipitation of molecules into protein crystals. In the case of the WT peptide, the precipitant concentration can be considered constant, as the concentration of PBS remains the same; the only variable is the protein concentration represented by circles in figure 6.4. The formation of amyloid fibrils has similarities with crystal formation in

that both require the generation of a critical nucleus (seed). This event is characterised by a slow lag phase; adding preformed seeds to solutions can speed up fibril or crystal growth. After this seed forms, assembly speeds up as monomers add to the growing fibre or crystal, inevitably affected by monomer concentration. The similarities between fibre and crystal growth have been observed previously (Come et al., 1993). At 5 mg/ml there are very few, short fibres at time 0. This is represented by circle 1 on the diagram, positioned on the edge of the undersaturation and metastable zones. The appearance of fibrils means that a nucleus has formed, however the short length of the fibres suggests that it is still early in the growth phase, which is limited by the lower monomer concentration. When the concentration is raised to 10 and 20 mg/ml (circles 2 and 3 respectively) longer fibres appear at time 0, some of which are bundled (more so at 20 mg/ml). As the solution becomes more supersaturated more nuclei will form, therefore more fibres will form and the increased monomer concentration can promote faster lengthening of the fibres. After 7 days, the crystals formed at 5 mg/ml are considerably wider (around 1 μm) than those species seen at 10 and 20 mg/ml. This is likely to be due to the slower, more controlled addition of monomer (or possibly small oligomers) to the seed, enabling growth in three dimensions. As fibres appear first, it is possible that they themselves act as a seed for crystal growth. Alternatively, crystal growth may occur through a separate pathway and with a different nuclear precursor. As fibres disappear in the 5 mg/ml sample, it is conceivable that fragments are able to dissociate from the fibres to form crystals on the separate pathway. At the higher concentrations at 7 days the crystals formed are much thinner, approximately 100 nm. This would suggest that at higher concentrations of monomer, when assembly is faster, addition is favoured in the hydrogen bonding direction. The striations in the crystal at 5 mg/ml corroborate this interpretation; although growth is occurring to a greater extent in three dimensions than at the higher concentrations, the favoured hydrogen bonding means that the crystals are more ordered in this direction than in the lateral direction, which causes the striated appearance.

It is clear that lowering concentration slows down the reaction from monomer to fibril and this correlates with the ability to form wider crystals. It is not possible to ascertain from electron micrographs whether there are any differences in terms of how the

peptide is arranged within the fibres and crystals that arise from preparation at different concentrations, but there are structural variations at a macromolecular level.

The KFFEAAAKKFFE crystals that underwent X-ray fibre and electron diffraction (Makin et al., 2005) were prepared at pH 7.4. Since the previous results clearly show that there is a relationship between net charge and the propensity to form fibrils or crystals the effect of changing the pH was further investigated. In addition, buffers were prepared without NaCl to confirm that the charge-charge interactions were important in assembly and were not being screened. Samples were set up in phosphoric acid (pH 2), phosphate buffer (pH 7.4) or disodium hydrogen phosphate (pH 12) and agitated for 7 days. There were no fibres or crystals visible by EM at either pH 2 or pH 12. At pH 7.4 the WT peptide formed crystals (data not shown) that looked very similar to those formed in PBS (see figure 6.3b at 5 mg/ml), indicating that neutral pH, and therefore a charge of +1, is optimal for assembly of the WT peptide. This is consistent with other studies that have highlighted the importance of charge in amyloid formation. Lopez de la Paz *et. al.* reported that highly charged peptides encouraged repulsion whereas neutral charges promote amorphous aggregation and therefore concluded that a charge of +1 was optimal for self-assembly (Lopez de la Paz and Serrano, 2004). In addition, the phosphate buffer did not contain NaCl, but the peptide was still able to form crystals suggesting that the charge-charge interactions are important and the NaCl is not able to screen them at the concentration used here of 10 mM. Previous work has assessed the ability of NaCl to screen charges and indicated that it is relatively inefficient at doing so, especially at low concentrations like that used in this work (Perez-Jimenez et al., 2004). Although it is clear that NaCl has no effect on assembly, for reasons of consistency with the previous studies of Makin *et. al*. PBS was used for the rest of the experiments, although NaCl was replaced with NaF in order to carry out CD experiments. Similar to water, at pH 2 the peptide would carry an overall charge of +4 whereas at pH 12 the overall charge would be -3. The reason for the inability of the peptide to form fibres or crystals, as before, is likely to be because the high net charge at these pH's cause repulsion of molecules. In addition, the charges at the N and C termini would no longer be zwitterionic at high or low pH's; at pH 2 the N terminus would be positively charged and the C terminus would have no charge and at

pH 12 the N terminus would have no charge and the C terminus would be negatively charged. The charges at the ends of the peptides therefore may also influence assembly.

Further biophysical characterisation was carried out on the wild-type peptide at 5 mg/ml in PBS (pH 7.4). Circular dichroism, intrinsic phenylalanine fluorescence and ThT binding were measured at time 0 and after 7 days (figure 6.5).

iii) iv)

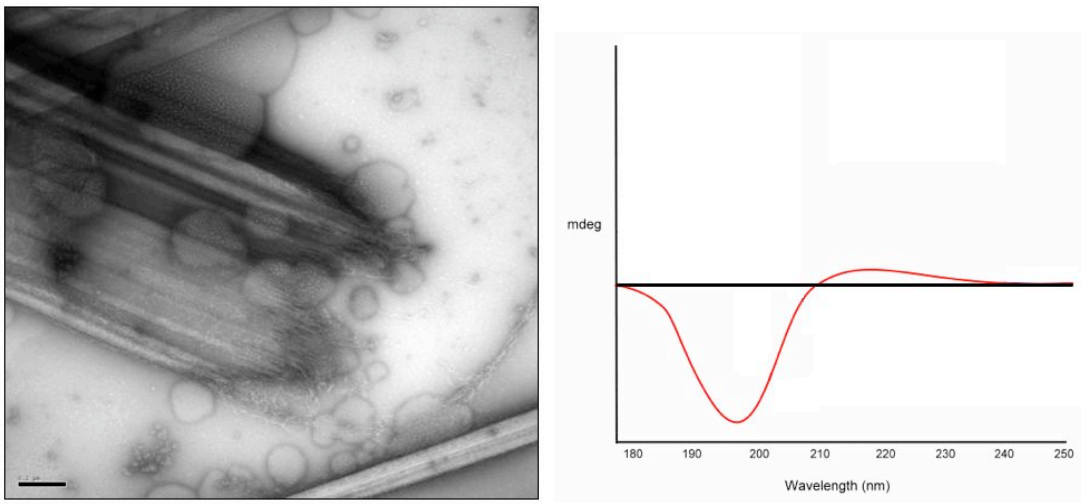


**Figure 6.5. KFFEAAAKKFFE in water (i) and PBS (ii). Electron micrographs at time 0 (a-scale bar 200 nm) and 7 days (b – scale bar 500 nm), far-UV CD spectra (c), intrinsic phenylalanine fluorescence (d) and Thioflavin T binding (e) at time 0 and after 7 days agitation. iii) A magnified image of the end of a crystal formed from the WT peptide in PBS (scale bar 200 nm). iv) Typical random coil spectrum (reproduced from www.proteinchemist.com).** Peptide was prepared at 5 mg/ml. The solubility of the peptide is indicated in the figure based on observation of a precipitate forming after dissolution and centrifugation; where no pellet was observed the box is coloured green (i.e more soluble), where a small pellet formed the box is coloured yellow and where a large pellet formed the box is coloured orange (i.e. less soluble). Where a precipitate was observed experiments were only carried out on the supernatant and the pellet was discarded. For spectroscopic measurements samples were diluted 1/10 with the appropriate buffer (PBS or water). In the case of CD this enabled the collection of low wavelength data. ThT was added to a final concentration of 50 μM and allowed to bind for 5 minutes before measurements were taken. The approximate widths of the species observed in EM are indicated in nm (measurements made using ImageJ (Abramoff et al., 2004).

In water, no fibrous crystals form (probably because the charge on the peptide at the low pH is too high and peptides cannot associate) and it may be assumed that the peptide is therefore in a monomeric state. The positive charge on both sides of the peptide (figure 6.5i) will aid in this repulsion. The lack of any assembly correlates with the results from CD, intrinsic fluorescence and ThT fluorescence as no change is observed after 7 days in any of these spectra. CD has been used previously on amyloid forming proteins to monitor the transition of monomeric peptide into β-sheet containing amyloid fibrils, for example α-synuclein (Serpell et al., 2000a) and in many

cases a random coil (positive signal at ~215 nm and negative signal at 195 nm) to β-sheet (positive signal at 195 nm and negative signal at 218 nm) transition is observed, as may be expected. The positions and intensities of the positive and negative signals observed in CD spectra result from the long-range order of the ϕ and ψ angles that the amino acid adopts in a particular conformation i.e. secondary structure. There are two electronic transitions in an amide bond, n→π* and π→π* that are positioned at approximately 220 nm and 190 nm respectively and are responsible for the positive and negative peaks in a random coil spectra (Rodger and Norden, 1997). For the WT peptide in water the spectra at both time 0 and 7 days are most consistent with random coil although there are three notable discrepancies when compared with a typical spectrum from poly-L-lysine (figure 6.5iv.) Firstly, the positive peak is red-shifted to the higher wavelength of 220 nm and the negative maxima blue-shifted to 190 nm. Secondly, there is a small but distinct negative peak at approximately 200 nm, indicated by the arrow in the figure. Lastly, the negative minimum at 195 nm in the classic spectrum (figure 6.5iv) is far more intense than the positive signal at 215 nm, whereas in the WT spectrum the ratio is much lower with MRE's for the negative and positive signals around 17000 and 5000 respectively. These shifts and changes in intensity may be due to the influence of the phenylalanine residues which although have maximum absorption in the near-UV region (250-300 nm) are known to also contribute to far-UV spectra (Rodger and Norden, 1997). CD can be highly sensitive to aromatic interactions and π-π stacking from species as small as dimers can greatly affect the spectra obtained (A.Rodger, personal communication). Alternatively, the spectra could be interpreted as an inverted β-sheet, although the lack of any fibril formation from EM would suggest that this explanation be precluded. It is possible that small, β-sheet containing species are formed by the WT peptide in water not visible by EM. However, in order to generate an inverted β-sheet signal some kind of orientation would have to occur and this is unlikely with small oligomeric species that are unlikely to display linearity.

To investigate these unusual CD spectra further and test for the effects of orientation a setup was employed where the sample was positioned at both 0° and 90° to the detector. A directionally dependent sample may be unintentionally aligned in different

ways e.g. pipetting or sliding the quartz cuvettes together, or it may be inherently oriented due to the linear nature of the fibres. Aligned, non-isotropic samples will exhibit linear dichroism (LD) as, due to inefficiencies in the photoelastic modulator, some linearly polarised light will exit along with the circularly polarised light. As LD effects are more powerful than CD it is possible that a LD signal could overwhelm or at least contribute to the CD spectra (Davidsson et al., 1980; Drake et al., 1988; Rodger et al., 2010). Therefore, if there were LD contributions, rotating the cuvette by 90° should invert the spectrum if the contribution was 100% or at least affect it if it was less than this (also see chapter 4, figure 4.8). The positioning of the cuvette in the spectrometer and the resulting spectra recorded from these positions for the WT peptide overlaid onto the spectra for time 0 and 7 days are shown below:

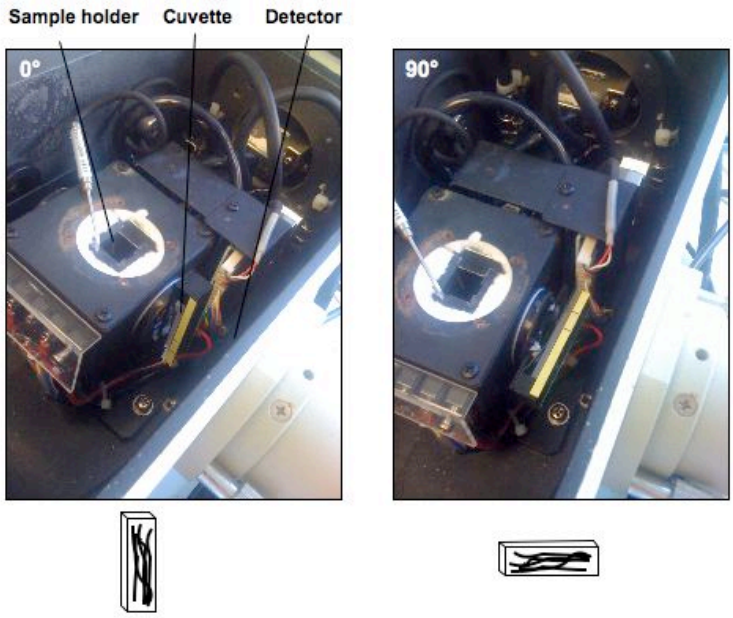


**Figure 6.6. Sample set-up for determining degree of alignment of amyloid species within the cuvette and whether linear dichroism is contributing to CD spectra.** Previous CD readings were taken with the sample in the cuvette and held in position in the sample holder. Here, readings were taken with the cuvette placed at the end of the sample holder, closer to the detector, where the cuvette could then be rotated 90°.

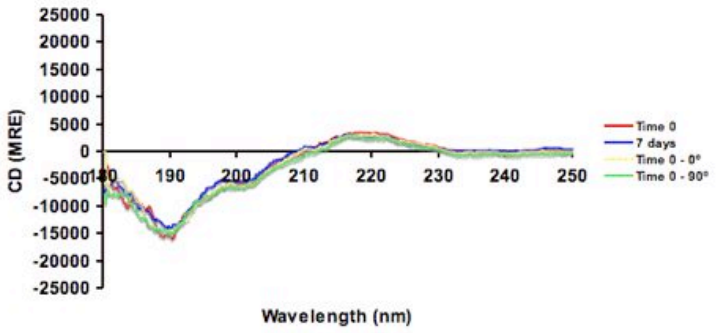


**Figure 6.7. CD spectra of KFFEAAAKKFFE in PBS in the sample holder at the original position, at 0° and at 90° to the detector.** The red and blue lines are the sample in the sample holder at time 0 and 7 days respectively (see figure 6.5ii.c), the yellow line is the sample placed closer to the detector (0° in figure 6.6) and the green line is the sample close to the detector but rotated 90°.

Because LD signals are orientation dependent, rotation will affect the spectrum and a rotation of 90° should invert the signal. Conversely, CD has no directional dependence and rotation will not affect the signal. Figure 6.7 clearly shows that rotating the sample has no effect on the signal. Therefore, the signal observed, although markedly different from the generally observed random coil spectrum, is most likely to be due to soluble, disordered peptide. However, it cannot be determined whether this is peptide is assembled into small oligomers, or whether it is monomeric.

CD experiments carried out by other groups on short peptides that are able to form amyloid-like fibrils have also shown spectra that differ from those classically reported for protein secondary structure. β-sheets normally show a negative maximum at around 216-218 nm. However, positive maxima at 200 and 217 nm have been observed for a dipeptide based on phenylalanine (Gupta M, 2007) and for the peptide FFKLVFF in methanol and TFE (Krysmann et al., 2007). The peak at 200 nm is thought to arise from a $\pi \rightarrow \pi^*$ transition and the 217 nm peak from an $n \rightarrow \pi^*$ transition (Gupta M, 2007). CD on FF nanotubes showed positive maxima at 200 nm and 217 nm, although these peaks were not ascribes to any particular transitions (Adler-Abramovich et al., 2006), whilst another group found that an Fmoc-FF hydrogel produced a spectrum with a negative at 218 nm that was attributed to β-sheet. Similarly, CD spectra from AFA showed positive maxima at 197 nm and 217 nm, this time thought to be due to a β-turn (Motta et al., 2005). A polyproline type II-like

conformation, with a predominant negative peak at around 200 nm and a relative positive at 217 nm (Drake et al., 1988) has been observed at early stages for the peptide Ac-A4KA2Y-NH2, which at later time points became characteristic of β-sheet as fibrils formed (Measey et al., 2009). Krysmann *et. al* also carried out CD on KLVFF at a concentration of 0.03 wt% (0.3 mg/ml) in water and PBS and 0.036 wt% and 0.018 wt% in TFE (Krysmann et al., 2008). In water and PBS there is a positive maximum at 198 nm and a broad peak at 210-220 nm, similar to previous work. In TFE the peak is at 196 nm and the broad peak is split into two maxima at 212 nm and 217 nm. This splitting is better resolved at the higher concentration. In addition all three samples showed negative maxima at 228 nm although the ellipticity was increased in the TFE samples. In another study on a related peptide, YYKLVFFC, a CD spectrum was observed that had positive maxima at 200 nm and 228 nm and a negative at 195 nm (Hamley et al., 2010). The authors claim that these spectral features are due to π-π stacking interactions between phenylalanine residues. The peaks at around 218 nm are consistent with the results shown here and are also likely to result from aromatic interference in the far-UV. Therefore, the CD spectra observed here, with a minimum at 190 nm, a shoulder minimum at approximately 202 nm and a maximum at ~219 nm probably arises either from disordered peptide but which does not correspond to the classically observed random coil spectra due to aromatic contributions, or it arises from some small but structured species that possibly influence the spectra due to some kind of aromatic interaction.

The peak for the intrinsic phenylalanine fluorescence (figure 6.5c) is at 283 nm and is the same intensity at both time 0 and 7 days. The fluorescence spectrum of phenylalanine in solution, with a similarly positioned peak at 280 nm is shown below.

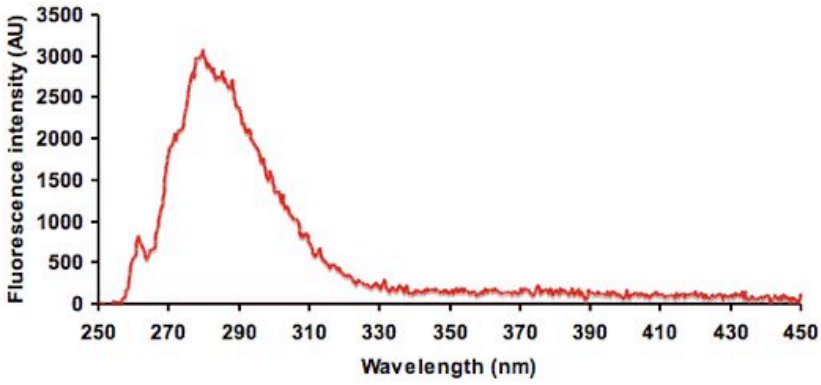


**Figure 6.8. Fluorescence spectrum of phenylalanine in solution (Du et al., 1998).**

Intrinsic fluorescence of phenylalanine has been used previously to help confirm the role of π-π stacking interactions in the self-assembly of amyloid (Krysmann et al., 2008). A spectrum with a peak at 313 nm was obtained with a very dilute solution (0.000003 wt% or 0.03 μg/ml) of the peptide KLVFF, thought to be due to the stacking of the phenylalanine units (Krysmann et al., 2007). The emission maximum observed here from the phenylalanine residues in the WT peptide is similar to that displayed by the amino acid on its own in solution (figure 6.8). For the WT peptide in water there is no additional emission peak at 313 nm, as expected for an unassembled disordered peptide that would not contain any stacked residues. Relating this to the CD data, this would suggest that if the reason for the unusual CD was due to soluble but structured species there was ether no π-π stacking in them, or it was not significant enough to be present in the intrinsic phenylalanine spectrum. Similarly, there is no thioflavin T fluorescence (figure 6.5ii.e) indicating that no amyloid-like structures have formed, consistent with other results.

In PBS (figure 6.5ii), very small fibres form at time 0 (approximately 10 nm in width and 1 μm in length) with crystals forming after 7 days. It is likely that this is due to the lowering of the net charge to +1 in this solvent. The alternating arrangement of amino acids within a β-strand may also have an effect; there is an overall positive charge on one side of the peptide (+2) and overall negative charge on the other side (-1) which possibly encourages assembly in the sheet-spacing direction as well as the charged N and C termini potentiating lateral (peptide end-to-end) assembly, thus leading to

crystal formation i.e. growth in all directions. However, the CD and intrinsic fluorescence spectra change only very little in intensity over time. Furthermore, the CD signal for the WT peptide in PBS is very similar to that in water (figure 6.5i and ii.c), despite the presence of microcrystals in EM. This could be explained if the signal is not coming from the assembled species i.e. the crystals, and is from soluble peptide that may be present, perhaps because not all of the initially solubilised peptide is incorporated into the crystals. It is also possible that monomers or oligomers are continually undergoing association and disassociation with the crystal and a constant pool of monomeric peptide is maintained in equilibrium with peptide assembled into crystals. The enlarged EM image of the end of a crystal (figure 6.5iv) shows what appear to be fibrils protruding from the end of the crystal suggesting that the crystal is composed of amyloid like fibres that are more ordered in their packing away from the ends. At this location, these fibres appear more disordered and may be less stable, providing a reservoir for the monomer visible to CD that is undergoing on-off reactions. The large size of the crystals means that they may precipitate out of solution and therefore become essentially invisible to CD spectroscopy, hence no β-sheet type structure is observed. There is a reduction in the intensity of the positive and negative signals in PBS compared to water (-17000 to -14000 and +4500 to +3000 respectively), likely to be due to the size of the crystals that form in PBS. Large aggregates in CD experiments can have two effects (see part 2.2.4). Firstly, they may scatter the light away from the detector, which would result in a false increase in absorbance, as is seen when baselines lie above zero in regions where there should be no absorbance (the raising of these baselines often correlating to increasing particle size). Secondly, absorbance flattening can reduce intensity of spectra in regions where proteins do absorb, due to a decrease in the concentration of soluble particles able to absorb light as they aggregate. The reduction in the signals observed here is therefore probably due to absorbance flattening, i.e. there is a reduction in soluble species, likely because they have been incorporated into larger aggregates, which are not contributing to CD.

The maximum intrinsic phenylalanine fluorescence for the WT peptide in PBS was the same as for the unassembled peptide in water, with a peak at 282 nm. However, there is an additional peak present at 302 nm, indicated by the arrow in the diagram.

Although this peak is at a lower wavelength than reported by Krysmann *et. al*. it may be due to π-π stacking within the fibres observed at time 0 and the crystals. Interestingly, this peak is also a feature at time 0, despite the presence of very few fibres by EM suggesting that aromatic interactions may manifest at very early stages of assembly. These observations validate the model previously proposed for the peptide which suggests π-π stacking as a structural feature and driving force of fibril assembly (Makin et al., 2005). The ThT data after 7 days (figure 6.5e) shows a peak at 485 nm indicating that the microcrystals are amyloid-like, consistent with previous data.

These results corroborate previous observations on KFFEAAKKFFE. The peptide does not appear to assemble in water but forms amyloid-like microcrystals in PBS. There is a difference in intrinsic phenylalanine fluorescence between unassembled and assembled WT peptide, namely that an additional peak at 303 nm appears when crystals form which could be attributed to π-π stacking. Furthermore, ThT fluoresces when added to microcrystals but not early stage species or monomeric peptide, confirming that the crystals are amyloid-like. These results provide a basis for comparison for the rest of the variants.

### 6.2.2. Capped peptide

Experiments were carried out on a variant of the WT peptide with capped, uncharged ends to determine the importance of the charges at the N and C terminus in fibril and crystal formation. Electron micrographs of the capped peptide at various concentrations are shown in figure 6.9 below.

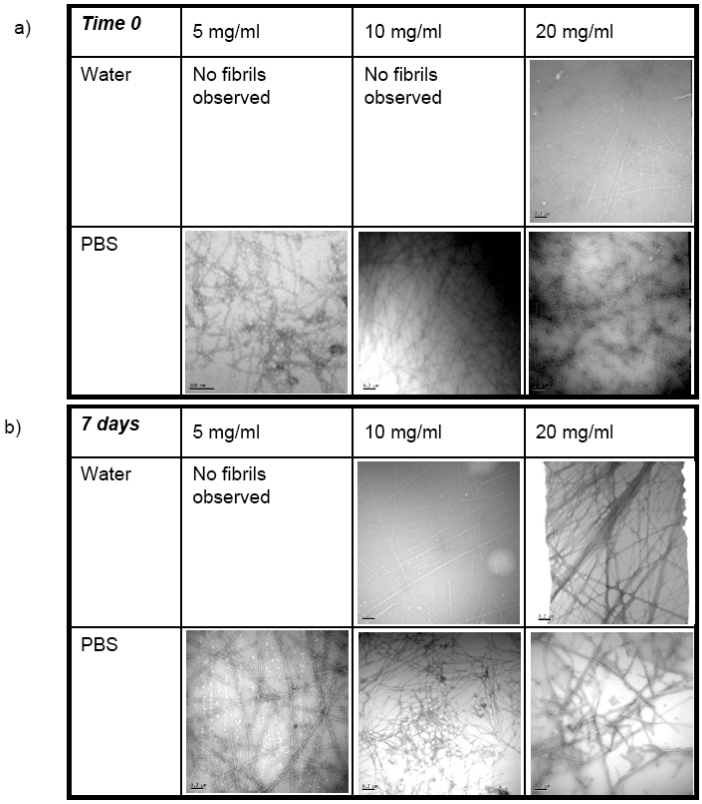


**Figure 6.9. Electron micrographs of Ac-KFFEAAAKKFFE-NH2 at time 0 (a) and after 7 days agitation (b) at 5, 10 and 20 mg/ml.** Peptides were dissolved in either water or PBS (pH 7.4). Scale bars are 200 nm.

The capped peptide has a net charge of +3 in water and, like the WT peptide, +1 in PBS. In water, at 5 and 10 mg/ml no fibres form at time 0. However, unlike the WT peptide, at 20 mg/ml fibres did form in water, even at time 0 (although far fewer were observed than at later time points). Furthermore, fibres eventually formed in water at 10 mg/ml after the solution had been agitated for 7 days, indicating that the slightly lower net charge enables fibril formation when the concentration is sufficiently high. In water, the glutamate residues will carry no charge, so no salt bridge should form, based on the WT model. However, fibres do form, implying that the salt bridge is not an absolute requirement for structural maintenance. Alternatively, the structure in

fibres formed from the capped peptide may differ significantly to the WT model. However, the slower formation of these fibres and their lower abundance means that the net charge still plays an important role and higher charges, as for the WT peptide, diminish the propensity for assembly. Fibres form in PBS at all concentrations and at all time points and appear similar to each other in morphology with widths of individual fibres consistently between approximately 5-50 nm and some of the wider assemblies being visibly composed of smaller protofilaments. In PBS, even at time 0 at the lowest concentration tested (5 mg/ml), far more material was observed by EM than for the WT peptide again suggesting that by reducing the charge and eliminating the charge at the ends of the peptide the propensity to form fibres is greatly increased. Unlike the WT peptide, changing concentrations did not appear to affect the overall morphology of this peptide and no large crystalline species are seen. This implies that the charges at the N and C termini are essential for the lateral association associated with crystal formation and corroborates the previous suggestion that assembly is favoured in the hydrogen bonding direction. As assembly along the fibril axis is not impeded by the potential for assembly in the lateral direction, fibrillisation is faster.

As for the WT peptide, assembly of the capped peptide was monitored at different pHs (figure 6.10).

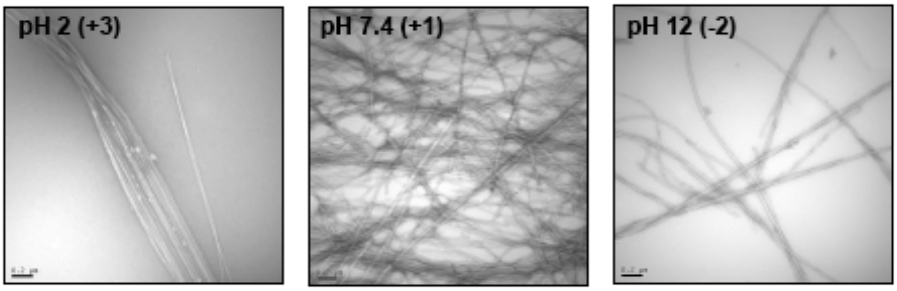


**Figure 6.10. Electron micrographs of Ac-KFFEAAAKKFFE-NH2 at various pH's.** The peptide was dissolved to a concentration of 5 mg/ml and agitated for 7 days. Buffer concentrations are all 10 mM. Scale bars are 200 nm.

In contrast to the WT peptide, at both pH 2 and pH 12 the capped peptide did form fibrils after 7 days agitation (figure 6.10) although compared to the fibrils seen at neutral pH these were in very low abundance. At pH 2 and 12 the net charges on the

peptide are +3 and –2 respectively. These lower charges along with the uncharged peptide ends may be responsible for the peptide being able to form fibres. In addition, one of the termini on the WT peptide will still be charged at high or low pH's which may lead to repulsion in the lateral direction, whereas for the capped peptide changes in pH will have no effect on the N and C terminus and there will be no additional repulsion. These results add to the conclusion that the capped peptide is much more fibrillogenic than the WT peptide and that growth in three dimensions can only occur when the charges on the N and C termini are maintained. Furthermore, lateral crystal growth, encouraged by charged peptide termini and illustrated in the WT structure shown in figure 6.1a (Makin et al., 2005), competes with growth in the hydrogen bonding direction and whilst it may be much less energetically favourable, indicated by the fact that the crystals are long and striated, it is still able to proceed and hinder growth in the fibre axis direction to some extent. As this possibility is completely abolished by the removal of charges, the assembly of β-strands by hydrogen bonding is allowed to fully proceed and fibres form much faster for the capped peptide than crystals do for the WT peptide. The material observed at pH 7.4 appeared very similar to those formed at the same concentration of 5 mg/ml in PBS again confirming that NaCl is not having an effect on assembly (figures 6.9 and 6.10). Therefore, as for the WT peptide, of the conditions tested here, neutral pH is optimal (although unlike the WT peptide not absolutely necessary) for assembly of the capped peptide and the absence of NaCl does not appear to have an effect.

As for the WT peptide, similar biophysical studies were carried out on the capped peptide. The results are shown in figure 6.11.

In water, at 5 mg/ml no fibres form after 7 days, consistent with previous results. It may therefore be expected that the peptide is monomeric and would show spectra similar to the WT peptide in water. Although the intensities of both the CD and phenylalanine fluorescence data do not change over time as expected, the spectral features are somewhat different to the WT peptide in water. The negative peak is slightly red-shifted to 192 nm and the shoulder at approximately 200 nm is much more pronounced. Furthermore, the intensity at 220 nm is much lower compared to the WT in water. In addition, another negative maxima is present for the capped peptide with a broad minima around 235 nm. Raising the concentration confirms the presence of this minimum (data not shown). These results may suggest the presence of some soluble ordered structure that is not random coil but that is not large enough to be visible by EM. This is supported by the presence of a small peak at 303 nm in the phenylalanine fluorescence spectrum (shown by the arrow) that may be due to aromatic interactions. Previous results showing that the capped peptide is able to fibrillise in water also support this possibility. The absence of any ThT fluorescence also most likely indicates no amyloid-like structure is present.

In PBS, the capped peptide fibrillises quickly and thin fibres around 5-10 nm wide are visible from time 0. At later time points these fibres are slightly wider but show a similar morphology to the fibres at time 0. Like the WT peptide, the capped peptide has a net charge of +1 and an overall charge of +2 on one side of the β-strand and -1 on the other (figure 6.11ii). Once again, these charges would encourage assembly in the sheet-spacing direction, however, the lack of any charged ends will prevent growth in the third dimension (laterally), therefore prohibiting crystal formation. The CD spectrum for both time points are similar but differ in intensity; the loss of intensity likely to be due to absorbance flattening from a reduction in soluble species over time. Compared to the WT peptide, the spectra show similar energy positioning (negative at ~190 nm and ~ 200 nm and positive at ~ 220 nm) although as for the capped peptide in water, the ratio of intensities are changed considerably. EM shows that, in PBS, the capped peptides forms fibres morphologically very distinct from the crystals formed by the WT peptide after 7 days. It is possible that the reason for the different CD signal is the different species that are formed by these two peptides in PBS. Whilst the CD

spectra for the WT peptide in PBS do not appear to be influenced by the crystals, probably due to their large size, the fibres formed by the capped peptide may be visible to CD and therefore may affect the spectra. It likely that aromatic contributions would affect CD for the capped peptide as well as the WT peptide (which would again explain the unusual profile), but the differences do suggest that either the fibres themselves are contributing, or that if like the WT peptide the signal arises from soluble species i.e. those not incorporated into the fibre, that these are discrete from the soluble material that is present in the WT sample.

There is a peak at 303 nm in the intrinsic fluorescence at both time 0 and 7 days although it is decreased at 7 days. The lack of any ThT fluorescence would indicate that the fibres observed are not amyloid-like, however, ThT binding efficiency is known to vary, especially with short peptides (Khurana et al., 2005; Pedersen et al., 2006a) and whilst a positive result confirms an amyloid–like structure, a negative result does not discount it. It is possible that ThT does not bind to the capped peptide, even if it is amyloid like. The mechanism by which positively charged ThT binds to amyloid is not fully understood (see 2.4.3) but it is known to be affected by pH and therefore to some extent by charge-charge interactions. It is therefore possible that abolishing the charges at the ends of the peptide will influence ThT binding ability.

The EM results for the WT and capped peptides indicate that changing the pH and concentration can affect fibril or crystal formation and highlight the importance of maintaining these factors. From these results it can be concluded that net charge, including charges at the C- and N-terminus of the peptide ($COO^-$ and $NH_3^+$ at pH 7.4 respectively) is at least partly a determinant of fibril or crystal formation and therefore interesting to investigate further using the variants of the WT type peptide specified previously. Furthermore, it is proposed from these results that the phenylalanine residues are making a significant contribution to some of the spectra observed. The roles of aromatic and charge-charge interactions are explored in the next sections using standard concentrations of 5 mg/ml in water and in PBS.

### 6.2.3. Phenylalanine/Alanine (F/A) variants

As for the previous studies, electron microscopy was used initially to determine which of the F/A variants were able to form fibres or crystals. Samples were set up at a concentration of 5 mg/ml in either PBS (pH 7.4) or water then agitated for 7 days and electron micrographs taken.

For all of the F/A variants no fibres were visible by EM after 7 days agitation at 5 mg/ml both in water and PBS. Replacing any of the phenylalanine residues therefore abolishes the ability to form amyloid under these conditions, highlighting the importance of aromatic interactions in amyloid formation (Reches and Gazit, 2003). Phenylalanine residues are hydrophobic and this property may also be important in driving assembly as hydrophobic residues are known to increase the propensity to form amyloid in some systems (Pawar et al., 2005; Pedersen et al., 2006b; Tartaglia et al., 2008), For example, $A\beta_{1-42}$ is more fibrillogenic than $A\beta_{1-40}$, thought to be partly due to the additional isoleucine and alanine residues that increase its hydrophobicity (Jarrett et al., 1993a). It is likely that the combination of reducing hydrophobicity (alanine has a lower hydropathy index (1.8) compared to that of phenylalanine which is 2.8) and restricting aromatic interactions prevents fibril formation.

Given that none of the F/A variants formed amyloid under these conditions they would serve as a useful control system. It would be expected that CD, intrinsic phenylalanine fluorescence and ThT fluorescence curves would be the same at time 0 and after 7 days agitation for a particular sample. These experiments were carried out on one of the peptides to verify this hypothesis. The results for F2AF3A are shown below and are representative of all the F/A variants. In a similar fashion to the WT peptide, they could serve as a basis for comparison for further work on the lysine variants as they were shown not to assemble under any circumstances.

CD spectra from F2AF3A in both water and PBS are similar and do not change significantly over time. In contrast with that observed for the WT peptide, these results show classic random coil features with positive and negative maxima at 218 nm and 195 nm respectively. Furthermore, the intensities are consistent with a typical random structure (figure 6.5iv). The slight change in PBS over time is within experimental error and not significant. These spectra could therefore be assigned as characteristic of a monomeric state. The only peak observed for the phenylalanine fluorescence is at 282 nm; the lack of any signal at longer wavelengths indicates that no stacking of aromatic residues is taking place. The lack of any ThT fluorescence correlates with these results i.e. that no amyloid-like structure is formed. Comparing these results with previous data it appears that F2AF3A is completely disordered whereas for the WT peptide in water there may be interactions taking place that are affecting the spectra observed, although if any structures are formed, they are not visible by EM. Alternatively, the removal of two of the four phenylalanine residues may abolish the far-UV aromatic effect on CD spectra. These results confirm the importance of phenylalanine residues in amyloid assembly and highlight how they can contribute to spectroscopic data, whether it is through the amino acid itself or from $\pi$-$\pi$ stacking interactions between two or more residues. Charge-charge interactions were investigated next using K/R and K/A variants.

### 6.2.4. Lysine variants: Lysine to arginine (K/R) substitutions

The previous results demonstrate the importance of phenylalanine in the assembly of KFFEAAAKKFFE. The final characteristic of this peptide that was investigated was the role of proposed electrostatic interactions between the lysine and glutamate resides in the sequence. Figures 6.13-6.18 show the EM and biophysical data for the K/R variants of the peptide i.e. where lysine had been substituted with arginine. Arginine was used to replace lysine due to its close similarity and therefore would act as a potential control. Any differences in results between the K/R variants and the WT peptide would indicate that lysine is specifically required to generate the structure shown in figure 6.1. These variants share the same overall net charge in water and in PBS as the WT peptide, +4 and +1 respectively.

In water (figures 6.13i-6.18i), like the WT peptide, although the peptides were very soluble and no visible precipitate was observed after centrifugation, no fibrils formed for any of the K/R variants. The high net charge on these peptides is probably responsible for both the solubility and the lack of assembly due to repulsion. Furthermore, all of the K/R variants in water showed similar CD and phenylalanine fluorescence spectra to the WT peptide in water and they did not change over time. For CD, there was a minimum at 190 nm with a small shoulder at 200 nm and a small positive peak at around 220 nm, and no signals at 303 nm were observed in any of the phenylalanine fluorescence spectra. It was proposed earlier that the unusual CD spectra arising from the WT peptide (and similar to those observed here) was due either to aromatic influence in the far-UV from disordered peptide (with no aromatic interactions taking place), or because there were some small, soluble structured species present that may contain aromatic interactions and which could affect spectra. The lack of any peaks in phenylalanine fluorescence spectra would suggest that there are no aromatic interactions occurring and therefore for these variants and the WT peptide in water the former is perhaps more likely. Furthermore, as for the WT peptide in water, there was no ThT fluorescence at 485 nm. The only feature of the K/R variants in water that differed significantly to the WT peptide is the appearance of a broad peak at approximately 520 nm in the ThT data for the K8R and K1R peptides

(figures 6.13i and 6.16i respectively) and is considerably more intense for K1R (at time 0 only). It is unknown at present what fluorescence intensity at this wavelength may arise from but there are similarly positioned peaks in the PBS data (figures 6.13ii and 6.16ii) suggesting this fluorescence is from something characteristic of the way that ThT binds to this peptide.

Electron micrographs of the arginine variants at time 0 and at 7 days in PBS show that pH 7.4 potentiates assembly. Like the WT peptide, this may be explained by the reduced net charge of +1 on the peptides at this pH, therefore lowering repulsion and facilitating assembly. However, only K9R (figure 6.15ii), K1RK8R (figure 6.17ii) and K1RK9R (6.18ii) formed crystals that were similar in morphology to the WT peptide. K8R (figure 6.13ii), K8RK9R (figure 6.14ii), and K1R (figure 6.16ii) all formed fibrillar looking species although those formed by K8R were narrow, short fibrils and were in very low abundance. Interestingly, lysine to arginine mutations appeared to dramatically affect the solubility of the peptides in PBS. The WT and capped peptides easily solubilised in PBS, as did K8R. However, despite having the same net charge, all of the other K/R variants formed visible precipitates on solubilisation. This difference in solubility must be due to the chemical differences between lysine and arginine. Lysine and arginine are the least hydrophobic amino acids, although it is not completely agreed which is most hydrophilic, therefore this property is unlikely to have a significant impact on solubility (Janin, 1979; Kyte and Doolittle, 1982; Rose et al., 1985; Wolfenden et al., 1981). Previous experiments using RNase Sa variants in which the threonine residue at position 76 was systematically mutated to each of the twenty amino acids showed that at pH 7 the T76R variant had a lower solubility than the T76K variant (Trevino et al., 2007). The contribution of lysine and arginine to solubility has been said to be a complex balance between the residue charge, the net charge of the protein or peptide and the ability to bind water, with the guanidinium group found to be the most weakly hydrated group known (Trevino et al., 2007). This may explain why the arginine variants are generally less soluble than the WT peptide. Moreover, as soon as aggregation proceeds, it is likely that certain charges will be screened and this will also affect solubility. Because only the supernatant was used for experiments, those samples that showed a lower solubility would have a lower peptide

concentration. This explains why there are no, or very little CD, intrinsic phenylalanine fluorescence or ThT fluorescence signals for the K/R variants that were poorly soluble (K8RK9R, K9R, K1RK9R) as indicated by the orange background at time 0, and there was little material observed in EM even after 7 days The only exception is the ThT fluorescence for K1RK9R that increased dramatically after 7 days, suggesting that even though there was little material present the binding affinity was high for this particular morphology.

The CD spectra for all of the K/R variants (except those that were poorly soluble that gave no signal) in PBS were similar to the WT, with two minima at 190 nm and 202 nm and a small maximum at 220 nm and which did not change over time despite there being no or little material in EM images at time 0 and fibres and crystals present after seven days. This corroborates the CD data previously observed and would suggest the spectra arise from material in solution, which may be early precursors to the larger species observed at later time points. A constant pool of these small species may be maintained through on-off reactions with the larger aggregates. The exception to this was K1RK8R that did show an increase in signal over time and at day 7 the spectrum resembled that of the capped peptide in PBS. This may be because at time 0 the lower solubility of the peptide meant that there was not enough soluble material to gain a CD signal. However, after 7 days, crystals had formed and it is possible that these crystals act as a reservoir for soluble, dissociated species that are at a higher local concentration at the ends of the crystals - sufficiently high to give a CD signal.

No peaks at 303 nm in intrinsic phenylalanine fluorescence spectra are observed in any cases for K/R variants in PBS. Although in some cases this may be due to the low solubility of the peptide (the signals at 303 nm observed previously are weak compared to the fluorescence of phenylalanine alone at 282 nm), even for those samples that were more soluble (K1R and K1RK8R) there is no additional peak at 303 nm, despite EM images showing that the peptide had assembled. This may indicate that the arginine imposes conformational changes to the WT structure, as WT crystals did show an additional peak at 303 nm. It is conceivable that even slight changes to peptide packing induced by the larger arginine residue may affect the positioning of

the phenylalanine residues within the structure. If indeed the peak at 303 nm is representative of π-π stacking, these results may reflect the disruption of this interaction, caused by the presence of the larger arginine.

It is clear from the results in figures 6.13ii-6.18ii that replacing lysine with arginine at certain positions has a significant effect on the morphology of the species observed by EM. K8R (figure 6.13ii) was the most soluble of the K/R variants but had the least amyloid-forming propensity as indicated by EM results. This would imply that having a lysine residue at this position is important for assembly. In the model for the WT structure, K8 is not involved in any salt bridges. Figure 6.19 below shows the model of the WT peptide as it is believed to exist within the crystals (Makin et al., 2005).

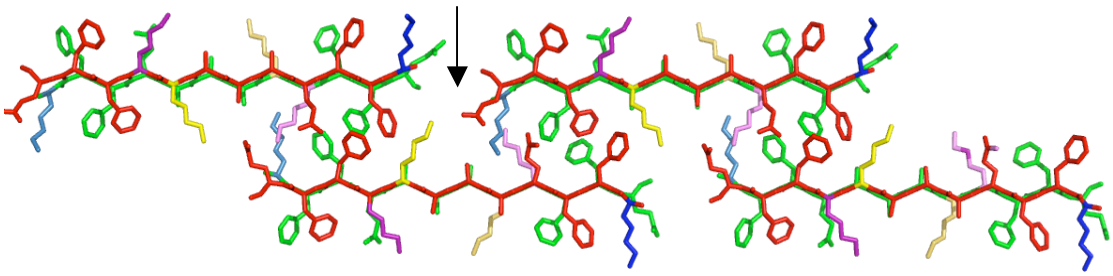

**Figure 6.19. Structural model of KFFEAAAKKFFE crystals in PBS (Makin et al., 2005).** View is looking down the fibre axis. Two layers of β-strands are shown, the top layer in red and the lower layer with β-strands anti-parallel to the red β-strands are in green. K1 and K9 (involved in salt bridges with glutamate residues on the green molecules on the lower layer) are coloured blue and purple respectively. K8 is coloured yellow. The corresponding residues on the antiparallel green strand below are coloured pale. Also refer to figure 6.1 a.

K8 in figure 6.19 is coloured yellow. Replacing this residue with arginine may impose a steric hindrance and impede assembly. Figure 6.2 shows the chemical properties of lysine and arginine. It is possible that arginine is too large (173.4 Å) to be accommodated and interferes with peptide association. There may be an interaction between K8 and E12 on the diagonally opposite molecule, indicated by the arrow. The CD spectra are similar to the WT peptide both at time 0 and day 7 and, like the WT peptide, K8R assemblies at day 7 are able to bind ThT and cause significant

fluorescence, despite their low abundance. These data suggest that the species formed by K8R are, like the WT peptide, invisible to CD but that they are amyloid like and hence able to bind ThT.

It may be expected that replacing lysine at position 8 with arginine in the double variants would also have a negative effect on assembly. However, this was not the case. The other variants that had a mutation at K8 were K8RK9R (figure 6.14ii) and K1RK8R (figure 6.17ii). Both of these peptides assembled in PBS although the morphologies were somewhat different to each other. K8RK9R formed fibrils that at high resolution (shown in the inset in figure 6.14ii) could be seen to be composed of varying numbers of even numbers of protofilaments (2,4 or 6) each approximately 10 nm in width. K1RK8R on the other hand formed small, fibrillar looking species initially and larger crystals at later time points. K1 is blue in figure 6.19 and K9 is purple. K1 and K9 are on the same side of the peptide. It would appear that the extra mutation at either position 1 or position 9 rescues the ability to form amyloid, although it causes quite different species to be produced.

All of the arginine variants that replaced lysine in the positions where the salt bridge is believed to be located, that is, position 1 and position 9, assemble, although again the species appeared remarkably different. Lateral association is greatly affected in K1R and K8RK9R. The sample that produced most similar looking material to the WT peptide was K9R. K1RK9R crystals also looked similar to the WT and in addition crystals were present at time 0, suggesting this mutant increased propensity for amyloid formation. Arginine has a greater β-sheet forming propensity compared to lysine (93 compared to 74 – figure 6.2) and which may explain the appearance of material at earlier time points for some of the K/R variants compared to the WT peptide. K1RK9R also strongly bound ThT, as did the WT sample, possibly suggesting similar modes of binding and therefore similar molecular arrangements. The low solubility of the K9R variant meant that ThT measurements on this peptide were inconclusive. Like K8RK9R, K1R formed material that appeared more like fibres than crystals and lateral association was significantly impeded. This may indicate that replacing lysine with arginine at position 1, 8, or at positions 8 and 9 together, somehow either facilitates

growth in the hydrogen bonding direction, or impedes it in the lateral direction and hence wider crystals do not form. The difference in size of the arginine residue may have an effect on the electrostatic interaction with the glutamate residue on the β-strand below, specifically a salt bridge can only be said to have formed if the charged groups on the paired residues are within 4 Å of each other (Kumar and Nussinov, 2002). As the measured distance according to the model is approximately 4 Å, it is possible that the presence of arginine instead of lysine could affect this distance and therefore the integrity of the stabilising interaction. Indeed, it has been shown that salt bridges can be both stabilising and destabilising (Hendsch and Tidor, 1999; Kumar and Nussinov, 2002; Schueler and Margalit, 1995). However, as K1RK9R formed crystals that from EM and biophysical methods resembled the WT, it might be expected that the structure in maintained in this variant. Other work has shown that arginine and lysine do contribute differently to structural stability through their ability to form hydrogen bonds (Klumpp et al., 2003). It is generally accepted that these electrostatic interactions are not the driving force in protein folding (Kumar and Nussinov, 2002), and from the previous results the essential role of aromatic residues in assembly is clear. Therefore it is likely that replacing lysine with arginine has three outcomes. Firstly, K/R mutations could affect peptide packing and consequently the aromatic interactions, which may explain the lack of a peak in phenylalanine fluorescence at 303 nm. Secondly, these mutations may affect the salt bridges formed to potentially form more or less stable structures, depending on which interaction is affected. Lastly, there appears to be a role for lysine in lateral association, as some of the variants did not form crystals.

The lysine to arginine mutations were originally expected to have little impact on the species observed by EM and the biophysical data gained for these peptides (and therefore act as controls), but this was not the case. The absence of a peak at 303 nm in the phenylalanine fluorescence scans is particularly interesting and suggests that a particular type of packing and aromatic interaction is required for generation of this peak. It is not to say that there are no aromatic interactions in these variants but that they are perhaps flexible in nature and only particular conformations will be able to exhibit this specific fluorescence. Despite the K/R variants showing some unexpected

differences to the WT peptide in PBS, there was a great deal of similarity for most of them and in water the results correlated well. These results highlight the ways in which very small chemical changes to sequence can affect assembly and structure and how peptides are able to adapt to these changes and assemble.

### 6.2.5. Lysine variants: Lysine to alanine (K/A) substitutions

The results from the K/R variants unexpectedly revealed that making very small changes in the chemical composition of the peptide side chains could affect assembly and potentially the structure of the species formed. In particular the presence of arginine instead of lysine may affect the peptide packing to influence the aromatic and charge-charge interactions and lateral assembly. To further test the role of lysine in assembly, lysine residues were mutated to alanine. The chemical properties of alanine are shown in figure 6.2. Alanine has a much smaller volume than arginine and is also much more hydrophobic, which partly contributes to its increased β-sheet forming propensity compared with lysine. Changing any of the lysine residues to alanine alters the overall net charge of the peptide, which from previous results is thought to influence amyloidogenic potential of this peptide. Electron micrographs and biophysical results from the alanine variants are shown in figures 6.20-6.25. These data showed the greatest deviations from the WT peptide, much more so than the arginine variants. Furthermore, many of the K/A variants show morphological and biophysical differences to each other indicating that each substitution, or combination of substitutions, can have significant effects.

The first striking observation made was that changing any of the lysine residues to alanine conferred the ability to form fibres in water, which the WT sequence and the arginine variants do not. This is probably partly due to the reduced charge on the peptides; the single K/A variants had a net charge of +3 and the double variants a net charge of +2 (table 6.1). In water, the salt bridge will be affected, as the glutamate residues will carry no charge and will therefore not be able to form any charge pairings with lysine. This may significantly change the peptide packing, as it is thought that the positions of the lysine and glutamate residues in the sequence influence the antiparallel arrangement. In addition, alanine variants assemble to form differing morphologies and in no cases did crystalline species of the type observed for the WT peptide form in either water or PBS (the average widths of the species as observed by EM are given in the figures). This corroborates previous indications that lysine plays a role in lateral association and crystal growth. In water, the N terminus will carry a positive charge and the C terminus will be uncharged. This may also help explain why end-to-end peptide assembly is limited in water. However, in PBS both ends are charged, yet still only fibres form. It is possible that this occurs by one of two mechanisms. Having lysine specifically present may promote lateral association only in the sheet spacing direction. The alternating residues on each β-strand will influence this association, K1 and K9 being on one side of the peptide and K8 (along with the glutamate residues) on the other side (see schematic in the top right of figure 6.5i and ii). Table 6.1 shows the overall net charges of the peptides in water and PBS, and how these charges are distributed on each side of the peptide.

| Peptide | Sequence | Net charge in water (pH 3.0) | Net charge in PBS (pH 7.4) |
|---|---|---|---|
| WT | KFFEAAAKKFFE | +4 (+2/+1) | +1 (+2/-1) |
| K8A | KFFEAAA**A**KFFE | +3 (+2/0) | -1 (+2/-2) |
| K8AK9A | KFFEAAA**AA**FFE | +2 (+1/0) | 0 (+1/-2) |
| K9A | KFFEAAAK**A**FFE | +3 (+1/+1) | 0 (+1/+1) |
| K1A | **A**FFEAAAKKFFE | +3 (+1/+1) | 0 (+1/-1) |
| K1AK8A | **A**FFEAAA**A**KFFE | +2 (+1/0) | -1 (+1/-2) |
| K1AK9A | **A**FFEAAAK**A**FFE | +2 (0/+1) | -1 (0/-1) |

**Table 6.1. Net charges of K/A variants and the distribution of these charges on either side of the peptide.** The numbers in brackets indicate the charges on either side of the peptide from charged residues and exclude the N and C termini. For example, KIAK8A in PBS will have a single positive charge on one side from K8 and two negatively charges on the opposite side from E4 and E12.

For the WT peptide and K/R variants, there will be an overall charge in PBS of +2 on one side of the peptide and -1 on the other side. These samples show a much higher degree of lateral association and crystals formed in most instances. None of the K/A variants share this distribution of charges, indicating that a combination of +2/-1 is optimal for lateral assembly in the sheet spacing direction. According to the model in figure 6.1, there are no electrostatic interactions in this direction; however, the charges may still be affecting how peptides associate end-to-end by imposing a different architecture. Conversely, it is also possible that lysine may hinder growth in the fibre axis (hydrogen bonding) direction, therefore its removal from certain positions allows lengthening of fibres to occur with greater propensity, out-competing lateral assembly and hence fibres form instead of crystals. These proposals are purely speculative and the way in which lysine may prevent peptide association in the fibre axis direction is not ascertained, although it may be that the larger size compared to alanine imposes steric hindrance thereby discouraging association in this direction. Lateral association in the third direction (peptide end-to-end) has been discussed previously using the capped peptide (section 6.3.2). As the WT peptide, K/R variants and K/A variants will all have positively charged N termini and uncharged C termini in water, and positively and negatively charged N and C termini respectively in PBS, lateral association in this direction will not differ. The formation of fibrils over crystals may also be due to the increased β-sheet forming propensity of alanine (83) over lysine (74), which would encourage assembly in the fibre axis direction. The β-sheet

forming propensity of arginine (93) is even higher than alanine, yet for most of these samples crystals formed. This again highlights the complexity of self-assembly of peptides into amyloid fibres and/or crystals, a process that is clearly determined by many factors some of which will inevitably override others and become the “driving force”.

The change in net charge of the K/A variants affects solubility. In water, where net charges were higher, the K/A variants were more soluble than their counterparts in PBS that had reduced net charges, as expected. The lower charged peptides correlate well to the appearance of a precipitate on dissolution and centrifugation. Those that had a charge of +3 were very soluble (indicated by a green box), those with a charge of +2 were less soluble (indicated by a yellow or orange box and a larger precipitate forming) and those with a charge of 0 or -1 (samples in PBS) were least soluble. The exceptions were K1AK8A and K1AK9A in water (figures 6.24i and 6.24ii respectively), which although having a slightly higher charge were relatively insoluble. There is an inverse relationship between solubility and the potential to form fibrils, as mentioned previously (section 6.3.1), with higher charges facilitating solubilisation but impeding fibrillisation due to repulsion (Calamai et al., 2003; Lopez De La Paz et al., 2002). In the case of the arginine variants solubility was much lower than for the WT peptide and consequently the abundance of material observed by EM, and the intensity of the spectroscopic and fluorescence signals, was dramatically reduced. This was also the case for some of the K/A variants and there was more material and more intense signals for all of the peptides in water. As for the arginine variants, the one exception to these data was ThT which for K1AK9A in water, K8A in PBS and K1AK8A in water and PBS showed a large increase in fluorescence over 7 days, despite there being little material present. These and the previous results show how the specificity and affinity of ThT binding varies dramatically and may indicate that it binds preferentially to some structures over others. In most cases for the K/A variants ThT fluorescence did not increase, indicating no binding, which apart from the samples mentioned generally correlates with the absence of crystalline material.

In water, despite the higher charges on the peptides than those in PBS, fibres formed in abundance but lateral association was limited. The fibres formed by K8A, K8AK9A and K9A variants in both water and PBS are mostly quite thin (3-12 nm wide), not straight, and tend not to bundle, although a larger aggregate can be seen in K8A in PBS. Close inspection of this image reveals this to be a bundle of fibres rather than a crystal of the type seen for the WT; each separate fibre can be identified whereas in the crystals this is not the case. In addition, there were far fewer fibres present in the K9A sample in PBS, likely to be due to lower solubility. K1A formed slightly wider fibres than the other variants in both water and PBS. In both samples a few, long, fibres appear at time 0 that go on to form very straight fibres that are of a slightly wider (30-40 nm) uniform width and which differ significantly in morphology from the fibres formed by the other K/A variants. The fibres formed by K1A in both water and PBS also show similar biophysical data to each other.

K1AK8A and K1AK9A behaved similarly when dissolved in water and PBS with low quantities of fibres of indeterminate length forming at time 0 that did not appear to change significantly after 7 days. Whilst there would clearly be less material due to the lower solubility of the peptides, the previous results from other poorly soluble peptides (K8A in PBS, K8AK9A in PBS and K1A in PBS) shows that propensity for fibril formation is not solely determined by peptide concentration, as these samples assembled despite low solubility. These two peptides seemed to show the lowest propensity for fibril formation and K1AK9A in PBS did not form fibres at all. This may be partly due to the involvement of these residues in the salt bridge, which will affect the stability of the fibres. However, K1AK9A did form few fibrils in water, again indicating a role for net charge in fibril formation (the net charge in water is +1 and in PBS is -1). This result supports the work of Lopez de la Paz *et.al.* who suggested an optimum peptide net charge of +1 for fibril formation. Other work investigating the effects of pH and net charge showed that high positive or negative net charges impede aggregation into amyloid (Lopez De La Paz et al., 2002; Picotti et al., 2007). Many proteins that have a high content of acidic residues aggregate preferentially at low pH's where the acidic residues are protonated and the negative net charge is reduced (Fandrich and Dobson, 2002; Uversky and Fink, 2004). Furthermore, many natively

unfolded proteins do not self-assemble; this is believed to partly be due to high net charge (Uversky et al., 2000). Modulating the net charge by changing pH has demonstrated its importance in many amyloid aggregating systems (Calamai et al., 2003; Picotti et al., 2007; Schmittschmitt and Scholtz, 2003). Furthermore, fibril forming ability was at its maximum when the pH was near the pI of the protein and solubility was at a minimum (Schmittschmitt and Scholtz, 2003). This result and others support that solubility is a determinant of fibril formation, and that increasing solubility has an inverse relationship with fibrillisation (Shaw et al., 2001).

The ThT fluorescence for K1AK8A and K1AK9A in water increased over 7 days as fibrillisation proceeded as expected and was some of the most intense of all the samples tested, which did not appear to correlate with how much material was present. Similar results have been observed elsewhere (Pedersen et al., 2006a). Again, this result illustrates that caution should be taken when interpreting results from ThT experiments. The results obtained from the K/A variants partly served to test the structure previously proposed and this result showing that K1AK9A does not assemble in PBS supports the presence of a salt bridge in the WT crystals.

The models in figure 6.1 and 6.19 show the positions of the lysine residues in the proposed model for the crystals. In PBS, having all three lysine residues present seems to encourage crystal formation. Replacing K1 with alanine reduces lateral association, replacing K9, K8, a combination of both or K1 and K8 reduces it even further and replacing K1 and K9 together abolishes fibril formation in PBS on this time scale. This suggests having both salt bridges present is important for generation or maintenance of the WT crystalline structure. Net charge will have a role in peptide assembly but is not the only determinant, as some K/A variants with a net charge of -1 fibrillise in PBS whereas others do not. Variants that have a net charge of zero show great propensity to fibrillise despite low solubility (and therefore low concentration). When there is no net charge, peptides will aggregate through side-chain interactions and backbone hydrogen bonding only; there will be no electrostatic interactions. In water, in most cases, the fibres appear similar to their counterparts in PBS. These results suggest again that lysine plays an important role in lateral association and that its position in

the sequence is also influential. It is possible that by replacing K with A, the brick-like arrangement is disrupted. This would mean that the ends of the peptides might be less exposed and available to associate with, limiting lateral assembly.

Solubility affected the biophysical data and in some cases CD and intrinsic fluorescence signals were very low due to a lower peptide concentration and absorbance flattening. For the K/A samples dissolved in PBS, CD data was only obtained for K1A (which incidentally also had the most fibrils present by EM, despite the low solubility) and was similar to the WT peptide. K1A in water also showed similar CD data to the WT peptide and to K1R in PBS that in neither case changed significantly over 7 days. There is also a small peak in the phenylalanine fluorescence data for K1A in water, similar to the WT peptide although it is weak and no such peak can be observed for the sample in PBS. This CD spectrum is thought to arise from soluble species (and not from fibrils or crystals) that may be: i) monomeric ii) small oligomeric precursors iii) dissociated monomer or iv) dissociated oligomers.

The CD data for some of the K/A variants in water is revealing and shows spectra unlike those previously observed for the WT and K/R variants in either water or PBS. K8A and K9A both change significantly over time and are similar to each other. At time 0, the spectra are similar to the WT peptide in PBS and the majority of K/R variants. However, over time the spectra change and an intense positive peak emerges at 200 nm. There remains a negative peak at 190 nm and the data for K9A shows that the small positive peak at 220 nm is maintained although the intense peak in the K8A data would drown this out if it were present. There are far fewer fibrils at time 0 when this signal is present and the signal only changes when fibrils form. The inversion of the peak at 200 nm correlates with the formation of fibrils, suggesting that in this case the fibrils are visible to CD

K8AK9A and K1AK8A in water also share similar spectra that differ to the previously observed CD data. In both of these there is a positive maxima at approximately 192 nm and a less intense, broad minimum centred at around 220 nm. This CD spectrum resembles that of a $\beta$-sheet. In the K8AK9A sample it appears that the minima are split

at around 215 nm and 225 nm, which would be more typical of an $\alpha$-helical spectrum. It is difficult to ascertain this as it is clear that aromatic residues have a strong influence, which may explain this feature. Alternatively, it may arise from early stage soluble species that have a helical conformation. The data is similar at both time 0 and 7 days and EM images show that fibres are formed at very early time points. Over time there is a slight blue-shift in the data from the K8AK9A peptide. Shifted data has been observed previously with aggregating systems (Calloni et al., 2008; Capes et al., 2010; Castiglioni et al., 2007; Ji and Urry, 1969; Starck and Sutherland-Smith, 2010; Wallace and Mao, 1984). The ability to produce a CD spectra that reports on the structures observed by EM rather than the material in solution appears to correlate with the width of fibrils as these four cases all produced fibres of around 5-20 nm width, apart from K8A which additionally produced some wider fibrils. This would suggest that there is a limit to what CD can "see" and report on structurally.

CD data would imply that K8A and K9A in water share similar characteristics in their structure and assembly, as does K8AK9A with K1AK8A in water. In all cases fibres form suggesting association in the hydrogen bonding direction is favoured over the lateral directions. K8AK9A and K1AK8A both have a charge of +1 on one side of the peptide and no charge on the other side, the only difference being where this charge is located. In both peptides it would be expected that no salt bridge should form, as glutamate carries no charge. K8AK9A and K1AK8A gave the most $\beta$-sheet-type spectrum from all the variants tested. The absence of this spectrum for the other samples does not exclude that the other structures contain $\beta$-sheets but supports previous observations that CD on aggregating systems can be complicated by a number of factors, particularly when aromatic residues are present. Furthermore, non-aggregated material can be influential. K8A and K9A in water differ in the placement of charges on either side of the peptide. However, that they have produced a similar CD spectrum suggests structural similarities. K8A fibres are slightly wider however, suggesting perhaps that K9 is required for lateral assembly.

For some of the K/A variants there is no discernable peak at wavelengths longer than the dominant 282 nm peak in the phenylalanine fluorescence data. These are K8A in

water, K1A in PBS and K1AK8A in both solvents. The signal for K9A in PBS is too low to draw any conclusions. There are very weak fluorescence peaks at around 303 nm (when compared to the peak at around 282 nm) for K8A in PBS, K9A in water and PBS and K1A in water. Other samples also gave peaks at 303 nm that were quite prominent compared to the peak at 282 nm. These were K8AK9A in water and PBS K1AK9A in water and PBS. This last result was particularly unusual since no fibres were observed in EM, although it is possible that they were present but in extremely low abundance. Alternatively, the peak may arise from $\pi$-$\pi$ stacking between associated peptides that are too small to be seen using EM. These results suggest that replacing lysine with alanine is able to change the position of the peptides within the overall structure so that the aromatic interactions are affected.

The results from the K/A variants show that changing the sequence dramatically affects potential for assembly and possibly the arrangement of the peptides within the final structures formed. The lysine residue would appear important for crystal formation. The overall net charge is also important although not the overriding determinant. The results suggest that the structures formed by each variant are different.

### 6.2.6. Assessing cytotoxicity of assemblies formed from KFFEAAAKKFFE variants

In order to ascertain the cytotoxic potential of some of the assemblies formed from KFFEAAAKKFFE variants, toxicity assays were performed on SH-SY5Y neuroblastoma cells. The MTT assay is a common test that reports on cell survival and has been used previously with many disease-related amyloid-forming proteins to determine which species cause cell death, for example $\beta_2$-microglobulin (Xue et al., 2009a), A$\beta_{1\text{-}40}$ (Solomon et al., 1997) and IAPP (Brender et al., 2008). The cytotoxicity of designed peptides that from amyloid-like fibrils has been carried out previously and the fibrils formed were found not to be toxic (Fezoui et al., 2000). Similar studies were carried out with a selection of assemblies formed here. The current view of amyloid toxicity *in vivo* is that small, soluble early stage species and protofibrils are responsible for cell death and not the full-length fibrils (Bitan et al., 2005; Conway et al., 2000; Klein et al.,

2001). The variants in the previous chapters formed a wide variety of assemblies that varied in morphology. Leaving samples quiescent slowed growth, which further provided aggregates of varying size.

Peptides used for cytotoxicity assays were all prepared in PBS at 5 mg/ml as were as follows:

i) capped peptide at time 0

ii) capped peptide after 2 hours incubation

iii) K1AK8A left quiescent for four days

iv) K1AK9A left quiescent for four days

These peptides were chosen for these preliminary studies based on the appearance of material in EM images (figure 6.26). The capped peptide provided a fibrillar sample at later stages and was compared to the same sample prepared at time 0 which would have a higher concentration of monomeric peptide as per CD and EM results. K1AK8A assembled to form short, worm-like fibres and K1AK9A did not assemble to form any species observable by EM. The results can be seen in figure 6.26.

The overall trend is that none of the species showed any significant toxicity compared to the untreated control. However, at the 1 hour time point (that is, 1 hour after the samples were added to the cells) there does appear to be some toxicity from the K1AK8A variant (short fibres) at 50 μM and the capped peptide freshly prepared at 10 μM. In addition, the fibrillar sample appeared to exhibit some toxicity at early time points at 50 μM. It is likely that in these samples there is some monomeric peptide or small oligomers, especially at early stages. No toxicity at all was exhibited by K1AK9A, which did not assemble per EM. It is possible that this reduced propensity to assemble also reduces cytotoxic effects. It has been proposed previously that cytotoxicity is a generic response from misfolded protein aggregates, as oligomers formed from proteins unrelated to disease have shown to be toxic to cells (Bucciantini et al., 2004). However, the p values calculated from the data are low and the general trend is that these short peptides are not toxic to SH-SY5Y neuroblastoma cells. These results are preliminary but are a starting point for further toxicity characterisation of short amyloid-forming peptides that could then be related to structure.

## 6.3. Summary

Using a structural model previously determined (Makin et al., 2005), variants of the peptide KFFEAAAKKFFE (WT peptide) were examined to ascertain the contribution of particular residues to assembly and overall structure. In particular, the role of the phenylalanine and lysine residues were explored, as aromatic stacking and charge-charge interactions were thought to be important in fibril formation. The WT peptide forms crystalline species in PBS so the influence of the charges at the ends of the peptides in lateral assembly was also investigated. The model of KFFEAAAKKFFE as it exists within fibrous crystals featured antiparallel β-strands within each β-sheet. This arrangement was proposed as being partly determined by charge pairings between K1 on one peptide and E12 on the next peptide in the hydrogen bonding (fibre axis) direction, and similar interactions between K9 and E4. Furthermore, aromatic interactions via π-π stacking between phenylalanine residues were present in the model (Makin et al., 2005).

At 5 mg/ml, the WT peptide forms crystals in PBS after 7 days agitation that are around 1 μM in width. At higher concentrations (10 mg/ml and 20 mg/ml), the WT peptide forms thinner species after 7 days. At each concentration, fibres form at time 0 and abundance positively correlates with increasing concentration, possibly because more fibril nuclei are formed. These results suggest that bonding in the hydrogen bonding direction is favoured, particularly at higher concentrations. Lower concentration may promote more ordered growth, allowing the peptides to laterally associate to form the larger crystals, possibly with the fibrils acting as a nucleus. The net charge on the peptides in water is +1, previously described as the optimum charge for amyloid assembly (Lopez De La Paz et al., 2002). In water the peptides have a net charge of +4; these results show that this high net charge prevents assembly in water as no fibrils formed at any concentration tested. The WT peptide did not assemble at pH 2 (net charge of +4) or pH 12 (net charge of -3), showing that net charge is important and is not being screened by salts in PBS. CD spectra for the WT peptide at 5 mg/ml in PBS did not change over 7 days even though crystals formed. The crystals may be invisible to CD and only representative of what remains in solution. The CD spectra are unusual and may arise either from monomer that is disordered but which influence the signal by a high aromatic content, or from small assemblies that contain stacked aromatic residues. A tilt experiment confirmed that the CD spectrum is not due to LD effects. In water, the CD are the same as in PBS, supporting the view that this technique is only seeing what is in solution. However, intrinsic phenylalanine fluorescence and ThT fluorescence differed between WT in water and PBS and show that WT crystals cause additional phenylalanine fluorescence peaks to appear at 303 nm, which may be due to π-π stacking within the structure. The crystals also bind ThT, suggesting they are amyloid-like.

The peptide with capped ends had a lower net charge (+3) in water than the WT peptide (+4) and, as concentration was increased, was able to form few fibrils, which the WT could not. Furthermore, the capped peptide could fibrillise at pH 2 and pH 12. This may be due to a lower net charge. In PBS, the charge is the same as the WT (+1), but only fibres, not crystals, form. This may be because the competition for lateral peptide association is reduced as there are no charged ends. CD spectra for the capped

peptide in water are unusual although differ to the WT peptide, with the minimum at around 200 nm more pronounced, maybe due to oligomeric structures that are different to the WT structures. The presence of a peak at 303 nm for phenylalanine fluorescence suggests π-π stacking, it is possible that this arises from small structured species not visible by EM. This is supported by previous results indicating that the capped peptide can form fibrils in water at higher concentrations. In PBS again the CD spectrum is unusual and differs to the WT and the peak in the phenylalanine fluorescence spectra at 303 nm is clear. The capped peptide may adopt a different conformation in early stage species and fibrils compared to WT in PBS. No ThT binding was observed, maybe due to a different underlying structure.

Replacing any of the F residues in the WT sequence resulted in no fibril formation in either solvent. CD spectra were typically random coil corroborating earlier suggestions that the other CD data are influenced either by F contributions or aromatic stacking. As expected there was no peak in either intrinsic phenylalanine or ThT fluorescence spectra. The aromatic residues in this sequence are therefore essential for assembly.

K/R variants in water behaved the same as WT. In PBS however, results varied, indicating that very small chemical differences can have dramatic effects on assembly and structure. Changing K8 to R appeared to have to most effect and very short (and few) fibres formed. Only K9R, K1RK8R and K1RK9R formed crystals similar to WT crystals in PBS. Notable by its absence was a peak at 303 nm in phenylalanine fluorescence spectra, suggesting that replacing K with R changes the structure, possibly due to its larger size, that leads to a disruption in aromatic interactions.

K/A variants showed the most deviations from the WT peptide. Changing any of the K residues to A has a significant effect on morphology. All were able to fibrillise in water to a greater or lesser extent. This may be partly due to a reduced net charge. No crystals like those seen for WT formed in any samples. Lysine may play a role in end-to-end peptide association by changing the packing of the peptides that results in them not being able to associate in this direction to form crystals. K8A, K8AK9A and K9A all

generally form long, thin fibres in water and PBS. K1A formed thicker, straight fibres. K1AK8A and K1AK9A have a much lower fibril-forming propensity.

The results validate the role of the salt bridge in the model proposed previously (Makin et al., 2005). However, no salt bridges can form in any of the K/A variants in water, as the charge on glutamate residue will be zero, yet fibres do form and in most cases are similar in morphology to those in PBS. This may suggest similar underlying structures in both solvents. It also shows that whilst the salt bridge may be important in modulating the structure, it is not essential. In water, lateral association may be affected by charge distribution at the N and C termini. However, because the fibres in PBS appear similar it is unlikely that this is the reason for the limited lateral assembly for K/A variants.

Due to low solubility, CD and fluorescence signals were weak for many of the variants, especially in PBS. According to CD data, K8A and K9A are similar in water, as are K8AK9A and K1AK8A. The latter two showed more β-sheet like spectra than had been previously observed for any of the variants. This suggests a limit to the width of fibrils that CD can measure. K1A in water and PBS showed spectra similar to the WT peptide, thought to be due to what is in solution and not the assembled species, and these were slightly wider. Many of the variants in water showed a peak at 303 nm for intrinsic phenylalanine fluorescence spectra showing that aromatic interactions are maintained in some variants but less so in others, possibly due to variations in peptide packing induced by the mutations. Thioflavin T showed extremely varied binding that did not correlate with either how many fibrils were present or their morphology, highlighting its varying affinity for amyloid structures. Preliminary toxicity studies on a small selection of samples indicated that small oligomeric species may exert some toxic effects.

These results combined demonstrate the complicated nature of how amyloid structure is determined. Many factors contribute and changing conditions only slightly would appear to have dramatic effects on underlying structure. To further probe the peptide arrangements within these fibres, fibre diffraction was carried out on several of the peptide variants in the following chapter.

# 7. RESULTS AND DISCUSSION: Fibre diffraction analysis of variants of KFFEAAAKKFFE

## 7.1. Introduction

A model of the structure of the WT sequence KFFEAAAKKFFE as it exists within an amyloid-like crystal has been built previously using X-ray fibre and electron diffraction data (figure 7.1a) (Makin et al., 2005). The fibre diffraction pattern for the WT sequence is shown in figure 7.1b.

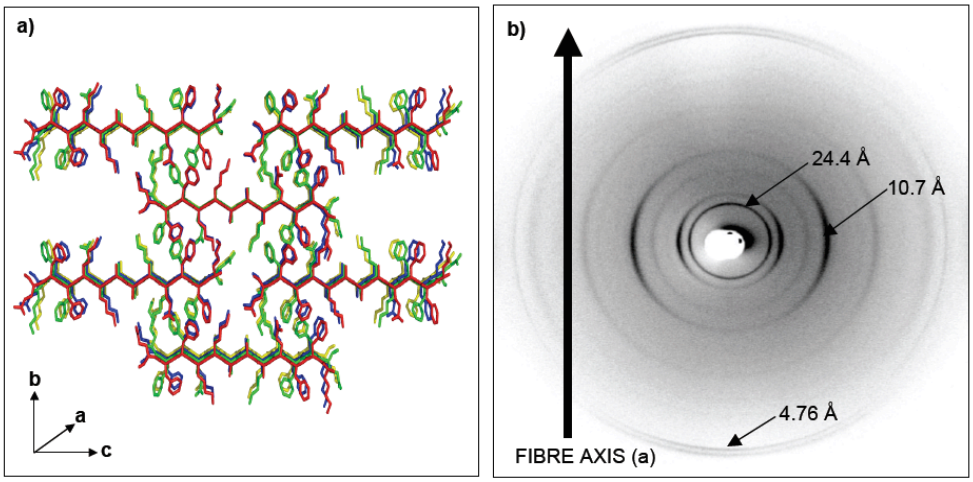


**Figure 7.1. a) Model structure of KFFEAAAKKFFE (Makin et al., 2005). b) X-ray diffraction pattern from a bundle of KFFEAAAKKFFE fibres.** Direction '*a*' refers to the hydrogen bonding distance between β-strands along the fibre axis and corresponds to the 4.76 Å meridional reflection. The 10.7 Å equatorial reflection arises from the distance between the β-sheets (*b*, sheet spacing direction). The 24.4 Å reflection, also on the equator, corresponds to direction *c* (chain length) and is equal to half the unit cell dimension of 48.8 Å.

To examine the internal architecture of the species formed by the variants in the previous chapter at a higher resolution, fibre diffraction was carried out on the variants of this peptide that formed abundant fibres or crystals after 7 days as shown by EM micrographs. Successful alignment relies partly on a high concentration of material; therefore early stage species were not investigated as in most cases there were insufficient amounts of fibres and crystals present. Analysis of fibre diffraction

patterns from the variants could aid in the determination of any possible structural differences that may exist between the WT sequence and the variants, using the known structure as a basis for comparison.

## 7.2. Results and discussion

Those samples that aligned and diffracted well were analysed using the program CLEARER (Sumner Makin et al., 2007). Initially, the positions of the diffraction signals were measured. The diffraction patterns and a list of the reflections for each sample are shown in figure 7.2 and table 7.1 below, with their probable indexings compared to the WT peptide (the shaded regions).

| | | Alanine variants | | | | | Arginine variants | | | |
|---|---|---|---|---|---|---|---|---|---|---|
| | a | b | c | d | e | f | g | h | i | j |
| **WT PBS [h k l]** | **Capped Water**** | **K8A Water** | **K8A PBS** | **K8AK9A Water** | **K9A Water** | **K1A Water** | **K8RK9R PBS** | **K9R PBS** | **K1RK8R PBS** | **K1RK9R PBS** |
| **Equatorial** | | | | | | | | | | |
| | | | | | 43.00 | | | | | **49.63** |
| | | | | *37.00* | | | **32.75** | 33.00 | | **35.84** |
| | | | | | | | | | | |
| 24.43 [0 0 2] **c** | 22.10 | **21.62** | **22.20** | *21.75* | | 23.2 | **26.57** (ring) | **24.40** | **25.38** | **26.02** |
| | | | | | | | | | 21.00 | *22.38* |
| 19.94 [0 1 1] | | | | | *19.36* | | | | | |
| | | | | | | | | | | *18.38* |
| | **15.63** | | *15.03* | | | | | | | |
| | | | | | *14.05* | | | | | |
| 13.27 [0 1 3] | *13.77* | | | | | | *12.59* | | | *13.32* |
| | **11.17** | | | | | | | | **11.18** | |
| | | | | | | | | | | **11.06** |
| 10.66 [0 2 0] **b** | | **10.66** | **10.70** | | | **10.40** | **10.51** | **10.70** | | |
| | | | | **9.84** | | | *9.80* | | | *9.68* |
| | | | | | **9.46** | | | | *9.50* | *9.40* |
| 9.33 [1 0 1] | | | | | | | *9.30* | | | |
| 8.69 [1 1 0] | **8.77** | | 8.99 | | | | *8.45* | | | |
| 7.93 [0 2 4] | | | *7.86* | | | *7.89* | | | *7.83* | |
| | | | | | | | *7.64* | | *7.61* | *7.60* |
| 7.19 [0 2 5] | | 7.15 | 7.15 | | | | | | | |
| | **7.09** | | | | | | *7.11* | | | |
| | | | | | **6.72** | | | | | |
| | **6.36** | | | | | | | | | *6.40* |
| 6.13 [1 0 6] | | | | | | *6.08* | | | | |
| 5.65 [1 3 1] | | | | *5.52* | | | | | *5.59* | |
| | **5.45** | | | | | | | | | |
| 5.33 [0 4 0] | **5.29** | 5.35 | 5.36 | | | | *5.27* | | | |
| | | | | | **5.16** | | | | | |
| | | | | | | | | | | |
| 4.91 [1 3 5] | | | | | | | | | | *4.84* |
| | | | | | | | | | *4.73* | |
| 4.66 [2 0 1] | | | | | | | | | *4.60* | |
| | | | | | **4.46** | | *4.58* | | *4.55* | |
| 4.37 [1 3 7] | | | | | | | | | | *4.34* |
| | | | 4.21 | | | | *4.26* | | *4.23* | |
| 4.00 [0 0 12] | | | | | | | *4.06* | | *4.00* | |
| **Meridional** | | | | | | | | | | |
| | 9.08 | | | | | | | | | |
| | **8.66** | 8.89 | 8.83 | | | *8.6* | *8.78* | | *8.76* | *8.83* |
| 4.76 [2 0 0] **a** | **4.60** | **4.67** | **4.67** | **4.70** | **4.59** | **4.66** | **4.65*** | **4.71** | **4.63** | **4.65** |
| | **4.44** | | | | | | *4.47* | *4.48* | **4.55** | *4.50* |
| | | | | | 4.26 | | 4.26 | | **4.35** | |
| | | | | | 4.06 | | | | | |
| | 3.11 | | | | 3.60 | | | | | *3.40* |
| | 2.27 | | | | | 2.37 | 2.35 | | 2.35 | |
| | 2.16 | | | | | | 2.21 | | | |
| | | | | | | | | | | |

| **Off-meridional** | | | | | | | | | | |
|---|---|---|---|---|---|---|---|---|---|---|
| | *7.86* | | | | | | | | *7.25* | *4.33* |
| | *6.03* | | | | | | | | *6.03* | |
| | *5.29* | | | | | | *5.53* | | *5.13* | |
| | *4.15* | | | | | | *4.26* | | | *3.97* |
| | *3.90* | | | | | | *3.70* | | | *3.85* |
| | *3.77* | | | | | | *3.62* | | *3.70* | *3.74* |
| | *3.53* | | | | | | *3.57* | | *3.62* | *3.57* |
| | *3.50* | | | | | | *3.50* | | *3.57* | *3.49* |
| | *3.22* | | | | | | | | | |

**Table 7.1. Reflection positions on fibre diffraction patterns from KFFEAAAKKFFE and variants.** Figures in bold represent strong reflections on the corresponding diffraction pattern. Figures in italics are weak reflections. Indexing for the WT peptide reflections are given in brackets underneath the relevant spacing (denoted by the Miller indices *h*, *k* and *l*) (Makin et al., 2005). Shaded areas represent the chain length (*c* direction), sheet spacing (*b* direction) and strand spacing (*a* direction). Units are given in Å.

- This reflection is a doublet composed of two reflections at approximately 4.70 and 4.60 Å

** Capped peptide was prepared at 10 mg/ml in water to ensure fibril formation

Table 7.1 lists the measured reflections in the experimental fibre diffraction patterns. The intensities of the reflections in each sample vary, some being stronger or weaker than others (shown in bold and italics respectively). Each variant has at least one strong equatorial reflection, which arises from the sheet spacing (*b* direction) or chain length (*c* direction) and an intense meridional reflection that corresponds to the distance between β-strands on the hydrogen bonding, or fibre axis, direction (*a*). Examination of the d-spacings given in table 7.1 reveals certain similarities and differences between the variants compared to the WT peptide and to each other. A visual assessment of the diffraction patterns shown in figure 7.2 shows how much more ordered the crystalline samples are compared to fibres. Figures 7.2a-f are diffraction patterns from fibrillar samples (capped peptide and alanine variants). The diffraction signals here are much more diffuse than those shown in figures 7.2g-j that are from the more crystalline K/R variants. Although information can be gained from all of these diffraction patterns those from the crystalline samples generally provide more detail, as the diffraction signals are sharper and there are more reflections. This would be expected from a sample that is more ordered and these results are similar to those from fibre diffraction on GNNQQNY fibres and crystals in chapters 4 and 5.

The only variant for which diffraction data was obtained in both PBS and water was K8A. K8A in PBS and water have very similar diffraction patterns (figure 7.2a and b)

and the positions of the reflections are also within experimental error. This indicates that K8A in water and in PBS are similar in structure. This is corroborated by electron micrographs (figure 6.2i and ii) that show that in both water and PBS K8A forms fibres of similar width (20-60 nm). The thioflavin T data does not appear to support this finding, as it seems to bind to the fibres in PBS preferentially over those in water. This discrepancy may be due to solution conditions, which can influence binding. In particular, low pH's have been seen to reduce ThT binding efficiency (Naiki and Nakakuki, 1996). Therefore, whilst the positive ThT result in PBS suggests that the fibres are amyloid-like, the negative result in water does not preclude it. Fibre diffraction data suggests that the fibres formed by K8A in water and PBS are similar in structure. The diffraction pattern from the fibres formed in PBS gave more detail and was used for further examinations, the results being also applicable to K8A in water.

The next step was to identify which of the variants shared structural similarities with the WT peptide, for which a model has been produced (figure 7.1a) (Makin et al., 2005). Initial examination of reflection positions reveals that some of the variants differ to the WT structure more than others. The low-angle reflection in the pattern from the WT structure at 24.43 Å arises from the chain (peptide) length and is indexed as [0 0 2] as it corresponds to approximately half the unit cell dimension in the *c* direction of 48.1 Å. The strongest reflections from the variants at approximately this position are given in bold and are in the shaded region alongside the WT position. It is clear that for most of the K/R variants this distance is slightly increased and for the K/A variants it is reduced compared to the WT distance, likely because of the different sizes of the residues. This may suggest that these mutations confer slightly different peptide packing arrangements within the structure and that the unit cell dimensions are altered. The chain length for the capped peptide also appeared more like the alanine variants than WT. This result correlates with EM results that show that the capped peptide and the K/A variants form fibres and the WT peptide and K/R variants form wider crystals and again imply a role for lysine in lateral association of peptides and crystal formation.

K9A in water diffracted to give a pattern that was unusual compared to the other variants that formed fibrils, as can be observed purely from a visual inspection (figure 7.2e). It is thought that this type of pattern arises due to the different texture of the sample. 'Texture' refers to the way individual fibres that are aligned within the bundle that is exposed to the X-rays are associated and can have a dramatic effect on the resultant diffraction image. Different alignment methods can produce samples with different textures. However, all of the samples here were aligned using the same method so the reason for the different texture must be due to an inherent property of the sample. Electron micrographs of K9A in water show the fibres to be extremely thin and of very uniform width and it is possible that these fibres do not align quite as well as the others and some may be oriented differently with respect to the X-ray beam compared to others within the "aligned" bundle. Alternatively, the different texture may be induced by the sample having a different conformation, such as a cylinder, were the 43 Å signal arises from the width across the cylinder. Although the pattern itself appears different, many of the diffraction signals are in similar positions to the other variants and the WT peptide. The 43 Å reflection is absent in the majority of other samples, and is similar to the width of the fibrils observed by EM (approximately 5 nm). It should be noted that there is a higher degree of error when measuring low angle reflections therefore this measurement is approximate. It is likely that the 19.36 Å reflection is related to this distance and would be indexed to [0 2 0]. The WT peptide was indexed to a $P2_12_12_1$ space group, which has systematic absences at odd [*h* 0 0], [0 *k* 0] and [0 0 *l*]. This means that for the WT peptide the [0 1 0] reflection at 43 Å does not appear on the diffraction image. Therefore, K9A in water may have a different symmetry arrangement to the WT peptide in PBS. Imperfect symmetry would also prevent the 43 Å reflection being systematically absent, which is another possible explanation for its appearance in the K9A diffraction pattern.

The next strongest reflection in the equatorial direction for the WT peptide is at 10.66 Å, indexed to [0 0 2] (half the *b* dimension of 21.3 Å) and representing the distance between the β-sheets in the structure. Again, the strongest corresponding reflections are given in bold and are present in the shaded area in table 7.1 alongside the WT reflection. Comparison of the reflections from the variants with the WT peptide

reveals that K8A of the alanine variants, and K8RK9R and K9R of the arginine variants have similar equatorial reflections to the WT peptide and that these mutations have less of a structural impact in this direction. The majority of alanine variants however have smaller *b* direction spacings. It is likely that the removal of lysine reduces steric hindrance, enabling the sheets to come closer together and it would appear that K9 has some influence in determining this distance as the greatest reduction was in the K8AK9A and K9A samples. For the K/R variants K1RK8R and K1RK9R gave the largest increases in sheet spacing (>11 Å) suggesting that K1 also affects the sheet spacing distance.

The capped peptide shows a strong equatorial reflection at a position more similar to the K/R variants than to the other fibrous samples (11.17 Å). This supports the role of alanine in reducing the sheet spacing direction and indicates that the capped peptide also adopts quite a different peptide packing arrangement to either the WT peptide or many of the other variants. However, the positions of the reflections (except the sheet spacing) for the capped peptide seem most similar to the K9A variant, which it also appears similar to in EM images. The K8AK9A variant also formed very thin fibres visible by EM in water and the reflection positions were similar to K9A in water. It is likely that K8AK9A, K9A and the capped peptide in water all adopt similar conformations that differ only in the sheet spacing direction and which are quite different to the WT peptide or K/R variants. The other equatorial reflections observed at higher angles are indexed as combinations of *h*, *k* and *l* and are used in later unit cell determination.

Meridional reflections correspond to distances in the fibre axis, or hydrogen bonding (*a*) direction. The presence of a strong meridional reflection at approximately 4.7 Å at 90° to the equatorial reflection at 10-11 Å in fibre diffraction patterns indicates a cross-β amyloid structure. For the WT peptide, the strong meridional signal was at 4.76 Å, which was indexed to [2 0 0] and was approximately half the unit cell *a* distance of 9.52 Å. This cell dimension reflects the antiparallel arrangement of peptides within each β-strand in the model for the WT peptide and is systematically absent in diffraction patterns owing to the odd [1 0 0] indexing. Many of the variants gave

diffraction patterns that featured a reflection at 8.6-8.9 Å although it is likely that this reflection is actually off-meridional and part of the 9.52 Å layer line. All of the variants gave strong meridional signals that were similar to the WT peptide suggesting that the hydrogen bonding distance is maintained in all of the peptides. In the more crystalline diffraction patterns (figures 7.2g-j) and the pattern from the capped peptide there are a number of weak off-meridional reflections, most of which are at positions less than 4 Å. Off-meridional reflections often arise from helical repeats and are indexed to [x x 0] or [x 0 x], for example, the 8.69 Å signal in the WT pattern, which was indexed to [1 1 0].

Following this initial analysis comparing reflections, the reflections from those experimental patterns that were sufficiently detailed were indexed to attempt to determine unit cell dimensions for the variants, which could then also be compared to the WT unit cell. K8AK9A in water, K1A in water and K9R in PBS contained few reflections and were exempted from unit cell calculations, as was K8A in water which was previously established as very similar to K8A in PBS. In order to compare to the WT peptide, the same indexing system was employed that was used for the WT. Using the program CLEARER (Sumner Makin et al., 2007), appropriate unit cell dimensions were input. Only *b* (sheet spacing) and *c* (chain length) dimensions were searched, the *a* direction was left as the default of 4.69 Å because there was very little variation in this direction. All angles were defined as 90°. Following this, the measured equatorial signals were entered and varied from [0 0 0] up to an appropriate possible indexing. The low angle reflections in table 7.1 that corresponded to the chain length (*b* direction) and sheet spacing (*a* direction) were defined as [0 0 2] and [0 2 0] respectively. For example, for K8A in PBS, unit cell dimensions of *b* = 15 Å and *c* = 25 Å were entered; the program will search double these distances. The following reflections were then input with the corresponding maximum and minimum possible indexing: 22.20 [0 0 2] (no maximum), 10.70 [0 2 0] (no maximum), 8.99 minimum: [0 0 0] maximum: [0 3 3], 7.15 minimum: [0 0 0] maximum: [0 3 4], and 5.36 minimum: [0 0 0] maximum: [0 4 4]. Using this indexing system would ensure that 22.2 Å would be defined as the *c* direction and 10.70 Å would be defined as the *b* direction, in keeping with the WT peptide. The program was then allowed to search the defined unit cell

space to index the reflections and possible unit cell dimensions generated. Only reflections up to a resolution of 4 Å were entered, those higher than this were not included in calculations as they could be indexed in many ways. Off-meridional or weak signals were also mostly not included in calculations. Possible unit cells for each sample are given in the table below (table 7.2). Further information is given in the appendix (iv).

| | **WT PBS** | **Capped Water** | **K8A PBS** | **K9A Water** | **K8RK9R PBS** | **K1RK8R PBS** | **K1RK9R PBS** |
|---|---|---|---|---|---|---|---|
| **B** | **21.3** | 21.80 | 21.60 | 18.35 | 21.26 | 22.80 | 21.93 |
| **C** | **48.1** | 31.05 | 47.92 | 38.92 | 51.71 | 50.12 | 53.30 |

**Table 7.2. Possible unit cell dimensions for some KFFEAAAKKFFE variants and the WT peptide.** Units are given in Å.

The unit cell generated for the capped peptide was similar in the *b* direction but differed significantly in the *c* direction and could not be indexed to a cell similar to the WT. It might be expected that the narrow filaments formed by the capped peptide would be in a different arrangement to those in the WT structure. K/A variants have overall smaller unit cell dimensions than WT. The chain length direction for K9A is considerably smaller, perhaps suggesting that the peptides are arranged more like the capped peptide than the WT peptide. The unit cell for K8A is very similar to the WT peptide even though fibres, and not crystals, were observed in EM images. However, the fibres formed by K8A tend to be wider and varied in width compared with the capped peptide and K9A, between approximately 20 nm and 60 nm, indicating that in these fibres the peptide arrangement seen in crystals of the WT peptide could be maintained. The fibres formed by K8A are also straighter than capped or K9A fibres suggesting that they are possibly more ordered and more like the WT than the other K/A variants. The unit cells generated for the K/R variants are generally bigger than the WT unit cell in both *b* and *c* directions which supports the view that the presence of arginine increases both the sheet spacing and the distance between peptides associated end-to-end.

The WT structure featured a brick-like arrangement of peptides, arising from the symmetry imposed by the space group (figure 7.3a). Fibre diffraction data supports a similar arrangement for the K/R variants, except with increased chain length dimensions and sheet spacings (figure 7.3b). K8A forms fibres as observed by EM although somewhat different in morphology to those formed by K9A and the capped peptide. The structural data presented here for K8A is in agreement with the WT peptide and indicates a similar structure for the fibres, except with limited lateral association (figure 7.3c). However, overall comparison of reflections, and the unit cell determined from these diffraction signals, for K9A and the capped peptide (figures 7.3 d and e respectively) suggests that there is a different peptide packing arrangement in these fibres.

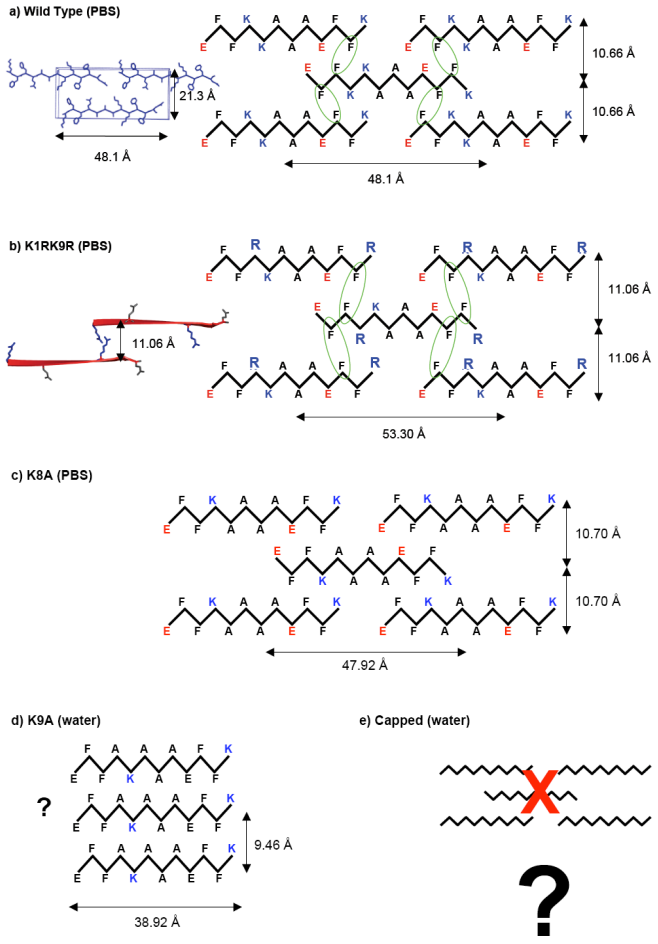


**Figure 7.3. Schematic showing possible peptide arrangements within WT, K/R and K/A structures.** a) WT structure with unit cell imposed and schematic showing the peptide arrangement in the WT peptide. Aromatic interactions are highlighted in the green circle. b) K1RK9R with model illustrating the spacing imposed by the presence of arginine. c) K8A. d) K9A. e) capped peptide, for which the structure is unknown but not likely to be similar to the WT arrangement. View is looking down the fibre axis.

## 7.3. Summary

In summary, the results from fibre diffraction reveal that the K/R variants share many structural similarities with the WT peptide that support the results from EM. It is likely that the anti-parallel arrangement of the peptides is maintained in the K/R variants in PBS. K (or R) and E residues would not pair if the β-strands were parallel and the salt bridge appears to offer some stabilising force as the fibril forming propensity of K1AK9A in PBS is significantly decreased (section 6.2.5). However, in water, there would be no such interaction due to the lack of any charge on glutamate residues. These results help to explain some of the results from the biophysical analyses in chapter 6. The K/R variants showed a longer chain length and sheet spacing when compared to the WT peptide and it is possible that this affected the aromatic interactions and could explain why the intrinsic phenylalanine fluorescence peak at 303 nm is missing for these variants. This would indicate that π-π stacking itself is not essential for fibril formation and it may be the hydrophobicity of phenylalanine that is more important.

The capped peptide and K9A appear to be quite different to the WT peptide and may form fibres that are similar in structure to one another. Indeed, EM images of K9A stood out, as they were much thinner and less straight than the other K/A variants and appeared more like the capped peptide at a macromolecular level. This may result from a different peptide packing arrangement for these fibres. Once again, the effect of making very small changes to sequence on overall structure is made clear and not only highlights the roles of individual amino acids in assembly and structure, but also where they are placed within the sequence.

## 7.4. Conclusions (chapters 6 and 7)

The purpose of the experiments carried out in chapters 6 and 7 was to gain insight into the roles of particular residues in the assembly and structure of amyloid-like fibrils and crystals, using a previously explored model as a basis for comparison. The simplicity of the system made it possible to draw specific conclusions. The questions to be answered were:

1. How do aromatic residues, in particular phenylalanine, and π-π stacking influence assembly and structure?
2. How do charged residues, in particular lysine, and electrostatic interactions influence assembly and structure?
3. How do charges at peptide ends influence assembly and structure?
4. What is the effect of changing the net charge?
5. Do short peptides exhibit any cytotoxicity?

Mutational scans, capping peptide ends, changing solution conditions, examining samples using different biophysical techniques and performing cytotoxicity assays were the techniques employed to answer these questions.

### 7.4.1. Aromatic interactions

No F/A variants fibrillised in water or PBS. This result strongly suggests that aromatic interactions drive assembly of this peptide. It also highlights that aromatic pairs are required. Furthermore, it would appear that aromaticity, and not just hydrophobicity, is required, as replacing phenylalanine with alanine, which is also hydrophobic, did not lead to fibril formation. In the F/A variants the salt bridge would still be able to form, but this propensity cannot overcome the barrier induced by disrupting the aromatic interactions.

The aromatic interactions were probed using the intrinsic fluorescence of the phenylalanine residue. The additional peak at 303nm observed for some variants was thought to be due to aromatic stacking, possibly over a long-range, and was disrupted in some variants, probably due to a change in the overall peptide arrangement.

### 7.4.2. Influence of charged residues

It is clear from EM that net charge strongly influences fibril formation. In water, where the overall net charges on the peptides are higher, the peptides are more soluble but less likely to form fibres due to increased repulsion. At 5 mg/ml, it seems that the threshold for fibril formation for the variants tested here is +4, under which fibrillisation is permitted. Peptides with a net charge of +2 or +3 i.e. K/A variants in water, formed fibres. These fibres were mostly very narrow and they resembled their counterparts in PBS by EM, biophysical methods and fibre diffraction. Therefore, whilst net charge may have a role in propensity to aggregate, it is unlikely that it influences structure. For fibrils to form at a high net charge, the repulsion induced must be overcome by another, stronger interaction, probably aromatic in nature. Therefore, electrostatic interactions probably play a secondary, although still important, stabilising role. K1 and K9 are involved in the salt bridge that is believed to stabilise the anti-parallel arrangement. Replacing both of these with alanine diminished the ability to form fibrils in PBS. This leads to an overall net charge of -1. Two other K/A variants share this net charge, both of which formed fibrils in PBS. Therefore, the overall net charge is not solely responsible for the inability of K1AK9A to fibrillise. It may be that disrupting both salt bridges prevents stabilisation, or it may be due to the charge distribution on either side of the peptide molecule. It would seem that the latter explanation is more likely, as in water there will be no salt bridge forming, yet the peptides form similar species in both solvents.

It is clear that lysine has a role in lateral association. Even changing lysine to arginine can have dramatic effects on assembly, possibly due to its larger size, although the location of the residue is important. The overall structure seen in the WT peptide appears to be maintained in the K/R variants, albeit with increased sheet spacings, which affects aromatic interactions as observed by EM studies. The K/R variants that formed narrower crystals could still contain the same packing arrangement as the WT. Crystal growth may be prevented by either because propensity to aggregate in the fibre axis direction is increased, or from a decreased propensity to aggregate laterally.

Differences were more significant when lysine was replaced with alanine as no crystals formed and they were able to fibrillise in water. The charge difference may play a role here. Also, alanine is more hydrophobic than lysine, which might facilitate association in the hydrogen bonding direction to form β-sheets. K1A and K8A appeared most similar to the WT peptide from EM, CD and fibre diffraction (although K8A CD was similar to K9A in water). However, although they were similar, other biophysical data showed differences, for example the ability to bind ThT. FD data showed that K8A fibrils were structurally similar in water and PBS, again showing that charge and pH affects aggregation and not structure.

### 7.4.3. Charges at peptide N and C termini

The charges at the N and C termini are important for association in the chain length direction. When both ends are uncharged, crystals cannot form, shown by the results from the capped peptide. The same is true when only the N terminus carries a positive charge i.e in water. Therefore it would seem that for crystals to form, N and C termini must be positively and negatively charged. However, charged ends do not *ensure* crystal formation. This is illustrated by the K/A variants in PBS, which have charged termini but do not form crystals. Charged ends are another factor that help determine assembly, and structure to some extent, but are by no means a driving force of fibril formation.

The experiments revealed some other points of interest. Firstly, atypical CD spectra were probably highly influenced by aromatic contributions, either from the residues themselves or from stacking in small structures not visible by EM. It would appear that in many cases not all of the peptide is incorporated into the fibrils or crystals formed and may be undergoing on-off reactions, maintaining a constant pool of small soluble species. In addition, the binding affinity of ThT appeared to vary greatly and even in water where binding is expected to significantly decrease in some cases fluorescence was observed. It may be concluded that for this system at least, and possibly for amyloid polymorphs formed from short peptides in general, ThT is an unreliable method for making any inferences into the nature of the species formed. In another

study it was claimed that monitoring intrinsic fluorescence (from tryptophan) was a more useful for examining fibrillisation than ThT fluorescence and the authors also highlight the poor correlation between fibril abundance and fluorescence (Pedersen et al., 2006a).

These results demonstrate the complexity of amyloid formation and the polymorphisms that can be induced by very small chemical or experimental modifications. Much effort has gone into establishing what drives assembly. A low net charge has been previously described as one of the three main promoters of aggregation into amyloid, along with high hydrophobicity, presence of aromatic residues and β-sheet forming propensity (DuBay et al., 2004; Jones et al., 2003; Pawar et al., 2005). Individual determinants of fibril formation may be placed in two hierarchies, one for assembly and one for structure, where at the top lies the fundamental driving force and at lower levels are less influential factors. Figure 7.4 illustrates the factors that can influence fibril formation, derived from the experiments here, and highlights the magnitude of each effect.

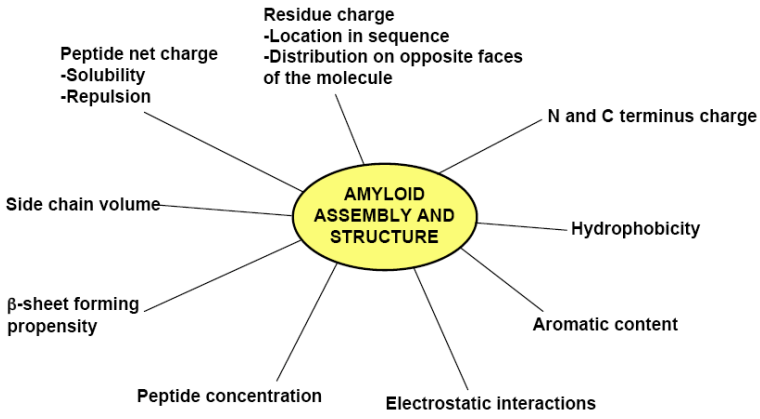


**Figure 7.4. Determinants of amyloid assembly and structure.**

These factors, some of which will be very subtle, each plays an important role firstly in whether aggregation can proceed in an ordered way, and secondly what the resulting structure is. Many of them are inextricably linked, for example final peptide concentration will depend partly on solubility. Which are the overriding driving forces will depend on the individual system. For example, hydrophobicity has previously

shown to have a greater influence than net charge in aggregation (Calamai et al., 2003). Here, aromatic content appears to be most important, at least in determining assembly. They will influence peptide arrangements within structures and bonding patterns. This may be illustrated using the WT peptide, for which most structural data is known. First, the presence of aromatic residues dictates the formation of a critical nucleus. It may be that this nucleus is formed of monomers whose phenylalanine residues intercalate rather than have any β-sheet content. Antiparallel β-sheets may form next, and this is governed by the charges. The overall net charge is +1, the charge on each side of the peptide is +2/-1 and the locations of these charges are in specific positions in the sequence. Because the aromatic residues have determined the association between the sheets, the peptide ends are left exposed – like "sticky ends" for further association through aromatic interactions, building up a brick like arrangement. For the fibrillar species, a completely different bonding pattern may be present whereby a brick like arrangement is not present and therefore lateral association is not able to proceed. The nature of the early stage species will also vary and may vary in cytotoxic effects, although the preliminary data here suggests that perhaps toxicity is inherent in prefibrillar aggregates.

Bonding in each of the three dimensions (fibre axis, sheet spacing and chain length) via hydrogen bonding and hydrophobic, side chain and electrostatic interactions appears to be competitive. Growth in any of these directions is therefore a fine balance that depends on the interactions mentioned above. It would seem that generally association is favoured in the hydrogen bonding direction, even in crystals. This is particularly promoted by raising the peptide concentration. The highly polymorphic nature of even short amyloidogenic peptides, and their ability to adapt to the mutations imposed upon them to form different structures, possible with different assembly pathways, is made clear from the data presented here. These results help to build a picture and clarify what determines the propensity to aggregate into amyloid, which may be distinct from those factors that dictate the formation of a particular structure.

# 8. DISCUSSION

The work presented here details the assembly and structure of two peptide model systems, both of which have been previously characterised structurally and therefore provide excellent starting points for further investigation. The yeast prion fragment GNNQQNY is known form fibres and crystals, the structure of the latter having been elucidated and proposed as relevant to the fibril structure (Nelson et al., 2005; Sawaya et al., 2007). All of the previous work on GNNQQNY focused on the structures of the final stage species formed and uncovered its polymorphic potential, with different models being proposed for both fibres and crystals (Diaz-Avalos et al., 2003; Nelson et al., 2005; Sawaya et al., 2007; van der Wel et al., 2007). However, no investigation had been carried out into the assembly of these structures, which would provide more insight into how the different polymorphisms arise. Furthermore, the two crystal structures for GNNQQNY differed significantly in the packing of the peptide and in particular around the location of the tyrosine residue. The research aims here were twofold; firstly, how do fibres and crystals of GNNQQNY form and are the resulting structures related to each other, or to the previously published models, and secondly, can the generation of these different polymorphic species be explained by the involvement of the tyrosine residue in assembly?

The second system examined was based on the sequence KFFEAAAKKFFE that has been structurally characterised previously using electron and fibre diffraction (Makin et al., 2005). Variants of this sequence were constructed to explore the roles of particular residues on assembly and structure of the peptide, using the well-characterised WT peptide as a basis for comparison. Polymorphism in amyloid fibrils is well known (Petkova et al., 2005) and short peptides able to form amyloid–like fibres and crystals can give more specific information on the sequence-structure relationships into how these different forms assemble and the impact they have on structure. In addition, by making small changes to sequence, the integrity of previous models can be tested. These results aimed to aid in the establishment of how amyloid-forming propensity and the polymorphisms observed in species formed from the same peptide are determined by sequence.

The first observation made for GNNQQNY was that, at concentrations of less than 10 mg/ml, fibres form initially followed by crystals. At a higher concentration a population of fibres is sustained. This was also the case for KFFEAAAKKFFE, where at time 0 fibres form, followed by crystals (figure 6.3). The ability to form wide, three-dimensional crystals therefore appears to be affected by concentration, with lower concentrations seeming to propagate wider crystals, possibly due to a more controlled growth mechanism. However, striations seen in crystals and the high length:width ratio would suggest that growth is favoured in the hydrogen-bonding direction along the fibre axis. Therefore, it is unlikely that crystals of amyloid forming proteins will assemble in the same manner as crystals of globular proteins, which may not exhibit such directionality. If the same peptide is able to form crystals and fibres under different conditions, are they structurally discrete from each other? This question will have an impact on which methods are deemed appropriate for use in amyloid structure determination.

It may seem logical if fibres form first and crystals at later time points that the crystals are composed of fibres that associate laterally to form the wider, striated, crystalline assemblies. However, the results here suggest that this is not the case. It would seem that, for those peptides that produced CD spectra that were not overwhelmed by LD contributions, there is a constant pool of monomeric or oligomeric peptide maintained in solution. The frayed ends of the crystals for KFFEAAAKKFFE suggest that the crystals are disordered at the ends and are possibly less stable, acting as a pool for monomer that is constantly dissociating and re-associating. Fragmentation as a mechanism for generation of oligomers has been observed previously (Collins et al., 2004; Xue et al., 2009a). In addition, many of the K/A variants were able to form fibres in water that never formed crystals and even forced alignment carried out in preparation for fibre diffraction experiments did not always induce the fibres to associate laterally. It would appear that in some cases fibres are the most stable conformation a peptide can adopt whereas for others a crystalline conformation is favoured, with fibres forming as an intermediate to which peptides add in all three directions but not equally favourably in all of them. A proposed mechanism for crystal formation from amyloidogenic peptide based on these results is shown in figure 8.1.

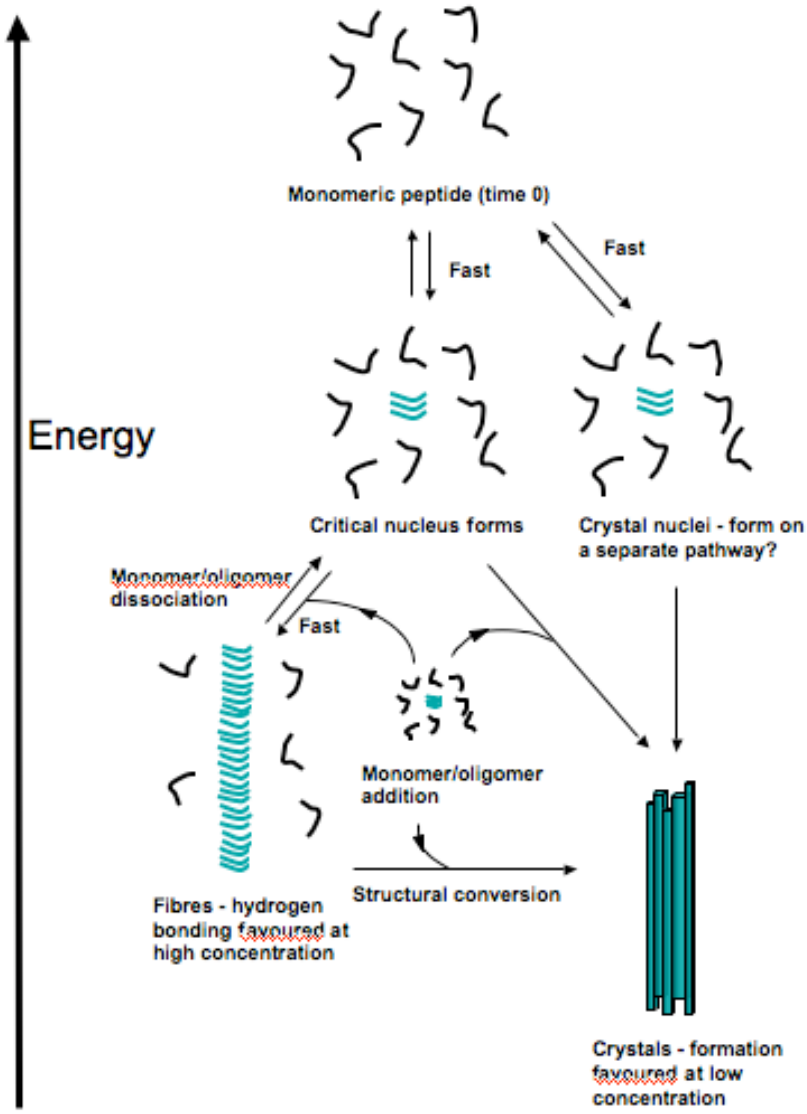


**Figure 8.1. Schematic showing assembly of monomer into fibres and crystals.**

The first step in the generation of both fibres and crystals is the formation of a critical nucleus. Crystal nuclei may form separately to fibril nuclei, although they may produce similar structures. This step is slow and is followed by the faster addition of monomer to form either a fibre or a crystal. In the cases where fibres are seen using EM at early time points and crystals later on, the fibre is potentially also acting as a nucleus to which monomers add in all directions, although preferentially in the fibre axis direction, eventually forming a crystal. Therefore, for amyloidogenic peptides that are able to form crystals, like those characterised here, the fibres observed at early time points are a stage in the crystallisation process. The crystal could be considered a

polymorph and while they may have fibrillar features, they are not composed of fibres. Therefore, fibres could be considered as on-pathway to crystal formation i.e Monomer⇔Fibril→Crystal, or off-pathway, meaning that Monomer⇔Fibril is a separate pathway to Monomer→Crystal. The reversible reactions (⇔) may sustain a population of monomer (or oligomer) for either fibril or crystal growth (figure 8.1). It would appear that once crystals are formed they do not revert back to fibres, indicating they are the most stable polymorph. A fine balance of conditions will be required for optimisation of crystal formation over fibril formation or vice versa. These will induce different bonding patterns and therefore potentially different structures between fibres and crystals.

Both fibril formation and crystal formation will be affected by a number of factors (figure 7.4). The aromatic residues in both of the systems tested here appear to play an essential role in fibril formation, and support previous observations that aromatic residues provide a driving force for fibril formation (Reches and Gazit, 2003). However, these results highlight that the driving force for assembly may be distinct from the driving force for determining structure. For GNNQQNY the tyrosine residue is probably important in both. MD simulations carried out on Y7A variants of this peptide showed that the peptide did not fibrillise (Gsponer et al., 2003) and it would be interesting to verify this experimentally. Aromatic residues are not always essential for fibrillisation in systems (Bemporad et al., 2006; Lopez de la Paz and Serrano, 2004; Tracz et al., 2004) and if the hypothesis that any polypeptide is able to form amyloid (under appropriate conditions) is correct (Dobson, 2003), aromaticity may prove less fundamental. For GNNQQNY, it would appear that the aromatic residue is responsible for polymorphism. This may not be true for the KFFEAAAKKFFE variants. Removing phenylalanine completely diminishes fibril-forming propensity, but other residues are highly influential in the species observed. Mutating aromatic residues in these systems may help to establish how the specific chemical nature of the residue affects fibrillisation. For example, phenylalanine could be replaced with valine, which is known to have a high β-sheet forming propensity (Du et al., 2003). Furthermore, factors particular to the experiment will be of importance. At lower concentrations, in both of the systems tested here, there is slower growth, which leads to bigger, wider crystals.

At high concentrations, longer crystals and even fibres are formed from the same peptide. This supports the view that hydrogen bonding is favoured at higher concentrations. More nuclei will form, although it is not ascertained whether fibril nuclei are distinct from crystal nuclei. The presence of alanine in the K/A variants may increase the propensity to form fibrils, and not crystals, further, due to its hydrophobicity. Alternatively, it may be that the presence of lysine promotes lateral association. This could be tested by performing an extensive scan of each residue with each of the other 19 amino acids and initially investigating by EM whether fibrils form. In particular the role of electrostatic interactions could be investigated further by mutating the glutamate residue. Overall it would seem that hydrogen bonding and association in sheet spacing and chain length directions are competitive. Backbone β-strand hydrogen bonding is generally the winner; it is just a matter of how much competition is provided (determined by the factors in figure 7.4) that decides how much lateral association there is.

To date, peptides up to only 7 residues in length have been crystallised and their structure as it exists in the crystal determined (Ivanova et al., 2009; Nelson et al., 2005; Sawaya et al., 2007; Wiltzius et al., 2008). It would seem that in order for crystals to be formed from amyloidogenic peptides they need to be able to order themselves in a very specific way, different to the way they order themselves in a fibre. An extended β-sheet may be essential for crystalline arrangements to form from amyloid proteins. This may help to explain why only short peptides can form single crystals, peptides that are slightly longer are able to form fibrous crystals and why longer proteins and peptides do not form crystals at all. The brick like arrangement seen for KFFEAAAKKFFE and the two GNNQQNY crystal structures would not be attained by a peptide or protein that formed a β-turn, or an even more complex tertiary structure. Furthermore, β-strands are known to twist, resulting in twisted β-sheets and therefore twisted fibril (Chothia, 1973). Twisting may be more pronounced in longer sequences, imposing greater heterogeneity and precluding crystallisation. These results show that for amyloid structure determination it may be preferable to use an arsenal of biophysical techniques to gain insights into assembly and structure, rather than rely on X-ray crystallography as a method. Caution should be taken, illustrated by the ThT

results, where binding did not correlate well to either fibril abundance or particular types of macromolecular structure.

Model systems like those described here can be useful in characterising determinants of protein misfolding and amyloid formation and their intricate relationships. They will help to provide rules that may be exploited for use in industry to create materials with similar physico-mechanical properties but which are non-toxic. The potential uses for these materials have been described previously (Cherny and Gazit, 2008). From a therapeutic perspective, model systems can give details on which fragments of larger proteins determine the amyloid state, and agents can be designed to counteract assembly. The emerging view is that small oligomeric species are toxic to cells (Caughey and Lansbury, 2003) and effort is now being placed into determining the structure of these species (Relini et al., 2010). The nature of the toxic species may turn out to be polymorphic, just as the higher species are, with toxicities that vary with structure (Bucciantini et al., 2004; Relini et al., 2010). Further toxicity studies with early stage species and fibrils that may provide a pool of monomeric peptide, like those used here, would be of interest. It is possible that disease related peptides form specific structures, or contain certain motifs, that are toxic, which short peptides cannot form. Comparison of oligomer structures to fibril structures will help to explain toxicity and whether it is a generic property of small misfolded oligomers, or whether there is a structural dependence. Methods for analysing structure of these small intermediates often involve labelling the peptide. If small chemical changes can affect assembly dramatically, as the results here show, then serious consideration should be given to the relevance of results using these methods to *in vivo* mechanisms.

## 8.1. Future directions

Both GNNQQNY and KFFEAAAKKFFE serve as useful and worthwhile model systems to study. The results and conclusions drawn demonstrate how even short peptides can provide a wealth of information on what drives the formation of the amyloid state. Carrying out further experiments on these peptides and variants thereof could extend the work presented here. Solid state NMR on both GNNQQNY and KFFEAAAKKFFE and

the related variants could provide restraints so that more detailed models could be built. In the case of GNNQQNY, the models of the fibres and crystals produced under the conditions used here could be compared to other solid state NMR data (van der Wel et. al., 2007), as well as the previously published crystal forms (Nelson et. al., 2005; Sawaya et. al., 2007). As mentioned above, the role of the tyrosine residue is GNNQQNY could be explored experimentally to determine how essential this residue is in assembly of fibres and crystals. The mechanism by which crystals form from fibres could also be investigated, although it is likely that the process is complex and techniques to study this may be limited. One method could be to determine the proportion of smaller species that are present throughout the assembly process, as it is proposed that fibres may be forming by dissociation and re-assembly into crystals. This could be carried out using, for example, solution NMR. ssNMR on KFFEAAAKKFFE and the related variants could also enable the building of more detailed structural models. Solution NMR studies on those peptide variants that appeared not to fibrillise would also help with interpretation of CD spectra and help to corroborate whether indeed small soluble species are forming.

A combination of mutagenesis and bioinformatical studies could provide further information on how specific residues contribute to assembly. Algorithms like those mentioned in chapter 1 could be used to design other variants based on these peptides and molecular dynamics simulations could aid in understanding how they assemble. In all cases it would be essential to verify these results and hypotheses experimentally. The results from the KFFEAAAKKFFE variants showed that side chains that may appear similar can have very specific effects due to their complex physico-chemical properties and “small” sequence changes may not be so. The role of lysine was shown to be particularly complex and it may be of benefit to perform the expeirments carried out here on other variants. For example lysine could be mutated to either leucine or isoleucine, which would diminish the positive charge but maintain the hydrophobic chain. This would test the importance of the hydrophobic chain in lysine. Furthermore, variants could be constructed that contain non-natural amino acids. Combined with structural methods, the results could give deep insight into the effect of very small chemical changes on assembly and structure. It would also be

worthwhile to add to the literature with more results from toxicity studies using these assemblies and how, if at all, the ability to cause cell death or infectivity relates to structure.

Many proteins and peptides are known to form amyloid polymorphs. Precisely how the generation of one conformation over another is favoured is unknown but will be a delicate balance of a variety of determinants. It is clear that even very small peptides can compensate for variables imposed upon them to form very different structures. Polymorphs may differ in their cytotoxic potential, which will impact on therapeutic design and in choosing potential biomaterials. Short sequences and different experimental procedures can help establish rules for amyloid formation.

# BIBLIOGRAPHY

Abe, H. and Nakanishi, H. (2003) Novel observation of a circular dichroism band originating from amyloid fibril. *Anal Sci*, **19**, 171-173.

Abramoff, M., Magelhaes, P. and Ram, S. (2004) Image Processing with ImageJ. *Biophotonics International*, **11**, 36-42.

Adachi, R., Yamaguchi, K., Yagi, H., Sakurai, K., Naiki, H. and Goto, Y. (2007) Flow-induced alignment of amyloid protofilaments revealed by linear dichroism. *J Biol Chem*, **282**, 8978-8983.

Adler-Abramovich, L., Reches, M., Sedman, V.L., Allen, S., Tendler, S.J. and Gazit, E. (2006) Thermal and chemical stability of diphenylalanine peptide nanotubes: implications for nanotechnological applications. *Langmuir*, **22**, 1313-1320.

Aggeli, A., Bell, M., Carrick, L.M., Fishwick, C.W., Harding, R., Mawer, P.J., Radford, S.E., Strong, A.E. and Boden, N. (2003) pH as a trigger of peptide beta-sheet self-assembly and reversible switching between nematic and isotropic phases. *J Am Chem Soc*, **125**, 9619-9628.

Aggeli, A., Nyrkova, I.A., Bell, M., Harding, R., Carrick, L., McLeish, T.C., Semenov, A.N. and Boden, N. (2001) Hierarchical self-assembly of chiral rod-like molecules as a model for peptide beta -sheet tapes, ribbons, fibrils, and fibers. *Proc Natl Acad Sci U S A*, **98**, 11857-11862.

Aldaye, F.A., Palmer, A.L. and Sleiman, H.F. (2008) Assembling materials with DNA as the guide. *Science*, **321**, 1795-1799.

Ali, F.E., Leung, A., Cherny, R.A., Mavros, C., Barnham, K.J., Separovic, F. and Barrow, C.J. (2006) Dimerisation of N-acetyl-L-tyrosine ethyl ester and Abeta peptides via formation of dityrosine. *Free Radic Res*, **40**, 1-9.

Alzheimer, A. (1904) Histologische Studien zur Differentialdiagnose der progressiven Paralyse. *Nissl's histologische und histopathologische Arbeiten*, **1**, 18-314.

Andersen, C.B., Hicks, M.R., Vetri, V., Vandahl, B., Rahbek-Nielsen, H., Thogersen, H., Thogersen, I.B., Enghild, J.J., Serpell, L.C., Rischel, C. and Otzen, D.E. (2010) Glucagon fibril polymorphism reflects differences in protofilament backbone structure. *J Mol Biol*, **397**, 932-946.

Andersson, D., Carlsson, U. and Freskgard, P.O. (2001) Contribution of tryptophan residues to the CD spectrum of the extracellular domain of human tissue factor: application in folding studies and prediction of secondary structure. *Eur J Biochem*, **268**, 1118-1128.

Anfinsen, C.B. (1973) Principles that govern the folding of protein chains. *Science*, **181**, 223-230.

Anfinsen, C.B., Redfield, R.R., Choate, W.L., Page, J. and Carroll, W.R. (1954) Studies on the gross structure, cross-linkages, and terminal sequences in ribonuclease. *J Biol Chem*, **207**, 201-210.

Anguiano, M., Nowak, R.J. and Lansbury, P.T., Jr. (2002) Protofibrillar islet amyloid polypeptide permeabilizes synthetic vesicles by a pore-like mechanism that may be relevant to type II diabetes. *Biochemistry*, **41**, 11338-11343.

Antzutkin, O.N., Balbach, J.J., Leapman, R.D., Rizzo, N.W., Reed, J. and Tycko, R. (2000) Multiple quantum solid-state NMR indicates a parallel, not antiparallel, organization of beta-sheets in Alzheimer's beta-amyloid fibrils. *Proc Natl Acad Sci U S A*, **97**, 13045-13050.

Antzutkin, O.N., Leapman, R.D., Balbach, J.J. and Tycko, R. (2002) Supramolecular structural constraints on Alzheimer's beta-amyloid fibrils from electron microscopy and solid-state nuclear magnetic resonance. *Biochemistry*, **41**, 15436-15450.

Asakura, S., Eguchi, G. and Iino, T. (1964) Reconstitution Of Bacterial Flagella In Vitro. *J Mol Biol*, **10**, 42-56.

Azriel, R. and Gazit, E. (2001) Analysis of the minimal amyloid-forming fragment of the islet amyloid polypeptide. An experimental support for the key role of the phenylalanine residue in amyloid formation. *J Biol Chem*, **276**, 34156-34161.

Badtke, M.P., Hammer, N.D. and Chapman, M.R. (2009) Functional amyloids signal their arrival. *Sci Signal*, **2**, pe43.

Balbach, J.J., Ishii, Y., Antzutkin, O.N., Leapman, R.D., Rizzo, N.W., Dyda, F., Reed, J. and Tycko, R. (2000) Amyloid fibril formation by A beta 16-22, a seven-residue fragment of the Alzheimer's beta-amyloid peptide, and structural characterization by solid state NMR. *Biochemistry*, **39**, 13748-13759.

Balbach, J.J., Petkova, A.T., Oyler, N.A., Antzutkin, O.N., Gordon, D.J., Meredith, S.C. and Tycko, R. (2002) Supramolecular structure in full-length Alzheimer's beta-amyloid fibrils: evidence for a parallel beta-sheet organization from solid-state nuclear magnetic resonance. *Biophys J*, **83**, 1205-1216.

Balbirnie, M., Grothe, R. and Eisenberg, D.S. (2001) An amyloid-forming peptide from the yeast prion Sup35 reveals a dehydrated beta-sheet structure for amyloid. *Proc Natl Acad Sci U S A*, **98**, 2375-2380.

Baldwin, A.J., Bader, R., Christodoulou, J., MacPhee, C.E., Dobson, C.M. and Barker, P.D. (2006) Cytochrome display on amyloid fibrils. *J Am Chem Soc*, **128**, 2162-2163.

Ban, T., Yamaguchi, K. and Goto, Y. (2006) Direct observation of amyloid fibril growth, propagation, and adaptation. *Acc Chem Res*, **39**, 663-670.

Banta, S., Megeed, Z., Casali, M., Rege, K. and Yarmush, M.L. (2007) Engineering protein and peptide building blocks for nanotechnology. *J Nanosci Nanotechnol*, **7**, 387-401.

Barnhart, M.M. and Chapman, M.R. (2006) Curli biogenesis and function. *Annu Rev Microbiol*, **60**, 131-147.

Baxa, U., Speransky, V., Steven, A.C. and Wickner, R.B. (2002) Mechanism of inactivation on prion conversion of the Saccharomyces cerevisiae Ure2 protein. *Proc Natl Acad Sci U S A*, **99**, 5253-5260.

Baxa, U., Wickner, R.B., Steven, A.C., Anderson, D.E., Marekov, L.N., Yau, W.M. and Tycko, R. (2007) Characterization of beta-sheet structure in Ure2p1-89 yeast prion fibrils by solid-state nuclear magnetic resonance. *Biochemistry*, **46**, 13149-13162.

Belorgey, D., Hagglof, P., Karlsson-Li, S. and Lomas, D.A. (2007) Protein misfolding and the serpinopathies. *Prion*, **1**, 15-20.

Bemporad, F., Taddei, N., Stefani, M. and Chiti, F. (2006) Assessing the role of aromatic residues in the amyloid aggregation of human muscle acylphosphatase. *Protein Sci*, **15**, 862-870.

Benyamini, H., Gunasekaran, K., Wolfson, H. and Nussinov, R. (2003) Beta2-microglobulin amyloidosis: insights from conservation analysis and fibril modelling by protein docking techniques. *J Mol Biol*, **330**, 159-174.

Benzinger, T.L., Gregory, D.M., Burkoth, T.S., Miller-Auer, H., Lynn, D.G., Botto, R.E. and Meredith, S.C. (1998) Propagating structure of Alzheimer's beta-amyloid(10-35) is parallel beta-sheet with residues in exact register. *Proc Natl Acad Sci U S A*, **95**, 13407-13412.

Benzinger, T.L., Gregory, D.M., Burkoth, T.S., Miller-Auer, H., Lynn, D.G., Botto, R.E. and Meredith, S.C. (2000) Two-dimensional structure of beta-amyloid(10-35) fibrils. *Biochemistry*, **39**, 3491-3499.

Berryman, J.T., Radford, S.E. and Harris, S.A. (2009) Thermodynamic description of polymorphism in Q- and N-rich peptide aggregates revealed by atomistic simulation. *Biophys J*, **97**, 1-11.

Berson, J.F., Theos, A.C., Harper, D.C., Tenza, D., Raposo, G. and Marks, M.S. (2003) Proprotein convertase cleavage liberates a fibrillogenic fragment of a resident glycoprotein to initiate melanosome biogenesis. *J Cell Biol*, **161**, 521-533.

Bhattacharjee S, G.T., Sándor Lovas, and Jonathan D. Hirst. (2003) Influence of Tyrosine on the Electronic Circular Dichroism of Helical Peptides. *J. Phys. Chem. B*, **107**, 8682–8688.

Biancalana, M. and Koide, S. (2010) Molecular mechanism of Thioflavin-T binding to amyloid fibrils. *Biochim Biophys Acta*.

Biancalana, M., Makabe, K., Koide, A. and Koide, S. (2009) Molecular mechanism of thioflavin-T binding to the surface of beta-rich peptide self-assemblies. *J Mol Biol*, **385**, 1052-1063.

Bitan, G., Fradinger, E.A., Spring, S.M. and Teplow, D.B. (2005) Neurotoxic protein oligomers--what you see is not always what you get. *Amyloid*, **12**, 88-95.

Blow, D. (2002) *Outline of crystallography for Biologists*.

Bousset, L., Savistchenko, J. and Melki, R. (2008) Assembly of the asparagine- and glutamine-rich yeast prions into protein fibrils. *Curr Alzheimer Res*, **5**, 251-259.

Brender, J.R., Hartman, K., Reid, K.R., Kennedy, R.T. and Ramamoorthy, A. (2008) A single mutation in the nonamyloidogenic region of islet amyloid polypeptide greatly reduces toxicity. *Biochemistry*, **47**, 12680-12688.

Broome, B.M. and Hecht, M.H. (2000) Nature disfavors sequences of alternating polar and non-polar amino acids: implications for amyloidogenesis. *J Mol Biol*, **296**, 961-968.

Bucciantini, M., Calloni, G., Chiti, F., Formigli, L., Nosi, D., Dobson, C.M. and Stefani, M. (2004) Prefibrillar amyloid protein aggregates share common features of cytotoxicity. *J Biol Chem*, **279**, 31374-31382.

Bucciantini, M., Giannoni, E., Chiti, F., Baroni, F., Formigli, L., Zurdo, J., Taddei, N., Ramponi, G., Dobson, C.M. and Stefani, M. (2002) Inherent toxicity of aggregates implies a common mechanism for protein misfolding diseases. *Nature*, **416**, 507-511.

Bulheller, B.M. and Hirst, J.D. (2009) DichroCalc--circular and linear dichroism online. *Bioinformatics*, **25**, 539-540.

Bulheller, B.M., Rodger, A. and Hirst, J.D. (2007) Circular and linear dichroism of proteins. *Phys Chem Chem Phys*, **9**, 2020-2035.

Brockwell, D.J. and Radford, S.E. (2007) Intermediates: ubiquitous species on folding energy landscapes? *Curr Opin Struct Biol,* **17**, 30-37

Cai, X.D., Golde, T.E. and Younkin, S.G. (1993) Release of excess amyloid beta protein from a mutant amyloid beta protein precursor. *Science*, **259**, 514-516.

Calabrese, M.F., Eakin, C.M., Wang, J.M. and Miranker, A.D. (2008) A regulatable switch mediates self-association in an immunoglobulin fold. *Nat Struct Mol Biol*, **15**, 965-971.

Calamai, M., Taddei, N., Stefani, M., Ramponi, G. and Chiti, F. (2003) Relative influence of hydrophobicity and net charge in the aggregation of two homologous proteins. *Biochemistry*, **42**, 15078-15083.

Calloni, G., Lendel, C., Campioni, S., Giannini, S., Gliozzi, A., Relini, A., Vendruscolo, M., Dobson, C.M., Salvatella, X. and Chiti, F. (2008) Structure and dynamics of a partially folded protein are decoupled from its mechanism of aggregation. *J Am Chem Soc*, **130**, 13040-13050.

Cannon, M.J., Williams, A.D., Wetzel, R. and Myszka, D.G. (2004) Kinetic analysis of beta-amyloid fibril elongation. *Anal Biochem*, **328**, 67-75.

Cao, P., Meng, F., Abedini, A. and Raleigh, D.P. (2010) The ability of rodent islet amyloid polypeptide to inhibit amyloid formation by human islet amyloid polypeptide has important implications for the mechanism of amyloid formation and the design of inhibitors. *Biochemistry*, **49**, 872-881.

Capes, J.S., Kiley, P.J. and Windle, A.H. (2010) Investigating the effect of pH on the aggregation of two surfactant-like octapeptides. *Langmuir*, **26**, 5637-5644.

Caplan, M.R., Schwartzfarb, E.M., Zhang, S., Kamm, R.D. and Lauffenburger, D.A. (2002) Control of self-assembling oligopeptide matrix formation through systematic variation of amino acid sequence. *Biomaterials*, **23**, 219-227.

Castelletto, V., Hamley, I.W., Harris, P.J., Olsson, U. and Spencer, N. (2009) Influence of the solvent on the self-assembly of a modified amyloid beta peptide fragment. I. Morphological investigation. *J Phys Chem B*, **113**, 9978-9987.

Castiglioni, E., Abbate, S., Longhi, G., Gangemi, R., Lauceri, R. and Purrello, R. (2007) Absorption flattening as one cause of distortion of circular dichroism spectra of Delta-RuPhen3. H2TPPS complex. *Chirality*, **19**, 642-646.

Caughey, B. and Lansbury, P.T. (2003) Protofibrils, pores, fibrils, and neurodegeneration: separating the responsible protein aggregates from the innocent bystanders. *Annu Rev Neurosci*, **26**, 267-298.

Cerpa, R., Cohen, F.E. and Kuntz, I.D. (1996) Conformational switching in designed peptides: the helix/sheet transition. *Fold Des*, **1**, 91-101.

Chakrabartty, A., Kortemme, T., Padmanabhan, S. and Baldwin, R.L. (1993) Aromatic side-chain contribution to far-ultraviolet circular dichroism of helical peptides and its effect on measurement of helix propensities. *Biochemistry*, **32**, 5560-5565.

Chapman, M.R., Robinson, L.S., Pinkner, J.S., Roth, R., Heuser, J., Hammar, M., Normark, S. and Hultgren, S.J. (2002) Role of Escherichia coli curli operons in directing amyloid fiber formation. *Science*, **295**, 851-855.

Chebaro, Y., Mousseau, N. and Derreumaux, P. (2009) Structures and thermodynamics of Alzheimer's amyloid-beta Abeta(16-35) monomer and dimer by replica exchange molecular dynamics simulations: implication for full-length Abeta fibrillation. *J Phys Chem B*, **113**, 7668-7675.

Chen, M., Margittai, M., Chen, J. and Langen, R. (2007) Investigation of alpha-synuclein fibril structure by site-directed spin labeling. *J Biol Chem*, **282**, 24970-24979.

Chen, R. and Edelhoch, H. (1975) *Biochemical fluorescence: concepts*.

Chernoff, Y.O. (2004) Amyloidogenic domains, prions and structural inheritance: rudiments of early life or recent acquisition? *Curr Opin Chem Biol*, **8**, 665-671.

Cherny, I. and Gazit, E. (2008) Amyloids: not only pathological agents but also ordered nanomaterials. *Angew Chem Int Ed Engl*, **47**, 4062-4069.

Chien, P., Weissman, J.S. and DePace, A.H. (2004) Emerging principles of conformation-based prion inheritance. *Annu Rev Biochem*, **73**, 617-656.

Chimon, S., Shaibat, M.A., Jones, C.R., Calero, D.C., Aizezi, B. and Ishii, Y. (2007) Evidence of fibril-like beta-sheet structures in a neurotoxic amyloid intermediate of Alzheimer's beta-amyloid. *Nat Struct Mol Biol*.

Chiti, F. and Dobson, C.M. (2006) Protein misfolding, functional amyloid, and human disease. *Annu Rev Biochem*, **75**, 333-366.

Chiti, F., Stefani, M., Taddei, N., Ramponi, G. and Dobson, C.M. (2003) Rationalization of the effects of mutations on peptide and protein aggregation rates. *Nature*, **424**, 805-808.

Choi, J.H., May, B.C., Wille, H. and Cohen, F.E. (2009) Molecular modeling of the misfolded insulin subunit and amyloid fibril. *Biophys J*, **97**, 3187-3195.

Chothia, C. (1973) Conformation of twisted beta-pleated sheets in proteins. *J Mol Biol*, **75**, 295-302.

Chou, P.Y. and Fasman, G.D. (1974) Prediction of protein conformation. *Biochemistry*, **13**, 222-245.

Citron, M., Oltersdorf, T., Haass, C., McConlogue, L., Hung, A.Y., Seubert, P., Vigo-Pelfrey, C., Lieberburg, I. and Selkoe, D.J. (1992) Mutation of the beta-amyloid precursor protein in familial Alzheimer's disease increases beta-protein production. *Nature*, **360**, 672-674.

Cobb, N.J., Sonnichsen, F.D., McHaourab, H. and Surewicz, W.K. (2007) Molecular architecture of human prion protein amyloid: a parallel, in-register beta-structure. *Proc Natl Acad Sci U S A*, **104**, 18946-18951.

Cohen. (1982) *Electron Microscopy of Protein*.

Cohen, A. (1986) General introduction and a brief history of the amyloid fibril, *in* Marrink, J., and Van Rijswijk, M. H. (Eds.), Amyloidosis, pp. 3–19, Nijhoff, Dordrecht.

Cohen, F.E., Pan, K.M., Huang, Z., Baldwin, M., Fletterick, R.J. and Prusiner, S.B. (1994) Structural clues to prion replication. *Science*, **264**, 530-531.

Collinge, J. (2001) Prion diseases of humans and animals: their causes and molecular basis. *Annu Rev Neurosci*, **24**, 519-550.

Collinge, J., Palmer, M.S. and Dryden, A.J. (1991) Genetic predisposition to iatrogenic Creutzfeldt-Jakob disease. *Lancet*, **337**, 1441-1442.

Collinge, J., Whitfield, J., McKintosh, E., Beck, J., Mead, S., Thomas, D.J. and Alpers, M.P. (2006) Kuru in the 21st century--an acquired human prion disease with very long incubation periods. *Lancet*, **367**, 2068-2074.

Collins, S.R., Douglass, A., Vale, R.D. and Weissman, J.S. (2004) Mechanism of prion propagation: amyloid growth occurs by monomer addition. *PLoS Biol*, **2**, e321.

Colon, W. and Kelly, J.W. (1992) Partial denaturation of transthyretin is sufficient for amyloid fibril formation in vitro. *Biochemistry*, **31**, 8654-8660.

Come, J.H., Fraser, P.E. and Lansbury, P.T., Jr. (1993) A kinetic model for amyloid formation in the prion diseases: importance of seeding. *Proc Natl Acad Sci U S A*, **90**, 5959-5963.

Compton, S.J. and Jones, C.G. (1985) Mechanism of dye response and interference in the Bradford protein assay. *Anal Biochem*, **151**, 369-374.

Conway, K.A., Harper, J.D. and Lansbury, P.T., Jr. (2000) Fibrils formed in vitro from alpha-synuclein and two mutant forms linked to Parkinson's disease are typical amyloid. *Biochemistry*, **39**, 2552-2563.

Cowgill, R.W. (1975) *Tyrosyl fluorescence in proteins and model peptides*.

Crick, F. (1970) Central dogma of molecular biology. *Nature*, **227**, 561-563.

Crick, F.H. (1958) On protein synthesis. *Symp Soc Exp Biol*, **12**, 138-163.

Dafforn, T.R., Rajendra, J., Halsall, D.J., Serpell, L.C. and Rodger, A. (2004) Protein fiber linear dichroism for structure determination and kinetics in a low-volume, low-wavelength couette flow cell. *Biophys J*, **86**, 404-410.

Dafforn, T.R. and Rodger, A. (2004) Linear dichroism of biomolecules: which way is up? *Curr Opin Struct Biol*, **14**, 541-546.

Davidsson, Norden and Seth. (1980) Measurement of oriented circular dichroism. *Chemical Physics Letters*, **70**.

de Vocht, M.L., Reviakine, I., Wosten, H.A., Brisson, A., Wessels, J.G. and Robillard, G.T. (2000) Structural and functional role of the disulfide bridges in the hydrophobin SC3. *J Biol Chem*, **275**, 28428-28432.

Der-Sarkissian, A., Jao, C.C., Chen, J. and Langen, R. (2003) Structural organization of alpha-synuclein fibrils studied by site-directed spin labeling. *J Biol Chem*, **278**, 37530-37535.

Derkatch, I.L., Bradley, M.E., Hong, J.Y. and Liebman, S.W. (2001) Prions affect the appearance of other prions: the story of [PIN(+)]. *Cell*, **106**, 171-182.

Deshpande, A., Mina, E., Glabe, C. and Busciglio, J. (2006) Different conformations of amyloid beta induce neurotoxicity by distinct mechanisms in human cortical neurons. *J Neurosci*, **26**, 6011-6018.

Diaz-Avalos, R., Long, C., Fontano, E., Balbirnie, M., Grothe, R., Eisenberg, D. and Caspar, D.L. (2003) Cross-beta order and diversity in nanocrystals of an amyloid-forming peptide. *J Mol Biol*, **330**, 1165-1175.

Dicko, C., Hicks, M.R., Dafforn, T.R., Vollrath, F., Rodger, A. and Hoffmann, S.V. (2008) Breaking the 200 nm limit for routine flow linear dichroism measurements using UV synchrotron radiation. *Biophys J*, **95**, 5974-5977.

Dickson, D.W. (2002) Misfolded, protease-resistant proteins in animal models and human neurodegenerative disease. *J Clin Invest*, **110**, 1403-1405.

Dill, K.A. and Chan, H.S. (1997) From Levinthal to pathways to funnels. *Nat Struct Biol*, **4**, 10-19.

Dobson, C.M. (2001) The structural basis of protein folding and its links with human disease. *Philos Trans R Soc Lond B Biol Sci*, **356**, 133-145.

Dobson, C.M. (2003) Protein folding and misfolding. *Nature*, **426**, 884-890.

Dodart, J.C., Bales, K.R., Gannon, K.S., Greene, S.J., DeMattos, R.B., Mathis, C., DeLong, C.A., Wu, S., Wu, X., Holtzman, D.M. and Paul, S.M. (2002) Immunization reverses memory deficits without reducing brain Abeta burden in Alzheimer's disease model. *Nat Neurosci*, **5**, 452-457.

Drake, A.F., Siligardi, G. and Gibbons, W.A. (1988) Reassessment of the electronic circular dichroism criteria for random coil conformations of poly(L-lysine) and the implications for protein folding and denaturation studies. *Biophys Chem*, **31**, 143-146.

Du, H., Fuh, R., Li, J., Corkan, A. and Lindsey, J. (1998) PhotochemCAD: A computer-aided design and research tool in photochemistry. *Photochem Photobiol*, **68**, 141-142.

Du, H.N., Tang, L., Luo, X.Y., Li, H.T., Hu, J., Zhou, J.W. and Hu, H.Y. (2003) A peptide motif consisting of glycine, alanine, and valine is required for the fibrillization and cytotoxicity of human alpha-synuclein. *Biochemistry*, **42**, 8870-8878.

DuBay, K.F., Pawar, A.P., Chiti, F., Zurdo, J., Dobson, C.M. and Vendruscolo, M. (2004) Prediction of the absolute aggregation rates of amyloidogenic polypeptide chains. *J Mol Biol*, **341**, 1317-1326.

Dusa, A., Kaylor, J., Edridge, S., Bodner, N., Hong, D.P. and Fink, A.L. (2006) Characterization of oligomers during alpha-synuclein aggregation using intrinsic tryptophan fluorescence. *Biochemistry*, **45**, 2752-2760.

Duysens, L.N. (1956) The flattening of the absorption spectrum of suspensions, as compared to that of solutions. *Biochim Biophys Acta*, **19**, 1-12.

Dzubiella, J. (2009) Salt-specific stability of short and charged alanine-based alpha-helices. *J Phys Chem B*, **113**, 16689-16694.

Eakin, C.M., Attenello, F.J., Morgan, C.J. and Miranker, A.D. (2004) Oligomeric assembly of native-like precursors precedes amyloid formation by beta-2 microglobulin. *Biochemistry*, **43**, 7808-7815.

Eanes, E.D. and Glenner, G.G. (1968) X-ray diffraction studies on amyloid filaments. *J Histochem Cytochem*, **16**, 673-677.

Eftink, M.R. and Ghiron, C.A. (1981) Fluorescence quenching studies with proteins. *Anal Biochem*, **114**, 199-227.

Eigen, M. (1996) Prionics or the kinetic basis of prion diseases. *Biophys Chem*, **63**, A1-18.

Esposito, L., Paladino, A., Pedone, C. and Vitagliano, L. (2008) Insights into structure, stability, and toxicity of monomeric and aggregated polyglutamine models from molecular dynamics simulations. *Biophys J*, **94**, 4031-4040.

Esposito, L., Pedone, C. and Vitagliano, L. (2006) Molecular dynamics analyses of cross-beta-spine steric zipper models: beta-sheet twisting and aggregation. *Proc Natl Acad Sci U S A*, **103**, 11533-11538.

Fagan, A.M., Watson, M., Parsadanian, M., Bales, K.R., Paul, S.M. and Holtzman, D.M. (2002) Human and murine ApoE markedly alters A beta metabolism before and after plaque formation in a mouse model of Alzheimer's disease. *Neurobiol Dis*, **9**, 305-318.

Fandrich, M. (2007) On the structural definition of amyloid fibrils and other polypeptide aggregates. *Cell Mol Life Sci*, **64**, 2066-2078.

Fandrich, M. and Dobson, C.M. (2002) The behaviour of polyamino acids reveals an inverse side chain effect in amyloid structure formation. *Embo J*, **21**, 5682-5690.

Fandrich, M., Meinhardt, J. and Grigorieff, N. (2009) Structural polymorphism of Alzheimer Abeta and other amyloid fibrils. *Prion*, **3**, 89-93.

Fasman, E.b.G.D. (1996) *Circular Dichroism and the Conformational Analysis of Biomolecules*.

Ferguson, N., Becker, J., Tidow, H., Tremmel, S., Sharpe, T.D., Krause, G., Flinders, J., Petrovich, M., Berriman, J., Oschkinat, H. and Fersht, A.R. (2006) General structural motifs of amyloid protofilaments. *Proc Natl Acad Sci U S A*, **103**, 16248-16253.

Fernandez-Escamilla, A.M., Rousseau, F., Schymkowitz, J. and Serrano, L. (2004) Prediction of sequence-dependent and mutational effects on the aggregation of peptides and proteins. *Nat Biotechnol*, **22**, 1302-1306.

Fezoui, Y., Hartley, D.M., Walsh, D.M., Selkoe, D.J., Osterhout, J.J. and Teplow, D.B. (2000) A de novo designed helix-turn-helix peptide forms nontoxic amyloid fibrils. *Nat Struct Biol*, **7**, 1095-1099.

Fowler, D.M., Koulov, A.V., Alory-Jost, C., Marks, M.S., Balch, W.E. and Kelly, J.W. (2006) Functional amyloid formation within mammalian tissue. *PLoS Biol*, **4**, e6.

Fowler, D.M., Koulov, A.V., Balch, W.E. and Kelly, J.W. (2007) Functional amyloid--from bacteria to humans. *Trends Biochem Sci*, **32**, 217-224.

Fraser, P.E., Duffy, L.K., O'Malley, M.B., Nguyen, J., Inouye, H., and Kirschner, D.A. (1991) Morphology and antibody recognition of synthetic beta amyloid peptides. *J Neurosci Res*, **28**, 474-485.

Fraser, P.E., McLachlan, D.R., Surewicz, W.K., Mizzen, C.A., Snow, A.D., Nguyen, J.T. and Kirschner, D.A. (1994) Conformation and fibrillogenesis of Alzheimer A beta peptides with selected substitution of charged residues. *J Mol Biol*, **244**, 64-73.

Gajdusek, D.C., Gibbs, C.J. and Alpers, M. (1966) Experimental transmission of a Kuru-like syndrome to chimpanzees. *Nature*, **209**, 794-796.

Gazit, E. (2002) A possible role for pi-stacking in the self-assembly of amyloid fibrils. *Faseb J*, **16**, 77-83.

Gebbink, M.F., Claessen, D., Bouma, B., Dijkhuizen, L. and Wosten, H.A. (2005) Amyloids--a functional coat for microorganisms. *Nat Rev Microbiol*, **3**, 333-341.

Gervais, F., Paquette, J., Morissette, C., Krzywkowski, P., Yu, M., Azzi, M., Lacombe, D., Kong, X., Aman, A., Laurin, J., Szarek, W.A. and Tremblay, P. (2007) Targeting soluble Abeta peptide with Tramiprosate for the treatment of brain amyloidosis. *Neurobiol Aging*, **28**, 537-547.

Gething, M.J. and Sambrook, J. (1992) Protein folding in the cell. *Nature*, **355**, 33-45.

Ghadiri, M.R., Granja, J.R., Milligan, R.A., McRee, D.E. and Khazanovich, N. (1993) Self-assembling organic nanotubes based on a cyclic peptide architecture. *Nature*, **366**, 324-327.

Ghanta, J., Shen, C.L., Kiessling, L.L. and Murphy, R.M. (1996) A strategy for designing inhibitors of beta-amyloid toxicity. *J Biol Chem*, **271**, 29525-29528.

Giasson, B.I., Murray, I.V., Trojanowski, J.Q. and Lee, V.M. (2001) A hydrophobic stretch of 12 amino acid residues in the middle of alpha-synuclein is essential for filament assembly. *J Biol Chem*, **276**, 2380-2386.

Gill, S.C. and von Hippel, P.H. (1989) Calculation of protein extinction coefficients from amino acid sequence data. *Anal Biochem*, **182**, 319-326.

Glabe, C.G. (2006) Common mechanisms of amyloid oligomer pathogenesis in degenerative disease. *Neurobiol Aging*, **27**, 570-575.

Glabe, C.G. and Kayed, R. (2006) Common structure and toxic function of amyloid oligomers implies a common mechanism of pathogenesis. *Neurology*, **66**, S74-78.

Glenner, G.G. (1980) Amyloid deposits and amyloidosis. The beta-fibrilloses (first of two parts). *N Engl J Med*, **302**, 1283-1292.

Glover, J.R., Kowal, A.S., Schirmer, E.C., Patino, M.M., Liu, J.J. and Lindquist, S. (1997) Self-seeded fibers formed by Sup35, the protein determinant of [PSI+], a heritable prion-like factor of S. cerevisiae. *Cell*, **89**, 811-819.

Goedert, M., Klug, A. and Crowther, R.A. (2006) Tau protein, the paired helical filament and Alzheimer's disease. *J Alzheimers Dis*, **9**, 195-207.

Goldsbury, C., Goldie, K., Pellaud, J., Seelig, J., Frey, P., Muller, S.A., Kistler, J., Cooper, G.J. and Aebi, U. (2000) Amyloid fibril formation from full-length and fragments of amylin. *J Struct Biol*, **130**, 352-362.

Gordon, D.J., Sciarretta, K.L. and Meredith, S.C. (2001) Inhibition of beta-amyloid(40) fibrillogenesis and disassembly of beta-amyloid(40) fibrils by short beta-amyloid congeners containing N-methyl amino acids at alternate residues. *Biochemistry*, **40**, 8237-8245.

Gordon, D.J., Tappe, R. and Meredith, S.C. (2002) Design and characterization of a membrane permeable N-methyl amino acid-containing peptide that inhibits Abeta1-40 fibrillogenesis. *J Pept Res*, **60**, 37-55.

Gosal, W.S., Morten, I.J., Hewitt, E.W., Smith, D.A., Thomson, N.H. and Radford, S.E. (2005) Competing pathways determine fibril morphology in the self-assembly of beta2-microglobulin into amyloid. *J Mol Biol*, **351**, 850-864.

Gosline, J.M., Guerette, P.A., Ortlepp, C.S. and Savage, K.N. (1999) The mechanical design of spider silks: from fibroin sequence to mechanical function. *J Exp Biol*, **202**, 3295-3303.

Govindarajan, S. and Goldstein, R.A. (1998) On the thermodynamic hypothesis of protein folding. *Proc Natl Acad Sci U S A*, **95**, 5545-5549.

Green, N.M. and Melamed, M.D. (1966) Optical rotatory dispersion, circular dichroism and far-ultraviolet spectra of avidin and streptavidin. *Biochem J*, **100**, 614-621.

Gregory, D.M., Benzinger, T.L., Burkoth, T.S., Miller-Auer, H., Lynn, D.G., Meredith, S.C. and Botto, R.E. (1998) Dipolar recoupling NMR of biomolecular self-assemblies: determining inter- and intrastrand distances in fibrilized Alzheimer's beta-amyloid peptide. *Solid State Nucl Magn Reson*, **13**, 149-166.

Griffith, J.S. (1967) Self-replication and scrapie. *Nature*, **215**, 1043-1044.

Griffiths, J.M., Ashburn, T.T., Auger, M., Costa, P.R., Griffin, R.G. and Lansbury, P.T. (1995) Rotational Resonance Solid-State Nmr Elucidates a Structural Model of Pancreatic Amyloid. *Journal of the American Chemical Society*, **117**, 3539-3546.

Groenning, M., Norrman, M., Flink, J.M., van de Weert, M., Bukrinsky, J.T., Schluckebier, G. and Frokjaer, S. (2007a) Binding mode of Thioflavin T in insulin amyloid fibrils. *J Struct Biol*, **159**, 483-497.

Groenning, M., Olsen, L., van de Weert, M., Flink, J.M., Frokjaer, S. and Jorgensen, F.S. (2007b) Study on the binding of Thioflavin T to beta-sheet-rich and non-beta-sheet cavities. *J Struct Biol*, **158**, 358-369.

Gsponer, J., Haberthur, U. and Caflisch, A. (2003) The role of side-chain interactions in the early steps of aggregation: Molecular dynamics simulations of an amyloid-forming peptide from the yeast prion Sup35. *Proc Natl Acad Sci U S A*, **100**, 5154-5159.

Guijarro, J.I., Sunde, M., Jones, J.A., Campbell, I.D. and Dobson, C.M. (1998) Amyloid fibril formation by an SH3 domain. *Proc Natl Acad Sci U S A*, **95**, 4224-4228.

Guo, Z. and Eisenberg, D. (2006) Runaway domain swapping in amyloid-like fibrils of T7 endonuclease I. *Proc Natl Acad Sci U S A*, **103**, 8042-8047.

Gupta M, B.A., Mishra A, Mathur P, Basu A, Ramakumar S, Chauhan VS. (2007) Self-Assembly of a Dipeptide- Containing Conformationally Restricted Dehydrophenylalanine Residue to Form Ordered Nanotubes. *Advanced Materials*, **19**, 858-861.

Haines, L.A., Rajagopal, K., Ozbas, B., Salick, D.A., Pochan, D.J. and Schneider, J.P. (2005) Light-activated hydrogel formation via the triggered folding and self-assembly of a designed peptide. *J Am Chem Soc*, **127**, 17025-17029.

Hamley, I.W., Castelletto, V., Moulton, C., Myatt, D., Siligardi, G., Oliveira, C.L., Pedersen, J.S., Abutbul, I. and Danino, D. (2010) Self-assembly of a modified amyloid peptide fragment: pH-responsiveness and nematic phase formation. *Macromol Biosci*, **10**, 40-48.

Hammar, M., Bian, Z. and Normark, S. (1996) Nucleator-dependent intercellular assembly of adhesive curli organelles in Escherichia coli. *Proc Natl Acad Sci U S A*, **93**, 6562-6566.

Hammer, N.D., Schmidt, J.C. and Chapman, M.R. (2007) The curli nucleator protein, CsgB, contains an amyloidogenic domain that directs CsgA polymerization. *Proc Natl Acad Sci U S A*, **104**, 12494-12499.

Hardy, J., Duff, K., Hardy, K.G., Perez-Tur, J. and Hutton, M. (1998) Genetic dissection of Alzheimer's disease and related dementias: amyloid and its relationship to tau. *Nat Neurosci*, **1**, 355-358.

Hardy, J. and Selkoe, D.J. (2002) The amyloid hypothesis of Alzheimer's disease: progress and problems on the road to therapeutics. *Science*, **297**, 353-356.

Harel, M., Sonoda, L.K., Silman, I., Sussman, J.L. and Rosenberry, T.L. (2008) Crystal structure of thioflavin T bound to the peripheral site of Torpedo californica acetylcholinesterase reveals how thioflavin T acts as a sensitive fluorescent reporter of ligand binding to the acylation site. *J Am Chem Soc*, **130**, 7856-7861.

Harper, J.D. and Lansbury, P.T., Jr. (1997) Models of amyloid seeding in Alzheimer's disease and scrapie: mechanistic truths and physiological consequences of the time-dependent solubility of amyloid proteins. *Annu Rev Biochem*, **66**, 385-407.

Harper, J.D., Lieber, C.M. and Lansbury, P.T., Jr. (1997a) Atomic force microscopic imaging of seeded fibril formation and fibril branching by the Alzheimer's disease amyloid-beta protein. *Chem Biol*, **4**, 951-959.

Harper, J.D., Wong, S.S., Lieber, C.M. and Lansbury, P.T. (1997b) Observation of metastable Abeta amyloid protofibrils by atomic force microscopy. *Chem Biol*, **4**, 119-125.

Hartl, F.U. and Hayer-Hartl, M. (2009) Converging concepts of protein folding in vitro and in vivo. *Nat Struct Mol Biol*, **16**, 574-581.

Hartley, D.M., Walsh, D.M., Ye, C.P., Diehl, T., Vasquez, S., Vassilev, P.M., Teplow, D.B. and Selkoe, D.J. (1999) Protofibrillar intermediates of amyloid beta-protein induce acute electrophysiological changes and progressive neurotoxicity in cortical neurons. *J Neurosci*, **19**, 8876-8884.

Hartley, D.M., Zhao, C., Speier, A.C., Woodard, G.A., Li, S., Li, Z. and Walz, T. (2008) Transglutaminase induces protofibril-like amyloid beta-protein assemblies that are protease-resistant and inhibit long-term potentiation. *J Biol Chem*, **283**, 16790-16800.

Hendsch, Z.S. and Tidor, B. (1999) Electrostatic interactions in the GCN4 leucine zipper: substantial contributions arise from intramolecular interactions enhanced on binding. *Protein Sci*, **8**, 1381-1392.

Hicks, M., Kowalski, J. and Rodger, A. (2010) LD Spectroscopy of natural and synthetic biomaterials. *Chem Reviews*, **in press**.

Higham, C.E., Jaikaran, E.T., Fraser, P.E., Gross, M. and Clark, A. (2000) Preparation of synthetic human islet amyloid polypeptide (IAPP) in a stable conformation to enable study of conversion to amyloid-like fibrils. *FEBS Lett*, **470**, 55-60.

Hilbich, C., Kisters-Woike, B., Reed, J., Masters, C.L. and Beyreuther, K. (1992) Substitutions of hydrophobic amino acids reduce the amyloidogenicity of Alzheimer's disease beta A4 peptides. *J Mol Biol*, **228**, 460-473.

Hill, A.F., Antoniou, M. and Collinge, J. (1999) Protease-resistant prion protein produced in vitro lacks detectable infectivity. *J Gen Virol*, **80 (Pt 1)**, 11-14.

Hill, E.K., Krebs, B., Goodall, D.G., Howlett, G.J. and Dunstan, D.E. (2006) Shear flow induces amyloid fibril formation. *Biomacromolecules*, **7**, 10-13.

Honig, B. (1999) Protein folding: from the levinthal paradox to structure prediction. *J Mol Biol*, **293**, 283-293.

Horwitz, J., Strickland, E.H. and Billups, C. (1970) Analysis of the vibrational structure in the near-ultraviolet circular dichroism and absorption spectra of tyrosine derivatives and ribonuclease-A at 77 degrees K. *J Am Chem Soc*, **92**, 2119-2129.

Hoshino, M., Katou, H., Hagihara, Y., Hasegawa, K., Naiki, H. and Goto, Y. (2002) Mapping the core of the beta(2)-microglobulin amyloid fibril by H/D exchange. *Nat Struct Biol*, **9**, 332-336.

Hosia, W., Bark, N., Liepinsh, E., Tjernberg, A., Persson, B., Hallen, D., Thyberg, J., Johansson, J. and Tjernberg, L. (2004) Folding into a beta-hairpin can prevent amyloid fibril formation. *Biochemistry*, **43**, 4655-4661.

Hsia, A.Y., Masliah, E., McConlogue, L., Yu, G.Q., Tatsuno, G., Hu, K., Kholodenko, D., Malenka, R.C., Nicoll, R.A. and Mucke, L. (1999) Plaque-independent disruption of neural circuits in Alzheimer's disease mouse models. *Proc Natl Acad Sci U S A*, **96**, 3228-3233.

Hughes, E., Burke, R.M. and Doig, A.J. (2000) Inhibition of toxicity in the beta-amyloid peptide fragment beta -(25-35) using N-methylated derivatives: a general strategy to prevent amyloid formation. *J Biol Chem*, **275**, 25109-25115.

Irvine, G.B., El-Agnaf, O.M., Shankar, G.M. and Walsh, D.M. (2008) Protein aggregation in the brain: the molecular basis for Alzheimer's and Parkinson's diseases. *Mol Med*, **14**, 451-464.

Ishii, Y., Yesinowski, J.P. and Tycko, R. (2001) Sensitivity enhancement in solid-state (13)C NMR of synthetic polymers and biopolymers by (1)H NMR detection with high-speed magic angle spinning. *J Am Chem Soc*, **123**, 2921-2922.

Ivanova, M.I., Sawaya, M.R., Gingery, M., Attinger, A. and Eisenberg, D. (2004) An amyloid-forming segment of beta2-microglobulin suggests a molecular model for the fibril. *Proc Natl Acad Sci U S A*, **101**, 10584-10589.

Ivanova, M.I., Sievers, S.A., Sawaya, M.R., Wall, J.S. and Eisenberg, D. (2009) Molecular basis for insulin fibril assembly. *Proc Natl Acad Sci U S A*, **106**, 18990-18995.

Ivanova, M.I., Thompson, M.J. and Eisenberg, D. (2006) A systematic screen of beta(2)-microglobulin and insulin for amyloid-like segments. *Proc Natl Acad Sci U S A*, **103**, 4079-4082.

Iwata, K., Fujiwara, T., Matsuki, Y., Akutsu, H., Takahashi, S., Naiki, H. and Goto, Y. (2006) 3D structure of amyloid protofilaments of beta2-microglobulin fragment probed by solid-state NMR. *Proc Natl Acad Sci U S A*, **103**, 18119-18124.

Jahn, T.R., Makin, O.S., Morris, K.L., Marshall, K.E., Tian, P., Sikorski, P. and Serpell, L.C. (2010) The common architecture of cross-beta amyloid. *J Mol Biol*, **395**, 717-727.

Jahn, T.R., Parker, M.J., Homans, S.W. and Radford, S.E. (2006) Amyloid formation under physiological conditions proceeds via a native-like folding intermediate. *Nat Struct Mol Biol*, **13**, 195-201.

Jahn, T.R. and Radford, S.E. (2005) The Yin and Yang of protein folding. *Febs J*, **272**, 5962-5970.

Jahn, T.R., Tennent, G.A. and Radford, S.E. (2008) A common beta-sheet architecture underlies in vitro and in vivo beta2-microglobulin amyloid fibrils. *J Biol Chem*, **283**, 17279-17286.

Janin, J. (1979) Surface and inside volumes in globular proteins. *Nature*, **277**, 491-492.

Jaroniec, C.P., MacPhee, C.E., Bajaj, V.S., McMahon, M.T., Dobson, C.M. and Griffin, R.G. (2004) High-resolution molecular structure of a peptide in an amyloid fibril determined by magic angle spinning NMR spectroscopy. *Proc Natl Acad Sci U S A*, **101**, 711-716.

Jarrett, J.T., Berger, E.P. and Lansbury, P.T., Jr. (1993a) The C-terminus of the beta protein is critical in amyloidogenesis. *Ann N Y Acad Sci*, **695**, 144-148.

Jarrett, J.T., Berger, E.P. and Lansbury, P.T., Jr. (1993b) The carboxy terminus of the beta amyloid protein is critical for the seeding of amyloid formation: implications for the pathogenesis of Alzheimer's disease. *Biochemistry*, **32**, 4693-4697.

Jarrett, J.T. and Lansbury, P.T., Jr. (1992) Amyloid fibril formation requires a chemically discriminating nucleation event: studies of an amyloidogenic sequence from the bacterial protein OsmB. *Biochemistry*, **31**, 12345-12352.

Jayasinghe, S.A. and Langen, R. (2004) Identifying structural features of fibrillar islet amyloid polypeptide using site-directed spin labeling. *J Biol Chem*, **279**, 48420-48425.

Jean, L., Lee, C.F., Shaw, M. and Vaux, D.J. (2008) Structural elements regulating amyloidogenesis: a cholinesterase model system. *PLoS ONE*, **3**, e1834.

Jelesarov, I., Durr, E., Thomas, R.M. and Bosshard, H.R. (1998) Salt effects on hydrophobic interaction and charge screening in the folding of a negatively charged peptide to a coiled coil (leucine zipper). *Biochemistry*, **37**, 7539-7550.

Ji, T.H. and Urry, D.W. (1969) Correlation of light scattering and absorption flattening effects with distortions in the circular dichroism patterns of mitochondrial membrane fragments. *Biochem Biophys Res Commun*, **34**, 404-411.

Jimenez, J.L., Guijarro, J.I., Orlova, E., Zurdo, J., Dobson, C.M., Sunde, M. and Saibil, H.R. (1999) Cryo-electron microscopy structure of an SH3 amyloid fibril and model of the molecular packing. *Embo J*, **18**, 815-821.

Jimenez, J.L., Nettleton, E.J., Bouchard, M., Robinson, C.V., Dobson, C.M. and Saibil, H.R. (2002) The protofilament structure of insulin amyloid fibrils. *Proc Natl Acad Sci U S A*, **99**, 9196-9201.

Jimenez, J.L., Tennent, G., Pepys, M. and Saibil, H.R. (2001) Structural diversity of ex vivo amyloid fibrils studied by cryo-electron microscopy. *J Mol Biol*, **311**, 241-247.

Jones, S., Manning, J., Kad, N.M. and Radford, S.E. (2003) Amyloid-forming peptides from beta2-microglobulin-Insights into the mechanism of fibril formation in vitro. *J Mol Biol*, **325**, 249-257.

Kagan, B.L., Azimov, R. and Azimova, R. (2004) Amyloid peptide channels. *J Membr Biol*, **202**, 1-10.

Kajava, A.V., Aebi, U. and Steven, A.C. (2005) The parallel superpleated beta-structure as a model for amyloid fibrils of human amylin. *J Mol Biol*, **348**, 247-252.

Kajava, A.V., Baxa, U., Wickner, R.B. and Steven, A.C. (2004) A model for Ure2p prion filaments and other amyloids: the parallel superpleated beta-structure. *Proc Natl Acad Sci U S A*, **101**, 7885-7890.

Kallberg, Y., Gustafsson, M., Persson, B., Thyberg, J. and Johansson, J. (2001) Prediction of amyloid fibril-forming proteins. *J Biol Chem*, **276**, 12945-12950.

Kayed, R., Bernhagen, J., Greenfield, N., Sweimeh, K., Brunner, H., Voelter, W. and Kapurniotu, A. (1999) Conformational transitions of islet amyloid polypeptide (IAPP) in amyloid formation in vitro. *J Mol Biol*, **287**, 781-796.

Kayed, R., Head, E., Thompson, J.L., McIntire, T.M., Milton, S.C., Cotman, C.W. and Glabe, C.G. (2003) Common structure of soluble amyloid oligomers implies common mechanism of pathogenesis. *Science*, **300**, 486-489.

Kayed, R., Sokolov, Y., Edmonds, B., McIntire, T.M., Milton, S.C., Hall, J.E. and Glabe, C.G. (2004) Permeabilization of lipid bilayers is a common conformation-dependent activity of soluble amyloid oligomers in protein misfolding diseases. *J Biol Chem*, **279**, 46363-46366.

Kelenyi, G. (1967) On the histochemistry of azo group-free thiazole dyes. *J Histochem Cytochem*, **15**, 172-180.

Kelly, S.M., Jess, T.J. and Price, N.C. (2005) How to study proteins by circular dichroism. *Biochim Biophys Acta*, **1751**, 119-139.

Kelly, S.M. and Price, N.C. (1997) The application of circular dichroism to studies of protein folding and unfolding. *Biochim Biophys Acta*, **1338**, 161-185.

Kelly, S.M. and Price, N.C. (2000) The use of circular dichroism in the investigation of protein structure and function. *Curr Protein Pept Sci*, **1**, 349-384.

Khan, M.A., Neale, C., Michaux, C., Pomes, R., Prive, G.G., Woody, R.W. and Bishop, R.E. (2007) Gauging a hydrocarbon ruler by an intrinsic exciton probe. *Biochemistry*, **46**, 4565-4579.

Khurana, R., Coleman, C., Ionescu-Zanetti, C., Carter, S.A., Krishna, V., Grover, R.K., Roy, R. and Singh, S. (2005) Mechanism of thioflavin T binding to amyloid fibrils. *J Struct Biol*, **151**, 229-238.

Kihara, M., Chatani, E., Iwata, K., Yamamoto, K., Matsuura, T., Nakagawa, A., Naiki, H. and Goto, Y. (2006) Conformation of amyloid fibrils of beta2-microglobulin probed by tryptophan mutagenesis. *J Biol Chem*, **281**, 31061-31069.

Kikuchi, T., Mizunoe, Y., Takade, A., Naito, S. and Yoshida, S. (2005) Curli fibers are required for development of biofilm architecture in Escherichia coli K-12 and enhance bacterial adherence to human uroepithelial cells. *Microbiol Immunol*, **49**, 875-884.

Kim, C.A. and Berg, J.M. (1993) Thermodynamic beta-sheet propensities measured using a zinc-finger host peptide. *Nature*, **362**, 267-270.

Kim, J., Basak, J.M. and Holtzman, D.M. (2009) The role of apolipoprotein E in Alzheimer's disease. *Neuron*, **63**, 287-303.

Kim, W. and Hecht, M.H. (2006) Generic hydrophobic residues are sufficient to promote aggregation of the Alzheimer's Abeta42 peptide. *Proc Natl Acad Sci U S A*, **103**, 15824-15829.

Kim, W. and Hecht, M.H. (2008) Mutations enhance the aggregation propensity of the Alzheimer's A beta peptide. *J Mol Biol*, **377**, 565-574.

Kimberly, W.T., LaVoie, M.J., Ostaszewski, B.L., Ye, W., Wolfe, M.S. and Selkoe, D.J. (2003) Gamma-secretase is a membrane protein complex comprised of presenilin, nicastrin, Aph-1, and Pen-2. *Proc Natl Acad Sci U S A*, **100**, 6382-6387.

Kirschner, D.A., Inouye, H., Duffy, L.K., Sinclair, A., Lind, M. and Selkoe, D.J. (1987) Synthetic peptide homologous to beta protein from Alzheimer disease forms amyloid-like fibrils in vitro. *Proc Natl Acad Sci U S A*, **84**, 6953-6957.

Klein, W.L., Krafft, G.A. and Finch, C.E. (2001) Targeting small Abeta oligomers: the solution to an Alzheimer's disease conundrum? *Trends Neurosci*, **24**, 219-224.

Klumpp, L.M., Mackey, A.T., Farrell, C.M., Rosenberg, J.M. and Gilbert, S.P. (2003) A kinesin switch I arginine to lysine mutation rescues microtubule function. *J Biol Chem*, **278**, 39059-39067.

Knaus, K.J., Morillas, M., Swietnicki, W., Malone, M., Surewicz, W.K. and Yee, V.C. (2001) Crystal structure of the human prion protein reveals a mechanism for oligomerization. *Nat Struct Biol*, **8**, 770-774.

Knowles, T.P., Fitzpatrick, A.W., Meehan, S., Mott, H.R., Vendruscolo, M., Dobson, C.M. and Welland, M.E. (2007) Role of intermolecular forces in defining material properties of protein nanofibrils. *Science*, **318**, 1900-1903.

Knowles, T.P., Oppenheim, T.W., Buell, A.K., Chirgadze, D.Y. and Welland, M.E. (2010) Nanostructured films from hierarchical self-assembly of amyloidogenic proteins. *Nat Nanotechnol*, **5**, 204-207.

Krammer, C., Kryndushkin, D., Suhre, M.H., Kremmer, E., Hofmann, A., Pfeifer, A., Scheibel, T., Wickner, R.B., Schatzl, H.M. and Vorberg, I. (2009) The yeast Sup35NM domain propagates as a prion in mammalian cells. *Proc Natl Acad Sci U S A*, **106**, 462-467.

Krammer, C., Suhre, M.H., Kremmer, E., Diemer, C., Hess, S., Schatzl, H.M., Scheibel, T. and Vorberg, I. (2008) Prion protein/protein interactions: fusion with yeast Sup35p-NM modulates cytosolic PrP aggregation in mammalian cells. *Faseb J*, **22**, 762-773.

Krebs, M.R., Bromley, E.H. and Donald, A.M. (2005) The binding of thioflavin-T to amyloid fibrils: localisation and implications. *J Struct Biol*, **149**, 30-37.

Krebs, M.R., Domike, K.R., Cannon, D. and Donald, A.M. (2008) Common motifs in protein self-assembly. *Faraday Discuss*, **139**, 265-274; discussion 309-225, 419-220.

Krysmann, M.J., Castelletto, V. and Hamley, I.W. (2007) Fibrillisation of hydrophobically modified amyloid peptide fragments in an organic solvent. *Soft Matter*, **3**, 1401-1406.

Krysmann, M.J., Castelletto, V., Kelarakis, A., Hamley, I.W., Hule, R.A. and Pochan, D.J. (2008) Self-assembly and hydrogelation of an amyloid peptide fragment. *Biochemistry*, **47**, 4597-4605.

Kumar, S. and Nussinov, R. (2002) Close-range electrostatic interactions in proteins. *Chembiochem*, **3**, 604-617.

Kwan, A.H., Winefield, R.D., Sunde, M., Matthews, J.M., Haverkamp, R.G., Templeton, M.D. and Mackay, J.P. (2006) Structural basis for rodlet assembly in fungal hydrophobins. *Proc Natl Acad Sci U S A*, **103**, 3621-3626.

Kyte, J. and Doolittle, R.F. (1982) A simple method for displaying the hydropathic character of a protein. *J Mol Biol*, **157**, 105-132.

Lakowicz, J.R. (1999) *Principles of Fluorescence Spectroscopy Second Edition*. Kluwer Academic/Plenum.

Lambert, M.P., Barlow, A.K., Chromy, B.A., Edwards, C., Freed, R., Liosatos, M., Morgan, T.E., Rozovsky, I., Trommer, B., Viola, K.L., Wals, P., Zhang, C., Finch, C.E., Krafft, G.A. and Klein, W.L. (1998) Diffusible, nonfibrillar ligands derived from Abeta1-42 are potent central nervous system neurotoxins. *Proc Natl Acad Sci U S A*, **95**, 6448-6453.

Lamm, M.S., Rajagopal, K., Schneider, J.P. and Pochan, D.J. (2005) Laminated morphology of nontwisting beta-sheet fibrils constructed via peptide self-assembly. *J Am Chem Soc*, **127**, 16692-16700.

Lansbury, P.T., Jr. (1992) In pursuit of the molecular structure of amyloid plaque: new technology provides unexpected and critical information. *Biochemistry*, **31**, 6865-6870.

Lansbury, P.T., Jr., Costa, P.R., Griffiths, J.M., Simon, E.J., Auger, M., Halverson, K.J., Kocisko, D.A., Hendsch, Z.S., Ashburn, T.T., Spencer, R.G. and et al. (1995) Structural model for the beta-amyloid fibril based on interstrand alignment of an antiparallel-sheet comprising a C-terminal peptide. *Nat Struct Biol*, **2**, 990-998.

Lashuel, H.A., Hartley, D., Petre, B.M., Walz, T. and Lansbury, P.T., Jr. (2002) Neurodegenerative disease: amyloid pores from pathogenic mutations. *Nature*, **418**, 291.

Lashuel, H.A. and Wall, J. (2005) Molecular Electron Microscopy Approaches to Elucidating the Mechanism of Amyloid Fibril Formation. *Methods Mol Biol.*, **299**, 81-101.

Lawrence, M.C. and Colman, P.M. (1993) Shape complementarity at protein/protein interfaces. *J Mol Biol*, **234**, 946-950.

Lee, K.Y. and Mooney, D.J. (2001) Hydrogels for tissue engineering. *Chem Rev*, **101**, 1869-1879.

Lee, S., Fernandez, E.J. and Good, T.A. (2007) Role of aggregation conditions in structure, stability, and toxicity of intermediates in the Abeta fibril formation pathway. *Protein Sci*, **16**, 723-732.

LeVine, H., 3rd. (1993) Thioflavine T interaction with synthetic Alzheimer's disease beta-amyloid peptides: detection of amyloid aggregation in solution. *Protein Sci*, **2**, 404-410.

LeVine, H., 3rd. (1999) Quantification of beta-sheet amyloid fibril structures with thioflavin T. *Methods Enzymol*, **309**, 274-284.

Levinthal, C. (1968) Are there pathways for proetin folding? *J. Chim. Phys*, **65**, 44-45.

Lewis, J., Dickson, D.W., Lin, W.L., Chisholm, L., Corral, A., Jones, G., Yen, S.H., Sahara, N., Skipper, L., Yager, D., Eckman, C., Hardy, J., Hutton, M. and McGowan, E. (2001) Enhanced neurofibrillary degeneration in transgenic mice expressing mutant tau and APP. *Science*, **293**, 1487-1491.

Lian, H.Y., Jiang, Y., Zhang, H., Jones, G.W. and Perrett, S. (2006) The yeast prion protein Ure2: structure, function and folding. *Biochim Biophys Acta*, **1764**, 535-545.

Liebman, S.W. and Sherman, F. (1979) Extrachromosomal psi+ determinant suppresses nonsense mutations in yeast. *J Bacteriol*, **139**, 1068-1071.

Lipfert, J., Franklin, J., Wu, F. and Doniach, S. (2005) Protein misfolding and amyloid formation for the peptide GNNQQNY from yeast prion protein Sup35: simulation by reaction path annealing. *J Mol Biol*, **349**, 648-658.

Litvinovich, S.V., Brew, S.A., Aota, S., Akiyama, S.K., Haudenschild, C. and Ingham, K.C. (1998) Formation of amyloid-like fibrils by self-association of a partially unfolded fibronectin type III module. *J Mol Biol*, **280**, 245-258.

Loo, D.T., Copani, A., Pike, C.J., Whittemore, E.R., Walencewicz, A.J. and Cotman, C.W. (1993) Apoptosis is induced by beta-amyloid in cultured central nervous system neurons. *Proc Natl Acad Sci U S A*, **90**, 7951-7955.

Lopez De La Paz, M., Goldie, K., Zurdo, J., Lacroix, E., Dobson, C.M., Hoenger, A. and Serrano, L. (2002) De novo designed peptide-based amyloid fibrils. *Proc Natl Acad Sci U S A*, **99**, 16052-16057.

Lopez de la Paz, M., Lacroix, E., Ramirez-Alvarado, M. and Serrano, L. (2001) Computer-aided design of beta-sheet peptides. *J Mol Biol*, **312**, 229-246.

Lopez de la Paz, M. and Serrano, L. (2004) Sequence determinants of amyloid fibril formation. *Proc Natl Acad Sci U S A*, **101**, 87-92.

Lu, Y., Derreumaux, P., Guo, Z., Mousseau, N. and Wei, G. (2009) Thermodynamics and dynamics of amyloid peptide oligomerization are sequence dependent. *Proteins*, **75**, 954-963.

Luca, S., Yau, W.M., Leapman, R. and Tycko, R. (2007) Peptide Conformation and Supramolecular Organization in Amylin Fibrils: Constraints from Solid-State NMR. *Biochemistry*, **46**, 13505-13522.

Luhrs, T., Ritter, C., Adrian, M., Riek-Loher, D., Bohrmann, B., Dobeli, H., Schubert, D. and Riek, R. (2005) 3D structure of Alzheimer's amyloid-beta(1-42) fibrils. *Proc Natl Acad Sci U S A*, **102**, 17342-17347.

Lynch, S.M., Zhou, C. and Messer, A. (2008) An scFv intrabody against the nonamyloid component of alpha-synuclein reduces intracellular aggregation and toxicity. *J Mol Biol*, **377**, 136-147.

MacPhee, C.E. and Woolfson, D.N. (2004) Engineered and designed peptide-based fibrous biomaterials. *Current Opinion in Solid State and Materials Science*, 141-149.

Maddelein, M.L., Dos Reis, S., Duvezin-Caubet, S., Coulary-Salin, B. and Saupe, S.J. (2002) Amyloid aggregates of the HET-s prion protein are infectious. *Proc Natl Acad Sci U S A*, **99**, 7402-7407.

Madine, J., Copland, A., Serpell, L.C. and Middleton, D.A. (2009) Cross-beta spine architecture of fibrils formed by the amyloidogenic segment NFGSVQFV of medin from solid-state NMR and X-ray fiber diffraction measurements. *Biochemistry*, **48**, 3089-3099.

Madine, J., Jack, E., Stockley, P.G., Radford, S.E., Serpell, L.C. and Middleton, D.A. (2008) Structural insights into the polymorphism of amyloid-like fibrils formed by region 20-29 of amylin revealed by solid-state NMR and X-ray fiber diffraction. *J Am Chem Soc*, **130**, 14990-15001.

Maji, S.K., Amsden, J.J., Rothschild, K.J., Condron, M.M. and Teplow, D.B. (2005) Conformational dynamics of amyloid beta-protein assembly probed using intrinsic fluorescence. *Biochemistry*, **44**, 13365-13376.

Makin, O.S., Atkins, E., Sikorski, P., Johansson, J. and Serpell, L.C. (2005) Molecular basis for amyloid fibril formation and stability. *Proc Natl Acad Sci U S A*, **102**, 315-320.

Makin, O.S. and Serpell, L.C. (2005a) Structures for amyloid fibrils. *Febs J*, **272**, 5950-5961.

Makin, O.S. and Serpell, L.C. (2005b) X-ray diffraction studies of amyloid structure. *Methods Mol Biol*, **299**, 67-80.

Malinchik, S.B., Inouye, H., Szumowski, K.E. and Kirschner, D.A. (1998) Structural analysis of Alzheimer's beta(1-40) amyloid: protofilament assembly of tubular fibrils. *Biophys J*, **74**, 537-545.

Manning, M.C., Illangasekare, M. and Woody, R.W. (1988) Circular dichroism studies of distorted alpha-helices, twisted beta-sheets, and beta turns. *Biophys Chem*, **31**, 77-86.

Margittai, M. and Langen, R. (2008) Fibrils with parallel in-register structure constitute a major class of amyloid fibrils: molecular insights from electron paramagnetic resonance spectroscopy. *Q Rev Biophys*, **41**, 265-297.

Marrington, R., Dafforn, T.R., Halsall, D.J., MacDonald, J.I., Hicks, M. and Rodger, A. (2005) Validation of new microvolume Couette flow linear dichroism cells. *Analyst*, **130**, 1608-1616.

Marrington, R., Dafforn, T.R., Halsall, D.J. and Rodger, A. (2004) Micro-volume couette flow sample orientation for absorbance and fluorescence linear dichroism. *Biophys J*, **87**, 2002-2012.

Marrington, R., Seymour, M. and Rodger, A. (2006) A new method for fibrous protein analysis illustrated by application to tubulin microtubule polymerisation and depolymerisation. *Chirality*, **18**, 680-690.

Marshall, K.E., Hicks, M.R., Williams, T.L., Hoffmann, S.V., Rodger, A., Dafforn, T.R. and Serpell, L.C. (2010) Characterizing the assembly of the Sup35 yeast prion fragment, GNNQQNY: structural changes accompany a fiber-to-crystal switch. *Biophys J*, **98**, 330-338.

Martel, A., Burghammer, M., Davies, R.J., Di Cola, E., Vendrely, C. and Riekel, C. (2008) Silk fiber assembly studied by synchrotron radiation SAXS/WAXS and Raman spectroscopy. *J Am Chem Soc*, **130**, 17070-17074.

Masters, C.L., Simms, G., Weinman, N.A., Multhaup, G., McDonald, B.L. and Beyreuther, K. (1985) Amyloid plaque core protein in Alzheimer disease and Down syndrome. *Proc Natl Acad Sci U S A*, **82**, 4245-4249.

Mattson, M.P. (1994) Secreted forms of beta-amyloid precursor protein modulate dendrite outgrowth and calcium responses to glutamate in cultured embryonic hippocampal neurons. *J Neurobiol*, **25**, 439-450.

McGlinchey, R.P., Shewmaker, F., McPhie, P., Monterroso, B., Thurber, K. and Wickner, R.B. (2009) The repeat domain of the melanosome fibril protein Pmel17 forms the amyloid core promoting melanin synthesis. *Proc Natl Acad Sci U S A*, **106**, 13731-13736.

McGowan, J.P. (1922) Scrapie in sheep. *Scott J Agric*, **5**, 365-375.

McLaurin, J., Kierstead, M.E., Brown, M.E., Hawkes, C.A., Lambermon, M.H., Phinney, A.L., Darabie, A.A., Cousins, J.E., French, J.E., Lan, M.F., Chen, F., Wong, S.S., Mount, H.T., Fraser, P.E., Westaway, D. and St George-Hyslop, P. (2006) Cyclohexanehexol inhibitors of Abeta aggregation prevent and reverse Alzheimer phenotype in a mouse model. *Nat Med*, **12**, 801-808.

McParland, V.J., Kad, N.M., Kalverda, A.P., Brown, A., Kirwin-Jones, P., Hunter, M.G., Sunde, M. and Radford, S.E. (2000) Partially unfolded states of beta(2)-microglobulin and amyloid formation in vitro. *Biochemistry*, **39**, 8735-8746.

McPherson, A. (1999) *Protein Crystallisation*.

Measey, T.J., Smith, K.B., Decatur, S.M., Zhao, L., Yang, G. and Schweitzer-Stenner, R. (2009) Self-aggregation of a polyalanine octamer promoted by its C-terminal tyrosine and probed by a strongly enhanced vibrational circular dichroism signal. *J Am Chem Soc*, **131**, 18218-18219.

Meinhardt, J., Sachse, C., Hortschansky, P., Grigorieff, N. and Fandrich, M. (2009) Abeta(1-40) fibril polymorphism implies diverse interaction patterns in amyloid fibrils. *J Mol Biol*, **386**, 869-877.

Meli, M., Morra, G. and Colombo, G. (2008) Investigating the mechanism of peptide aggregation: insights from mixed monte carlo-molecular dynamics simulations. *Biophys J*, **94**, 4414-4426.

Michelitsch, M.D. and Weissman, J.S. (2000) A census of glutamine/asparagine-rich regions: implications for their conserved function and the prediction of novel prions. *Proc Natl Acad Sci U S A*, **97**, 11910-11915.

Minor, D.L., Jr. and Kim, P.S. (1994a) Context is a major determinant of beta-sheet propensity. *Nature*, **371**, 264-267.

Minor, D.L., Jr. and Kim, P.S. (1994b) Measurement of the beta-sheet-forming propensities of amino acids. *Nature*, **367**, 660-663.

Moffat, J.R. and Smith, D.K. (2008) Metastable two-component gel-exploring the gel-crystal interface. *Chem Commun (Camb)*, 2248-2250.

Motta, A., Reches, M., Pappalardo, L., Andreotti, G. and Gazit, E. (2005) The preferred conformation of the tripeptide Ala-Phe-Ala in water is an inverse gamma-turn: implications for protein folding and drug design. *Biochemistry*, **44**, 14170-14178.

Mueller-Steiner, S., Zhou, Y., Arai, H., Roberson, E.D., Sun, B., Chen, J., Wang, X., Yu, G., Esposito, L., Mucke, L. and Gan, L. (2006) Antiamyloidogenic and neuroprotective functions of cathepsin B: implications for Alzheimer's disease. *Neuron*, **51**, 703-714.

Nagarkar, R.P., Hule, R.A., Pochan, D.J. and Schneider, J.P. (2008) De novo design of strand-swapped beta-hairpin hydrogels. *J Am Chem Soc*, **130**, 4466-4474.

Naiki, H., Higuchi, K., Hosokawa, M. and Takeda, T. (1989) Fluorometric determination of amyloid fibrils in vitro using the fluorescent dye, thioflavin T1. *Anal Biochem*, **177**, 244-249.

Naiki, H. and Nakakuki, K. (1996) First-order kinetic model of Alzheimer's beta-amyloid fibril extension in vitro. *Lab Invest*, **74**, 374-383.

Narayanan, S., Walter, S. and Reif, B. (2006) Yeast prion-protein, sup35, fibril formation proceeds by addition and substraction of oligomers. *Chembiochem*, **7**, 757-765.

Nelson, R. and Eisenberg, D. (2006) Recent atomic models of amyloid fibril structure. *Curr Opin Struct Biol*, **16**, 260-265.

Nelson, R., Sawaya, M.R., Balbirnie, M., Madsen, A.O., Riekel, C., Grothe, R. and Eisenberg, D. (2005) Structure of the cross-beta spine of amyloid-like fibrils. *Nature*, **435**, 773-778.

Nesloney, C.L. and Kelly, J.W. (1996) Progress towards understanding beta-sheet structure. *Bioorg Med Chem*, **4**, 739-766.

Nielsen, J.T., Bjerring, M., Jeppesen, M.D., Pedersen, R.O., Pedersen, J.M., Hein, K.L., Vosegaard, T., Skrydstrup, T., Otzen, D.E. and Nielsen, N.C. (2009) Unique identification of supramolecular structures in amyloid fibrils by solid-state NMR spectroscopy. *Angew Chem Int Ed Engl*, **48**, 2118-2121.

Nilsson, M.R. (2004) Techniques to study amyloid fibril formation in vitro. *Methods*, **34**, 151-160.

Norden, B. and Kurucsev, T. (1994) Analysing DNA complexes by circular and linear dichroism. *J Mol Recognit*, **7**, 141-155.

Olofsson, A., Sauer-Eriksson, A.E. and Ohman, A. (2006) The solvent protection of alzheimer amyloid-beta-(1-42) fibrils as determined by solution NMR spectroscopy. *J Biol Chem*, **281**, 477-483.

Olson, M.I. and Shaw, C.M. (1969) Presenile dementia and Alzheimer's disease in mongolism. *Brain*, **92**, 147-156.

Ono, K., Condron, M.M. and Teplow, D.B. (2009) Structure-neurotoxicity relationships of amyloid beta-protein oligomers. *Proc Natl Acad Sci U S A*, **106**, 14745-14750.

Orpiszewski, J. and Benson, M.D. (1999) Induction of beta-sheet structure in amyloidogenic peptides by neutralization of aspartate: a model for amyloid nucleation. *J Mol Biol*, **289**, 413-428.

Otzen, D.E., Kristensen, O. and Oliveberg, M. (2000) Designed protein tetramer zipped together with a hydrophobic Alzheimer homology: a structural clue to amyloid assembly. *Proc Natl Acad Sci U S A*, **97**, 9907-9912.

Otzen, D.E. and Oliveberg, M. (1999) Salt-induced detour through compact regions of the protein folding landscape. *Proc Natl Acad Sci U S A*, **96**, 11746-11751.

Padrick, S.B. and Miranker, A.D. (2001) Islet amyloid polypeptide: identification of long-range contacts and local order on the fibrillogenesis pathway. *J Mol Biol*, **308**, 783-794.

Padrick, S.B. and Miranker, A.D. (2002) Islet amyloid: phase partitioning and secondary nucleation are central to the mechanism of fibrillogenesis. *Biochemistry*, **41**, 4694-4703.

Palmer, M.S., Dryden, A.J., Hughes, J.T. and Collinge, J. (1991) Homozygous prion protein genotype predisposes to sporadic Creutzfeldt-Jakob disease. *Nature*, **352**, 340-342.

Pan, K.M., Baldwin, M., Nguyen, J., Gasset, M., Serban, A., Groth, D., Mehlhorn, I., Huang, Z., Fletterick, R.J., Cohen, F.E. and et al. (1993) Conversion of alpha-helices into beta-sheets features in the formation of the scrapie prion proteins. *Proc Natl Acad Sci U S A*, **90**, 10962-10966.

Paravastu, A.K., Leapman, R.D., Yau, W.M. and Tycko, R. (2008) Molecular structural basis for polymorphism in Alzheimer's beta-amyloid fibrils. *Proc Natl Acad Sci U S A*, **105**, 18349-18354.

Paravastu, A.K., Qahwash, I., Leapman, R.D., Meredith, S.C. and Tycko, R. (2009) Seeded growth of beta-amyloid fibrils from Alzheimer's brain-derived fibrils produces a distinct fibril structure. *Proc Natl Acad Sci U S A*, **106**, 7443-7448.

Patino, M.M., Liu, J.J., Glover, J.R. and Lindquist, S. (1996) Support for the prion hypothesis for inheritance of a phenotypic trait in yeast. *Science*, **273**, 622-626.

Pauling, L. and Corey, R.B. (1951) The pleated sheet, a new layer configuration of polypeptide chains. *Proc Natl Acad Sci U S A*, **37**, 251-256.

Pawar, A.P., Dubay, K.F., Zurdo, J., Chiti, F., Vendruscolo, M. and Dobson, C.M. (2005) Prediction of "aggregation-prone" and "aggregation-susceptible" regions in proteins associated with neurodegenerative diseases. *J Mol Biol*, **350**, 379-392.

Pedersen, J.S., Dikov, D., Flink, J.L., Hjuler, H.A., Christiansen, G. and Otzen, D.E. (2006a) The changing face of glucagon fibrillation: structural polymorphism and conformational imprinting. *J Mol Biol*, **355**, 501-523.

Pedersen, J.S., Dikov, D. and Otzen, D.E. (2006b) N- and C-terminal hydrophobic patches are involved in fibrillation of glucagon. *Biochemistry*, **45**, 14503-14512.

Pepys, M.B. (2006) Amyloidosis. *Annu Rev Med*, **57**, 223-241.

Pepys, M.B., Herbert, J., Hutchinson, W.L., Tennent, G.A., Lachmann, H.J., Gallimore, J.R., Lovat, L.B., Bartfai, T., Alanine, A., Hertel, C., Hoffmann, T., Jakob-Roetne, R., Norcross, R.D., Kemp, J.A., Yamamura, K., Suzuki, M., Taylor, G.W., Murray, S., Thompson, D., Purvis, A., Kolstoe, S., Wood, S.P. and Hawkins, P.N. (2002) Targeted pharmacological depletion of serum amyloid P component for treatment of human amyloidosis. *Nature*, **417**, 254-259.

Perez-Jimenez, R., Godoy-Ruiz, R., Ibarra-Molero, B. and Sanchez-Ruiz, J.M. (2004) The efficiency of different salts to screen charge interactions in proteins: a Hofmeister effect? *Biophys J*, **86**, 2414-2429.

Periole, X., Rampioni, A., Vendruscolo, M. and Mark, A.E. (2009) Factors that affect the degree of twist in beta-sheet structures: a molecular dynamics simulation study of a cross-beta filament of the GNNQQNY peptide. *J Phys Chem B*, **113**, 1728-1737.

Perutz, M. (1994) Polar zippers: their role in human disease. *Protein Sci*, **3**, 1629-1637.

Perutz, M.F., Finch, J.T., Berriman, J. and Lesk, A. (2002) Amyloid fibers are water-filled nanotubes. *Proc Natl Acad Sci U S A*, **99**, 5591-5595.

Petkova, A.T., Ishii, Y., Balbach, J.J., Antzutkin, O.N., Leapman, R.D., Delaglio, F. and Tycko, R. (2002) A structural model for Alzheimer's beta -amyloid fibrils based on experimental constraints from solid state NMR. *Proc Natl Acad Sci U S A*, **99**, 16742-16747.

Petkova, A.T., Leapman, R.D., Guo, Z., Yau, W.M., Mattson, M.P. and Tycko, R. (2005) Self-propagating, molecular-level polymorphism in Alzheimer's beta-amyloid fibrils. *Science*, **307**, 262-265.

Petkova, A.T., Yau, W.M. and Tycko, R. (2006) Experimental constraints on quaternary structure in Alzheimer's beta-amyloid fibrils. *Biochemistry*, **45**, 498-512.

Picotti, P., De Franceschi, G., Frare, E., Spolaore, B., Zambonin, M., Chiti, F., de Laureto, P.P. and Fontana, A. (2007) Amyloid Fibril Formation and Disaggregation of Fragment 1-29 of Apomyoglobin: Insights into the Effect of pH on Protein Fibrillogenesis. *J Mol Biol*.

Platt, G.W., Xue, W.F., Homans, S.W. and Radford, S.E. (2009) Probing dynamics within amyloid fibrils using a novel capping method. *Angew Chem Int Ed Engl*, **48**, 5705-5707.

Pochan, D.J., Schneider, J.P., Kretsinger, J., Ozbas, B., Rajagopal, K. and Haines, L. (2003) Thermally reversible hydrogels via intramolecular folding and consequent self-assembly of a de novo designed peptide. *J Am Chem Soc*, **125**, 11802-11803.

Prusiner, S.B. (1998) Prions. *Proc Natl Acad Sci U S A*, **95**, 13363-13383.

Prusiner, S.B., McKinley, M.P., Bowman, K.A., Bolton, D.C., Bendheim, P.E., Groth, D.F. and Glenner, G.G. (1983) Scrapie prions aggregate to form amyloid-like birefringent rods. *Cell*, **35**, 349-358.

Ptitsyn, O.B. (1991) How does protein synthesis give rise to the 3D-structure? *FEBS Lett*, **285**, 176-181.

Rajagopal, K., Lamm, M.S., Haines-Butterick, L.A., Pochan, D.J. and Schneider, J.P. (2009) Tuning the pH responsiveness of beta-hairpin peptide folding, self-assembly, and hydrogel material formation. *Biomacromolecules*, **10**, 2619-2625.

Ramachandran, S., Tseng, Y. and Yu, Y.B. (2005) Repeated rapid shear-responsiveness of peptide hydrogels with tunable shear modulus. *Biomacromolecules*, **6**, 1316-1321.

Rammensee, S., Slotta, U., Scheibel, T. and Bausch, A.R. (2008) Assembly mechanism of recombinant spider silk proteins. *Proc Natl Acad Sci U S A*, **105**, 6590-6595.

Rapoport, M., Dawson, H.N., Binder, L.I., Vitek, M.P. and Ferreira, A. (2002) Tau is essential to beta -amyloid-induced neurotoxicity. *Proc Natl Acad Sci U S A*, **99**, 6364-6369.

Rauscher, S., Baud, S., Miao, M., Keeley, F.W. and Pomes, R. (2006) Proline and glycine control protein self-organization into elastomeric or amyloid fibrils. *Structure*, **14**, 1667-1676.

Reches, M. and Gazit, E. (2003) Casting metal nanowires within discrete self-assembled peptide nanotubes. *Science*, **300**, 625-627.

Relini, A., Torrassa, S., Ferrando, R., Rolandi, R., Campioni, S., Chiti, F. and Gliozzi, A. (2010) Detection of populations of amyloid-like protofibrils with different physical properties. *Biophys J*, **98**, 1277-1284.

Ritter, C., Maddelein, M.L., Siemer, A.B., Luhrs, T., Ernst, M., Meier, B.H., Saupe, S.J. and Riek, R. (2005) Correlation of structural elements and infectivity of the HET-s prion. *Nature*, **435**, 844-848.

Rodger, A., Dafforn, T. and Norden, B. (2010) *Linear Dichroism and Circular Dichroism: A Textbook on Polarised-Light Spectroscopy*.

Rodger, A., Marrington, R., Geeves, M.A., Hicks, M., de Alwis, L., Halsall, D.J. and Dafforn, T.R. (2006) Looking at long molecules in solution: what happens when they are subjected to Couette flow? *Phys Chem Chem Phys*, **8**, 3161-3171.

Rodger, A. and Norden, B. (1997) *Circular Dichroism and Linear Dichroism*.

Rogers, D.M. and Hirst, J.D. (2004) First-principles calculations of protein circular dichroism in the near ultraviolet. *Biochemistry*, **43**, 11092-11102.

Roher, A.E., Baudry, J., Chaney, M.O., Kuo, Y.M., Stine, W.B. and Emmerling, M.R. (2000) Oligomerizaiton and fibril asssembly of the amyloid-beta protein. *Biochim Biophys Acta*, **1502**, 31-43.

Rose, G.D., Geselowitz, A.R., Lesser, G.J., Lee, R.H. and Zehfus, M.H. (1985) Hydrophobicity of amino acid residues in globular proteins. *Science*, **229**, 834-838.

Rousseau, F., Schymkowitz, J. and Serrano, L. (2006) Protein aggregation and amyloidosis: confusion of the kinds? *Curr Opin Struct Biol*, **16**, 118-126.

Sabate, R., Lascu, I. and Saupe, S.J. (2008) On the binding of Thioflavin-T to HET-s amyloid fibrils assembled at pH 2. *J Struct Biol*, **162**, 387-396.

Sachse, C., Fandrich, M. and Grigorieff, N. (2008) Paired beta-sheet structure of an Abeta(1-40) amyloid fibril revealed by electron microscopy. *Proc Natl Acad Sci U S A*, **105**, 7462-7466.

Sachse, C., Xu, C., Wieligmann, K., Diekmann, S., Grigorieff, N. and Fandrich, M. (2006) Quaternary structure of a mature amyloid fibril from Alzheimer's Abeta(1-40) peptide. *J Mol Biol*, **362**, 347-354.

Sakata, M., Chatani, E., Kameda, A., Sakurai, K., Naiki, H. and Goto, Y. (2008) Kinetic coupling of folding and prolyl isomerization of beta2-microglobulin studied by mutational analysis. *J Mol Biol*, **382**, 1242-1255.

Sawaya, M.R., Sambashivan, S., Nelson, R., Ivanova, M.I., Sievers, S.A., Apostol, M.I., Thompson, M.J., Balbirnie, M., Wiltzius, J.J., McFarlane, H.T., Madsen, A.O., Riekel, C. and Eisenberg, D. (2007) Atomic structures of amyloid cross-beta spines reveal varied steric zippers. *Nature*, **447**, 453-457.

Scheibel, T., Parthasarathy, R., Sawicki, G., Lin, X.M., Jaeger, H. and Lindquist, S.L. (2003) Conducting nanowires built by controlled self-assembly of amyloid fibers and selective metal deposition. *Proc Natl Acad Sci U S A*, **100**, 4527-4532.

Schellman. (1975) Circular Dicroism and Optical Rotation. *Chemical Reviews*, **75**, 323-331.

Schenk, D. (2002) Amyloid-beta immunotherapy for Alzheimer's disease: the end of the beginning. *Nat Rev Neurosci*, **3**, 824-828.

Schenk, D.B., Seubert, P., Grundman, M. and Black, R. (2005) A beta immunotherapy: Lessons learned for potential treatment of Alzheimer's disease. *Neurodegener Dis*, **2**, 255-260.

Scheuner, D., Eckman, C., Jensen, M., Song, X., Citron, M., Suzuki, N., Bird, T.D., Hardy, J., Hutton, M., Kukull, W., Larson, E., Levy-Lahad, E., Viitanen, M., Peskind, E., Poorkaj, P., Schellenberg, G., Tanzi, R., Wasco, W., Lannfelt, L., Selkoe, D. and Younkin, S. (1996) Secreted amyloid beta-protein similar to that in the senile plaques of Alzheimer's disease is increased in vivo by the presenilin 1 and 2 and APP mutations linked to familial Alzheimer's disease. *Nat Med*, **2**, 864-870.

Schmidt, M., Sachse, C., Richter, W., Xu, C., Fandrich, M. and Grigorieff, N. (2009) Comparison of Alzheimer A{beta}(1-40) and A{beta}(1-42) amyloid fibrils reveals similar protofilament structures. *Proc Natl Acad Sci U S A*.

Schmittschmitt, J.P. and Scholtz, J.M. (2003) The role of protein stability, solubility, and net charge in amyloid fibril formation. *Protein Sci*, **12**, 2374-2378.

Schneider, J.P., Pochan, D.J., Ozbas, B., Rajagopal, K., Pakstis, L. and Kretsinger, J. (2002) Responsive hydrogels from the intramolecular folding and self-assembly of a designed peptide. *J Am Chem Soc*, **124**, 15030-15037.

Schueler, O. and Margalit, H. (1995) Conservation of salt bridges in protein families. *J Mol Biol*, **248**, 125-135.

Seidel, C., Orth, A. and Greulich, K.O. (1993) Electronic effects on the fluorescence of tyrosine in small peptides. *Photochem Photobiol*, **58**, 178-184.

Selkoe, D.J. (1994) Normal and abnormal biology of the beta-amyloid precursor protein. *Annu Rev Neurosci*, **17**, 489-517.

Selkoe, D.J. (2000) Toward a comprehensive theory for Alzheimer's disease. Hypothesis: Alzheimer's disease is caused by the cerebral accumulation and cytotoxicity of amyloid beta-protein. *Ann N Y Acad Sci*, **924**, 17-25.

Selkoe, D.J. (2001) Presenilin, Notch, and the genesis and treatment of Alzheimer's disease. *Proc Natl Acad Sci U S A*, **98**, 11039-11041.

Serio, T.R., Cashikar, A.G., Kowal, A.S., Sawicki, G.J., Moslehi, J.J., Serpell, L., Arnsdorf, M.F. and Lindquist, S.L. (2000) Nucleated conformational conversion and the replication of conformational information by a prion determinant. *Science*, **289**, 1317-1321.

Serpell, L.C., Sunde, M., Fraser, P.E., Luther P.K., Morris E.P., Sangren, O., Lundgren, E. and Blake, C.C. (1995) Examination of the structure of the transthyretin amyloid fibril by image reconstruction from electron micrographs. *J Mol Biol*, **254**, 113-118.

Serpell, L.C. (2000) Alzheimer's amyloid fibrils: structure and assembly. *Biochim Biophys Acta*, **1502**, 16-30.

Serpell, L.C., Benson, M., Liepnieks, J.J. and Fraser, P.E. (2007) Structural analyses of fibrinogen amyloid fibrils. *Amyloid*, **14**, 199-203.

Serpell, L.C., Berriman, J., Jakes, R., Goedert, M. and Crowther, R.A. (2000a) Fiber diffraction of synthetic alpha-synuclein filaments shows amyloid-like cross-beta conformation. *Proc Natl Acad Sci U S A*, **97**, 4897-4902.

Serpell, L.C. and Smith, J.M. (2000) Direct visualisation of the beta-sheet structure of synthetic Alzheimer's amyloid. *J Mol Biol*, **299**, 225-231.

Serpell, L.C., Sunde, M., Benson, M.D., Tennent, G.A., Pepys, M.B. and Fraser, P.E. (2000b) The protofilament substructure of amyloid fibrils. *J Mol Biol*, **300**, 1033-1039.

Shaw, K.L., Grimsley, G.R., Yakovlev, G.I., Makarov, A.A. and Pace, C.N. (2001) The effect of net charge on the solubility, activity, and stability of ribonuclease Sa. *Protein Sci*, **10**, 1206-1215.

Shewmaker, F., Wickner, R.B. and Tycko, R. (2006) Amyloid of the prion domain of Sup35p has an in-register parallel beta-sheet structure. *Proc Natl Acad Sci U S A*, **103**, 19754-19759.

Shirahama, T., Benson, M.D., Cohen, A.S. and Tanaka, A. (1973) Fibrillar assemblage of variable segments of immunoglobulin light chains: an electron microscopic study. *J Immunol*, **110**, 21-30.

Shirahama, T. and Cohen, A.S. (1965) Structure of amyloid fibrils after negative staining and high-resolution electron microscopy. *Nature*, **206**, 737-738.

Siemers, E.R., Quinn, J.F., Kaye, J., Farlow, M.R., Porsteinsson, A., Tariot, P., Zoulnouni, P., Galvin, J.E., Holtzman, D.M., Knopman, D.S., Satterwhite, J., Gonzales, C., Dean, R.A. and May, P.C. (2006) Effects of a gamma-secretase inhibitor in a randomized study of patients with Alzheimer disease. *Neurology*, **66**, 602-604.

Sigurdsson, E.M. (2009) Tau-focused immunotherapy for Alzheimer's disease and related tauopathies. *Curr Alzheimer Res*, **6**, 446-450.

Sikorski, P. and Atkins, E. (2005) New model for crystalline polyglutamine assemblies and their connection with amyloid fibrils. *Biomacromolecules*, **6**, 425-432.

Sikorski, P., Atkins, E.D. and Serpell, L.C. (2003) Structure and texture of fibrous crystals formed by Alzheimer's abeta(11-25) peptide fragment. *Structure*, **11**, 915-926.

Sipe, J.D. and Cohen, A.S. (2000) Review: history of the amyloid fibril. *J Struct Biol*, **130**, 88-98.

Slotta, U., Hess, S., Spiess, K., Stromer, T., Serpell, L. and Scheibel, T. (2007) Spider silk and amyloid fibrils: a structural comparison. *Macromol Biosci*, **7**, 183-188.

Smith, C.K., Withka, J.M. and Regan, L. (1994) A thermodynamic scale for the beta-sheet forming tendencies of the amino acids. *Biochemistry*, **33**, 5510-5517.

Smith, J.F., Knowles, T.P., Dobson, C.M., Macphee, C.E. and Welland, M.E. (2006) Characterization of the nanoscale properties of individual amyloid fibrils. *Proc Natl Acad Sci U S A*, **103**, 15806-15811.

Smith, P.K., Krohn, R.I., Hermanson, G.T., Mallia, A.K., Gartner, F.H., Provenzano, M.D., Fujimoto, E.K., Goeke, N.M., Olson, B.J. and Klenk, D.C. (1985) Measurement of protein using bicinchoninic acid. *Anal Biochem*, **150**, 76-85.

Soderberg, L., Dahlqvist, C., Kakuyama, H., Thyberg, J., Ito, A., Winblad, B., Naslund, J. and Tjernberg, L.O. (2005) Collagenous Alzheimer amyloid plaque component assembles amyloid fibrils into protease resistant aggregates. *Febs J*, **272**, 2231-2236.

Solomon, B., Koppel, R., Frankel, D. and Hanan-Aharon, E. (1997) Disaggregation of Alzheimer beta-amyloid by site-directed mAb. *Proc Natl Acad Sci U S A*, **94**, 4109-4112.

Sondheimer, N. and Lindquist, S. (2000) Rnq1: an epigenetic modifier of protein function in yeast. *Mol Cell*, **5**, 163-172.

Sreerama, N., Manning, M.C., Powers, M.E., Zhang, J.X., Goldenberg, D.P. and Woody, R.W. (1999) Tyrosine, phenylalanine, and disulfide contributions to the circular dichroism of proteins: circular dichroism spectra of wild-type and mutant bovine pancreatic trypsin inhibitor. *Biochemistry*, **38**, 10814-10822.

Stahl, N. and Prusiner, S.B. (1991) Prions and prion proteins. *Faseb J*, **5**, 2799-2807.

Staniforth, R.A., Giannini, S., Higgins, L.D., Conroy, M.J., Hounslow, A.M., Jerala, R., Craven, C.J. and Waltho, J.P. (2001) Three-dimensional domain swapping in the folded and molten-globule states of cystatins, an amyloid-forming structural superfamily. *Embo J*, **20**, 4774-4781.

Stansfield, I. and Tuite, M.F. (1994) Polypeptide chain termination in Saccharomyces cerevisiae. *Curr Genet*, **25**, 385-395.

Starck, C.S. and Sutherland-Smith, A.J. (2010) Cytotoxic aggregation and amyloid formation by the myostatin precursor protein. *PLoS One*, **5**, e9170.

Stefani, M. (2008) Protein folding and misfolding on surfaces. *Int J Mol Sci*, **9**, 2515-2542.

Street, A.G. and Mayo, S.L. (1999) Intrinsic beta-sheet propensities result from van der Waals interactions between side chains and the local backbone. *Proc Natl Acad Sci U S A*, **96**, 9074-9076.

Strickland, E.H. (1974) Aromatic contributions to circular dichroism spectra of proteins. *CRC Crit Rev Biochem*, **2**, 113-175.

Strodel, B., Whittleston, C.S. and Wales, D.J. (2007) Thermodynamics and kinetics of aggregation for the GNNQQNY peptide. *J Am Chem Soc*, **129**, 16005-16014.

Stryer, L. (1999) *Biochemistry*. W.H. Freeman & Company.

Sudhakar, K., Wright, W., Williams, S., Phillips, C. and Vanderkooi, J. (1993) Phenylalanine fluorescence and phosphorescence used as a probe of conformation for cod parvalbumin. *Journal of Fluorescence*, **3**.

Sumner Makin, O. and Serpell, L.C. (2004) Structural characterisation of islet amyloid polypeptide fibrils. *J Mol Biol*, **335**, 1279-1288.

Sumner Makin, O., Sikorski, P. and Serpell, L. (2007) *CLEARER*: a new tool for the analysis of X-ray fibre diffraction patterns and diffraction simulation from atomic structural models. *Journal of Applied Crystallography*, **40**, 966-972.

Sunde, M., Kwan, A.H., Templeton, M.D., Beever, R.E. and Mackay, J.P. (2008) Structural analysis of hydrophobins. *Micron*, **39**, 773-784.

Sunde, M., Richardson, S.J., Chang, L., Pettersson, T.M., Schreiber, G. and Blake, C.C. (1996) The crystal structure of transthyretin from chicken. *Eur J Biochem*, **236**, 491-499.

Sunde, M., Serpell, L.C., Bartlam, M., Fraser, P.E., Pepys, M.B. and Blake, C.C. (1997) Common core structure of amyloid fibrils by synchrotron X-ray diffraction. *J Mol Biol*, **273**, 729-739.

Suzuki, N., Cheung, T.T., Cai, X.D., Odaka, A., Otvos, L., Jr., Eckman, C., Golde, T.E. and Younkin, S.G. (1994) An increased percentage of long amyloid beta protein secreted by familial amyloid beta protein precursor (beta APP717) mutants. *Science*, **264**, 1336-1340.

Taddei, N., Capanni, C., Chiti, F., Stefani, M., Dobson, C.M. and Ramponi, G. (2001) Folding and aggregation are selectively influenced by the conformational preferences of the alpha-helices of muscle acylphosphatase. *J Biol Chem*, **276**, 37149-37154.

Takasugi, N., Tomita, T., Hayashi, I., Tsuruoka, M., Niimura, M., Takahashi, Y., Thinakaran, G. and Iwatsubo, T. (2003) The role of presenilin cofactors in the gamma-secretase complex. *Nature*, **422**, 438-441.

Tan, S.Y. and Pepys, M.B. (1994) Amyloidosis. *Histopathology*, **25**, 403-414.

Tanaka, M., Collins, S.R., Toyama, B.H. and Weissman, J.S. (2006) The physical basis of how prion conformations determine strain phenotypes. *Nature*, **442**, 585-589.

Tartaglia, G.G., Pawar, A.P., Campioni, S., Dobson, C.M., Chiti, F. and Vendruscolo, M. (2008) Prediction of aggregation-prone regions in structured proteins. *J Mol Biol*, **380**, 425-436.

Tattum, M.H., Cohen-Krausz, S., Thumanu, K., Wharton, C.W., Khalili-Shirazi, A., Jackson, G.S., Orlova, E.V., Collinge, J., Clarke, A.R. and Saibil, H.R. (2006) Elongated oligomers assemble into mammalian PrP amyloid fibrils. *J Mol Biol*, **357**, 975-985.

Telling, G.C., Parchi, P., DeArmond, S.J., Cortelli, P., Montagna, P., Gabizon, R., Mastrianni, J., Lugaresi, E., Gambetti, P. and Prusiner, S.B. (1996) Evidence for the conformation of the pathologic isoform of the prion protein enciphering and propagating prion diversity. *Science*, **274**, 2079-2082.

Tillement, J.P., Lecanu, L. and Papadopoulos, V. (2010) Amyloidosis and neurodegenerative diseases: current treatments and new pharmacological options. *Pharmacology*, **85**, 1-17.

Tinker, D.A., Krebs, E.A., Feltham, I.C., Attah-Poku, S.K. and Ananthanarayanan, V.S. (1988) Synthetic beta-turn peptides as substrates for a tyrosine protein kinase. *J Biol Chem*, **263**, 5024-5026.

Tjernberg, L., Hosia, W., Bark, N., Thyberg, J. and Johansson, J. (2002) Charge attraction and beta propensity are necessary for amyloid fibril formation from tetrapeptides. *J Biol Chem*, **277**, 43243-43246.

Tjernberg, L.O., Callaway, D.J., Tjernberg, A., Hahne, S., Lilliehook, C., Terenius, L., Thyberg, J. and Nordstedt, C. (1999) A molecular model of Alzheimer amyloid beta-peptide fibril formation. *J Biol Chem*, **274**, 12619-12625.

Tjernberg, L.O., Naslund, J., Lindqvist, F., Johansson, J., Karlstrom, A.R., Thyberg, J., Terenius, L. and Nordstedt, C. (1996) Arrest of beta-amyloid fibril formation by a pentapeptide ligand. *J Biol Chem*, **271**, 8545-8548.

Torok, M., Milton, S., Kayed, R., Wu, P., McIntire, T., Glabe, C.G. and Langen, R. (2002) Structural and dynamic features of Alzheimer's Abeta peptide in amyloid fibrils studied by site-directed spin labeling. *J Biol Chem*, **277**, 40810-40815.

Touchette, J.C., Williams, L.L., Ajit, D., Gallazzi, F. and Nichols, M.R. (2010) Probing the amyloid-beta(1-40) fibril environment with substituted tryptophan residues. *Arch Biochem Biophys*, **494**, 192-197.

Toyama, B.H., Kelly, M.J., Gross, J.D. and Weissman, J.S. (2007) The structural basis of yeast prion strain variants. *Nature*, **449**, 233-237.

Tracz, S.M., Abedini, A., Driscoll, M. and Raleigh, D.P. (2004) Role of aromatic interactions in amyloid formation by peptides derived from human Amylin. *Biochemistry*, **43**, 15901-15908.

Trevino, S.R., Scholtz, J.M. and Pace, C.N. (2007) Amino acid contribution to protein solubility: Asp, Glu, and Ser contribute more favorably than the other hydrophilic amino acids in RNase Sa. *J Mol Biol*, **366**, 449-460.

Trovato, A., Seno, F. and Tosatto, S.C. (2007) The PASTA server for protein aggregation prediction. *Protein Eng Des Sel*, **20**, 521-523.

True, H.L., Berlin, I. and Lindquist, S.L. (2004) Epigenetic regulation of translation reveals hidden genetic variation to produce complex traits. *Nature*, **431**, 184-187.

True, H.L. and Lindquist, S.L. (2000) A yeast prion provides a mechanism for genetic variation and phenotypic diversity. *Nature*, **407**, 477-483.

Tsai, H.H., Reches, M., Tsai, C.J., Gunasekaran, K., Gazit, E. and Nussinov, R. (2005) Energy landscape of amyloidogenic peptide oligomerization by parallel-tempering molecular dynamics simulation: significant role of Asn ladder. *Proc Natl Acad Sci U S A*, **102**, 8174-8179.

Tuite, M.F. (2000) Yeast prions and their prion-forming domain. *Cell*, **100**, 289-292.

Tycko, R., Sciarretta, K.L., Orgel, J.P. and Meredith, S.C. (2009) Evidence for Novel -Sheet Structures in Iowa-mutant -Amyloid Fibrils. *Biochemistry*.

Ulijn, R.V. and Smith, A.M. (2008) Designing peptide based nanomaterials. *Chem Soc Rev*, **37**, 664-675.

Ulrih, N.P., Barry, C.H. and Fink, A.L. (2008) Impact of Tyr to Ala mutations on alpha-synuclein fibrillation and structural properties. *Biochim Biophys Acta*, **1782**, 581-585.

Uptain, S.M., Sawicki, G.J., Caughey, B. and Lindquist, S. (2001) Strains of [PSI(+)] are distinguished by their efficiencies of prion-mediated conformational conversion. *Embo J*, **20**, 6236-6245.

Uversky, V.N. and Fink, A.L. (2004) Conformational constraints for amyloid fibrillation: the importance of being unfolded. *Biochim Biophys Acta*, **1698**, 131-153.

Uversky, V.N., Gillespie, J.R. and Fink, A.L. (2000) Why are "natively unfolded" proteins unstructured under physiologic conditions? *Proteins*, **41**, 415-427.

Uversky, V.N., Li, J. and Fink, A.L. (2001) Evidence for a partially folded intermediate in alpha-synuclein fibril formation. *J Biol Chem*, **276**, 10737-10744.

van der Wel, P.C., Lewandowski, J.R. and Griffin, R.G. (2007) Solid-state NMR study of amyloid nanocrystals and fibrils formed by the peptide GNNQQNY from yeast prion protein Sup35p. *J Am Chem Soc*, **129**, 5117-5130.

Vassar, P.S. and Culling, C.F. (1959) Fluorescent stains, with special reference to amyloid and connective tissues. *Arch Pathol*, **68**, 487-498.

Ventura, S., Zurdo, J., Narayanan, S., Parreno, M., Mangues, R., Reif, B., Chiti, F., Giannoni, E., Dobson, C.M., Aviles, F.X. and Serrano, L. (2004) Short amino acid stretches can mediate amyloid formation in globular proteins: the Src homology 3 (SH3) case. *Proc Natl Acad Sci U S A*, **101**, 7258-7263.

Vestergaard, B., Groenning, M., Roessle, M., Kastrup, J.S., van de Weert, M., Flink, J.M., Frokjaer, S., Gajhede, M. and Svergun, D.I. (2007) A helical structural nucleus is the primary elongating unit of insulin amyloid fibrils. *PLoS Biol*, **5**, e134.

Vilar, M., Chou, H.T., Luhrs, T., Maji, S.K., Riek-Loher, D., Verel, R., Manning, G., Stahlberg, H. and Riek, R. (2008) The fold of alpha-synuclein fibrils. *Proc Natl Acad Sci U S A*, **105**, 8637-8642.

Vitagliano, L., Esposito, L., Pedone, C. and De Simone, A. (2008) Stability of single sheet GNNQQNY aggregates analyzed by replica exchange molecular dynamics: antiparallel versus parallel association. *Biochem Biophys Res Commun*, **377**, 1036-1041.

Volles, M.J., Lee, S.J., Rochet, J.C., Shtilerman, M.D., Ding, T.T., Kessler, J.C. and Lansbury, P.T., Jr. (2001) Vesicle permeabilization by protofibrillar alpha-synuclein: implications for the pathogenesis and treatment of Parkinson's disease. *Biochemistry*, **40**, 7812-7819.

Vollrath, F. (2000) Strength and structure of spiders' silks. *J Biotechnol*, **74**, 67-83.

Vuilleumier, S., Sancho, J., Loewenthal, R. and Fersht, A.R. (1993) Circular dichroism studies of barnase and its mutants: characterization of the contribution of aromatic side chains. *Biochemistry*, **32**, 10303-10313.

Wadsworth, J.D., Joiner, S., Linehan, J.M., Desbruslais, M., Fox, K., Cooper, S., Cronier, S., Asante, E.A., Mead, S., Brandner, S., Hill, A.F. and Collinge, J. (2008) Kuru prions and sporadic Creutzfeldt-Jakob disease prions have equivalent transmission properties in transgenic and wild-type mice. *Proc Natl Acad Sci U S A*, **105**, 3885-3890.

Wallace, B.A. and Mao, D. (1984) Circular dichroism analyses of membrane proteins: an examination of differential light scattering and absorption flattening effects in large membrane vesicles and membrane sheets. *Anal Biochem*, **142**, 317-328.

Walsh, D.M., Klyubin, I., Fadeeva, J.V., Rowan, M.J. and Selkoe, D.J. (2002) Amyloid-beta oligomers: their production, toxicity and therapeutic inhibition. *Biochem Soc Trans*, **30**, 552-557.

Walsh, D.M., Lomakin, A., Benedek, G.B., Condron, M.M. and Teplow, D.B. (1997) Amyloid beta-protein fibrillogenesis. Detection of a protofibrillar intermediate. *J Biol Chem*, **272**, 22364-22372.

Walsh, D.M. and Selkoe, D.J. (2007) A beta oligomers - a decade of discovery. *J Neurochem*, **101**, 1172-1184.

Wang, J., Tan, C., Chen, H.F. and Luo, R. (2008) All-atom computer simulations of amyloid fibrils disaggregation. *Biophys J*, **95**, 5037-5047.

Wasmer, C., Soragni, A., Sabate, R., Lange, A., Riek, R. and Meier, B.H. (2008) Infectious and noninfectious amyloids of the HET-s(218-289) prion have different NMR spectra. *Angew Chem Int Ed Engl*, **47**, 5839-5841.

Watt, B., van Niel, G., Fowler, D.M., Hurbain, I., Luk, K.C., Stayrook, S.E., Lemmon, M.A., Raposo, G., Shorter, J., Kelly, J.W. and Marks, M.S. (2009) N-terminal domains elicit formation of functional Pmel17 amyloid fibrils. *J Biol Chem*, **284**, 35543-35555.

Waxman, E.A., Mazzulli, J.R. and Giasson, B.I. (2009) Characterization of hydrophobic residue requirements for alpha-synuclein fibrillization. *Biochemistry*, **48**, 9427-9436.

Westermark, P., Benson, M.D., Buxbaum, J.N., Cohen, A.S., Frangione, B., Ikeda, S., Masters, C.L., Merlini, G., Saraiva, M.J. and Sipe, J.D. (2005) Amyloid: toward terminology clarification. Report from the Nomenclature Committee of the International Society of Amyloidosis. *Amyloid*, **12**, 1-4.

Westermark, P., Benson, M.D., Buxbaum, J.N., Cohen, A.S., Frangione, B., Ikeda, S., Masters, C.L., Merlini, G., Saraiva, M.J. and Sipe, J.D. (2007) A primer of amyloid nomenclature. *Amyloid*, **14**, 179-183.

Westermark, P., Engstrom, U., Johnson, K.H., Westermark, G.T. and Betsholtz, C. (1990) Islet amyloid polypeptide: pinpointing amino acid residues linked to amyloid fibril formation. *Proc Natl Acad Sci U S A*, **87**, 5036-5040.

White, H.E., Hodgkinson, J.L., Jahn, T.R., Cohen-Krausz, S., Gosal, W.S., Muller, S., Orlova, E.V., Radford, S.E. and Saibil, H.R. (2009) Globular Tetramers of beta(2)-Microglobulin Assemble into Elaborate Amyloid Fibrils. *J Mol Biol*.

Whitmore, L. and Wallace, B.A. (2008) Protein secondary structure analyses from circular dichroism spectroscopy: methods and reference databases. *Biopolymers*, **89**, 392-400.

Wickner, R.B. (1994) [URE3] as an altered URE2 protein: evidence for a prion analog in Saccharomyces cerevisiae. *Science*, **264**, 566-569.

Wickner, R.B., Dyda, F. and Tycko, R. (2008) Amyloid of Rnq1p, the basis of the [PIN+] prion, has a parallel in-register beta-sheet structure. *Proc Natl Acad Sci U S A*, **105**, 2403-2408.

Wiechelman, K.J., Braun, R.D. and Fitzpatrick, J.D. (1988) Investigation of the bicinchoninic acid protein assay: identification of the groups responsible for color formation. *Anal Biochem*, **175**, 231-237.

Williams, A.D., Portelius, E., Kheterpal, I., Guo, J.T., Cook, K.D., Xu, Y. and Wetzel, R. (2004) Mapping abeta amyloid fibril secondary structure using scanning proline mutagenesis. *J Mol Biol*, **335**, 833-842.

Wiltzius, J.J., Sievers, S.A., Sawaya, M.R., Cascio, D., Popov, D., Riekel, C. and Eisenberg, D. (2008) Atomic structure of the cross-beta spine of islet amyloid polypeptide (amylin). *Protein Sci*, **17**, 1467-1474.

Wisniewski, T., Ghiso, J. and Frangione, B. (1991) Peptides homologous to the amyloid protein of Alzheimer's disease containing a glutamine for glutamic acid substitution have accelerated amyloid fibril formation. *Biochem Biophys Res Commun*, **180**, 1528.

Wolfe, M.S., Xia, W., Ostaszewski, B.L., Diehl, T.S., Kimberly, W.T. and Selkoe, D.J. (1999) Two transmembrane aspartates in presenilin-1 required for presenilin endoproteolysis and gamma-secretase activity. *Nature*, **398**, 513-517.

Wolfenden, R., Andersson, L., Cullis, P.M. and Southgate, C.C. (1981) Affinities of amino acid side chains for solvent water. *Biochemistry*, **20**, 849-855.

Wood, S.P., Blundell, T.L., Wollmer, A., Lazarus, N.R. and Neville, R.W. (1975) The relation of conformation and association of insulin to receptor binding; x-ray and circular-dichroism studies on bovine and hystricomorph insulins. *Eur J Biochem*, **55**, 531-542.

Woody, A.Y. and Woody, R.W. (2003) Individual tyrosine side-chain contributions to circular dichroism of ribonuclease. *Biopolymers*, **72**, 500-513.

Woody, R.W. (1978) Aromatic side-chain contributions to the far ultraviolet circular dichroism of peptides and proteins. *Biopolymers*, **17**, 1451-1467.

Woody, R.W. (1994) Contributions of tryptophan side chains to the far-ultraviolet circular dichroism of proteins. *Eur Biophys J*, **23**, 253-262.

Woolfson, D.N. and Ryadnov, M.G. (2006) Peptide-based fibrous biomaterials: Some things old, new and borrowed. *Curr Opin Chem Biol*, **10**, 559-567.

Wosten, H.A. (2001) Hydrophobins: multipurpose proteins. *Annu Rev Microbiol*, **55**, 625-646.

Wu, C., Biancalana, M., Koide, S. and Shea, J.E. (2009) Binding modes of thioflavin-T to the single-layer beta-sheet of the peptide self-assembly mimics. *J Mol Biol*, **394**, 627-633.

Xu, S., Bevis, B. and Arnsdorf, M.F. (2001) The assembly of amyloidogenic yeast sup35 as assessed by scanning (atomic) force microscopy: an analogy to linear colloidal aggregation? *Biophys J*, **81**, 446-454.

Xue, W.F., Hellewell, A.L., Gosal, W.S., Homans, S.W., Hewitt, E.W. and Radford, S.E. (2009a) Fibril fragmentation enhances amyloid cytotoxicity. *J Biol Chem*, **284**, 34272-34282.

Xue, W.F., Homans, S.W. and Radford, S.E. (2009b) Amyloid fibril length distribution quantified by atomic force microscopy single-particle image analysis. *Protein Eng Des Sel*, **22**, 489-496.

Yang, D.S., Yip, C.M., Huang, T.H., Chakrabartty, A. and Fraser, P.E. (1999) Manipulating the amyloid-beta aggregation pathway with chemical chaperones. *J Biol Chem*, **274**, 32970-32974.

Zamyatnin, A.A. (1972) Protein volume in solution. *Prog Biophys Mol Biol*, **24**, 107-123.

Zerovnik, E., Skarabot, M., Skerget, K., Giannini, S., Stoka, V., Jenko-Kokalj, S. and Staniforth, R.A. (2007) Amyloid fibril formation by human stefin B: influence of pH and TFE on fibril growth and morphology. *Amyloid*, **14**, 237-247.

Zhang, A., Qi, W., Good, T.A. and Fernandez, E.J. (2009) Structural differences between Abeta(1-40) intermediate oligomers and fibrils elucidated by proteolytic fragmentation and hydrogen/deuterium exchange. *Biophys J*, **96**, 1091-1104.

Zhang, F., Lin, X.J., Ji, L.N., Du, H.N., Tang, L., He, J.H., Hu, J. and Hu, H.Y. (2008) Assembly of alpha-synuclein fibrils in nanoscale studied by peptide truncation and AFM. *Biochem Biophys Res Commun*, **368**, 388-394.

Zhang, S., Holmes, T., Lockshin, C. and Rich, A. (1993) Spontaneous assembly of a self-complementary oligopeptide to form a stable macroscopic membrane. *Proc Natl Acad Sci U S A*, **90**, 3334-3338.

Zhang, S. and Rich, A. (1997) Direct conversion of an oligopeptide from a beta-sheet to an alpha-helix: a model for amyloid formation. *Proc Natl Acad Sci U S A*, **94**, 23-28.

Zhao, Y., Yokoi, H., Tanaka, M., Kinoshita, T. and Tan, T. (2008) Self-assembled pH-responsive hydrogels composed of the RATEA16 peptide. *Biomacromolecules*, **9**, 1511-1518.

Zheng, J., Ma, B., Tsai, C.J. and Nussinov, R. (2006) Structural stability and dynamics of an amyloid-forming peptide GNNQQNY from the yeast prion sup-35. *Biophys J*, **91**, 824-833.

Zibaee, S., Makin, O.S., Goedert, M. and Serpell, L.C. (2007) A simple algorithm locates beta-strands in the amyloid fibril core of alpha-synuclein, Abeta, and tau using the amino acid sequence alone. *Protein Sci*, **16**, 906-918.

Zurdo, J., Guijarro, J.I., Jimenez, J.L., Saibil, H.R. and Dobson, C.M. (2001) Dependence on solution conditions of aggregation and amyloid formation by an SH3 domain. *J Mol Biol*, **311**, 325-340.

# APPENDIX

## i. Short sequences that form amyloid-like structures

| Sequence | From | Reference | Notes |
|---|---|---|---|
| KFFK and EFFE | Designed | (Tjernberg 2002) | Only form fibres when mixed in equimolar quantities, not alone. |
| KFFEAAAKKFFE | Designed | (Hosia, 2004; Makin, 2005) | |
| LVFFA | Aβ 17-21 | (Esler 1996; Findeis, 1999) | Aβ inhibitor |
| QKLVFF | Aβ 15-20 | (Tjernberg, 1996) | Aβ inhibitor |
| LPFFD | Designed | (Soto, 1998) | Aβ inhibitor |
| KLVFFAE | Aβ 16-22 | (Balbach, 2000) | |
| F19 | | (Esler 1996; Wurth 2002) | |
| EVHHQKLVFFAEDVG | Aβ 11-25 | (Sikorski, 2003) | FF interactions |
| NFGAIL/ FGAIL | IAPP | (Tenidis, 2000) | GAIL does not form fibres. |
| DFNKF | Human calcitonin 15-19 | (Reches, 2002; Haspel, 2005; Zanuy, 2004) | |
| 59-71, 59-79 | $\beta_2$ –microglobulin | (Jones, 2003) | |
| NFGAILSS | IAPP 22-29 | (Westermark, 1990; Goldsbury, 2000; Moriarty, 1999) | |
| NNFGAIL<br>SSTNVG | IAPP 21-27<br>IAPP 28-33 | (Wiltzius 2008) | |
| VYK | Tau | (Goux, 2004) | |
| NFGSQV | Medin | (Reches, 2004) | |
| VEALYL | Insulin | (Sawaya, 2007) | |
| LYQLEN | Insulin | (Sawaya, 2007) | |
| VAQKTV | α-synuclein | (Madine, 2008) | |
| NFLVH | IAPP | (Mazor, 2002) | |
| SFNNGDCCFILD | Gelsolin | (Maury, 1992) | |
| SFFSFLGEAFD | Serum amyloid A | (Westermark, 1992) | |

## ii. Amyloid structures in the Protein Data Bank

| Code | Sequence | Reference | Method | Parent Protein | Other notes |
|---|---|---|---|---|---|
| 1yjp | GNNQQNY – 1 | Nelson Nature 2005 | XRD | Sup35 7-13 | |
| 1yjo | NNQQNY | Nelson Nature 2005 | XRD | Sup35 8-13 | + zinc acetate |
| 2onv | GGVVIA | Sawaya Nature 2007 | XRD | A beta 37-42 | |
| 2on9 | VQIVYK – 1 | Sawaya Nature 2007 | XRD | tau 306-311 | |
| 2okz | MVGGVV – 2 | Sawaya Nature 2007 | XRD | A beta 35-40 | |
| 2ol9 | SNQNNF | Sawaya Nature 2007 | XRD | Human prion 170-175 | |
| 2olx | NNQQ – 2 | Sawaya Nature 2007 | XRD | Sup35 8-11 | |
| 2omm | GNNQQNY – 2 | Sawaya Nature 2007 | XRD | Sup35 7-13 | |
| 2omp | LYQLEN | Sawaya Nature 2007 | XRD | Insulin chain A 13-18 | |
| 2omq | VEALYL | Sawaya Nature 2007 | XRD | Insulin chain B 12-17 | |
| 2onw | SSTSSA | Sawaya Nature 2007 | XRD | RNase A 15-20 | |
| 2onx | NNQQ – 1 | Sawaya Nature 2007 | XRD | Sup35 8-11 | |
| 2ona | MVGGVV – 1 | Sawaya Nature 2007 | XRD | A beta 35-40 | |
| 3dgj | NNFGAIL | Wiltzius Protein Sci 2008 | XRD | IAPP 21-27 | |
| 3dg1 | SSTNVG – 1 | Wiltzius Protein Sci 2008 | XRD | IAPP 61-66 | |
| 3hyd | LVEALYL | Ivanova PNAS 2009 | XRD | Insulin 11-17 | |
| 3fpo | HSSNNF | Wiltzius NSMB 2009 | XRD | IAPP 51-56 | |
| 3fqp | VQIVYK – 2 | Wiltzius NSMB 2009 | XRD | Tau 623-628 | |
| 3fr1 | NFLVHS | Wiltzius NSMB 2009 | XRD | IAPP 47-52 | |
| 3fth | NFLVHSS | Wiltzius NSMB 2009 | XRD | IAPP 47-53 | + Sulphate ligand |
| 3ftk | NVGSNTY – 1 | Wiltzius NSMB 2009 | XRD | IAPP 64-70 | |
| 3ftl | NVGSNTY – 2 | Wiltzius NSMB 2009 | XRD | IAPP 64-70 | |
| 3ftr | SSTNVG – 2 | Wiltzius NSMB 2009 | XRD | IAPP 61-66 | |
| 3fva | NNQNTF | Wiltzius NSMB 2009 | XRD | Elk prion 173-178 | |
| 3fod | AILSST | Wiltzius NSMB 2009 | XRD | IAPP 58-63 | |
| 2bfi | KFFEAAAKKFFE | Makin PNAS | XRFD | Designed | |

| | | | | | |
|---|---|---|---|---|---|
| | | 2005 | | | |
| 2beg | A beta 42 | Luhrs PNAS 2005 | ssNMR | A beta 42 | |
| 1rvs | YTIAALLSPYS | Jaroniec PNAS 2004 | ssNMR | Transthyretin 1-11 | |
| 28ed | Beta 2 m 40-61 | Iwata PNAS 2006 | ssNMR | Beta 2 m K3 peptide | |
| 2rnm | HET-s 218-289 | Wasmer Science 2008 | ssNMR | HET-s prion forming domain | |
| 2nnt | 40 residues | Ferguson PNAS 2006 | ssNMR | $2^{nd}$ WW domain of CA150 | |
| 2kib | SNNFGAILSS | Nielsen Angewandte 2009 | ssNMR | IAPP 20-29 | |

Total of 32 structures as at 27/11/09

25 crystal structures from Eisenberg group – 13 in 1 form, 6 in 2 forms

## iii. Signal position prediction – 1YJP

DiffractionSettings: Pixel: 400 µm, λ: 1.5419 Å, Sample to plate: 160 mm, X-ray beam, Fibre (Untitled).

Range of Miller Indices: D-spacing: Infinity Å to 2.745276E-10 Å, h: 0 to 20, k: 0 to 20 and l: 0 to 20.

Fibre Axis: (0.0, 1.0, 0.0)

Beam Orientation: (0.0, 0.0, 1.0)

*Signal Positions and Resolutions*

| h | k | l | d-spacing | $(x_{imageplate}, y_{imageplate})$ | $(x_{imageplate}, y_{imageplate})$ | Coordinates |
|---|---|---|---|---|---|---|
| 0 | 0 | 1 | 22.444 | (28, 0) | (-28, 0) | (∞, ∞, 22.44443) |
| 0 | 0 | 2 | 11.222 | (55, 0) | (-55, 0) | (∞, ∞, 11.222215) |
| 0 | 0 | 3 | 7.481 | (84, 0) | (-84, 0) | (∞, ∞, 7.4814763) |
| 0 | 0 | 4 | 5.611 | (113, 0) | (-113, 0) | (∞, ∞, 5.6111073) |
| 0 | 0 | 5 | 4.489 | (144, 0) | (-144, 0) | (∞, ∞, 4.488886) |
| 0 | 0 | 6 | 3.741 | (176, 0) | (-176, 0) | (∞, ∞, 3.7407382) |
| 0 | 0 | 7 | 3.206 | (211, 0) | (-211, 0) | (∞, ∞, 3.206347) |
| 0 | 0 | 8 | 2.806 | (249, 0) | (-249, 0) | (∞, ∞, 2.8055537) |
| 0 | 1 | 0 | 4.87 | (0, 132) | | (∞, 4.87, -∞) |
| 0 | 1 | 1 | 4.759 | (19, 134) | (-19, 134) | (∞, 4.87, 22.44443) |
| 0 | 1 | 2 | 4.467 | (53, 135) | (-53, 135) | (∞, 4.87, 11.222215) |
| 0 | 1 | 3 | 4.081 | (83, 136) | (-83, 136) | (∞, 4.87, 7.4814763) |
| 0 | 1 | 4 | 3.678 | (114, 139) | (-114, 139) | (∞, 4.87, 5.6111073) |
| 0 | 1 | 5 | 3.301 | (146, 142) | (-146, 142) | (∞, 4.87, 4.488886) |
| 0 | 1 | 6 | 2.967 | (180, 146) | (-180, 146) | (∞, 4.87, 3.7407382) |
| 1 | 0 | 0 | 20.972 | (29, 0) | (-29, 0) | (21.94, -∞, 71.40576) |
| 1 | 0 | 1 | 13.476 | (46, 0) | (-46, 0) | (21.94, -∞, 17.076807) |
| 1 | 0 | 2 | 8.87 | (70, 0) | (-70, 0) | (21.94, -∞, 9.698056) |
| 1 | 0 | 3 | 6.471 | (97, 0) | (-97, 0) | (21.94, -∞, 6.771951) |
| 1 | 0 | 4 | 5.062 | (126, 0) | (-126, 0) | (21.94, -∞, 5.2023067) |
| 1 | 0 | 5 | 4.147 | (157, 0) | (-157, 0) | (21.94, -∞, 4.223385) |
| 1 | 0 | 6 | 3.509 | (190, 0) | (-190, 0) | (21.94, -∞, 3.5545268) |
| 1 | 0 | 7 | 3.039 | (225, 0) | (-225, 0) | (21.94, -∞, 3.068559) |
| 1 | 1 | 0 | 4.744 | (22, 134) | (-22, 134) | (21.94, 4.87, 71.40576) |
| 1 | 1 | 1 | 4.58 | (42, 134) | (-42, 134) | (21.94, 4.87, 17.076807) |
| 1 | 1 | 2 | 4.269 | (69, 135) | (-69, 135) | (21.94, 4.87, 9.698056) |
| 1 | 1 | 3 | 3.891 | (98, 137) | (-98, 137) | (21.94, 4.87, 6.771951) |
| 1 | 1 | 4 | 3.51 | (128, 140) | (-128, 140) | (21.94, 4.87, 5.2023067) |
| 1 | 1 | 5 | 3.157 | (160, 144) | (-160, 144) | (21.94, 4.87, 4.223385) |
| 1 | 1 | 6 | 2.847 | (194, 148) | (-194, 148) | (21.94, 4.87, 3.5545268) |
| 2 | 0 | 0 | 10.486 | (59, 0) | (-59, 0) | (10.97, -∞, 35.70288) |
| 2 | 0 | 1 | 8.583 | (73, 0) | (-73, 0) | (10.97, -∞, 13.781047) |
| 2 | 0 | 2 | 6.738 | (93, 0) | (-93, 0) | (10.97, -∞, 8.5384035) |

| | | | | | | |
|---|---|---|---|---|---|---|
| 2 | 0 | 3 | 5.388 | (118, 0) | (-118, 0) | (10.97, -∞, 6.1853476) |
| 2 | 0 | 4 | 4.435 | (146, 0) | (-146, 0) | (10.97, -∞, 4.849028) |
| 2 | 0 | 5 | 3.748 | (176, 0) | (-176, 0) | (10.97, -∞, 3.987537) |
| 2 | 0 | 6 | 3.235 | (209, 0) | (-209, 0) | (10.97, -∞, 3.3859756) |
| 2 | 0 | 7 | 2.842 | (245, 0) | (-245, 0) | (10.97, -∞, 2.9421253) |
| 2 | 1 | 0 | 4.417 | (57, 135) | (-57, 135) | (10.97, 4.87, 35.70288) |
| 2 | 1 | 1 | 4.236 | (72, 136) | (-72, 136) | (10.97, 4.87, 13.781047) |
| 2 | 1 | 2 | 3.947 | (93, 137) | (-93, 137) | (10.97, 4.87, 8.5384035) |
| 2 | 1 | 3 | 3.613 | (119, 139) | (-119, 139) | (10.97, 4.87, 6.1853476) |
| 2 | 1 | 4 | 3.279 | (148, 142) | (-148, 142) | (10.97, 4.87, 4.849028) |
| 2 | 1 | 5 | 2.97 | (180, 146) | (-180, 146) | (10.97, 4.87, 3.987537) |
| 3 | 0 | 0 | 6.991 | (90, 0) | (-90, 0) | (7.3133335, -∞, 23.801922) |
| 3 | 0 | 1 | 6.179 | (102, 0) | (-102, 0) | (7.3133335, -∞, 11.551625) |
| 3 | 0 | 2 | 5.279 | (121, 0) | (-121, 0) | (7.3133335, -∞, 7.6264625) |
| 3 | 0 | 3 | 4.492 | (144, 0) | (-144, 0) | (7.3133335, -∞, 5.692269) |
| 3 | 0 | 4 | 3.858 | (170, 0) | (-170, 0) | (7.3133335, -∞, 4.5406795) |
| 3 | 0 | 5 | 3.356 | (200, 0) | (-200, 0) | (7.3133335, -∞, 3.7766368) |
| 3 | 0 | 6 | 2.957 | (233, 0) | (-233, 0) | (7.3133335, -∞, 3.2326853) |
| 3 | 1 | 0 | 3.996 | (90, 137) | (-90, 137) | (7.3133335, 4.87, 23.801922) |
| 3 | 1 | 1 | 3.825 | (103, 138) | (-103, 138) | (7.3133335, 4.87, 11.551625) |
| 3 | 1 | 2 | 3.579 | (122, 140) | (-122, 140) | (7.3133335, 4.87, 7.6264625) |
| 3 | 1 | 3 | 3.302 | (146, 142) | (-146, 142) | (7.3133335, 4.87, 5.692269) |
| 3 | 1 | 4 | 3.024 | (174, 146) | (-174, 146) | (7.3133335, 4.87, 4.5406795) |
| 3 | 1 | 5 | 2.763 | (205, 150) | (-205, 150) | (7.3133335, 4.87, 3.7766368) |
| 4 | 0 | 0 | 5.243 | (122, 0) | (-122, 0) | (5.485, -∞, 17.85144) |
| 4 | 0 | 1 | 4.803 | (134, 0) | (-134, 0) | (5.485, -∞, 9.943089) |
| 4 | 0 | 2 | 4.291 | (151, 0) | (-151, 0) | (5.485, -∞, 6.8905234) |
| 4 | 0 | 3 | 3.801 | (173, 0) | (-173, 0) | (5.485, -∞, 5.272) |
| 4 | 0 | 4 | 3.369 | (199, 0) | (-199, 0) | (5.485, -∞, 4.2692018) |
| 4 | 0 | 5 | 3.002 | (229, 0) | (-229, 0) | (5.485, -∞, 3.586925) |
| 4 | 1 | 0 | 3.568 | (123, 140) | (-123, 140) | (5.485, 4.87, 17.85144) |
| 4 | 1 | 1 | 3.42 | (136, 141) | (-136, 141) | (5.485, 4.87, 9.943089) |
| 4 | 1 | 2 | 3.22 | (154, 143) | (-154, 143) | (5.485, 4.87, 6.8905234) |
| 4 | 1 | 3 | 2.996 | (177, 146) | (-177, 146) | (5.485, 4.87, 5.272) |
| 4 | 1 | 4 | 2.771 | (204, 150) | (-204, 150) | (5.485, 4.87, 4.2692018) |
| 5 | 0 | 0 | 4.194 | (155, 0) | (-155, 0) | (4.388, -∞, 14.281153) |
| 5 | 0 | 1 | 3.92 | (167, 0) | (-167, 0) | (4.388, -∞, 8.727767) |
| 5 | 0 | 2 | 3.598 | (184, 0) | (-184, 0) | (4.388, -∞, 6.2841177) |
| 5 | 0 | 3 | 3.272 | (206, 0) | (-206, 0) | (4.388, -∞, 4.909522) |
| 5 | 0 | 4 | 2.967 | (232, 0) | (-232, 0) | (4.388, -∞, 4.0283546) |
| 5 | 1 | 0 | 3.178 | (158, 144) | (-158, 144) | (4.388, 4.87, 14.281153) |

| | | | | | | |
|---|---|---|---|---|---|---|
| 5 | 1 | 1 | 3.054 | (171, 145) | (-171, 145) | (4.388, 4.87, 8.727767) |
| 5 | 1 | 2 | 2.894 | (189, 148) | (-189, 148) | (4.388, 4.87, 6.2841177) |
| 6 | 0 | 0 | 3.495 | (191, 0) | (-191, 0) | (3.6566668, -∞, 11.900961) |
| 6 | 0 | 1 | 3.309 | (203, 0) | (-203, 0) | (3.6566668, -∞, 7.7771797) |
| 6 | 0 | 2 | 3.09 | (221, 0) | (-221, 0) | (3.6566668, -∞, 5.7758126) |
| 6 | 0 | 3 | 2.861 | (243, 0) | (-243, 0) | (3.6566668, -∞, 4.5936823) |
| 6 | 1 | 0 | 2.84 | (195, 149) | (-195, 149) | (3.6566668, 4.87, 11.900961) |
| 7 | 0 | 0 | 2.996 | (229, 0) | (-229, 0) | (3.1342857, -∞, 10.200824) |
| 7 | 0 | 1 | 2.862 | (243, 0) | (-243, 0) | (3.1342857, -∞, 7.013322) |
| | | | | | | |

## iv. Signal position prediction – 2OMM

DiffractionSettings: Pixel: 400 µm, λ: 1.5419 Å, Sample to plate: 160 mm, X-ray beam, Fibre (Untitled).

Range of Miller Indices: D-spacing: Infinity Å to 2.745276E-10 Å, h: 0 to 20, k: 0 to 20 and l: 0 to 20.

Fibre Axis: (0.0, 1.0, 0.0)

Beam Orientation: (0.0, 0.0, 1.0)

*Signal Positions and Resolutions*

| h | k | l | d-spacing | $(x_{imageplate}, y_{imageplate})$ | $(x_{imageplate}, y_{imageplate})$ | Coordinates |
|---|---|---|---|---|---|---|
| 0 | 0 | 1 | 37.55 | (16, 0) | (-16, 0) | (∞, ∞, 37.55) |
| 0 | 0 | 2 | 18.775 | (33, 0) | (-33, 0) | (∞, ∞, 18.775) |
| 0 | 0 | 3 | 12.517 | (50, 0) | (-50, 0) | (∞, ∞, 12.516666) |
| 0 | 0 | 4 | 9.387 | (66, 0) | (-66, 0) | (∞, ∞, 9.3875) |
| 0 | 0 | 5 | 7.51 | (83, 0) | (-83, 0) | (∞, ∞, 7.51) |
| 0 | 0 | 6 | 6.258 | (101, 0) | (-101, 0) | (∞, ∞, 6.258333) |
| 0 | 0 | 7 | 5.364 | (119, 0) | (-119, 0) | (∞, ∞, 5.364286) |
| 0 | 0 | 8 | 4.694 | (137, 0) | (-137, 0) | (∞, ∞, 4.69375) |
| 0 | 1 | 0 | 4.93 | (0, 130) | | (∞, 4.93, -∞) |
| 0 | 1 | 1 | 4.888 | (0, 131) | | (∞, 4.93, 37.55) |
| 0 | 1 | 2 | 4.768 | (27, 132) | (-27, 132) | (∞, 4.93, 18.775) |
| 0 | 1 | 3 | 4.587 | (46, 133) | (-46, 133) | (∞, 4.93, 12.516666) |
| 0 | 1 | 4 | 4.365 | (65, 133) | (-65, 133) | (∞, 4.93, 9.3875) |
| 0 | 1 | 5 | 4.121 | (83, 135) | (-83, 135) | (∞, 4.93, 7.51) |
| 0 | 1 | 6 | 3.873 | (101, 136) | (-101, 136) | (∞, 4.93, 6.258333) |
| 1 | 0 | 0 | 23.32 | (26, 0) | (-26, 0) | (23.32, -∞, -∞) |
| 1 | 0 | 1 | 19.811 | (31, 0) | (-31, 0) | (23.32, -∞, 37.55) |
| 1 | 0 | 2 | 14.624 | (42, 0) | (-42, 0) | (23.32, -∞, 18.775) |
| 1 | 0 | 3 | 11.029 | (56, 0) | (-56, 0) | (23.32, -∞, 12.516666) |
| 1 | 0 | 4 | 8.708 | (72, 0) | (-72, 0) | (23.32, -∞, 9.3875) |
| 1 | 0 | 5 | 7.148 | (88, 0) | (-88, 0) | (23.32, -∞, 7.51) |
| 1 | 0 | 6 | 6.044 | (105, 0) | (-105, 0) | (23.32, -∞, 6.258333) |
| 1 | 0 | 7 | 5.228 | (122, 0) | (-122, 0) | (23.32, -∞, 5.364286) |
| 1 | 1 | 0 | 4.823 | (18, 132) | (-18, 132) | (23.32, 4.93, -∞) |
| 1 | 1 | 1 | 4.784 | (24, 132) | (-24, 132) | (23.32, 4.93, 37.55) |
| 1 | 1 | 2 | 4.672 | (38, 132) | (-38, 132) | (23.32, 4.93, 18.775) |
| 1 | 1 | 3 | 4.501 | (54, 133) | (-54, 133) | (23.32, 4.93, 12.516666) |
| 1 | 1 | 4 | 4.29 | (70, 134) | (-70, 134) | (23.32, 4.93, 9.3875) |
| 1 | 1 | 5 | 4.058 | (88, 135) | (-88, 135) | (23.32, 4.93, 7.51) |
| 1 | 1 | 6 | 3.82 | (105, 136) | (-105, 136) | (23.32, 4.93, 6.258333) |
| 2 | 0 | 0 | 11.66 | (53, 0) | (-53, 0) | (11.66, -∞, -∞) |
| 2 | 0 | 1 | 11.135 | (56, 0) | (-56, 0) | (11.66, -∞, 37.55) |

| | | | | | | |
|---|---|---|---|---|---|---|
| 2 | 0 | 2 | 9.905 | (63, 0) | (-63, 0) | (11.66, -∞, 18.775) |
| 2 | 0 | 3 | 8.532 | (73, 0) | (-73, 0) | (11.66, -∞, 12.516666) |
| 2 | 0 | 4 | 7.312 | (86, 0) | (-86, 0) | (11.66, -∞, 9.3875) |
| 2 | 0 | 5 | 6.314 | (100, 0) | (-100, 0) | (11.66, -∞, 7.51) |
| 2 | 0 | 6 | 5.514 | (115, 0) | (-115, 0) | (11.66, -∞, 6.258333) |
| 2 | 0 | 7 | 4.873 | (132, 0) | (-132, 0) | (11.66, -∞, 5.364286) |
| 2 | 1 | 0 | 4.541 | (51, 133) | (-51, 133) | (11.66, 4.93, -∞) |
| 2 | 1 | 1 | 4.508 | (53, 133) | (-53, 133) | (11.66, 4.93, 37.55) |
| 2 | 1 | 2 | 4.414 | (61, 133) | (-61, 133) | (11.66, 4.93, 18.775) |
| 2 | 1 | 3 | 4.269 | (72, 134) | (-72, 134) | (11.66, 4.93, 12.516666) |
| 2 | 1 | 4 | 4.088 | (85, 135) | (-85, 135) | (11.66, 4.93, 9.3875) |
| 2 | 1 | 5 | 3.886 | (100, 136) | (-100, 136) | (11.66, 4.93, 7.51) |
| 3 | 0 | 0 | 7.773 | (81, 0) | (-81, 0) | (7.7733335, -∞, -∞) |
| 3 | 0 | 1 | 7.612 | (82, 0) | (-82, 0) | (7.7733335, -∞, 37.55) |
| 3 | 0 | 2 | 7.182 | (87, 0) | (-87, 0) | (7.7733335, -∞, 18.775) |
| 3 | 0 | 3 | 6.604 | (95, 0) | (-95, 0) | (7.7733335, -∞, 12.516666) |
| 3 | 0 | 4 | 5.987 | (106, 0) | (-106, 0) | (7.7733335, -∞, 9.3875) |
| 3 | 0 | 5 | 5.401 | (118, 0) | (-118, 0) | (7.7733335, -∞, 7.51) |
| 3 | 0 | 6 | 4.875 | (132, 0) | (-132, 0) | (7.7733335, -∞, 6.258333) |
| 3 | 1 | 0 | 4.163 | (80, 134) | (-80, 134) | (7.7733335, 4.93, -∞) |
| 3 | 1 | 1 | 4.138 | (82, 134) | (-82, 134) | (7.7733335, 4.93, 37.55) |
| 3 | 1 | 2 | 4.065 | (87, 135) | (-87, 135) | (7.7733335, 4.93, 18.775) |
| 3 | 1 | 3 | 3.95 | (96, 135) | (-96, 135) | (7.7733335, 4.93, 12.516666) |
| 3 | 1 | 4 | 3.806 | (106, 136) | (-106, 136) | (7.7733335, 4.93, 9.3875) |
| 3 | 1 | 5 | 3.641 | (119, 137) | (-119, 137) | (7.7733335, 4.93, 7.51) |
| 4 | 0 | 0 | 5.83 | (109, 0) | (-109, 0) | (5.83, -∞, -∞) |
| 4 | 0 | 1 | 5.761 | (110, 0) | (-110, 0) | (5.83, -∞, 37.55) |
| 4 | 0 | 2 | 5.568 | (114, 0) | (-114, 0) | (5.83, -∞, 18.775) |
| 4 | 0 | 3 | 5.285 | (121, 0) | (-121, 0) | (5.83, -∞, 12.516666) |
| 4 | 0 | 4 | 4.953 | (129, 0) | (-129, 0) | (5.83, -∞, 9.3875) |
| 4 | 0 | 5 | 4.605 | (140, 0) | (-140, 0) | (5.83, -∞, 7.51) |
| 4 | 1 | 0 | 3.764 | (110, 137) | (-110, 137) | (5.83, 4.93, -∞) |
| 4 | 1 | 1 | 3.746 | (111, 137) | (-111, 137) | (5.83, 4.93, 37.55) |
| 4 | 1 | 2 | 3.691 | (115, 137) | (-115, 137) | (5.83, 4.93, 18.775) |
| 4 | 1 | 3 | 3.605 | (122, 138) | (-122, 138) | (5.83, 4.93, 12.516666) |
| 4 | 1 | 4 | 3.494 | (131, 139) | (-131, 139) | (5.83, 4.93, 9.3875) |
| 5 | 0 | 0 | 4.664 | (138, 0) | (-138, 0) | (4.664, -∞, -∞) |
| 5 | 0 | 1 | 4.628 | (139, 0) | (-139, 0) | (4.664, -∞, 37.55) |
| 5 | 0 | 2 | 4.526 | (143, 0) | (-143, 0) | (4.664, -∞, 18.775) |
| 5 | 0 | 3 | 4.37 | (148, 0) | (-148, 0) | (4.664, -∞, 12.516666) |
| 5 | 0 | 4 | 4.177 | (156, 0) | (-156, 0) | (4.664, -∞, 9.3875) |

| | | | | | | |
|---|---|---|---|---|---|---|
| 5 | 1 | 0 | 3.388 | (140, 140) | (-140, 140) | (4.664, 4.93, -∞) |
| 5 | 1 | 1 | 3.374 | (141, 140) | (-141, 140) | (4.664, 4.93, 37.55) |
| 5 | 1 | 2 | 3.334 | (145, 140) | (-145, 140) | (4.664, 4.93, 18.775) |
| 6 | 0 | 0 | 3.887 | (169, 0) | (-169, 0) | (3.8866668, -∞, -∞) |
| 6 | 0 | 1 | 3.866 | (170, 0) | (-170, 0) | (3.8866668, -∞, 37.55) |
| 6 | 0 | 2 | 3.806 | (173, 0) | (-173, 0) | (3.8866668, -∞, 18.775) |
| 6 | 0 | 3 | 3.712 | (178, 0) | (-178, 0) | (3.8866668, -∞, 12.516666) |
| 6 | 1 | 0 | 3.052 | (172, 143) | (-172, 143) | (3.8866668, 4.93, -∞) |
| 7 | 0 | 0 | 3.331 | (202, 0) | (-202, 0) | (3.3314285, -∞, -∞) |
| 7 | 0 | 1 | 3.318 | (203, 0) | (-203, 0) | (3.3314285, -∞, 37.55) |

## v. Diffraction signal indexing from KFFEAAAKKFFE variants used for unit cell determination

| Measured Resolution (Å) | Miller Indices | | | Predicted Resolution (Å) |
|---|---|---|---|---|
| | h | k | l | |
| 21.1 | 0 | 1 | 0 | 21.797377 |
| 15.63 | 0 | 0 | 2 | 15.526486 |
| 11.17 | 0 | 2 | 0 | 10.898688 |
| 8.77 | 0 | 2 | 2 | 8.920408 |
| 7.09 | 0 | 3 | 1 | 7.0747137 |
| 6.36 | 0 | 2 | 4 | 6.3231144 |
| 5.45 | 0 | 4 | 0 | 5.449344 |
| 5.29 | 0 | 3 | 4 | 5.30484 |

Table A1. Comparison of observed reflections with signals calculated from the unit cell for capped peptide.

| Measured Resolution (Å) | Miller Indices | | | Predicted Resolution (Å) |
|---|---|---|---|---|
| | h | k | l | |
| 22.2 | 0 | 0 | 2 | 23.96094 |
| 10.7 | 0 | 2 | 0 | 10.800426 |
| 8.99 | 0 | 2 | 3 | 8.94724 |
| 7.15 | 0 | 3 | 1 | 7.1203604 |
| 5.36 | 0 | 4 | 1 | 5.3662486 |

Table A2. Comparison of observed reflections with signals calculated from the unit cell for K8A in PBS.

| Measured Resolution (Å) | Miller Indices | | | Predicted Resolution (Å) |
|---|---|---|---|---|
| | h | k | l | |
| 19.36 | 0 | 0 | 2 | 19.463964 |
| 9.46 | 0 | 2 | 0 | 9.173728 |
| 6.72 | 0 | 2 | 4 | 6.6754403 |
| 5.16 | 0 | 3 | 4 | 5.178218 |
| 4.46 | 0 | 4 | 2 | 4.4645686 |

Table A3. Comparison of observed reflections with signals calculated from the unit cell for K9A in water.

| Measured Resolution (Å) | Miller Indices | | | Predicted Resolution (Å) |
|---|---|---|---|---|
| | h | k | l | |
| 26.57 | 0 | 0 | 2 | 25.85589 |
| 10.51 | 0 | 2 | 0 | 10.631978 |
| 9.8 | 0 | 2 | 2 | 9.833107 |
| 9.3 | 0 | 1 | 5 | 9.3006 |
| 7.11 | 0 | 3 | 0 | 7.0879855 |

Table A4. Comparison of observed reflections with signals calculated from the unit cell for K8RK9R in PBS

| Measured Resolution (Å) | Miller Indices | | | Predicted Resolution (Å) |
|---|---|---|---|---|
| | h | k | l | |
| 25.38 | 0 | 0 | 2 | 25.05971 |
| 21.0 | 0 | 1 | 1 | 20.75244 |
| 11.18 | 0 | 2 | 0 | 11.399312 |
| 9.5 | 0 | 2 | 3 | 9.416183 |
| 7.83 | 0 | 1 | 6 | 7.8433514 |
| 7.61 | 0 | 3 | 0 | 7.599541 |

Table A5. Comparison of observed reflections with signals calculated from the unit cell for K1RK8R in PBS

| Measured Resolution (Å) | Miller Indices | | | Predicted Resolution (Å) |
|---|---|---|---|---|
| | H | k | l | |
| 26.02 | 0 | 0 | 2 | 26.65193 |
| 22.38 | 0 | 1 | 0 | 21.934841 |
| 13.32 | 0 | 0 | 4 | 13.325965 |
| 11.06 | 0 | 2 | 0 | 10.967421 |
| 9.68 | 0 | 1 | 5 | 9.588299 |
| 9.4 | 0 | 2 | 3 | 9.33268 |
| 7.6 | 0 | 2 | 5 | 7.644415 |

Table A6. Comparison of observed reflections with signals calculated from the unit cell for K1RK9R in PBS

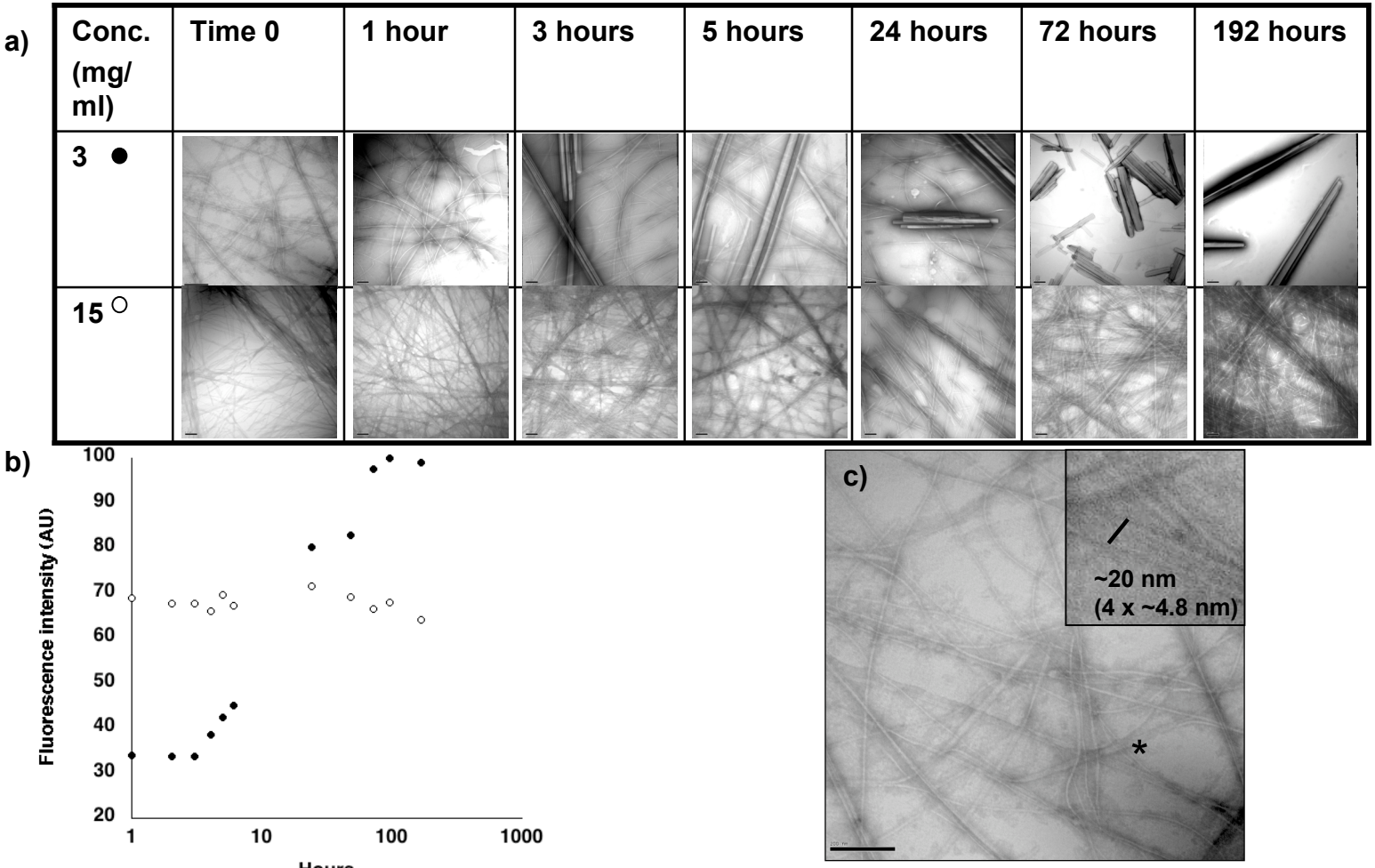


**Figure 4.5. Detailed assembly of GNNQQNY at 3 mg/ml and 15 mg/ml over time.** a) Electron micrographs of species formed as time proceeds. b) Tyrosine fluorescence at 305 nm against time for 3 mg/ml (closed circles) and 15 mg/ml (open circles). There is no lag phase for the 15 mg/ml sample, the lag phase for 3 mg/ml is approximately 3 hours. c) Enlargement of 3 mg/ml, time 0 showing lateral association of fibres. The inset shows a higher magnification of the fibres next to the asterisk (*). The width of the ribbon is around 20 nm and is composed of 4 subunits (protofilaments) of around 4.8 nm each. Scale bars are 200 nm.

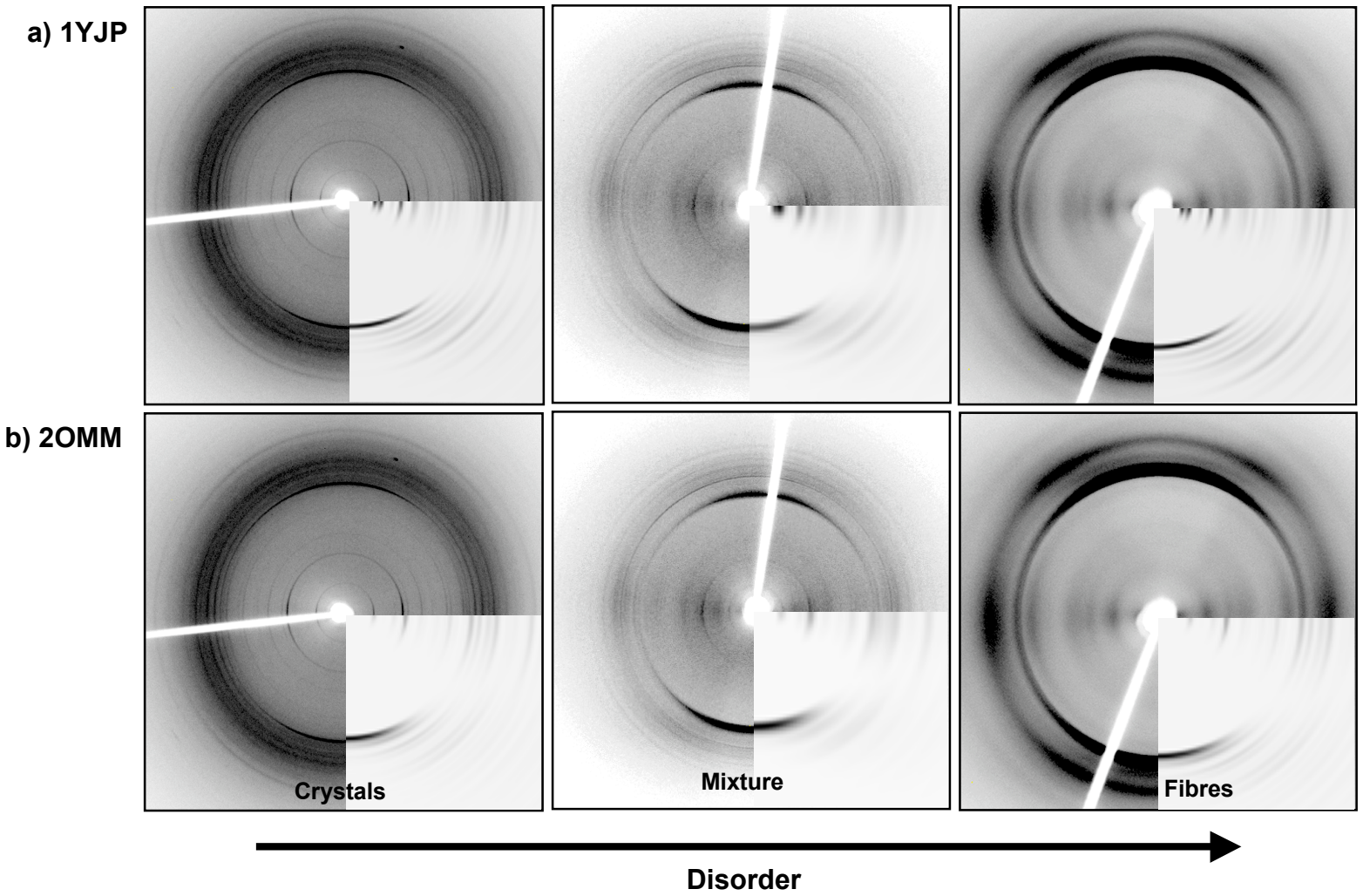


**Figure 5.4. Comparison of experimental and calculated fibre diffraction patterns.** Calculated patterns are shown in the bottom right hand corner of each image and have been sized to correspond to the experimental diffraction settings. Crystalline, mixed fibres and crystals and fibrillar samples are compared to simulated diffraction patterns from the crystal structure of a) 1YJP and b) 2OMM.

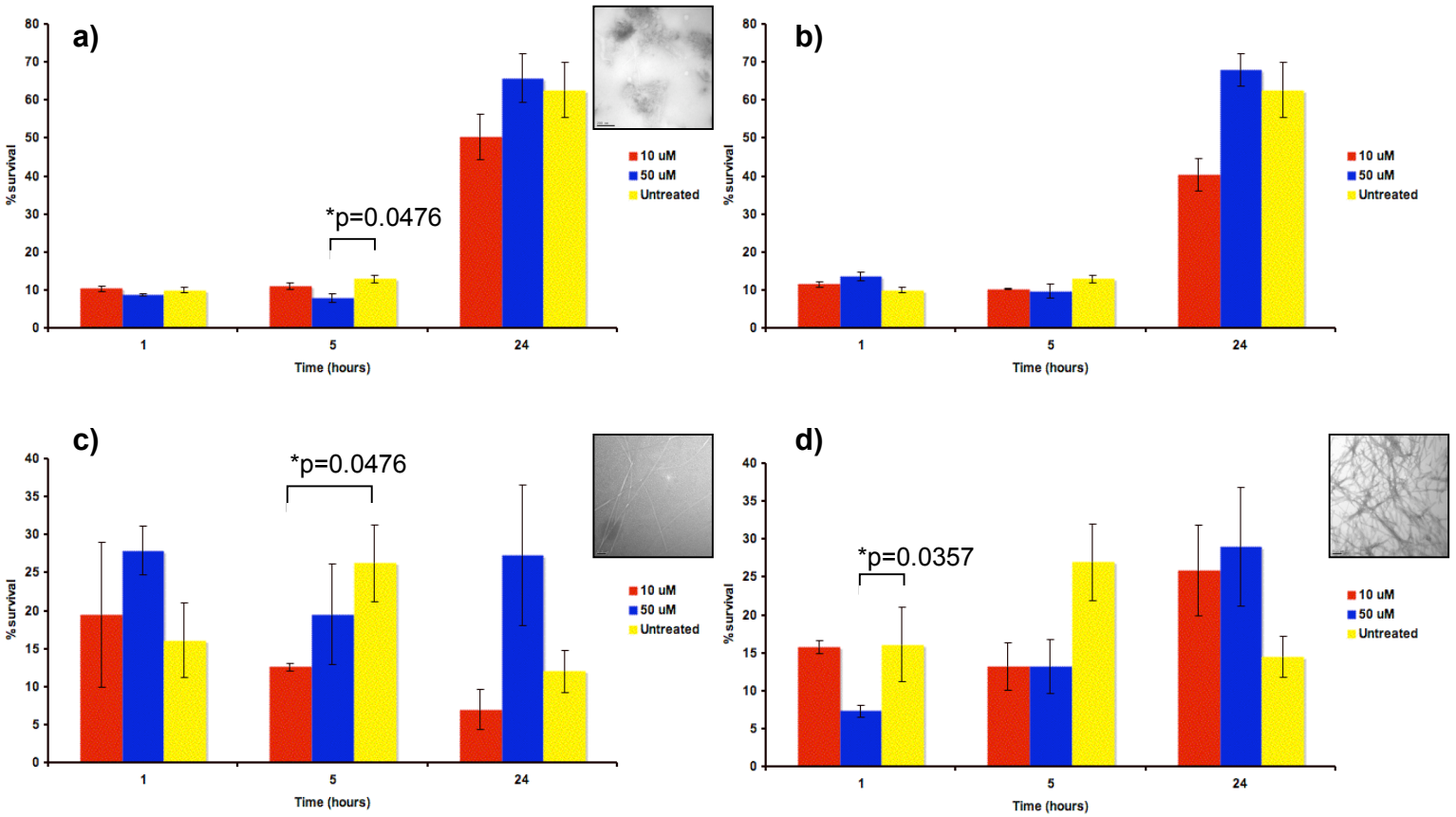


**Figure 6.26 % cell survival measured using the MTT assay for various KFFEAAAKKFFE variants diluted to 10 μM and 50 μM added to SHSY5Y cells after 1, 5 and 24 hours.** a) K1AK8A left quiescent for four days, b) K1AK9A left quiescent for four days, c) Freshly prepared capped peptide, d) fibres formed from capped peptide after 2 hours agitated incubation. Significant p values are shown. All variants were prepared at 5 mg/ml in PBS, EM images of each sample at the time of addition to cells are shown in the insets. Scale bars are 200 nm.

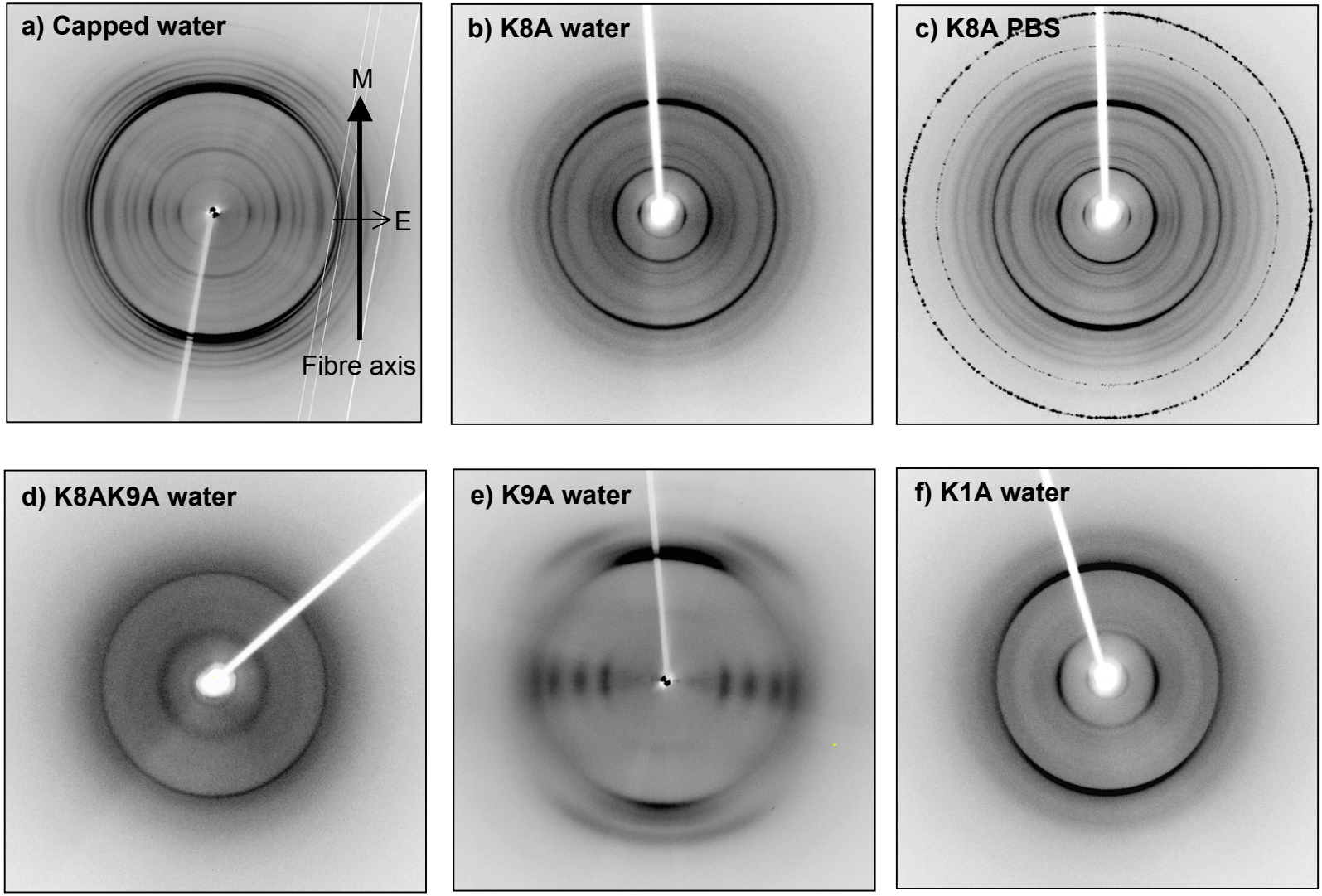
a) Capped water
M
E
Fibre axis
b) K8A water
c) K8A PBS
d) K8AK9A water
e) K9A water
f) K1A water

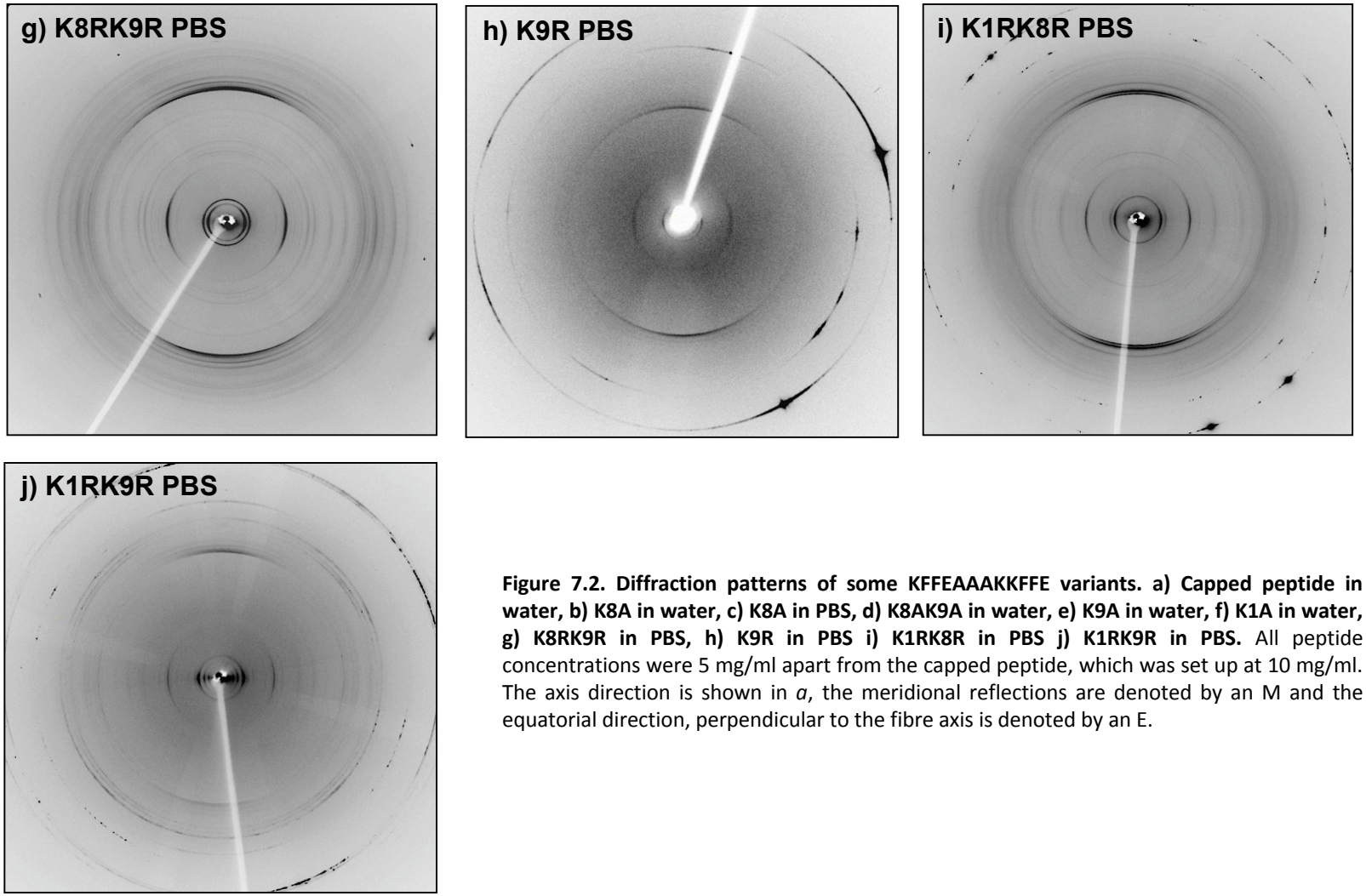


**Figure 7.2. Diffraction patterns of some KFFEAAAKKFFE variants. a) Capped peptide in water, b) K8A in water, c) K8A in PBS, d) K8AK9A in water, e) K9A in water, f) K1A in water, g) K8RK9R in PBS, h) K9R in PBS i) K1RK8R in PBS j) K1RK9R in PBS.** All peptide concentrations were 5 mg/ml apart from the capped peptide, which was set up at 10 mg/ml. The axis direction is shown in *a*, the meridional reflections are denoted by an M and the equatorial direction, perpendicular to the fibre axis is denoted by an E.

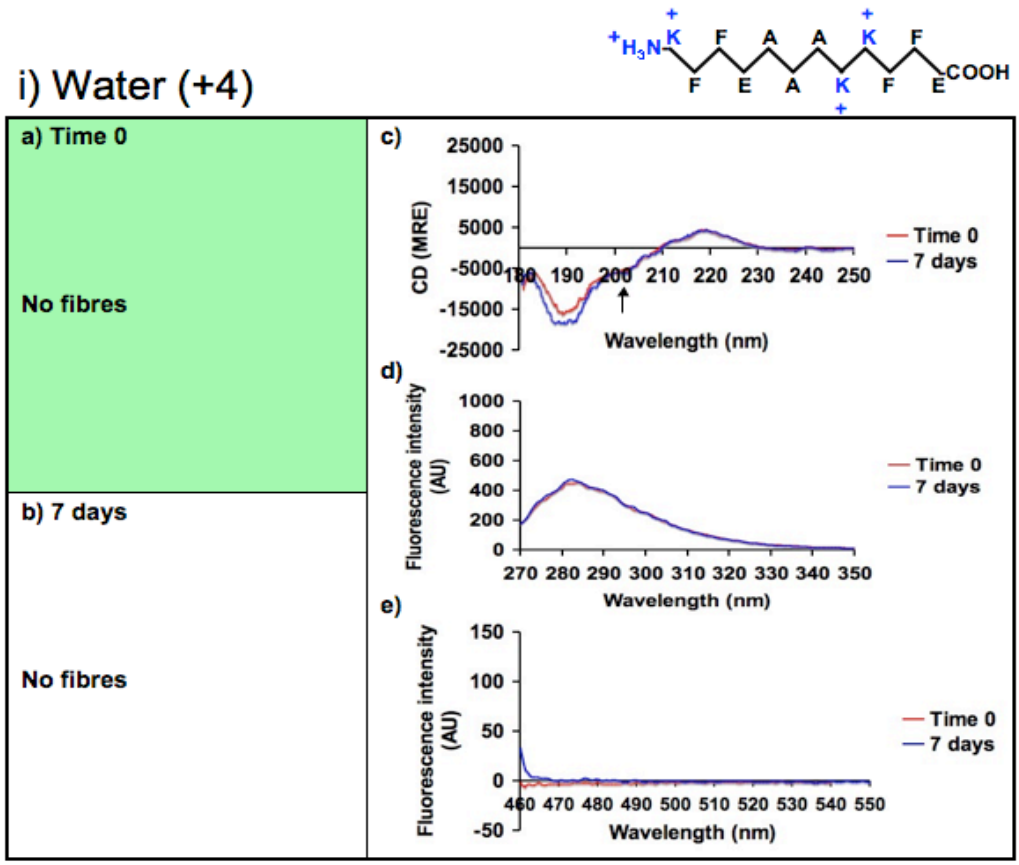
i) Water (+4)
a) Time 0
No fibres
b) 7 days
No fibres
c)
CD (MRE)
Wavelength (nm)
Time 0
7 days
d)
Fluorescence intensity (AU)
Wavelength (nm)
Time 0
7 days
e)
Fluorescence intensity (AU)
Wavelength (nm)
Time 0
7 days

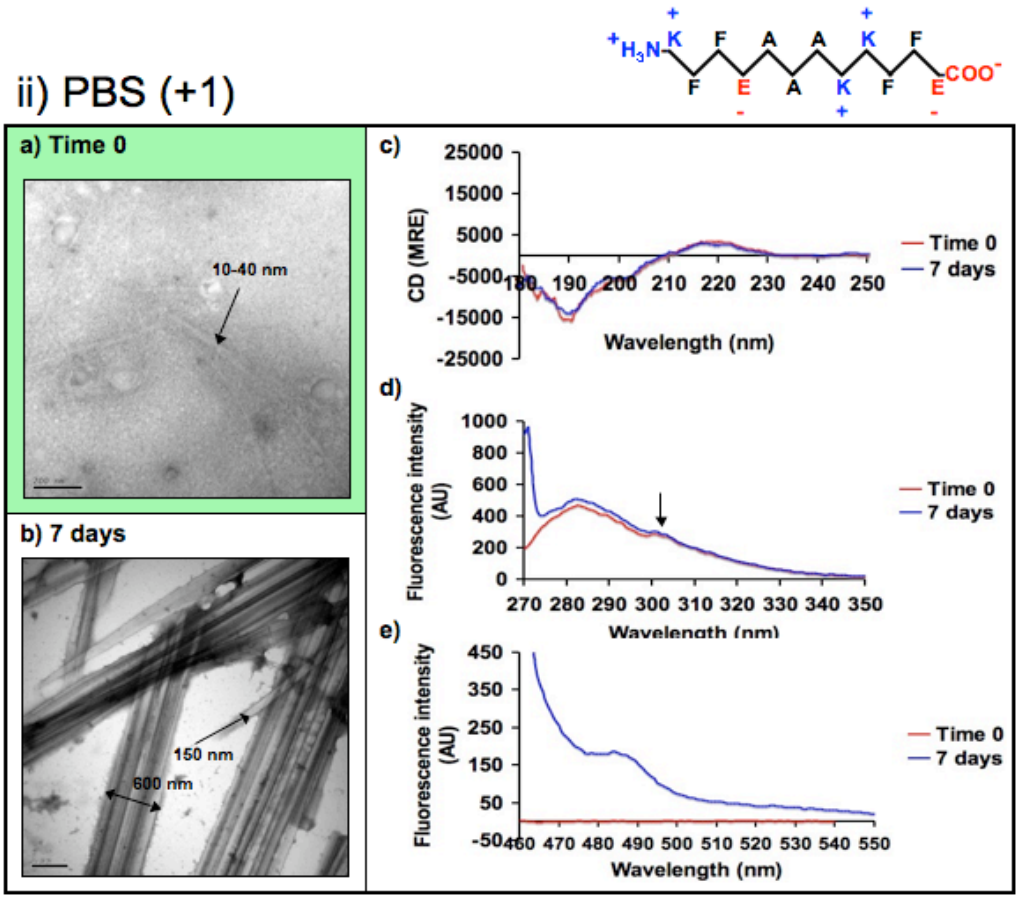
ii) PBS (+1)
a) Time 0
10-40 nm
b) 7 days
150 nm
600 nm
c)
CD (MRE)
Wavelength (nm)
Time 0
7 days
d)
Fluorescence intensity (AU)
Time 0
7 days
e)
Fluorescence intensity (AU)
Wavelength (nm)
Time 0
7 days

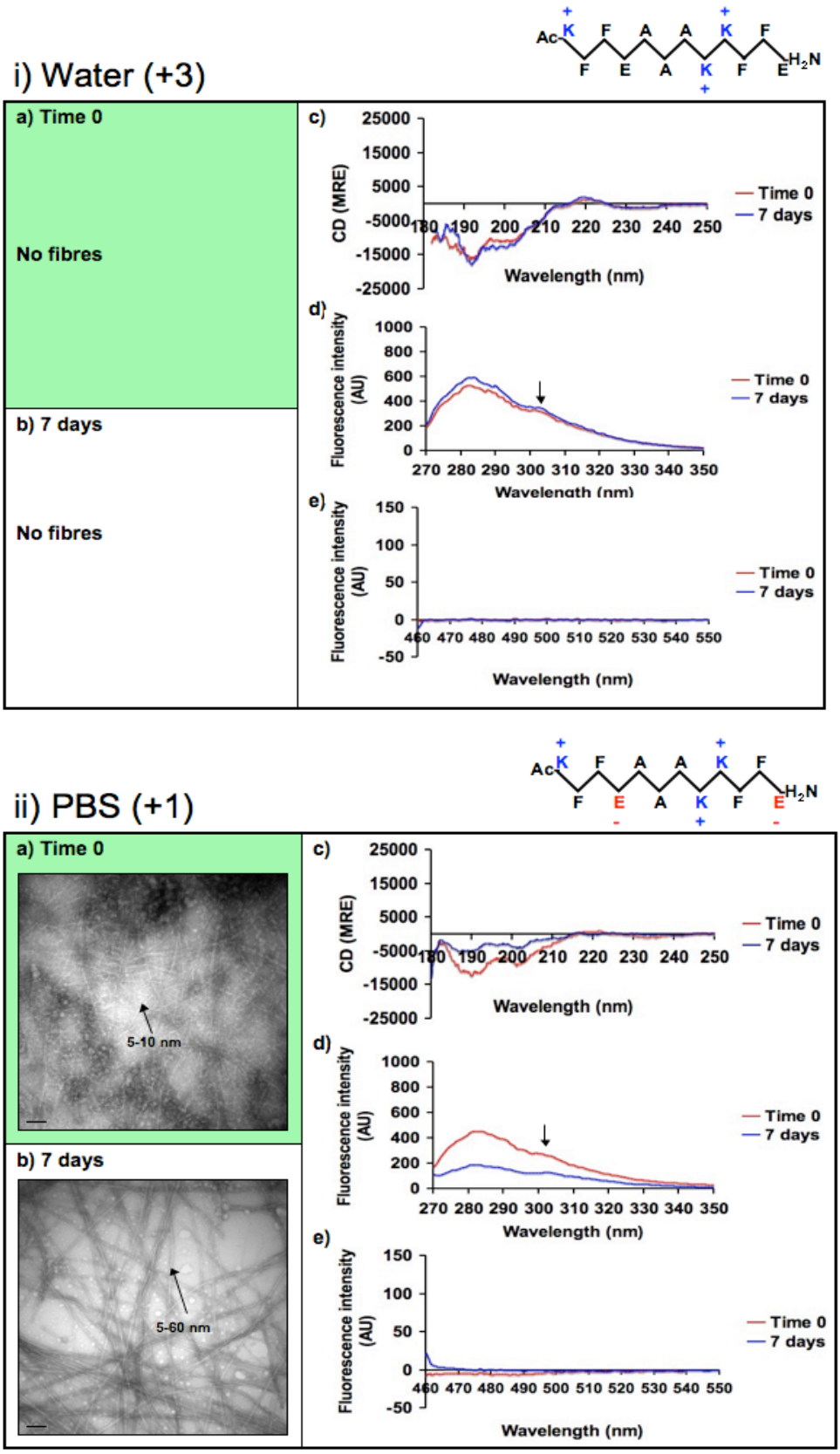


**Figure 6.11. Ac-KFFEAAAKKFFE-NH2 in water (i) and 10 mM PBS (ii). Electron micrographs at time 0 (a) and 7 days (b), far-UV CD spectra (c), intrinsic phenylalanine fluorescence (d) and Thioflavin T binding (e) at time 0 and after 7 days agitation.** For experimental details see legend for figure 6.5. Scale bars are 200 nm.

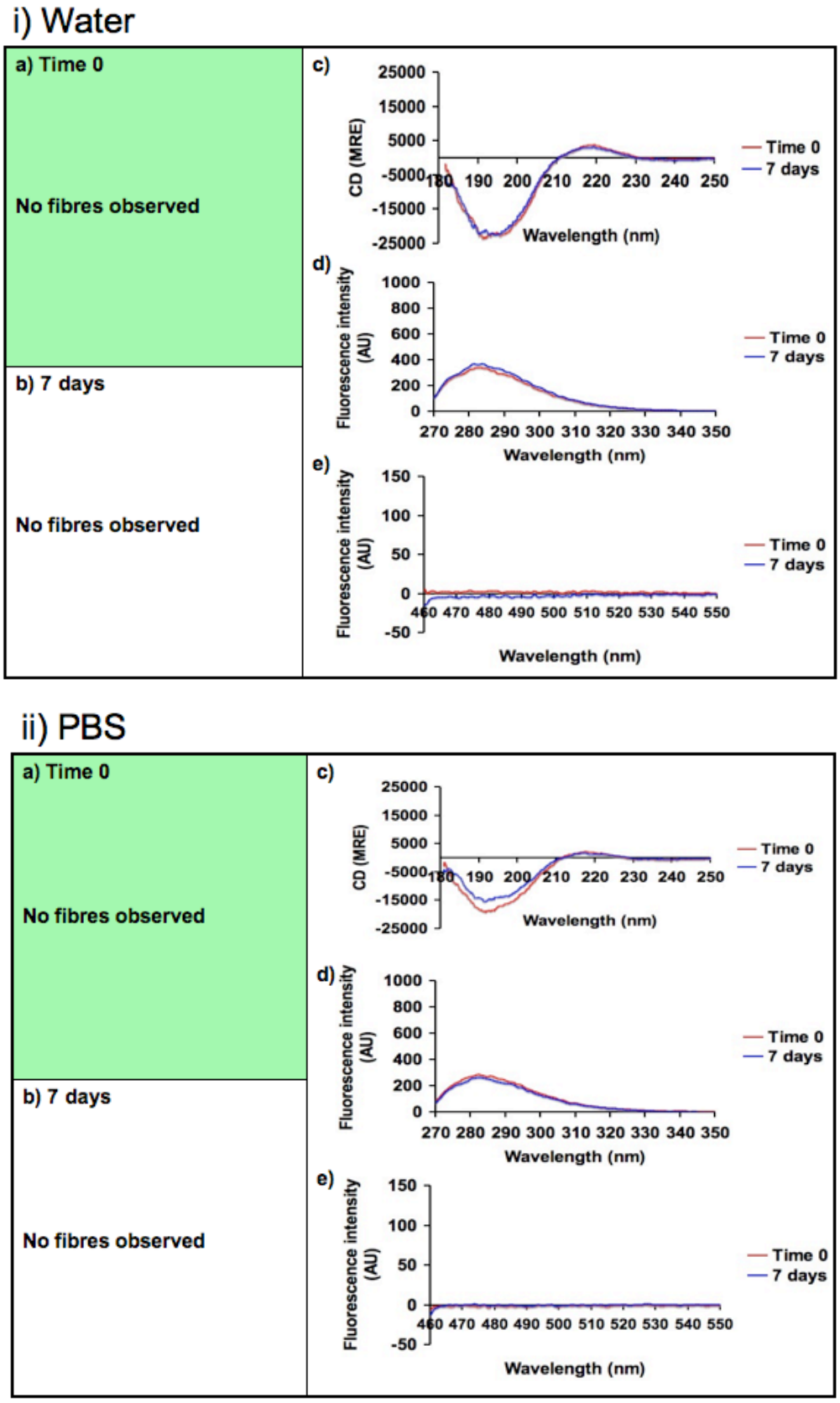


**Figure 6.12. K<u>AA</u>EAAAKKFFE in water (i) and 10 mM PBS (ii). Electron micrographs at time 0 (a) and 7 days (b), far-UV CD spectra (c), intrinsic phenylalanine fluorescence (d) and Thioflavin T binding (e) at time 0 and after 7 days agitation.** For experimental details see legend for figure 6.5.

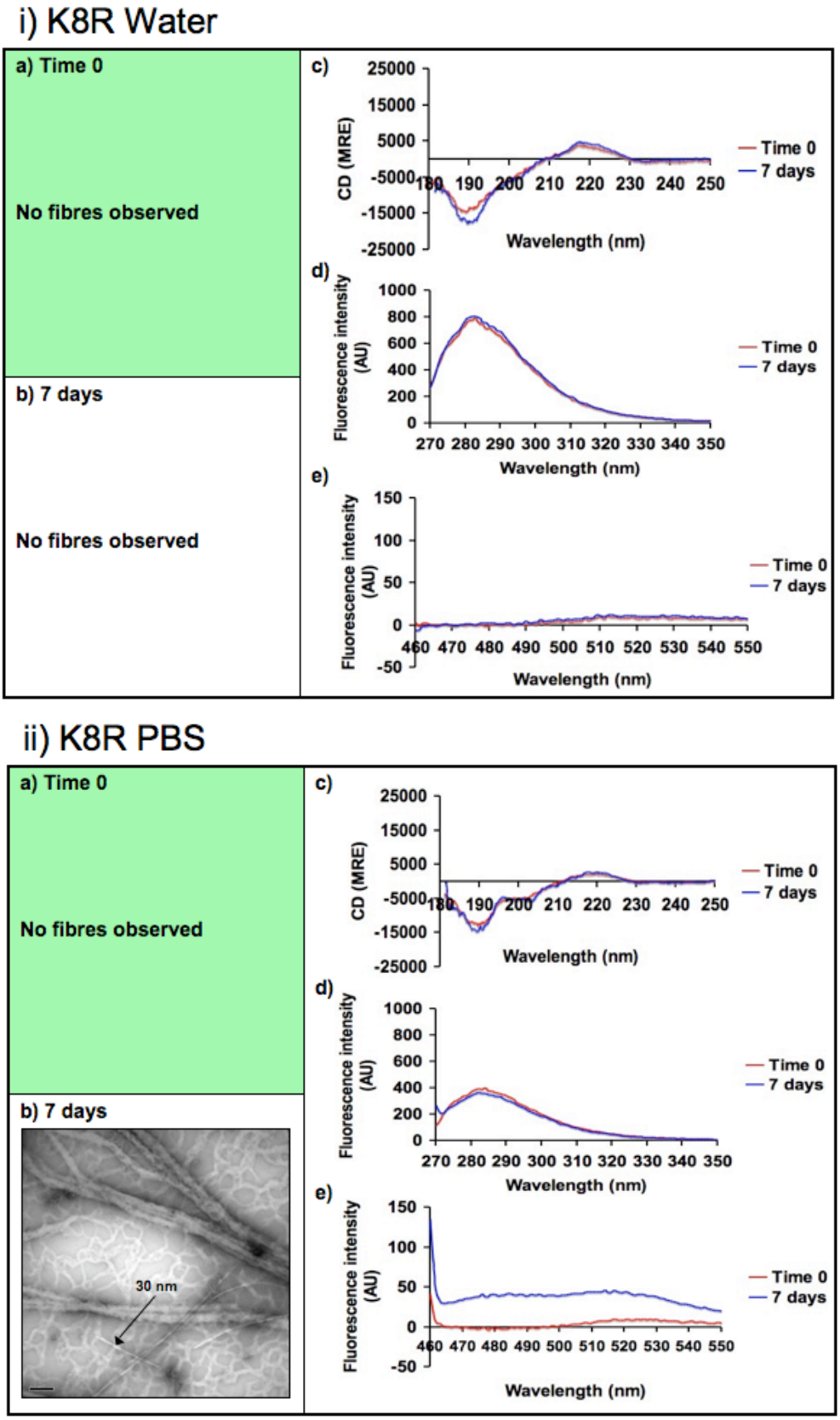


**Figure 6.13. KFFEAAARKFFE in water (i) and 10 mM PBS (ii). Electron micrographs at time 0 (a) and 7 days (b), far-UV CD spectra (c), intrinsic phenylalanine fluorescence (d) and Thioflavin T binding (e) at time 0 and after 7 days agitation.** For experimental details see legend for figure 6.5. Scale bars are 200 nm.

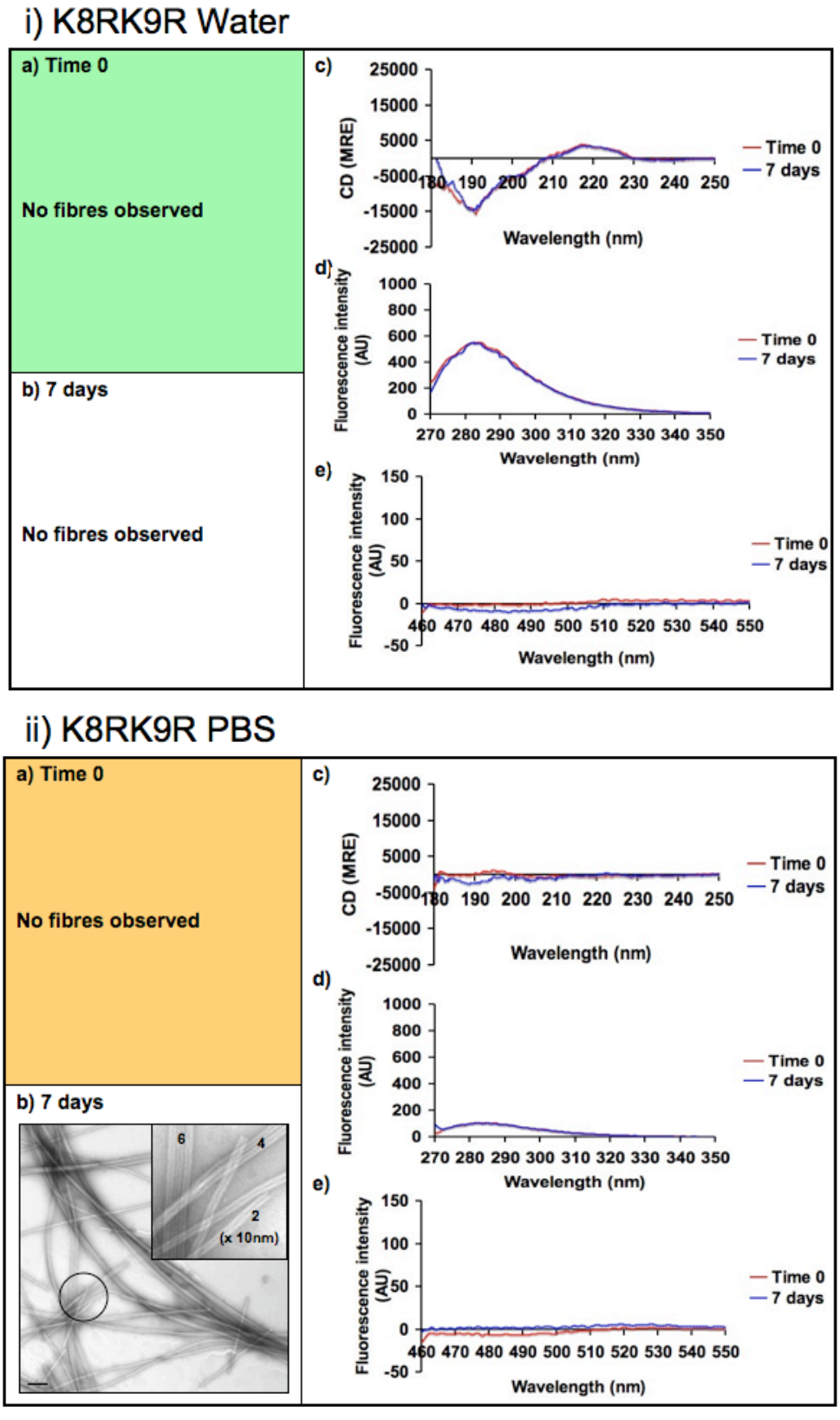


**Figure 6.14. KFFEAAARRFFE in water (i) and 10 mM PBS (ii). Electron micrographs at time 0 (a) and 7 days (b), far-UV CD spectra (c), intrinsic phenylalanine fluorescence (d) and Thioflavin T binding (e) at time 0 and after 7 days agitation.** For experimental details see legend for figure 6.5. Scale bars are 200 nm.

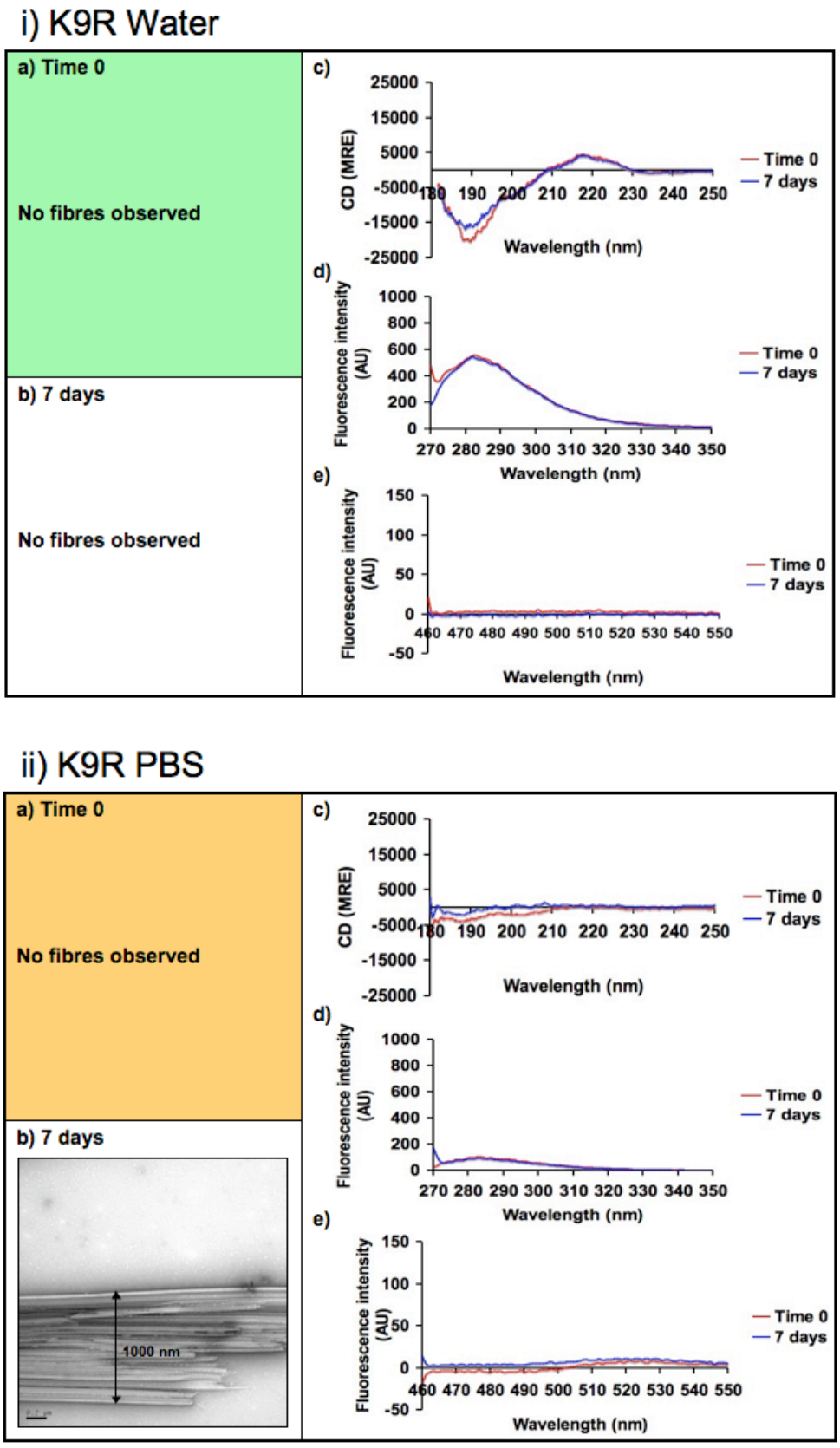


**Figure 6.15. KFFEAAAKRFFE in water (i) and 10 mM PBS (ii). Electron micrographs at time 0 (a) and 7 days (b), far-UV CD spectra (c), intrinsic phenylalanine fluorescence (d) and Thioflavin T binding (e) at time 0 and after 7 days agitation.** For experimental details see legend for figure 6.5. Scale bars are 200 nm.

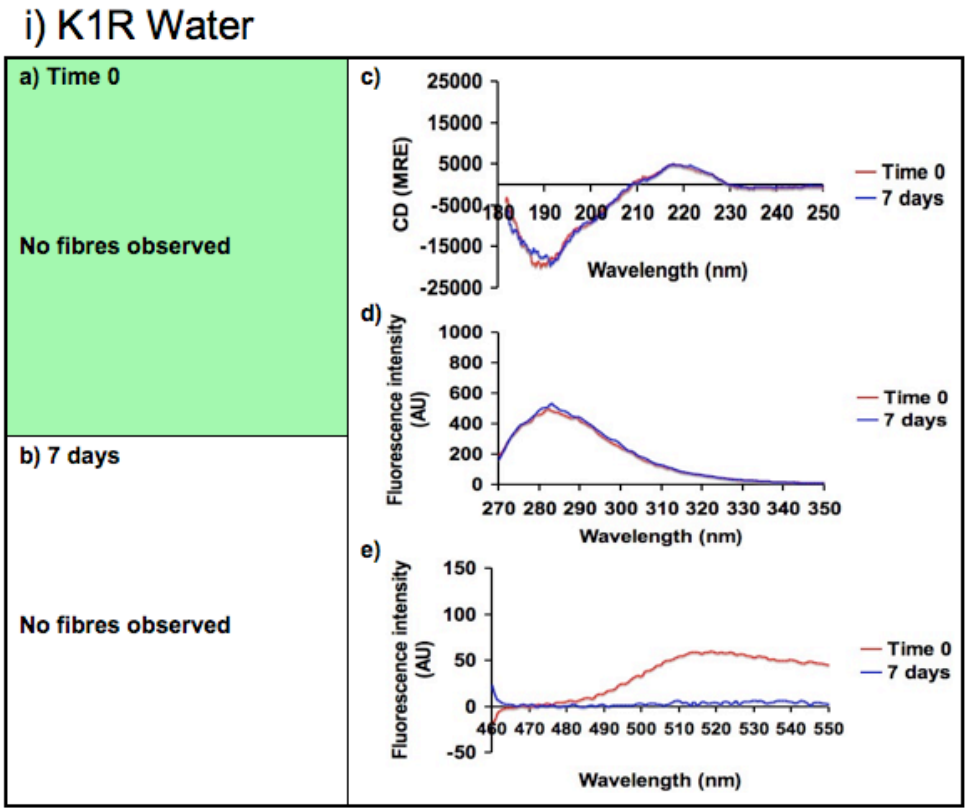


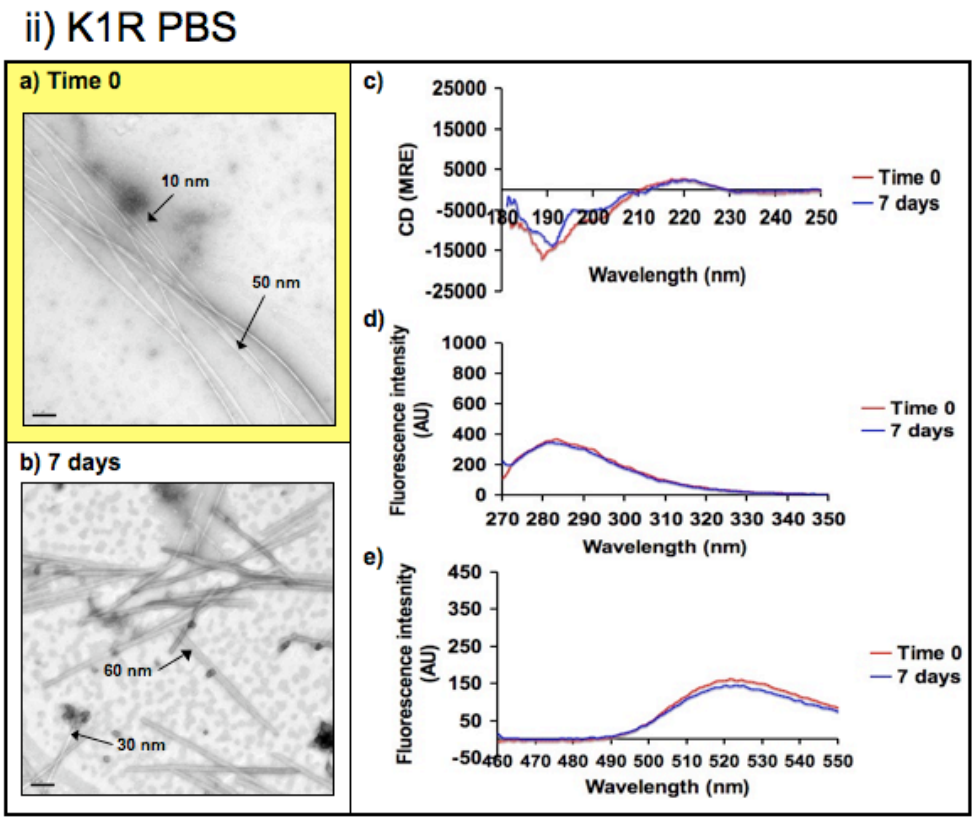


**Figure 6.16. RFFEAAAKKFFE in water (i) and 10 mM PBS (ii). Electron micrographs at time 0 (a) and 7 days (b), far-UV CD spectra (c), intrinsic phenylalanine fluorescence (d) and Thioflavin T binding (e) at time 0 and after 7 days agitation.** For experimental details see legend for figure 6.5. Scale bars are 200 nm. The scale for the ThT fluorescence is increased in ii.

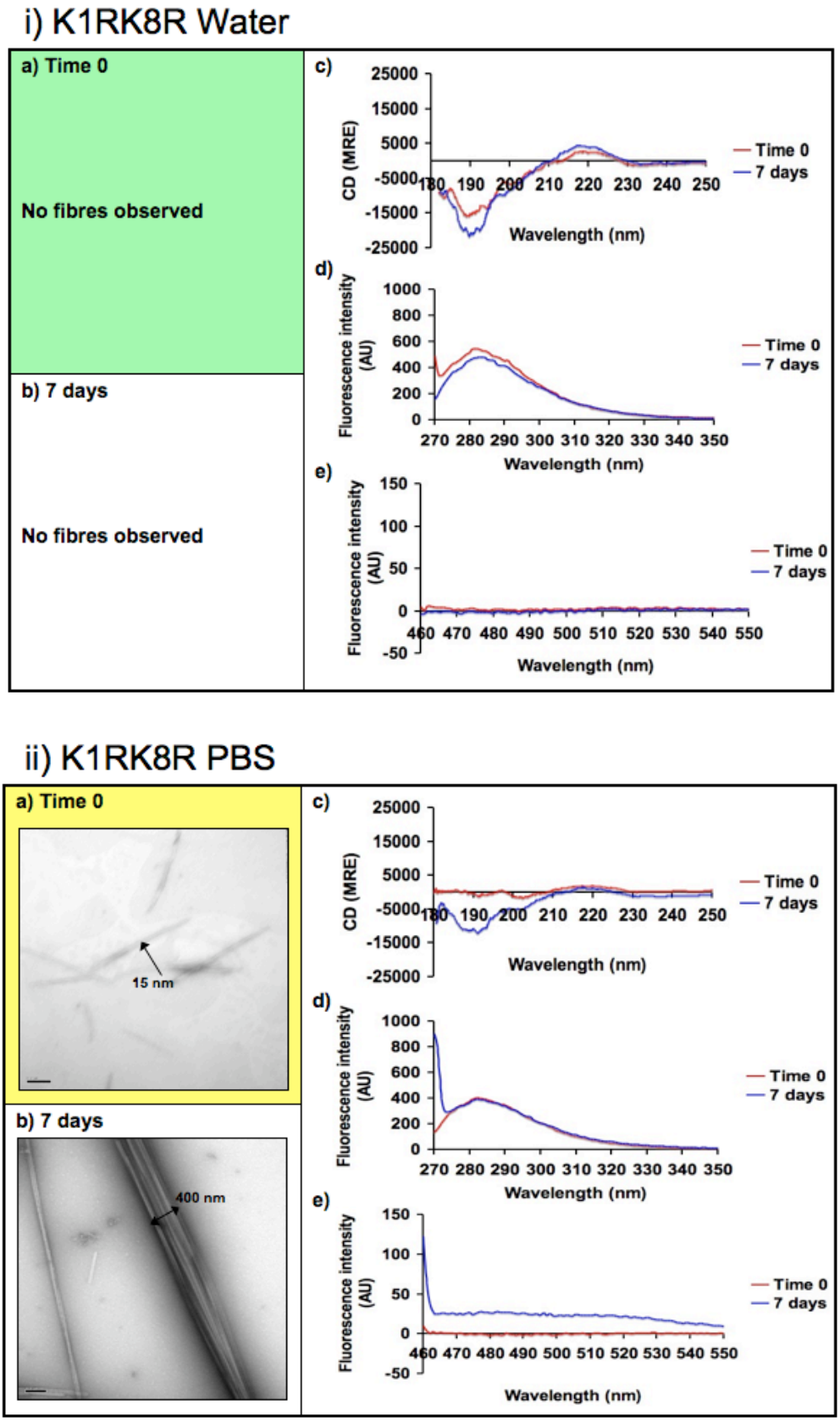


**Figure 6.17. RFFEAAARKFFE in water (i) and 10 mM PBS (ii). Electron micrographs at time 0 (a) and 7 days (b), far-UV CD spectra (c), intrinsic phenylalanine fluorescence (d) and Thioflavin T binding (e) at time 0 and after 7 days agitation.** For experimental details see legend for figure 6.5. Scale bars are 200 nm.

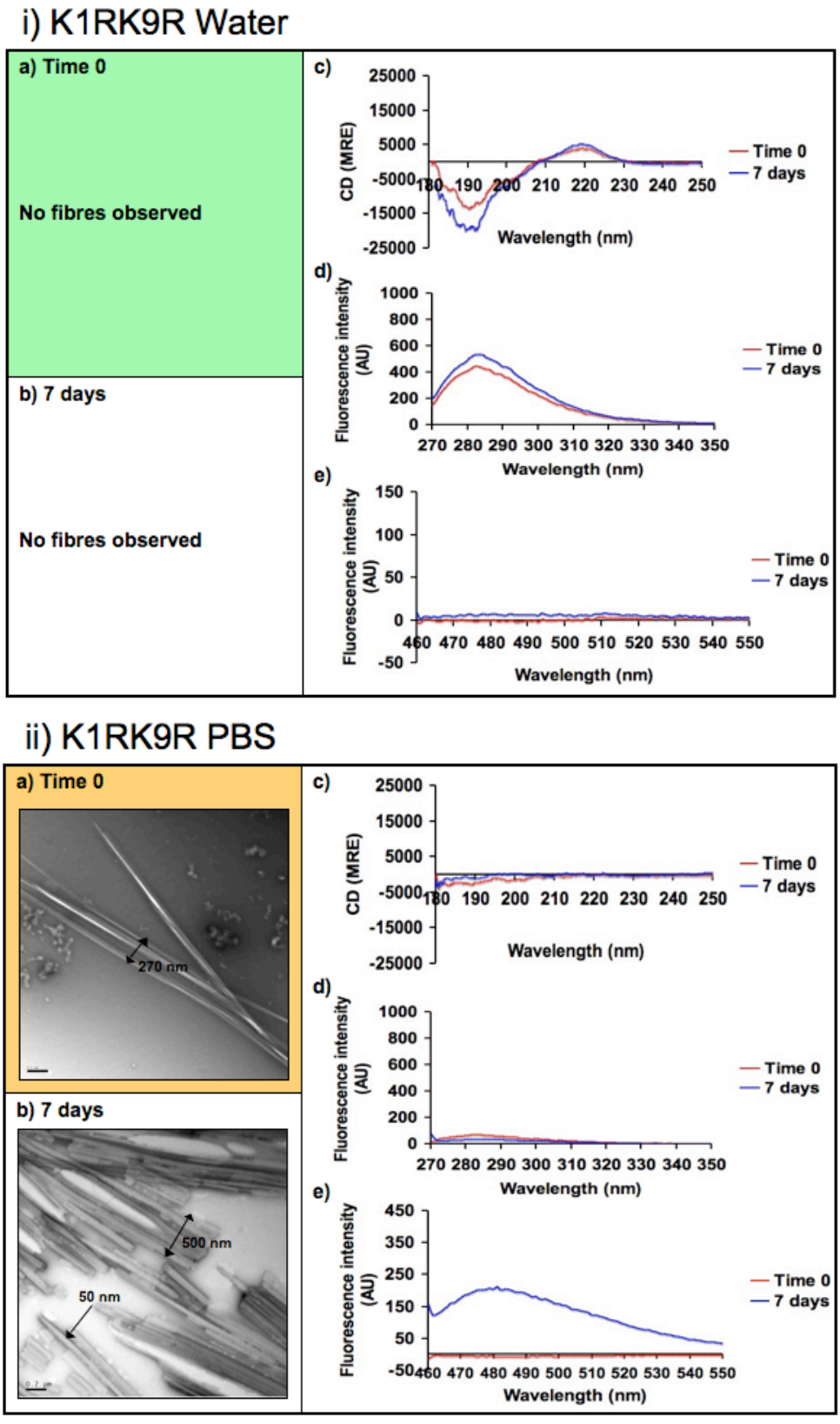


**Figure 6.18. RFFEAAAKRFFE in water (i) and 10 mM PBS (ii). Electron micrographs at time 0 (a) and 7 days (b), far-UV CD spectra (c), intrinsic phenylalanine fluorescence (d) and Thioflavin T binding (e) at time 0 and after 7 days agitation.** For experimental details see legend for figure 6.5. Scale bars are 200 nm. The scale for the ThT fluorescence is increased in ii.

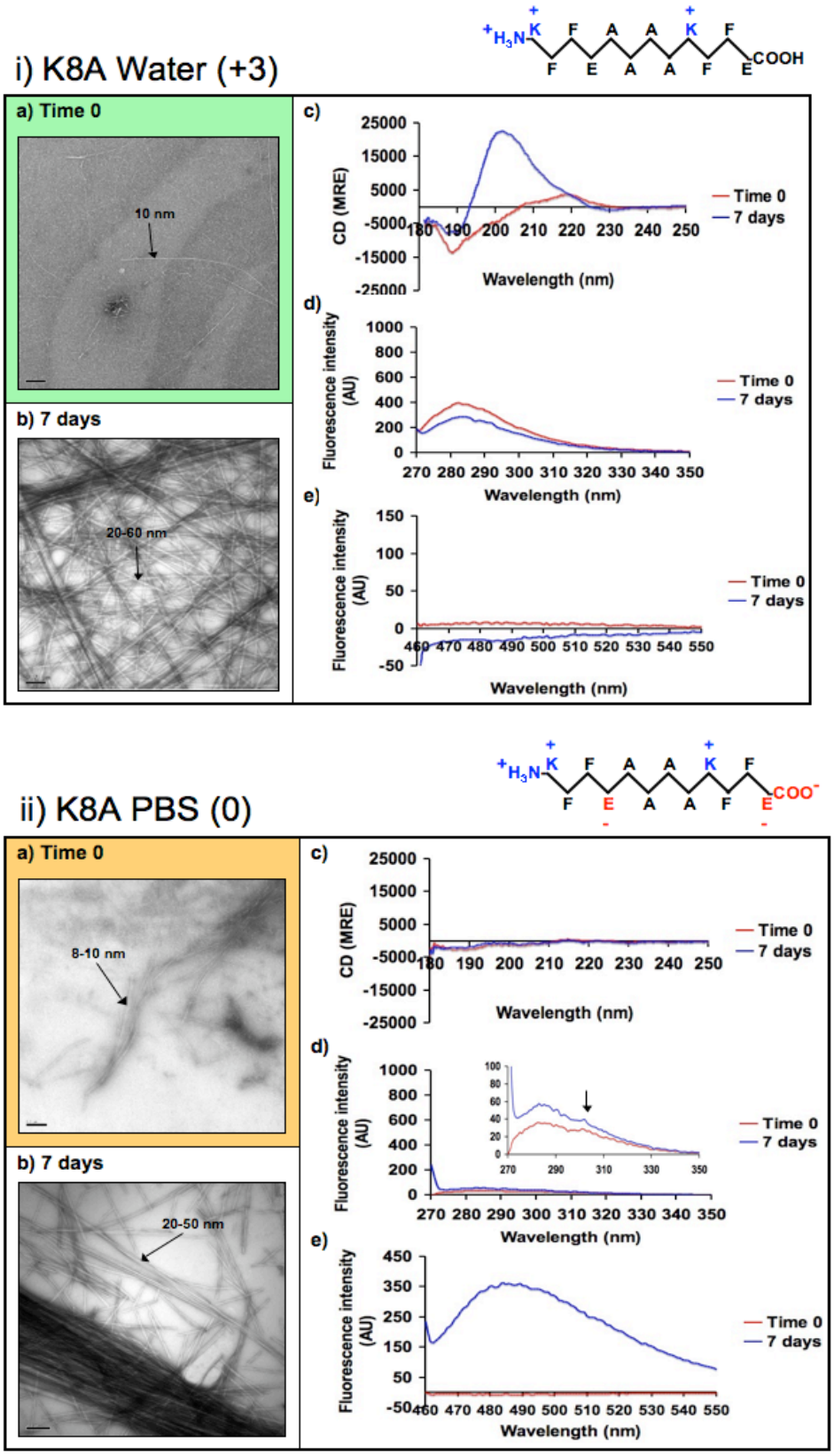


**Figure 6.20. KFFEAAAAKFFE in water (i) and 10 mM PBS (ii). Electron micrographs at time 0 (a) and 7 days (b), far-UV CD spectra (c), intrinsic phenylalanine fluorescence (d) and Thioflavin T binding (e) at time 0 and after 7 days agitation.** For experimental details see legend for figure 6.5. Scale bars are 200 nm. The net charge on the peptide is given in brackets.

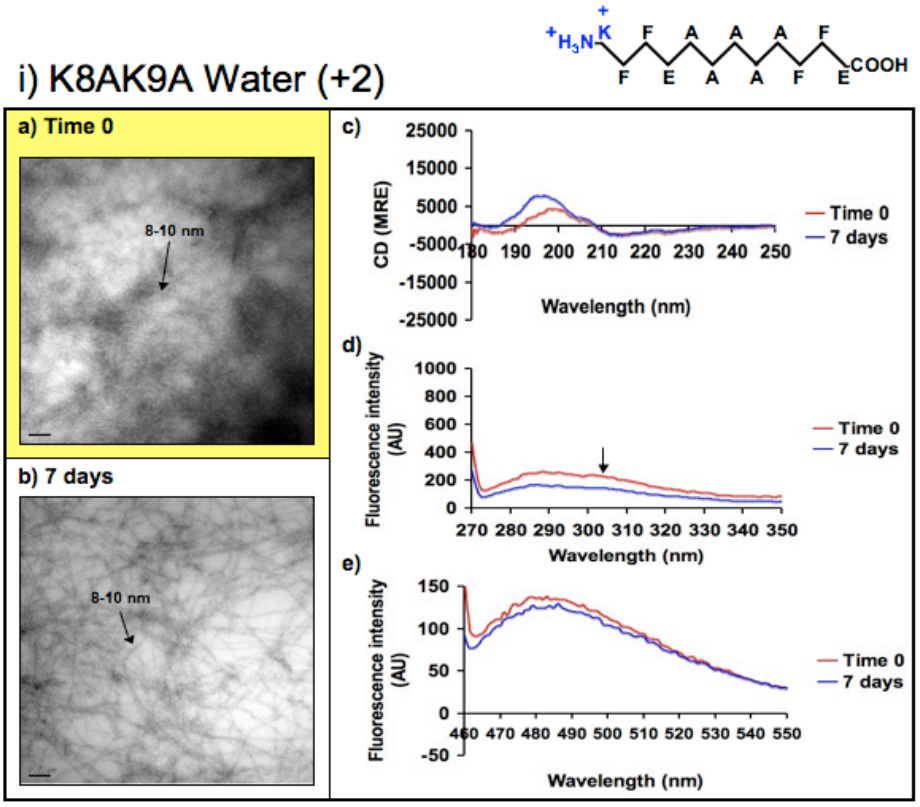


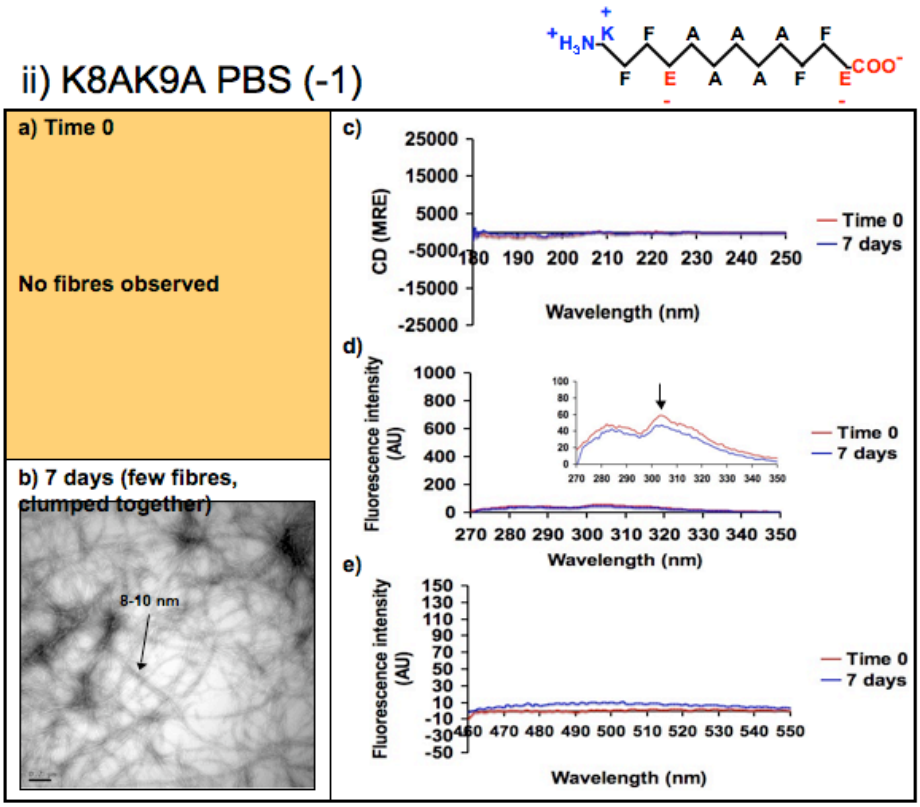


**Figure 6.21. KFFEAAAAAFFE in water (i) and 10 mM PBS (ii). Electron micrographs at time 0 (a) and 7 days (b), far-UV CD spectra (c), intrinsic phenylalanine fluorescence (d) and Thioflavin T binding (e) at time 0 and after 7 days agitation.** For experimental details see legend for figure 6.5. Scale bars are 200 nm. The net charge on the peptide is given in brackets.

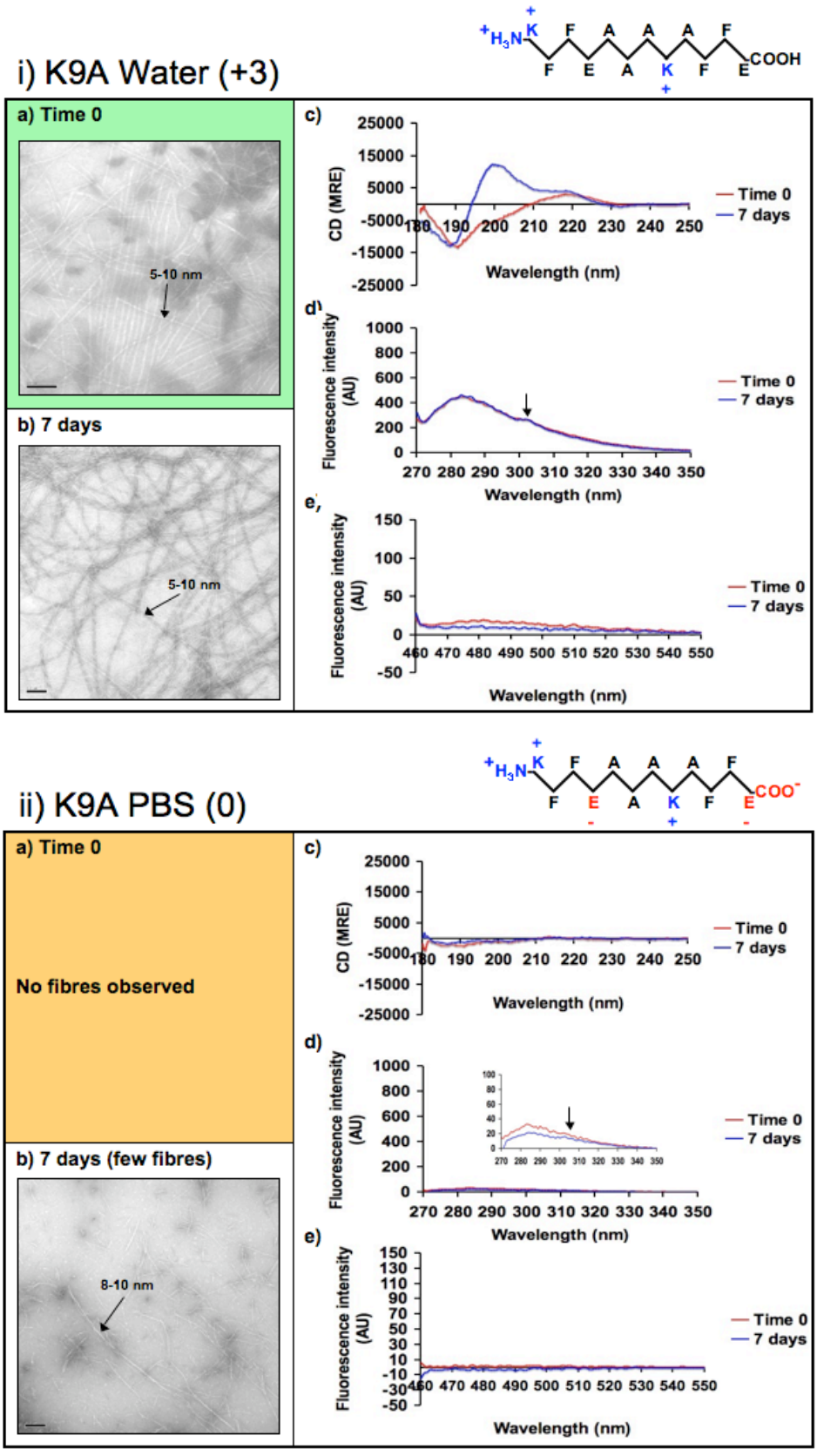


**Figure 6.22. KFFEAAAKAFFE in water (i) and 10 mM PBS (ii). Electron micrographs at time 0 (a) and 7 days (b), far-UV CD spectra (c), intrinsic phenylalanine fluorescence (d) and Thioflavin T binding (e) at time 0 and after 7 days agitation.** For experimental details see legend for figure 6.5. Scale bars are 200 nm. The net charge on the peptide is given in brackets.

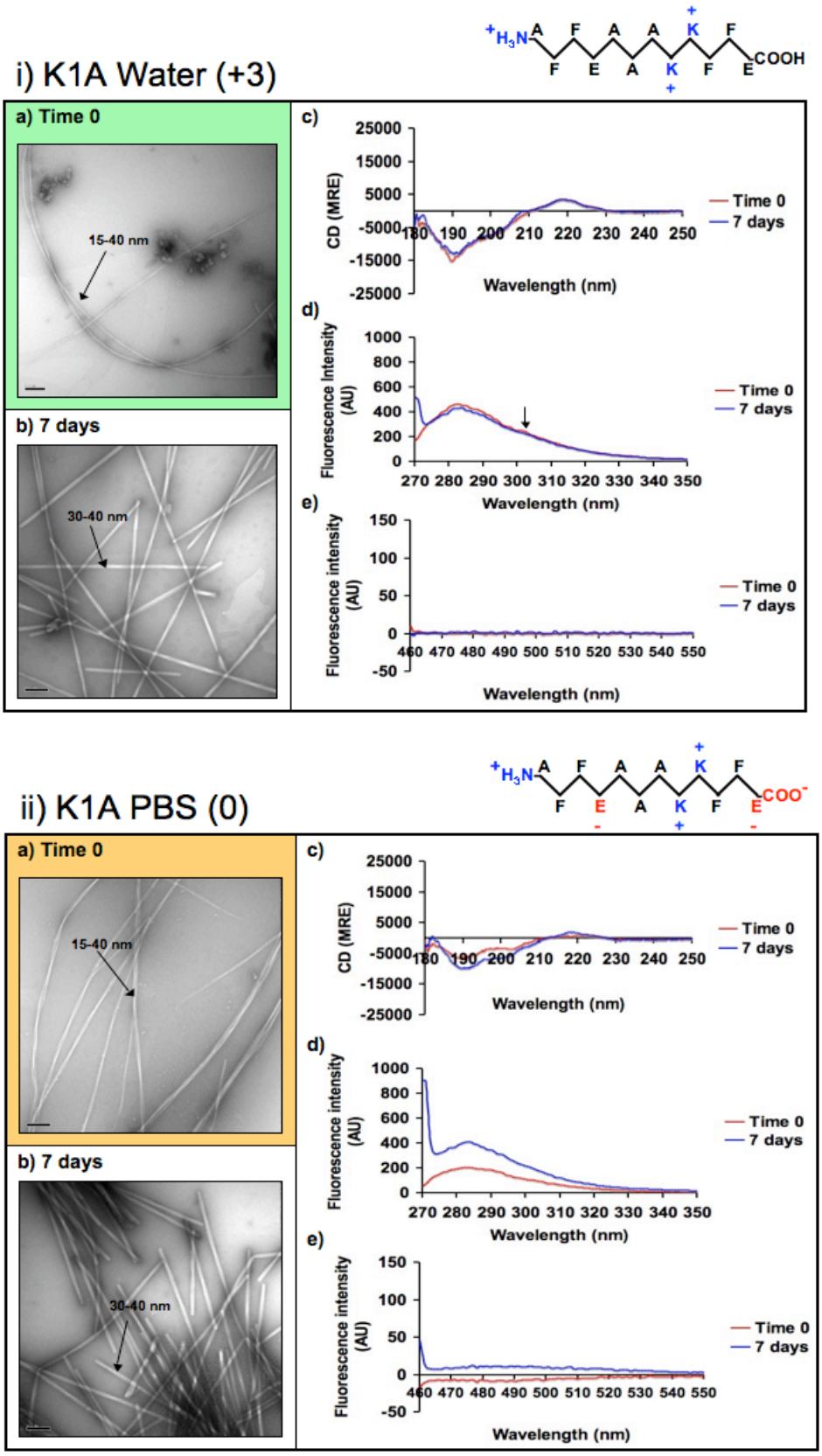


**Figure 6.23. AFFEAAAKKFFE in water (i) and 10 mM PBS (ii). Electron micrographs at time 0 (a) and 7 days (b), far-UV CD spectra (c), intrinsic phenylalanine fluorescence (d) and Thioflavin T binding (e) at time 0 and after 7 days agitation.** For experimental details see legend for figure 6.5. Scale bars are 200 nm. The net charge on the peptide is given in brackets.

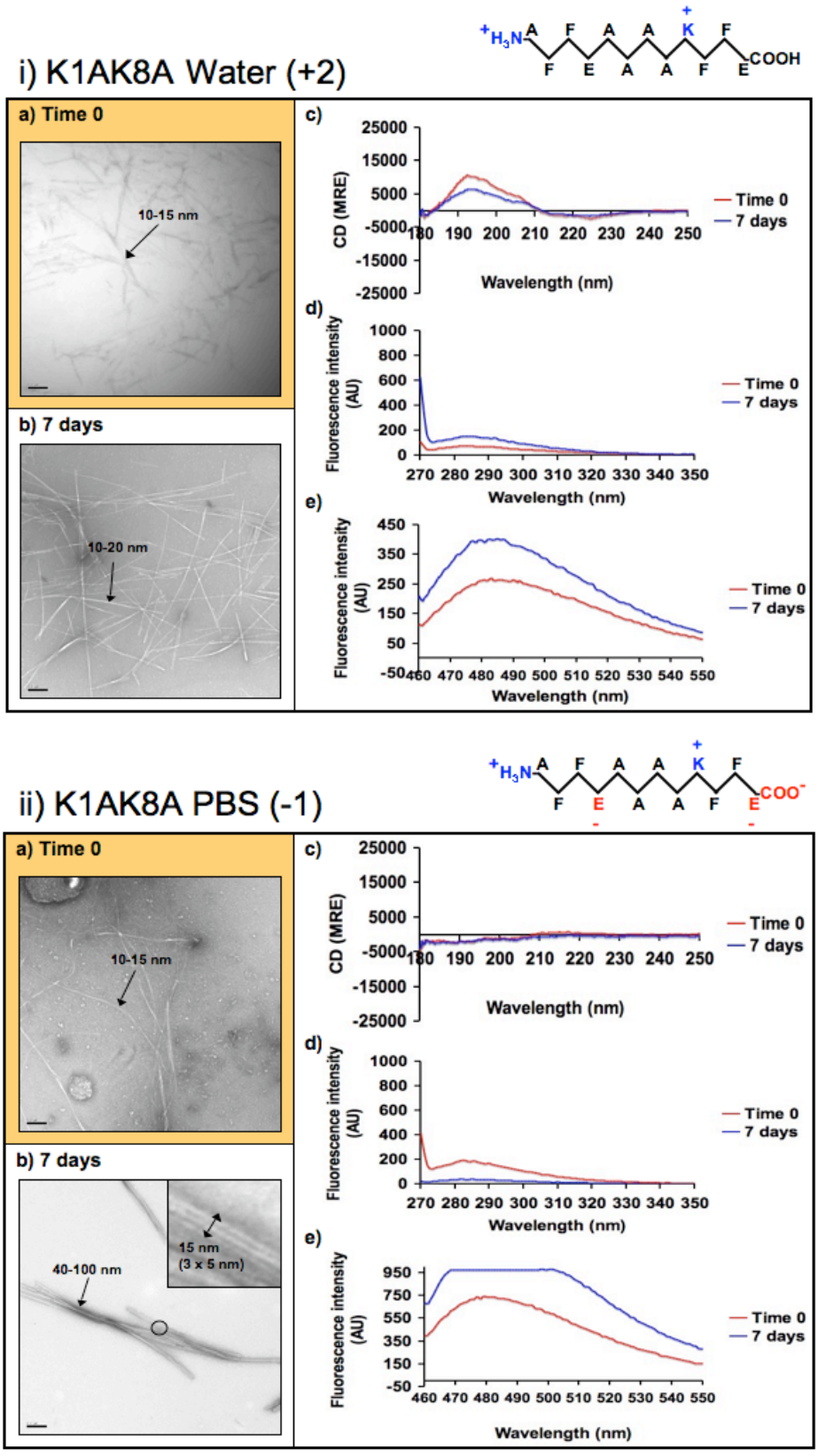


**Figure 6.24. AFFEAAAAKFFE in water (i) and 10 mM PBS (ii). Electron micrographs at time 0 (a) and 7 days (b), far-UV CD spectra (c), intrinsic phenylalanine fluorescence (d) and Thioflavin T binding (e) at time 0 and after 7 days agitation.** For experimental details see legend for figure 6.5. Scale bars are 200 nm. The net charge on the peptide is given in brackets.

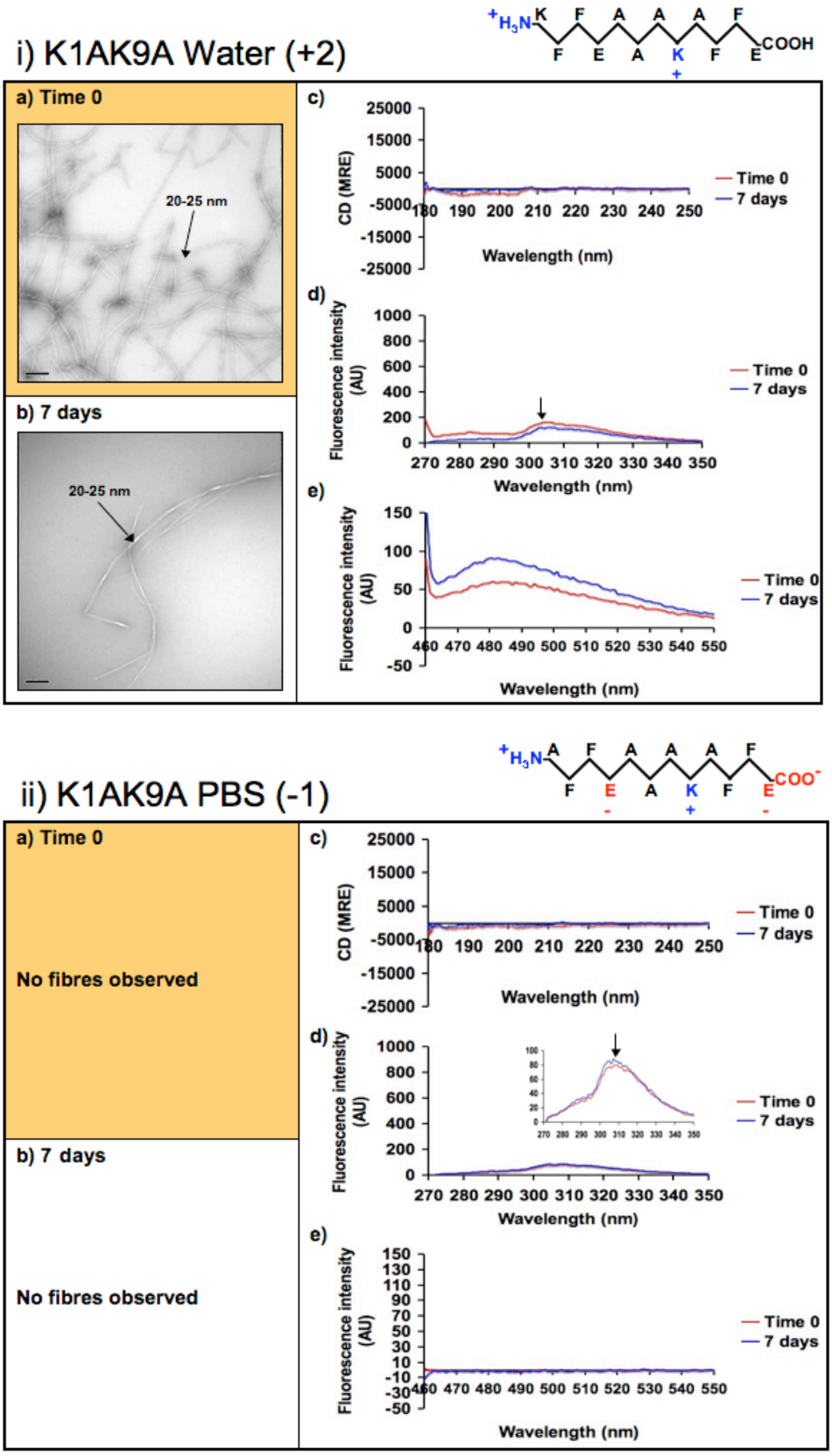


**Figure 6.25. AFFEAAAKAFFE in water (i) and 10 mM PBS (ii). Electron micrographs at time 0 (a) and 7 days (b), far-UV CD spectra (c), intrinsic phenylalanine fluorescence (d) and Thioflavin T binding (e) at time 0 and after 7 days agitation.** For experimental details see legend for figure 6.5. Scale bars are 200 nm. The net charge on the peptide is given in brackets.

# Characterizing the Assembly of the Sup35 Yeast Prion Fragment, GNNQQNY: Structural Changes Accompany a Fiber-to-Crystal Switch

Karen E. Marshall,[†] Matthew R. Hicks,[‡§] Thomas L. Williams,[†] Søren Vrønning Hoffmann,[¶] Alison Rodger,[‡] Timothy R. Dafforn,[§] and Louise C. Serpell[†*]

[†]Department of Biochemistry, School of Life Sciences, University of Sussex, Falmer, BN1 9QG United Kingdom; [‡]Department of Chemistry, University of Warwick, Coventry, CV4 7AL United Kingdom; [§]School of Biosciences, University of Birmingham, Birmingham, B15 2TT United Kingdom; and [¶]Institute for Storage Ring Facilities, Aarhus University, Aarhus, DK-8000 Denmark

ABSTRACT Amyloid-like fibrils can be formed by many different proteins and peptides. The structural characteristics of these fibers are very similar to those of amyloid fibrils that are deposited in a number of protein misfolding diseases, including Alzheimer's disease and the transmissible spongiform encephalopathies. The elucidation of two crystal structures from an amyloid-like fibril-forming fragment of the yeast prion, Sup35, with sequence GNNQQNY, has contributed to knowledge regarding side-chain packing of amyloid-forming peptides. Both structures share a cross-$\beta$ steric zipper arrangement but vary in the packing of the peptide, particularly in terms of the tyrosine residue. We investigated the fibrillar and crystalline structure and assembly of the GNNQQNY peptide using x-ray fiber diffraction, electron microscopy, intrinsic and quenched tyrosine fluorescence, and linear dichroism. Electron micrographs reveal that at concentrations between 0.5 and 10 mg/mL, fibers form initially, followed by crystals. Fluorescence studies suggest that the environment of the tyrosine residue changes as crystals form. This is corroborated by linear dichroism experiments that indicate a change in the orientation of the tyrosine residue over time, which suggests that a structural rearrangement occurs as the crystals form. Experimental x-ray diffraction patterns from fibers and crystals also suggest that these species are structurally distinct. A comparison of experimental and calculated diffraction patterns contributes to an understanding of the different arrangements accessed by the peptide.

## INTRODUCTION

Many diseases, including Alzheimer's disease and the transmissible spongiform encephalopathies, involve the deposition of normally soluble protein in the form of amyloid fibrils, and this process is thought to be a key factor in their pathology (1). Amyloid is defined by a variety of criteria, including staining by the dye Congo Red and a long, unbranched appearance when viewed by electron microscopy (EM). There is strong evidence that amyloid has a structure known as cross-$\beta$ (first observed in the egg stalk of the lacewing *Chrysopa* (2)), which shows characteristic reflections at 4.7 Å and 10–11 Å in x-ray fiber diffraction patterns arising from the hydrogen bonding between $\beta$-strands and the spacing between $\beta$-sheets, respectively (3,4). This characteristic cross-$\beta$ pattern is also used as a diagnostic tool to identify amyloid fibrils (5). To understand how proteins misfold and assemble to form these well-ordered fibers, and to gain insight into how they may cause disease, detailed structural knowledge is required. To date, crystallization of full-length amyloid-forming peptides and proteins related to disease has not been possible, so structural information has been obtained by other methods, including solid-state NMR (6), cryo-EM (7–9), atomic force microscopy (10), and x-ray fiber diffraction (11). Recent advances have also been made using model systems comprised of short synthetic peptides, often fragments from proteins associated with disease (11,12). The structures of short peptides ($\leq$7 amino acids) that form amyloid fibers and microcrystals were recently solved by x-ray crystallography, and these structures share a ''steric zipper'' arrangement (13,14). The accumulation of these data has led to the definition of eight different classes of steric zipper that depend on the orientation of $\beta$-strands and $\beta$-sheets in relation to one another (14). One of these, the seven-residue peptide GNNQQNY, is a motif from the N-terminus of the yeast prion-like protein, Sup35. The role of Sup35 in its native state is to terminate translation in yeast, but it has also shown the ability to transmit its alternative conformation and take part in prion-like activity (15). GNNQQNY was previously shown to exhibit amyloid-forming properties similar to those of the full-length peptide (15), and, depending on the concentration and incubation time, this peptide can form both fibrils and microcrystals. However, the methods used to achieve these different species vary, and heterogeneous solutions are often produced (13,15–17). The concentrations required to form fibrils in particular vary greatly, and their presence has been reported at concentrations as low as 0.3 mg/mL (13). Conversely, Diaz-Avalos et al. (16) reported that neither fibers nor crystals form at $\leq$5 mg/mL, even after prolonged periods, and that much higher concentrations are required (>20 mg/mL) to form fibers, in agreement with other groups (17). Initial studies using a concentration of 10 mg/mL produced crystals that were subjected to powder and electron diffraction (15,16). Further work produced larger crystals that were of sufficient size for structure determination by x-ray

*Submitted August 12, 2009, and accepted for publication October 15, 2009.*

*Correspondence: L.C.Serpell@sussex.ac.uk

Editor: Kathleen B. Hall.



0006-3495/10/01/0330/9 $2.00

doi: 10.1016/j.bpj.2009.10.020

crystallography. Two crystal structures have been solved that both contain pairs of parallel $\beta$-sheets with side chains interdigitating in an anhydrous steric zipper (13,14). However, the two structures differ considerably in the packing of the peptide, crystallizing in monoclinic (1yjp.pdb) (13) or orthorhombic (2omm.pdb) (14) forms (see Fig. S1 in the Supporting Material). Solid-state NMR measurements carried out on the two different crystal forms corroborate previous findings that the two forms are similar and share a cross-$\beta$ arrangement, with the main differences being in the environment of the tyrosine residue (17). In the monoclinic form, the side chain appears to be immobile and responsible for stabilizing the interaction between pairs of sheets across the wet interface via $\pi$-$\pi$ interactions, whereas in the orthorhombic form it has no such role (17). Furthermore, solid-state NMR experiments on fibrillar forms of GNNQQNY show similarities to the orthorhombic form of the crystals, suggesting that the mobile tyrosine residue is responsible for polymorphisms within fibrillar structures (17).

The importance of aromatic interactions in amyloid formation was discussed previously (18), which would imply that the tyrosine residue of GNNQQNY is important for fibril formation and/or the overall stability of the fiber. Nelson et al. (13) suggested that fibril formation proceeds initially by the formation of a nucleus consisting of $\beta$-sheets held together by side-chain interactions. The stability of such a nucleus has been verified by molecular-dynamics simulations on GNNQQNY (19), indicating that interactions in the steric zipper by even a limited number of $\beta$-strands may be responsible for the overall stability of the fiber (19). It is conceivable that alternative structures could arise from different bonding patterns between side chains, as evidenced by the two crystal forms (13,14,20). It is unclear at present whether either or any of these crystal structures truly represent the structure of the fibril, or whether it takes on some entirely different arrangement.

Most of the work on GNNQQNY to date has focused on structural characterization of the end-point species formed after fibrillization and crystallization, and has uncovered variations in morphology. In this work we investigated the actual assembly process using a number of biophysical techniques to gain insight into the pathways by which fibers and crystals form. The role of the tyrosine residue in driving fibril or crystal formation is of particular interest. Measurement of intrinsic and quenched tyrosine fluorescence can provide information regarding the environment of the tyrosine residue, and was previously used to follow structural changes that occur during amyloid fibril formation (21,22). Similarly, circular dichroism (CD) is classically used to obtain information on protein secondary structure and can report on these changes as fibrillization proceeds, typically from random coil or folded native structures to $\beta$-sheet-containing species (23). However, it is known that aromatic residues can contribute significantly to CD spectra in both the near- and far-UV regions (24,25). Furthermore, aromatic residues in close proximity can undergo coupling of their transitions and intensify these contributions, which can complicate data interpretation. In this study, we used linear dichroism (LD) to obtain information on both the secondary structure and the orientation of chromophores within the larger structure (see Rodger and Nordén for an overview (26)). This method can give information regarding the orientation of the $\pi$-$\pi^*$ transitions in the peptide bond of $\beta$-sheet structures that absorb light at ~195 nm. The sign of the LD signal at this wavelength therefore identifies the orientation of $\beta$-strands relative to a larger structure, in this case a peptide fiber. In addition, it is also possible to determine the orientation of aromatic side chains within peptide fibers. Furthermore, the LD signal can be measured in real time to follow the kinetic processes that occur during fiber formation, and to identify changes in backbone and aromatic side-chain orientation that occur during this process. Fiber diffraction analysis of the different species that form over time can also reveal how the morphology changes as assembly proceeds.

Because the peptide GNNQQNY is one of the few amyloidogenic peptides that have been characterized structurally by x-ray crystallography, it provides an excellent model system for further investigation into the process of fibrillization. In this work, we investigate the assembly and accompanying structural changes that occur in the formation of GNNQQNY fibers and crystals. Fluorescence studies indicate that the assembly process is accompanied by a change in the environment of the C-terminal tyrosine residue. This is correlated to morphological changes observed by EM that indicate a development of amyloid-like fibrils to larger crystalline assemblies. LD indicates that the orientation of the tyrosine residue is also altered with the assembly process. Finally, x-ray fiber diffraction of fibers and crystals indicates structural differences between these two morphological forms, and a comparison of the fiber patterns calculated from the two crystal forms suggests that whereas the crystals are consistent with the orthorhombic structure, the fibers may represent an alternative packing arrangement.

## MATERIALS AND METHODS

### Peptide synthesis and sample preparation

$NH_3$+-GNNQQNY-COO- was purchased from Pepceuticals (Biocity, Nottingham, UK) at >97% purity. Stock solutions were made up in Milli-Q (Millipore, Billerica, MA) 0.2 $\mu$m filtered water at concentrations of 2–3 mg/mL. The concentration was determined using a molar extinction coefficient of 1490 $M^{-1}$ $cm^{-1}$ and by measuring absorbance at a wavelength of 280 nm using an Eppendorf biophotometer (Eppendorf AG, Hamburg, Germany).

### Electron microscopy

4 $\mu$L of solution were placed onto carbon-coated copper grids (Agar Scientific, Essex, UK), blotted, and then negatively stained with 4 $\mu$L of 2% uranyl acetate and blotted. The grid was allowed to air-dry before it was

examined in a Hitachi 7100 microscope (Hitachi, Germany) fitted with a Gatan Ultrascan 1000 CCD camera (Gatan, Abingdon, UK). Aliquots of samples were taken at various time points for each experiment. Measurements were made using ImageJ (27).

## Tyrosine fluorescence

Immediately after the addition of water to obtain a final peptide concentration of 3 mg/mL, the samples were centrifuged at 13,000 rpm for 5 min to remove any preformed aggregates. Any pellet that formed was discarded. The samples were placed in a quartz cuvette (Starna, Essex, UK) with a 1 cm pathlength, and the fluorescence from tyrosine was monitored at various time points using a Varian Cary Eclipse fluorimeter (Varian, Oxford, UK) with an excitation wavelength of 278 nm. Fluorescence intensities at the peak of 305 nm were plotted against time. Excitation and emission slits were set to 5 and 10 nm, respectively. The scan rate was set to 600 nm/min with 1 nm data intervals and an averaging time of 0.1 s. Experiments were carried out in triplicate to confirm trends.

## Acrylamide quenching

Samples were prepared as for the tyrosine fluorescence experiments, with identical fluorimeter settings. Quenching effects were observed on fibrils (time 0) and crystals (168 h). At each time point, acrylamide was titrated into the sample at increasing concentrations between 0.1 and 0.4 M, and a fluorescence reading was taken. A reading was also taken with no acrylamide present. The data were fitted to the Stern-Volmer equation, which is used to describe collisional quenching:

$$F_0/F = 1 + K_{SV}[Q],$$

where $F_0$ is the fluorescence intensity in the absence of acrylamide, $F$ is the fluorescence intensity in the presence of acrylamide, $Q$ is the concentration of acrylamide, and $K_{SV}$ is the Stern-Volmer quenching constant (28). Linear plots of $F_0/F$ against $[Q]$ gave $K_{SV}$ values for fibrils and crystals; higher values indicate that the tyrosine is more easily quenched and therefore more solvent-accessible.

## Linear dichroism

Peptide was preincubated for several weeks in water to enable the formation of crystals at a concentration of 2 mg/mL and was diluted to 0.2 mg/mL. Equilibrium LD measurements were performed on a Jasco J-815 spectropolarimeter (Great Dunmow, UK) from 350–180 nm with a bandwidth of 2 nm, scanning speed of 100 nm/min, response of 1 s, standard sensitivity, and data pitch of 0.2 nm. Alignment of the samples was achieved using a microvolume Couette cell with a rotation speed of 3000 rpm, which was built in-house (equivalent models are available from Kromatek, Great Dunmow, UK). Eight spectra were averaged and a water baseline spectrum was subtracted from this to account for the inherent LD signal of the system originating from the optics and the detector. LD spectra are reported in $\delta$ absorbance units.

For kinetics experiments, LD spectroscopy was performed on freshly solubilized peptide. The peptide was dissolved in water at a concentration of 2 mg/mL. Alignment was induced by using a microvolume Couette cell (Kromatek, Great Dunmow, UK) with a pathlength of 0.5 mm (29). Experiments were carried out on the UV1 beamline at the Synchrotron Radiation Facility ASTRID at the Institute for Storage Ring Facilities, Aarhus University (Aarhus, Denmark) and on a Jasco J-815 spectropolarimeter. ASTRID provided a much enhanced signal/noise ratio, which allowed the rapid scanning required for kinetic measurements of samples that inherently scatter light at low wavelengths, such as protein fibers. Spectra were measured between 180 nm and 350 nm at 1 nm steps using the low-energy grating of the UV1 beamline at a spectral resolution of ~1 nm. The beamline was set up as described previously (30). Spectra were measured at a cell rotation speed of 3000 rpm and a water baseline spectrum was subtracted from this to account for the inherent LD signal of the system originating from the optics and the detector. Synchrotron radiation spectra are reported in the output signal from the lock-in amplifier (in millivolts). In terms of $\delta$ absorbance units, 1 mV is ~$6 \times 10^{-4}$ Å.

## X-ray fiber diffraction

A stock solution of peptide at 10 mg/mL was incubated at room temperature. At various time points, aliquots were taken to check for the presence of fibers, crystals, or a mixture of both using EM. For the samples containing fibers and a mixture of crystals and fibers, 20 $\mu$L of solution were placed between two wax-filled capillaries and allowed to air-dry at room temperature. Alternatively, the crystalline sample was placed into a siliconized 0.7 mm capillary tube, sealed with wax at one end, and allowed to dry over a few weeks at room temperature. The resulting sample was a disk in which the crystals were generally oriented across the capillary. The capillary containing the dried disk was sealed at the top end. The fiber or disk sample was placed on a goniometer head, and data were collected with the use of a Rigaku (Sevenoaks, UK) rotating anode (CuK$\alpha$) and Raxis IV++ detector (Sevenoaks, UK), with a specimen-to-film distance of 160 mm or 250 mm.

## X-ray diffraction simulation from coordinates

Diffraction patterns were calculated from model coordinates from 1yjp.pdb and 2omm.pdb using the published unit cell dimensions. This was done using the fiber diffraction analysis program Clearer (31), which generates fiber diffraction patterns from input structural coordinates, as previously described (31,32). The fiber axis was assigned to be parallel to the hydrogen-bonding direction of the coordinates, and the beam direction was perpendicular. The calculated diffraction pattern took into account the diffraction settings associated with the experimental data collection (specimen-to-detector distance, pixel size) to allow direct comparison between experimental and calculated diffraction patterns.

# RESULTS

## EM reveals that GNNQQNY forms fibers followed by crystals

At all concentrations between 0.5 and 10 mg/mL, electron micrographs show that immediately after dissolving in water, the peptide GNNQQNY forms fibrils that eventually develop to form crystalline assemblies, with very little or no fibrils present (data are shown only for a 3 mg/mL sample). Even at very low concentrations, some fibrillar material was observed at time ''zero'' (despite the attempted removal of preformed aggregates by centrifugation), although it was much less abundant, and the crystals that formed at later time points were generally smaller in width. The time it takes for these transitions to occur varies depending on the concentration, but after several days, in all cases only crystals were present. Fig. 1, *a–e*, shows electron micrographs of a 3 mg/mL sample of GNNQQNY at time 0, 3, 24, 72, and 192 h. At time 0 (Fig. 1 *a*) the fibrils show the long, unbranching appearance characteristic of amyloid. Individual fibrils are ~5–10 nm wide, and even at this stage there appears to be some lateral association of fibrils into ribbons of ~20–25 nm (denoted by * and shown in the inset of Fig. 1). By 3 h (Fig. 1 *b*) the average width of the ribbons increases to ~30–60 nm and there are far fewer smaller-width fibrils. Much larger crystalline species (~150–350 nm wide)

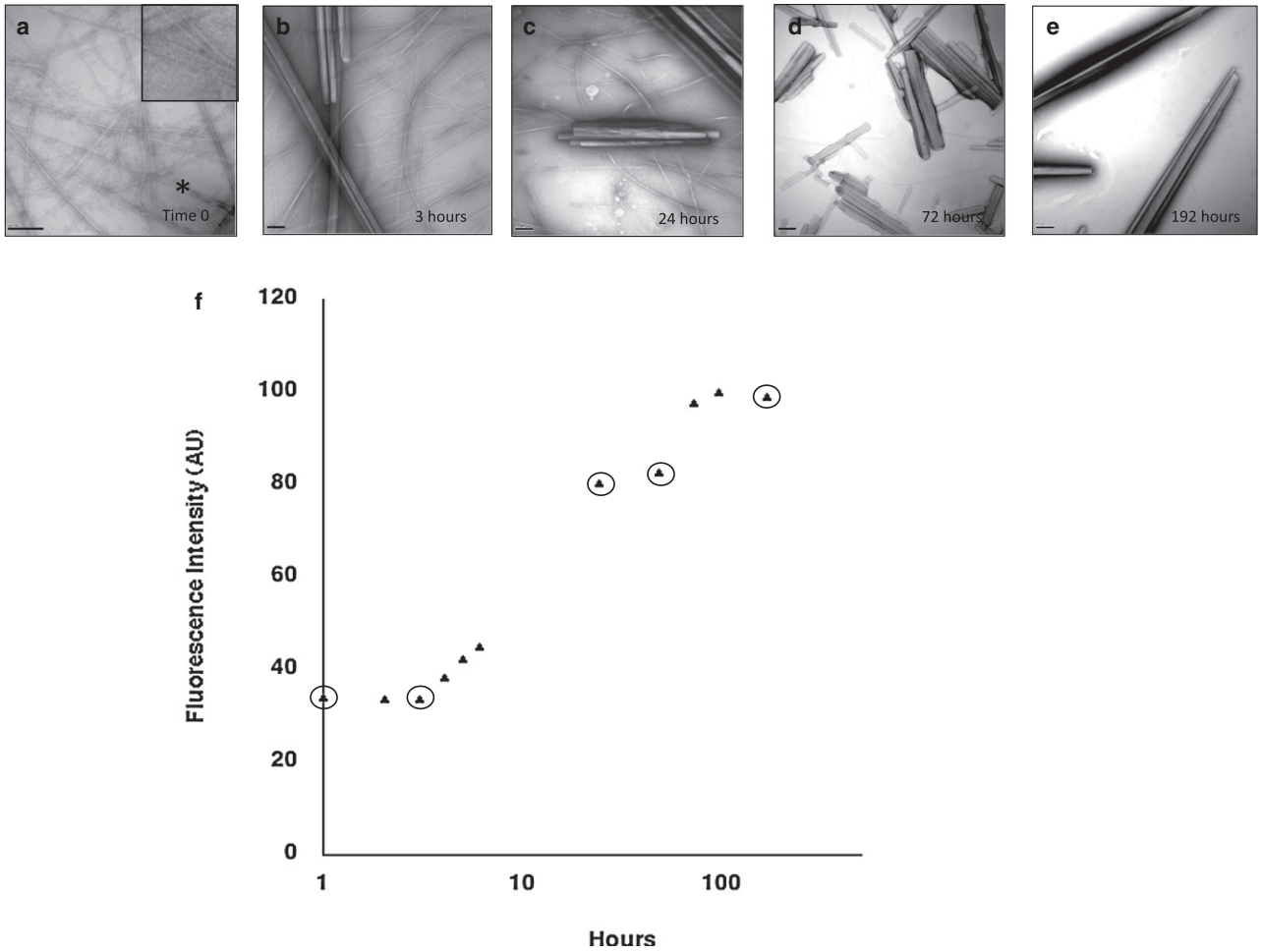


FIGURE 1 Changes in the morphology and tyrosine fluorescence of GNNQQNY over time. (*a–e*) EM images of GNNQQNY taken at various time points. Scale bars are 200 nm in all images. (*f*) Increase in tyrosine fluorescence intensity at 305 nm over time. Circled data points correspond to EM images shown in *a–e*.

are also present. At 24 h (Fig. 1 *c*) the average sizes are uniform but there are fewer fibrils or ribbons in the background, and by 72 h (Fig. 1 *d*) the fibrillar material has disappeared completely.

## An increase in intrinsic tyrosine fluorescence correlates with the transition from fibers to crystals

Structural information obtained from previous crystallization and solid-state NMR experiments (13,14,17) suggests that tyrosine plays an important role in this assembly. We investigated this further using intrinsic fluorescence and quenching experiments. A representative concentration of 3 mg/mL was used to compare the morphological changes observed by EM with any changes in tyrosine fluorescence, which would indicate a change in the environment of the tyrosine residue. Fig. 1 *f* shows that the tyrosine fluorescence increases over time, with a lag phase up to 3 h, followed by an increase in intensity up to ~72 h, at which point the fluorescence intensity reaches a plateau. These changes correspond to the initial formation of crystalline assemblies (3 h), the gradual disappearance of fibrils up to 72 h (during which time the tyrosine fluorescence increases), and finally the presence of crystals only. At this point, there are no further changes in fluorescence or hence in the environment of the tyrosine residue. Other concentrations ranging from 0.5 to 10 mg/mL were explored and showed a similar correlation between intrinsic fluorescence and morphology (data not shown).

## Tyrosine is more easily quenched and more solvent-exposed in fibers than in crystals

Various agents can be used to quench the fluorescence of a fluorophore and give further information on the extent to which that residue is accessible to solvent. Acrylamide was used previously to quench tyrosine fluorescence (33,34), and was used here to generate a Stern-Volmer plot (Fig. S2). $K_{sv}$ values were calculated as 13.6 $\pm$ 0.6 $M^{-1}$ for fibers (present at time 0) and 10.4 $\pm$ 0.1 $M^{-1}$ for crystals (present

at 168 h). Higher $K_{sv}$ values suggest that tyrosine is more readily quenched and is therefore more solvent-accessible in fibers than in crystals, in agreement with the intrinsic fluorescence data.

## LD supports a cross-$\beta$ structure and reveals a change in the orientation of the tyrosine residue over time

LD has the potential to report directional information regarding the orientation of the peptide backbone and the side chains in both fiber and crystal states and as a function of time. To examine the spectra arising from the backbone orientation of the GNNQQNY peptide in crystals, we diluted preincubated peptide 10-fold at a concentration of 2 mg/mL. This was necessary to reduce the high absorbance and light scattering at low wavelength that left insufficient light intensity at the detector below ~215 nm (Fig. 2 *a*). The spectra were taken while the solution was rotated in a Couette cell so that the long axes of the crystals were oriented with the direction of flow. These data show a dominant backbone transition for the $\beta$-structure at ~195 nm (35) arising from a transition dipole moment that is oriented perpendicular to the $\beta$-strands. This is consistent with the cross-$\beta$ structure shown previously (35). The LD signal in the aromatic region (Fig. 2 *b*) shows two maxima at 278 nm and 286 nm. This is evidence of exciton coupling of the tyrosine residues, which occurs when the tyrosines are in close proximity. The positive signals appearing at the same time, at ~230–240 nm, are also consistent with exciton coupling of the tyrosine residues (36).

LD was then used to examine the development of these features during the fiber formation process. To allow direct comparison with other kinetic data collected in this study, the peptide was not diluted and rotated in a Couette cell to induce alignment. This prevented LD data from being recorded in the far-UV region (due to absorbance and light scattering), so instead only the signals in the $n$-$\pi$* (very low intensity for $\beta$-sheets) and aromatic regions were measured (>215 nm). In the kinetics experiment (Fig. 2 *b*), the presence of an increasing LD signal over time means that the fibers/crystals are growing and/or aligning more effectively. The increased light scattering over time (as observed by the increase in the baseline signal outside the wavelength where there are absorbance bands (300–320 nm)) is indicative of an increase in the size and/or number of the particles in the sample, consistent with fiber and/or crystal growth. The presence of an aromatic LD signal at ~280 nm indicates that the tyrosine residues are ordered within the fibers and crystals. The transitions for tyrosine are illustrated in Fig. 2 *c*. Furthermore, there is a change in the sign of the aromatic LD signal over time (when the sloping baseline due to light scattering is taken into consideration; Fig. 2 *b*, *inset*), indicating that the tyrosine side chain changes its orientation early in the kinetics process.

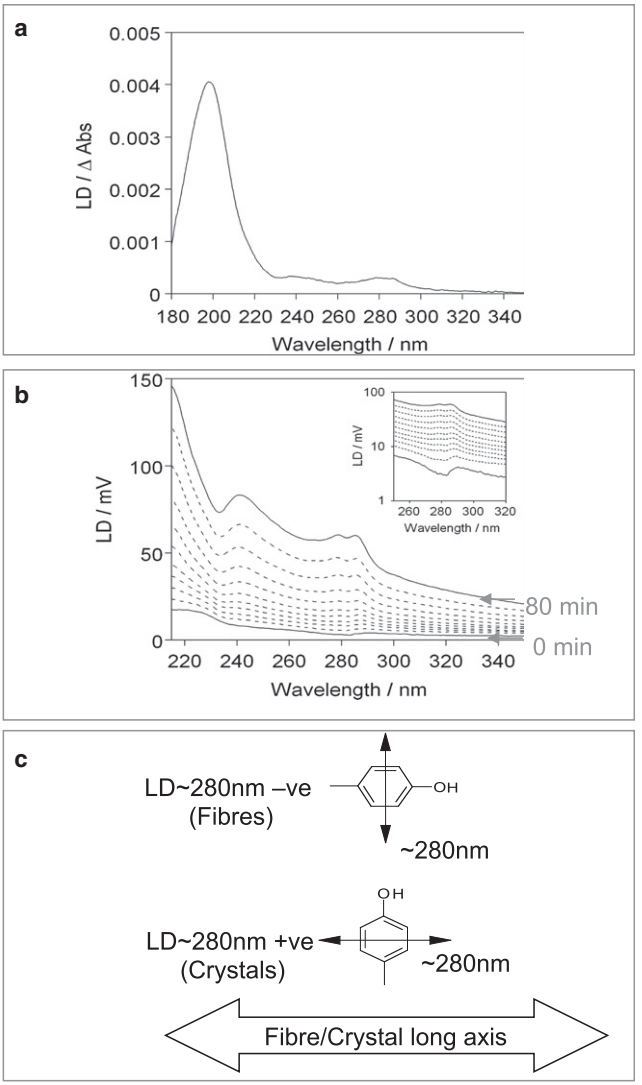


FIGURE 2 (*a*) LD spectrum of mature G1 peptide sample at 0.2 mg/mL. A strong $\pi$-$\pi$* transition at ~195 nm is consistent with the formation of cross-$\beta$ structure. There are aromatic signals at ~280 nm resulting from ordered tyrosine side chains in the structure. (*b*) Kinetics of fiber/crystal formation by G1 peptide at 2 mg/mL. Spectra were measured at 8 min intervals. The inset shows the aromatic region plot on a log scale showing the inversion of the aromatic signal at early time points. Units are in millivolts, as explained in Materials and Methods. (*c*) Direction of the transitions that give rise to the LD signals observed in the near-UV region for fibers and crystals.

## Experimental and calculated fiber diffraction analyses of GNNQQNY fibers and crystals imply structural differences between fibers and crystals

Diffraction patterns from partially aligned fibrils and crystal preparations of GNNQQNY were collected and revealed the expected cross-$\beta$ patterns (Fig. 3) with a strong meridional reflection at 4.7 Å. Of interest, the three patterns collected gave slightly different positions of equatorial diffraction signals (Table 1) and had different reflections on the equator (19 Å in the crystals, and 31.3 Å and 13.7 Å in the fibers),

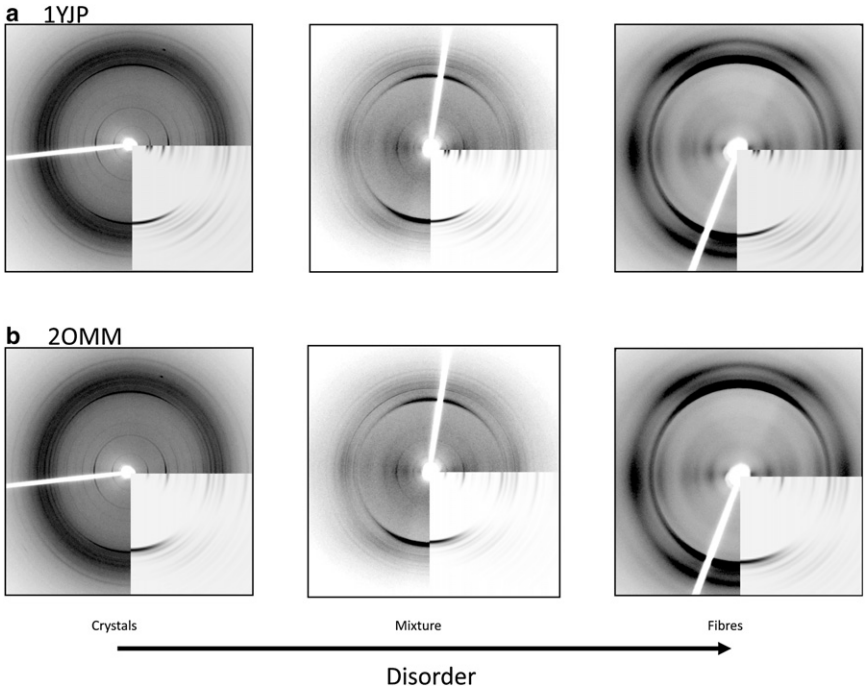


FIGURE 3 Comparison of experimental and simulated fiber diffraction patterns. Simulations are shown in the bottom right-hand corner of each image and were calculated to correspond to the experimental diffraction settings. Fiber axis is vertical. Crystalline, mixed fibers and crystals, and fibrillar samples are compared with simulated diffraction patterns from the crystal structure of (*a*) 1yjp and (*b*) 2omm.

suggesting that their internal architecture varies. Strong reflections at ~10–11 Å on the equator often arise from the sheet spacings, whereas the low-angle reflections are from the chain length, or the width of the protofilaments. A comparison between the signal positions from the three preparations suggests that the positions of the reflections are combined in the preparation known to contain a mixture of both fibers and crystals.

To relate the GNNQQNY preparations with the published crystal structure, we calculated the diffraction patterns from the crystal structure coordinates, 1yjp and 2omm (Fig. S2). These structures crystallize in different unit cells and space groups (13,14), giving rise to different packing of the peptide chains and environments of the tyrosine residue. The 1yjp structure has a very wide separation of sheets at the wet interface, with a spacing of ~15 Å. The position of the meridional reflections arising from the hydrogen bonding between $\beta$-strands differs between the two structures (Table 2 and Fig. S1) and the equatorial positions show clear differences that are likely to arise from the different packing arrangements. A close examination and comparison of the experimental and calculated diffraction patterns (Fig. 3) shows a reasonable match between the equatorials of the experimental pattern from crystalline fibers and mixed preparations with the calculated pattern from the 2omm structure (Fig. 3 *b*). In the 1yjp pattern, the positions of the equatorial reflections are not similar to experimental data. Of interest, the equatorial reflections in the diffraction pattern from fibrils do not match either calculated pattern well (in particular, the strong 13.7 Å reflection is missing in both), which may indicate that fibers rearrange structurally to become crystals, consistent with our other data.

**TABLE 1 Comparison of reflection positions measured from experimental diffraction patterns (only the most intense reflections are shown)**

| | Crystals | Mixture | Fibers |
|---|---|---|---|
| Equatorial reflections (Å) | | | 31.3 |
| | 19.7 | 19.3 | |
| | | 13.7 | 13.7 |
| | 9.9 | 9.9 | 9.2 |
| | 7.4 | 7.4 | 7.9 |
| Meridional reflections (Å) | 4.75 | 4.72 | 4.75 |

## DISCUSSION

The relationship between the structures of crystals and amyloid-like fibrils formed from the peptide GNNQQNY has been studied previously (13–17), and it has been proposed that the crystals share many structural similarities

**TABLE 2 Comparison of reflection positions measured from fiber diffraction patterns calculated from monoclinic and orthorhombic crystal coordinates (only the most intense reflections are shown)**

| | 1yjp | 2omm |
|---|---|---|
| Equatorial reflections (Å) | 22.6 | |
| | | 19.6 |
| | 18.0 | |
| | 11.2 | 11.5 |
| | 8.9 | 9.3 |
| | | 5.5 |
| Meridional reflection (Å) | | 4.85 |
| Meridional reflection (Å) | 4.75 | |

with the fibrils (14). Here, we present data that suggest that although there are some fundamental structural similarities between fibers and crystals, there are also some important differences. We probed the structural environment of the tyrosine residue and found that the tyrosine exists in a different conformation in the crystals compared to the fibers. The assembly of crystals is preceded by fibril formation, and the gradual disappearance of fibrillar material formed from the peptide GNNQQNY, as well as the increasing width of ribbons and crystals as observed by EM, could be explained in two possible ways. The fibers may be laterally associating in some manner to form the crystals, or, more likely, there may be a separate pathway that leads to the formation of crystals, possibly involving fragmentation or monomer dissociation of the fibrils. In either case, it is possible that some structural rearrangement is taking place as the crystals form, and that this crystal form is the most stable arrangement. This was the basis for our further investigations.

The comparatively lower intensity in tyrosine fluorescence observed for fibrils compared to crystals implies that the tyrosine residues are significantly more solvent-exposed in the fibrils, either because they are located on the surface or because they are exposed to solvent present within the structure. This result is corroborated by the $K_{sv}$ values obtained for fibers and crystals calculated from acrylamide quenching experiments. The tyrosine residue is located at the C-terminus, and therefore burial of the tyrosine as crystals form might be expected. This is consistent with the observed increase in fluorescence intensity accompanying the observed morphological changes from narrow fibrils to crystals. However, this change in solvent exposure does not preclude the possibility that the tyrosine residues may also be undergoing structural rearrangements as they participate in these different species, or that their mobility may drive the formation of polymorphisms in the fibrils. The data from acrylamide quenching experiments can be fitted to a straight line (see Fig. S2), consistent with simple collision quenching taking place.

From our EM results, we know that fibers are formed immediately on dissolution of peptide with water, and we can therefore assume that the LD signal at time 0 is specific to fibrillar material. At the end of the LD experiment, crystals are observed in electron micrographs, and the final LD signal is different from that of the fibrillar material. The flow that the peptide experiences in the Couette cell is likely responsible for the crystals forming more quickly than in other experiments (37). The change in the near-UV signal over time at ~280 nm can only be due to a change in the orientation of the tyrosine residue: in the fibers it has one orientation with respect to the fiber axis, whereas in crystals it has another.

The observed splitting of the 280 nm tyrosine peak suggests coupling of the tyrosine residues, which would be the case if they were in close proximity. This proximity could arise either from stacking in the hydrogen-bonding direction, or possibly from interactions between sheets.

The transition moment that gives rise to the signals at ~280 nm in tyrosine is illustrated in Fig. 2 *c*. Thus, in fibers the tyrosine residue is oriented such that, on average, the transition moment shown is pointing more perpendicular than parallel to the fiber long axis. In crystals, the tyrosine transition moment that absorbs at ~280 nm is oriented more parallel to the crystal long axis, giving rise to a positive LD signal in this region (Fig. 2 *c*). Given that for fibers and crystals (which have rotational symmetry about the long axis),

$$\mathrm{LD} = \frac{3}{2}S\left(3\cos^2\alpha - 1\right),$$

where $\alpha$ is the angle between the fiber (or crystal axis) and the 280 nm transition polarization, and $S$ is the degree of orientation, a positive signal means that the transition moment is $<54.7^\circ$ from the alignment axis (fiber/crystal long axis) and a negative signal means that this angle is $>54.7^\circ$. It is important to note the sloping baseline that is seen in these spectra is indicative of large structures scattering the light. Thus, when we refer to a negative signal in this context, we mean a signal that drops below this sloping baseline. It is possible in some cases to correct for this light scattering; however, when the particles that are scattering the light are large (relative to the wavelength of the light), the scattering becomes complex (Mie scattering), and this process can introduce artifacts into the data. For this reason, we did not process the data to correct for light scattering.

Fiber diffraction analysis suggests that the packing of the GNNQQNY peptides within the initially formed fibrils may differ from the published crystal structures, and that rearrangements take place accompanying the conversion to crystals. This could be a conversion from a possibly hydrated wider sheet spacing in the fibrils to a steric zipper arrangement with a dry interface in the crystals. This is seen in the gradual change in the diffraction patterns from fibers, to mixtures of crystals and fibers to the final crystals, and from our other results that suggest that this rearrangement may involve changes in the orientation of the tyrosine. It is even conceivable from this and other work (18) that such aromatic interactions may be a driving force for these changes to take place. Aromatic residues feature in many amyloid-forming proteins (e.g., FF pairs in A$\beta$ and serum amyloid protein), and their presence may play an important role in assembly and/or structural stability. In addition, our analysis indicates that the crystals that form under the conditions used here are consistent with the crystal structure represented by the orthorhombic crystal form (14) (Fig. 3 *b* and Tables 1 and 2).

## CONCLUSIONS

Our results suggest that GNNQQNY initially forms fibers and then crystals. The pathway by which this occurs is

unclear, but we propose that it is either by lateral association of fibers or, more likely, by fragmentation of existing fibers being replaced by crystal nuclei. In all concentrations tested, we noted that the formation of crystals was favored as time proceeded, indicating that crystals are the most stable species. In this work, we used the fluorescent characteristics of the tyrosine residue to monitor assembly. Tyrosine is more buried in fibers than in crystals, suggesting a change in its environment between the two species. LD and fiber diffraction data report that the two species are structurally distinct in terms of both peptide chain packing and the position of the tyrosine residue. LD enables the tyrosine transition to be followed as a function of time, and fiber diffraction analysis indicates that the fibrils may be structurally different from either crystal structure, whereas crystals show similarities to the orthorhombic crystal structure for GNNQQNY. These results may suggest the importance of aromatic interactions in the assembly of fibrils and crystals, and their potential role in driving the formation of different structural species. In addition, the work presented here highlights the structural variations that may exist between these species (i.e., fibers and crystals), and the important implications these differences will have in their characterization.

## SUPPORTING MATERIAL

Two figures are available at http://www.biophysj.org/biophysj/supplemental/S0006-3495(09)01627-0.

The authors thank Julian Thorpe for help with the electron microscopy, and Cedric Dicko for help with the LD analysis.

L.S. received funding from the Biotechnology and Biological Sciences Research Council and Alzheimer's Research Trust, and a donation from Michael Chowen. M.H. and A.R. received funding from the Engineering and Physical Sciences Research Council and the Biotechnology and Biological Sciences Research Council. S.V.H. received funding from the Danish Council for Independent Research | Natural Sciences, and the Lundbeck Foundation.

## REFERENCES

1. Pepys, M. B. 2006. Amyloidosis. *Annu. Rev. Med.* 57:223–241.
2. Geddes, A. J., K. D. Parker, …, E. Beighton. 1968. "Cross-$\beta$" conformation in proteins. *J. Mol. Biol.* 32:343–358.
3. Serpell, L. C., M. Sunde, and C. C. Blake. 1997. The molecular basis of amyloidosis. *Cell. Mol. Life Sci.* 53:871–887.
4. Makin, O. S., and L. C. Serpell. 2005. Structures for amyloid fibrils. *FEBS J.* 272:5950–5961.
5. Westermark, P., M. D. Benson, …, J. D. Sipe. 2007. A primer of amyloid nomenclature. *Amyloid.* 14:179–183.
6. Tycko, R. 2004. Progress towards a molecular-level structural understanding of amyloid fibrils. *Curr. Opin. Struct. Biol.* 14:96–103.
7. White, H. E., J. L. Hodgkinson, …, H. R. Saibil. 2009. Globular tetramers of $\beta$ (2)-microglobulin assemble into elaborate amyloid fibrils. *J. Mol. Biol.* 389:48–57.
8. Vilar, M., H. T. Chou, …, R. Riek. 2008. The fold of $\alpha$-synuclein fibrils. *Proc. Natl. Acad. Sci. USA.* 105:8637–8642.
9. Sachse, C., M. Fändrich, and N. Grigorieff. 2008. Paired $\beta$-sheet structure of an A$\beta$ (1-40) amyloid fibril revealed by electron microscopy. *Proc. Natl. Acad. Sci. USA.* 105:7462–7466.
10. Ding, T. T., and J. D. Harper. 1999. Analysis of amyloid-$\beta$ assemblies using tapping mode atomic force microscopy under ambient conditions. *Methods Enzymol.* 309:510–525.
11. Makin, O. S., P. Sikorski, and L. C. Serpell. 2006. Diffraction to study protein and peptide assemblies. *Curr. Opin. Chem. Biol.* 10:417–422.
12. Marshall, K. E., and L. C. Serpell. 2009. Structural integrity of $\beta$-sheet assembly. *Biochem. Soc. Trans.* 37:671–676.
13. Nelson, R., M. R. Sawaya, …, D. Eisenberg. 2005. Structure of the cross-$\beta$ spine of amyloid-like fibrils. *Nature.* 435:773–778.
14. Sawaya, M. R., S. Sambashivan, …, D. Eisenberg. 2007. Atomic structures of amyloid cross-$\beta$ spines reveal varied steric zippers. *Nature.* 447:453–457.
15. Balbirnie, M., R. Grothe, and D. S. Eisenberg. 2001. An amyloid-forming peptide from the yeast prion Sup35 reveals a dehydrated $\beta$-sheet structure for amyloid. *Proc. Natl. Acad. Sci. USA.* 98:2375–2380.
16. Diaz-Avalos, R., C. Long, …, D. L. Caspar. 2003. Cross-$\beta$ order and diversity in nanocrystals of an amyloid-forming peptide. *J. Mol. Biol.* 330:1165–1175.
17. van der Wel, P. C., J. R. Lewandowski, and R. G. Griffin. 2007. Solid-state NMR study of amyloid nanocrystals and fibrils formed by the peptide GNNQQNY from yeast prion protein Sup35p. *J. Am. Chem. Soc.* 129:5117–5130.
18. Gazit, E. 2002. A possible role for $\pi$-stacking in the self-assembly of amyloid fibrils. *FASEB J.* 16:77–83.
19. Esposito, L., C. Pedone, and L. Vitagliano. 2006. Molecular dynamics analyses of cross-$\beta$-spine steric zipper models: $\beta$-sheet twisting and aggregation. *Proc. Natl. Acad. Sci. USA.* 103:11533–11538.
20. Berryman, J. T., S. E. Radford, and S. A. Harris. 2009. Thermodynamic description of polymorphism in Q- and N-rich peptide aggregates revealed by atomistic simulation. *Biophys. J.* 97:1–11.
21. Maji, S. K., J. J. Amsden, …, D. B. Teplow. 2005. Conformational dynamics of amyloid $\beta$-protein assembly probed using intrinsic fluorescence. *Biochemistry.* 44:13365–13376.
22. Padrick, S. B., and A. D. Miranker. 2002. Islet amyloid: phase partitioning and secondary nucleation are central to the mechanism of fibrillogenesis. *Biochemistry.* 41:4694–4703.
23. Kirkitadze, M. D., M. M. Condron, and D. B. Teplow. 2001. Identification and characterization of key kinetic intermediates in amyloid $\beta$-protein fibrillogenesis. *J. Mol. Biol.* 312:1103–1119.
24. Sreerama, N., M. C. Manning, …, R. W. Woody. 1999. Tyrosine, phenylalanine, and disulfide contributions to the circular dichroism of proteins: circular dichroism spectra of wild-type and mutant bovine pancreatic trypsin inhibitor. *Biochemistry.* 38:10814–10822.
25. Bhattacharjee, S., G. Tóth, …, J. D. Hirst. 2003. Influence of tyrosine on the electronic circular dichroism of helical peptides. *J. Phys. Chem. B.* 107:8682–8688.
26. Rodger, A., and B. Nordén. 1997. Circular Dichroism and Linear Dichroism. Oxford University Press, Oxford, UK.
27. Abramoff, M. D., P. J. Magelhaes, and S. J. Ram. 2004. Image Processing with Image. *J. Biophotonics Int.* 11:36–42.
28. Lakowicz, J. R. 1999. Principles of Fluorescence Spectroscopy, 2nd ed. Kluwer Academic/Plenum, London, UK.
29. Rodger, A., R. Marrington, …, T. R. Dafforn. 2006. Looking at long molecules in solution: what happens when they are subjected to Couette flow? *Phys. Chem. Chem. Phys.* 8:3161–3171.
30. Dicko, C., M. R. Hicks, …, S. V. Hoffmann. 2008. Breaking the 200 nm limit for routine flow linear dichroism measurements using UV synchrotron radiation. *Biophys. J.* 95:5974–5977.

31. Zibaee, S., O. S. Makin, …, L. C. Serpell. 2007. A simple algorithm locates $\beta$-strands in the amyloid fibril core of $\alpha$-synuclein, A$\beta$, and $\tau$ using the amino acid sequence alone. *Protein Sci.* 16:906–918.

32. Madine, J., E. Jack, …, D. A. Middleton. 2008. Structural insights into the polymorphism of amyloid-like fibrils formed by region 20–29 of amylin revealed by solid-state NMR and X-ray fiber diffraction. *J. Am. Chem. Soc.* 130:14990–15001.

33. Padrick, S. B., and A. D. Miranker. 2001. Islet amyloid polypeptide: identification of long-range contacts and local order on the fibrillogenesis pathway. *J. Mol. Biol.* 308:783–794.

34. Dusa, A., J. Kaylor, …, A. L. Fink. 2006. Characterization of oligomers during $\alpha$-synuclein aggregation using intrinsic tryptophan fluorescence. *Biochemistry.* 45:2752–2760.

35. Dafforn, T. R., J. Rajendra, …, A. Rodger. 2004. Protein fiber linear dichroism for structure determination and kinetics in a low-volume, low-wavelength couette flow cell. *Biophys. J.* 86:404–410.

36. Khan, M. A., C. Neale, …, R. E. Bishop. 2007. Gauging a hydrocarbon ruler by an intrinsic exciton probe. *Biochemistry.* 46:4565–4579.

37. Hill, E. K., B. Krebs, …, D. E. Dunstan. 2006. Shear flow induces amyloid fibril formation. *Biomacromolecules.* 7:10–13.